

Aqueous and Mineral Intrinsic Bioremediation Assessment (AMIBA) Protocol



Technology Transfer Division

By

Lonnie Kennedy, Ph.D., P.G.
Earth Science Services
5815 Hickory Bend, Norman, OK 73026
lonniekennedy@hotmail.com

Jess Everett, Ph.D. P.E.
Rowan University
201 Mullica Hill Road, Suite 5325
Glassboro, NJ 08028
everett@rowan.edu

James Gonzales
HQ AFCEE/ER
3207 N. Road, Building 532
Brooks AFB, TX 78235
james.gonzales@hqafcee.brooks.af.mil

[Viewing Instructions](#)

[Begin Document](#)

This document presents graphics as imbedded objects as shown on the left. There are two types of graphics objects, 2D and 3D. In both cases, clicking on the thumbnail image will activate and enlarge the graphic. To return to the text click on the “Home” symbol.

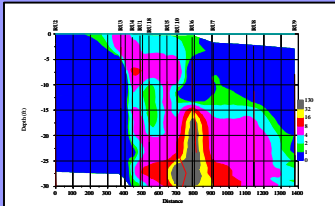


Figure i

An example of a 2D graphic is shown on the left (Figure i). All 2D graphics are archived in one of two portable document files (pdf) so you can view many graphic images serially. The thumbnail link will show the appropriate graphic image and the “Home” icon on that image will return to the proper page in the text. However, if you scroll to a different image on another page the “Home” icon may be linked to a different page in the text. Although you can view all the 2D graphics you must return to the image you started with to return to the correct position in the text. Figure i is a concentration profile of dissolved Fe through a line of section. Click on the thumbnail to activate the graphic then return by clicking on the “Home” icon.

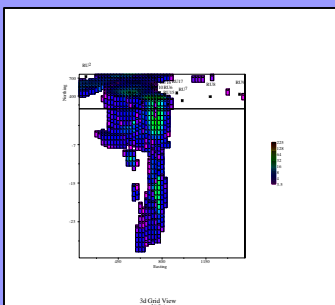


Figure ii 3D (mg/Kg)

An example of a 3D graphic is shown on the left (Figure ii). As above, clicking on the thumbnail image will activate and enlarge the graphic. 3D graphics rotate or slice through the geostatistical model. They are designated with the word “3D” in the caption followed by the units of the image. When a 3D image is activated can click on the graphic to rotate or slice through it. Clicking on the “Home” icon on a 3D graphic will always return you to correct position in the text document. Figure ii is a 3D geologic model of chromium extractable sulfide, mostly pyrite (FeS_2), for the study area. Click on the thumbnail to view the model. Clicking on a model image will rotate to the next orientation. Click on the “Home” icon to return back to this page.

Click on the “Begin Document” icon below to view the AMIBA protocol.

Begin Document

Table of Contents

1. INTRODUCTION	1
1.1. PURPOSE	1
1.2. RATIONALE FOR AMIBA.....	2
2. AMIBA THEORY AND BACKGROUND.....	11
2.1. MICROBIAL ENVIRONMENT	12
2.2. BIOREMEDIATION PROCESSES/REDOX ZONE DEVELOPMENT.....	14
2.3. ELECTRON ACCEPTOR OCCURRENCE IN THE SUBSURFACE.....	19
2.3.1. <i>Oxygen</i>	19
2.3.2. <i>Nitrate</i>	21
2.3.3. <i>Iron</i>	22
2.3.4. <i>Sulfate</i>	24
2.3.5. <i>Comparison of Electron Acceptor Abundance by Type</i>	27
2.4. IRON MICROBIAL GEOCHEMICAL PROCESSES	28
2.5. SULFUR MICROBIAL GEOCHEMICAL PROCESSES.....	41
2.6. Fe^{3+} AND SO_4 REDOX ZONE DELINEATION FROM PRIOR STUDIES	49
2.7. INTRINSIC BIOREMEDIATION SUMMARY	53
3. AMIBA SAMPLING AND LABORATORY PROTOCOL	55
3.1. OBJECTIVE OF METHODS DEVELOPMENT.....	55
3.2. SAMPLE PLANNING AND BORING PLACEMENT.....	57
3.3. FIELD OBSERVATIONS.....	60
3.4. FIELD SAMPLE COLLECTION AND PRESERVATION	63

3.5.	WEAK ACID SOLUTION (WAS) IRON ANALYSIS.....	67
3.5.1.	<i>WAS Method Background</i>	67
3.5.2.	<i>Weak Acid Iron Mineral Extraction Method Description</i>	71
3.6.	STRONG ACID SOLUTION (SAS) FE AND EXTENDED SULFIDE ANALYSIS	72
3.6.1.	<i>Method Background</i>	72
3.6.2.	<i>Method Description</i>	75
3.6.3.	<i>Laboratory Testing and Discussion</i>	79
3.7.	PORE WATER EXTRACTION.....	80
3.7.1.	<i>Method Background</i>	80
3.7.2.	<i>Sample Collection</i>	81
3.7.3.	<i>Laboratory Analysis</i>	82
3.8.	FIELD EXAMPLES OF FE AND S EXTRACTION	83
3.9.	FE AND S EXTRACTION SUMMARY	88
4.	AMIBA DATA ANALYSES	93
4.1.	EXPRESSED AND ASSIMILATIVE CAPACITY	93
4.2.	EXPRESSED AND ASSIMILATIVE CAPACITY – AQUEOUS COMPOUNDS	94
4.3.	EXPRESSED AND ASSIMILATIVE CAPACITY – SOLID COMPOUNDS	99
4.4.	SULFIDE INDEXING OF AQUEOUS EC	105
4.5.	TOTAL EXPRESSED CAPACITY	107
4.6.	HYDROCARBON MASS CALCULATIONS.....	108
4.7.	INDEX OF EXPRESSED CAPACITY	111
4.8.	GEOSTATISTICAL APPROACH.....	112
4.9.	DATA DISTRIBUTION AND DIMENSIONAL ANALYSES.....	120

4.10.	PLUME FOOTPRINT.....	128
4.11.	RATE CONSTANT DETERMINATION	129
5.	AMIBA EXAMPLE AT WESTOVER AIR FORCE BASE.....	132
5.1.	EXECUTIVE SUMMARY.....	132
5.2.	INTRODUCTION	136
5.2.1.	<i>Scope and Purpose.....</i>	<i>136</i>
5.2.2.	<i>Site Background.....</i>	<i>138</i>
5.2.3.	<i>Hydrogeology.....</i>	<i>142</i>
5.2.4.	<i>Known Fuel Distribution</i>	<i>144</i>
5.2.5.	<i>Review of Prior Natural Attenuation Studies.....</i>	<i>145</i>
5.2.6.	<i>Overview of Approach</i>	<i>147</i>
5.3.	METHODS	148
5.3.1.	<i>Sample Planning.....</i>	<i>148</i>
5.3.2.	<i>Drilling and Lithologic Logging.....</i>	<i>150</i>
5.3.3.	<i>Sediment and Pore Water Collection.....</i>	<i>151</i>
5.3.4.	<i>Monitoring Well Sampling.....</i>	<i>152</i>
5.3.5.	<i>Laboratory Analytical.....</i>	<i>153</i>
5.4.	DATA ANALYSES METHODS	155
5.5.	AMIBA RESULTS	159
5.5.1.	<i>Geologic Observations.....</i>	<i>159</i>
5.5.2.	<i>BTEX Mass and Distribution</i>	<i>162</i>
5.5.3.	<i>Sulfate Analyses</i>	<i>166</i>
5.5.4.	<i>Iron Reduction</i>	<i>170</i>

5.5.5.	<i>Oxygen and Nitrate Reduction</i>	179
5.5.6.	<i>Expressed Capacity Index</i>	180
5.5.7.	<i>Comparison of AMIBA EC to Prior Protocol</i>	182
5.5.8.	<i>Rate Constant Analysis</i>	185
5.5.9.	<i>Groundwater Modeling</i>	186
5.6.	DISCUSSION AND RECOMMENDATIONS	191
5.7.	CONCLUSIONS.....	196
6.	REFERENCES	198

Definitions

Acid Volatile Sulfide (AVS): The fraction of mineral sulfide extractable by acid solution correlating to FeS species.

Assimilative Capacity (AC): The potential ability of the aquifer system to degrade hydrocarbon through specific redox processes based on electron acceptor mass. Functionally, AC only has significance if contaminant oxidation is limited by electron acceptor availability or arrested if a required electron acceptor is unavailable.

Chromium Extractable Sulfides (CrES): The fraction of mineral sulfides extractable by chromium solution following AVS removal correlating to S^0 and FeS_2 .

Bioavailable Fe^{3+} : Fe^{3+} that can immediately be used as an electron acceptor should sufficient labile electron donor be available under proper environmental conditions for iron reduction. Bioavailable iron is normally a fraction of the bulk Fe^{3+} present in most soils as determined by a weak acid extraction.

Biogenic Fe^{2+} : The Fe^{2+} created by the direct enzymatic reduction of Fe^{3+} or abiotically by reaction with sulfides that were produced by SO_4^{2-} reduction.

Expressed Capacity (EC): The mass of hydrocarbon that has been destroyed via a specific redox process based on the measured mass of reduced electron acceptors or expressed product.

Expressed Product (EP): The reduced product of a former electron acceptor compound which has been reduced by microbial respiration.

Iron Reserve: Fe^{3+} potentially useable as an electron acceptor by bacteria but not immediately available. This is SAS Fe^{3+} minus WAS Fe^{3+} iron.

Plume Fingerprint: A comparison of the distribution of organic contaminant and respiratory end-product used to determine if the plume is growing or shrinking.

Reactive iron: Iron that is dissolved by a weak acid solution (WAS). Used to measure bioavailable Fe^{3+} and biogenic Fe^{2+} .

SAS Fe: Strong acid solution extracted iron using 6 N HCl. Can be further divided into SAS Fe^{2+} + SAS Fe^{3+} . This may be referred to as "Bulk Fe".

Total Sulfides: AVS + CrES extracted sulfides.

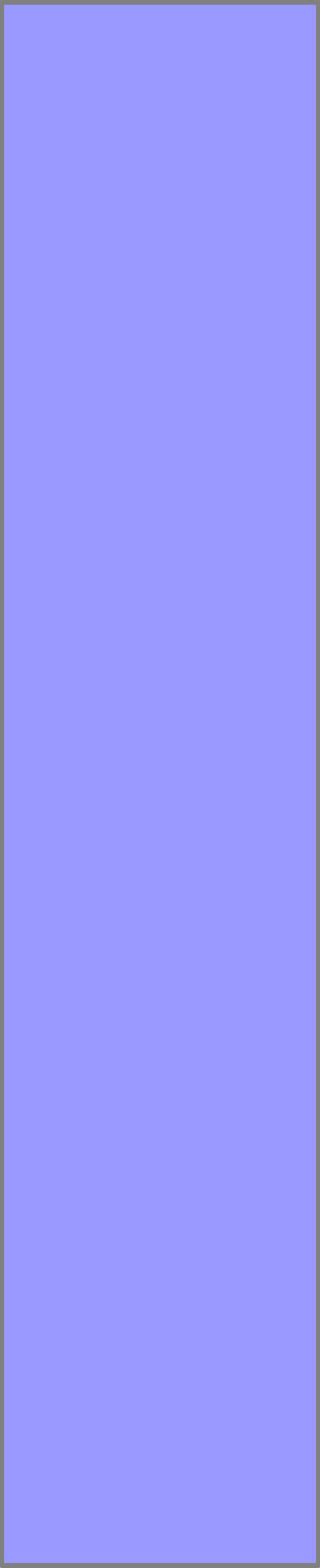
WAS Fe: Weak acid solution extracted iron using 0.5 N HCl.



1. INTRODUCTION

1.1. Purpose

Our understanding of natural aquifer restoration is continuously evolving, precipitating the need for the periodic update of technical procedures. This document is a supplement to the Technical Protocol for Implementing Intrinsic Remediation with Long-Term Monitoring for Natural Attenuation of Fuel Contamination Dissolved in Groundwater, Volumes 1 and 2 (Wiedemeier et al., 1999). The above referenced document remains central to understanding the scope of natural attenuation of hydrocarbon fuels; however, as its title implies, emphasis was placed on the aqueous system. Though relying heavily on the previous work, this publication focuses on important mineral/microbial interactions to provide a more comprehensive understanding of intrinsic bioremediation. This document presents the concept of Aqueous and Mineralogical Intrinsic Bioremediation Assessment (AMIBA). Key to AMIBA is examining in greater detail aqueous and

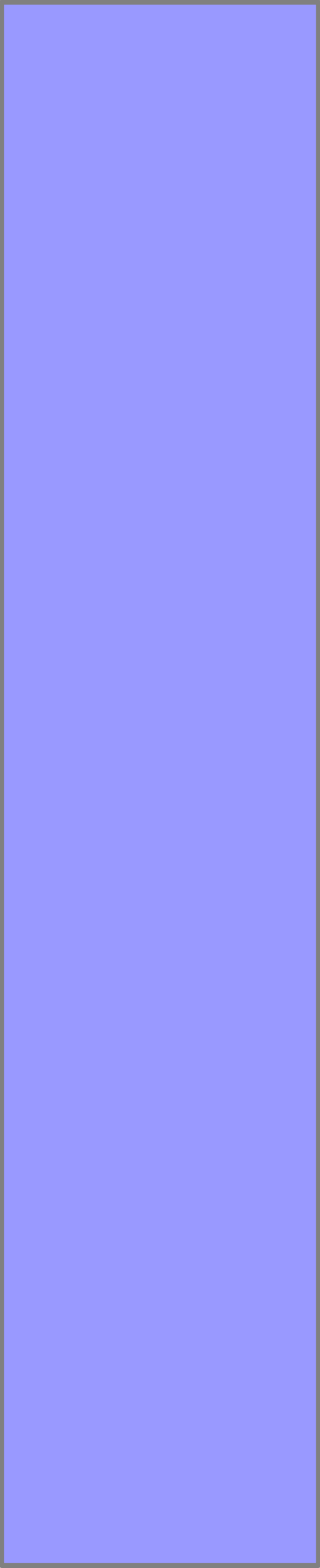


mineral interactions facilitated by microbial processes mostly related to iron and sulfur biogeochemistry.

Perhaps more than any other realm of environmental science, natural attenuation is an interdisciplinary study. It is assumed that the reader has a basic understanding of hydrogeology, environmental science, microbiology and engineering as related to natural attenuation. Many of the necessary fundamental concepts can be found in Wiedemeier et al. (1999) and are revisited here only as is necessary to address the subject at hand. The intended audience for this document is United States Air Force personnel and their contractors, scientists, consultants, regulatory personnel, and others charged with remediating groundwater contaminated with fuel hydrocarbons.

1.2. Rationale for AMIBA

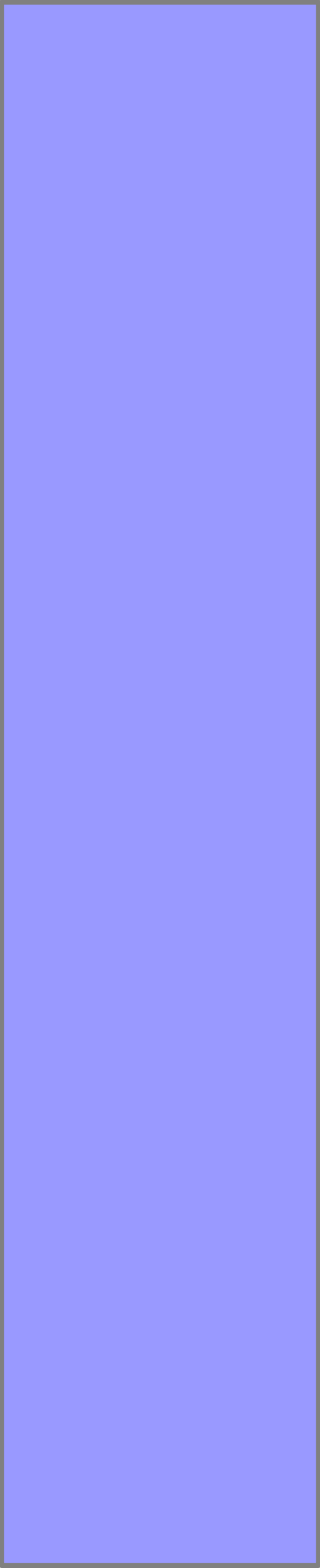
Natural attenuation is recognized as an effective remediation for hydrocarbon fuels. The AFCEE Remediation Matrix - Hierarchy of Preferred Alternatives has identified intrinsic remediation as the first option to be evaluated for Air Force sites. Natural attenuation is often regarded as a cost effective alternative to engineered treatment systems.



However, it should also be considered as a supplement to engineered remediation. Moreover, in many cases, natural attenuation is the only treatment technology that can practically be applied, irrespective of cost considerations.

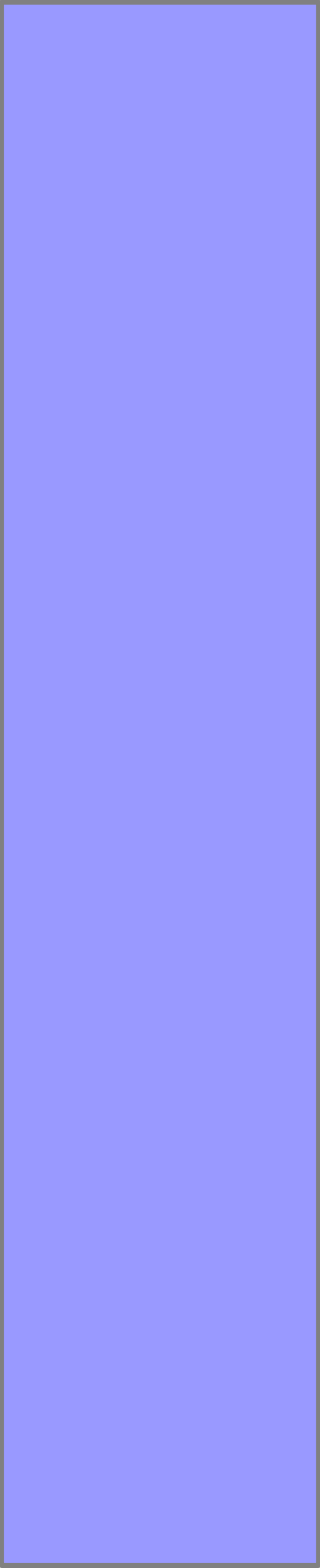
When successful, a natural attenuation assessment demonstrates that intrinsic bioremediation: 1) has historically been effective in contaminant abatement; and 2) will continue to restore the site in a timely manner, so a more costly, engineered remediation system can be avoided. As presented below, an examination of both the aqueous and mineral systems can significantly improve the understanding of natural attenuation as opposed to examining predominantly the aqueous components, as has previously been the practice. With AMIBA, the effectiveness of intrinsic bioremediation in controlling hydrocarbon may be tangibly demonstrated to the satisfaction of a regulator, enabling more rapid site closure or relaxation of monitoring requirements.

Natural attenuation includes many abiotic processes, including advection, dispersion, and volatilization, that collectively decrease contaminant concentrations. However,



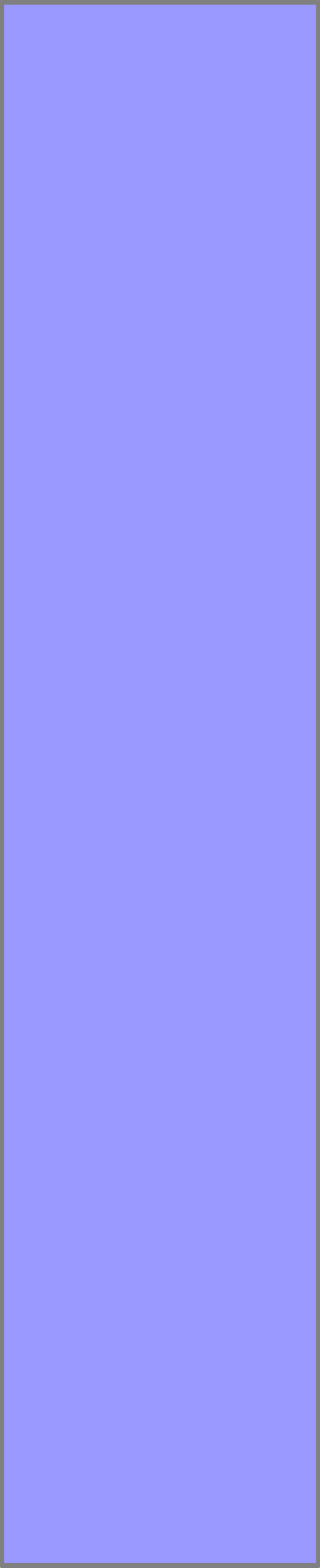
intrinsic bioremediation is often the chief destructive mechanism. Determining the efficacy of natural attenuation has been accomplished by performing natural attenuation studies that typically relying on aqueous data supplied from groundwater analyses. Using the aqueous approach, it is possible to roughly identify operative redox zones and/or daughter products and thus confirm that remediation via microbial oxidation/reduction is likely occurring. However, at the conclusion of such a study, the historical destructive efficiency of intrinsic bioremediation at a site cannot be reasonably quantified. Thus, extended periods of monitoring are necessary to confirm plume stabilization and decay. However, AMIBA can often substantially quantify the mass percent of hydrocarbon fuel destroyed by microbial processes.

Clearly establishing the efficacy of intrinsic bioremediation using aqueous data alone can sometimes be difficult. Normally, evidence of ongoing intrinsic bioremediation is provided by trying to observe a consistent decrease in dissolved phase contaminant concentrations. However, seasonal or periodic variations in recharge and



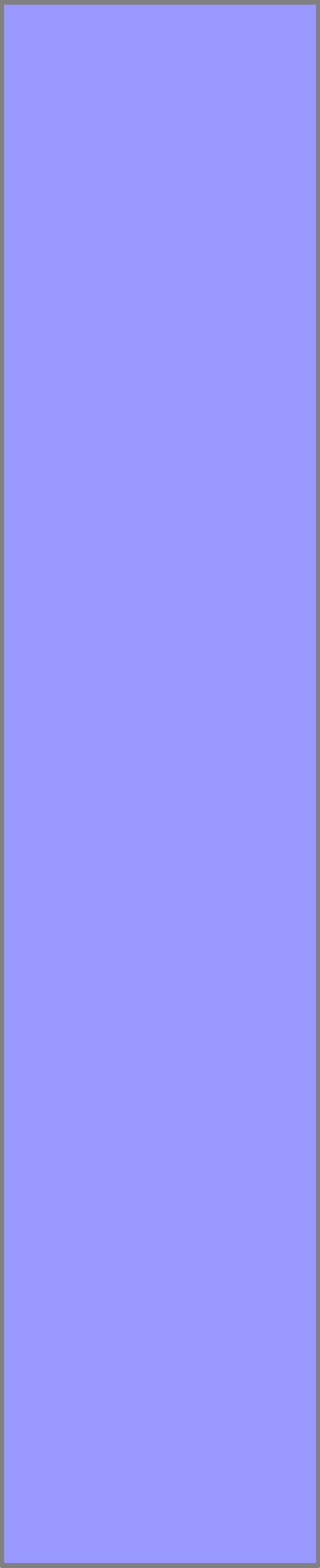
groundwater elevations can cause significant fluctuations in contaminant concentrations in monitoring wells for successive sampling events. Thus, the desired progressive decrease in contaminant concentrations over time may not be readily apparent or statistically defensible. Additionally, in some cases, there is little apparent decrease in dissolved contaminant concentrations in monitoring wells over time, suggesting that intrinsic bioremediation is inactive or ineffective. This condition may occur, for example, where source concentrations exceed the solubility limit of the groundwater. However, if key indicators in the soil system are examined, one can often find that considerable contaminant degradation is occurring that is simply not reflected in the groundwater.

For an engineered treatment system, an efficiency study would be conducted to determine its effectiveness after some period of operation. Bioremediation is a de facto treatment system, operational since near the date of the first release. As such, intrinsic bioremediation should also be routinely examined for cleanup efficiency, which is only possible with an adequate site assessment similar to the



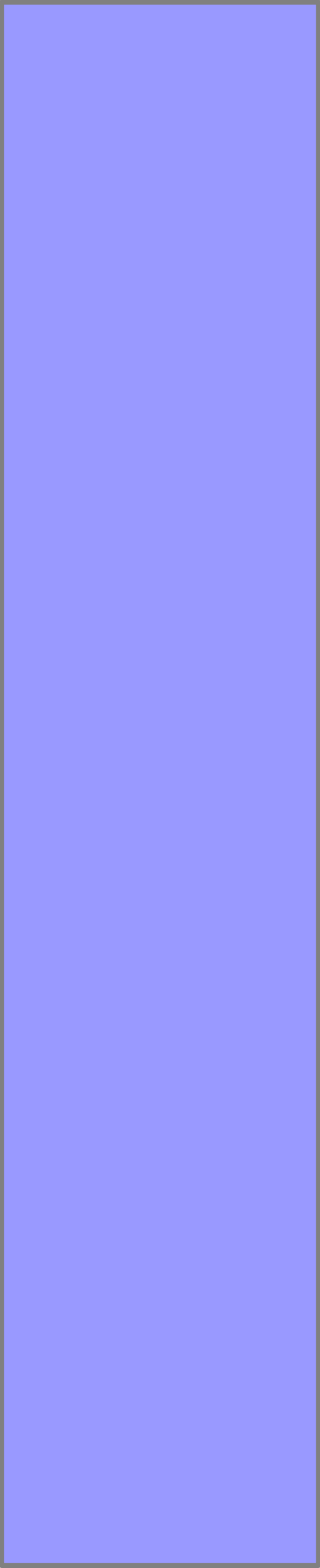
type described here. As described below, AMIBA can produce a defensible value for the percent contaminant remediated by natural attenuation. It can also help define the maximum historical extent of plume migration (plume footprint) to effectively demonstrate plume contraction.

One major objective of a traditional natural attenuation assessment is to assess future contaminant concentrations using a predictive model. However, there is often considerable uncertainty regarding the rate of source decay and source loading, factors that strongly affect simulation outcomes. Dissolved fuel concentrations in groundwater along with other hydrological site data are normally used to estimate dissolved phase degradation rate constants (Wiedemeier et al. 1999, Buscheck and Alcantar, 1995). However, if only dissolved phase degradation is assumed, one can at best only demonstrate a stable plume using a model. Source mass and a source decay term is required before plume retreat can be simulated with defensible results. An AMIBA study can aid in quantifying mass loading and source decay rates in support of predictive modeling



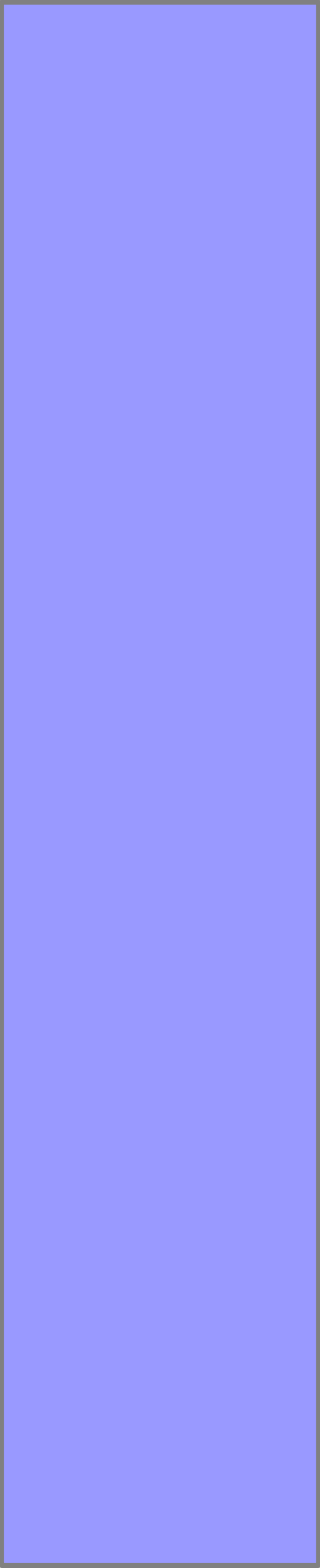
It can be argued that the importance of natural attenuation is marginal, in light of the growing tendency to rely on Risk Based Corrective Action (RBCA) for site closure. However, success in RBCA does not infer that contaminants are absent from the site. In fact, when a “no action” recommendation is made using RBCA, we are relying exclusively on natural attenuation processes for complete site restoration if any level of contaminant is present. RBCA is strengthened when key input factors are supplied from a comprehensive natural attenuation assessment rather than relying on generalized data. Thus, the need for improved natural attenuation assessment is even more critical when RBCA is considered.

AMIBA can more fully quantify the role of natural attenuation, often reducing the need for engineered remediation. However, data gathered during AMIBA will almost certainly aid in the feasibility assessment process. Should remediation be required, a natural attenuation study as described below can significantly improve system design and implementation. For example, an AMIBA assessment



will characterize the spatial distribution of the contaminants enabling more effective source removal or control. In addition, an engineered treatment system is rarely 100% effective. So, the role of natural attenuation in treating residual contaminants should be assessed as part of life-cycle-management. In some cases, considering the combined effects of engineered treatment with natural attenuation could allow an earlier cessation of treatment activities.

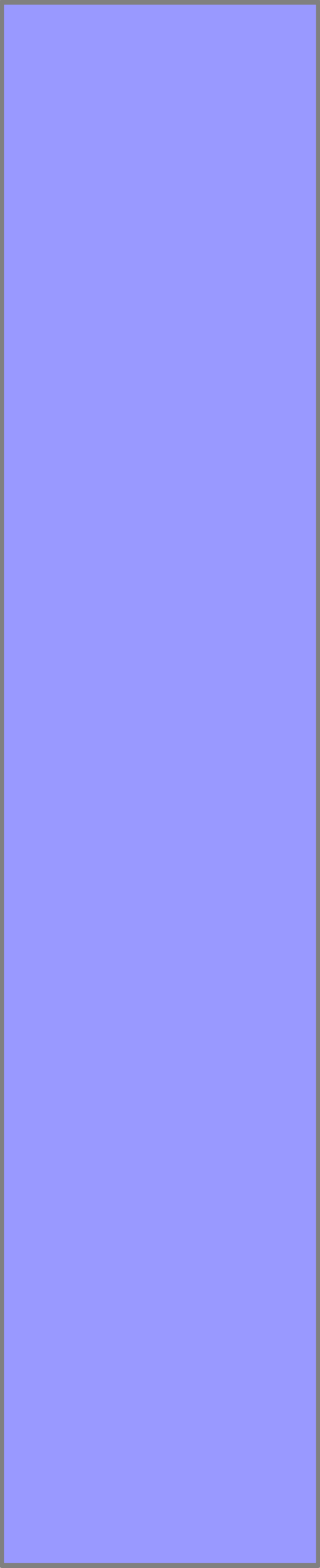
With AMIBA, the role of natural attenuation in augmenting, or hindering, engineered treatment can also be assessed. The concept that natural attenuation might inhibit engineered treatment is a fact not often recognized. For example, as shown below, intrinsic bioremediation processes can produce quite large amounts of reduced reactive mineral species that can strongly compete with bacteria as a sink for oxygen should sparging or the chemical addition of oxygen be considered as a treatment. Indeed, the chemical oxygen demand from minerals generated during natural attenuation can be many times greater than the targeted contaminant. Abiotic mineral



demand cannot be determined by examining groundwater data alone. Using AMIBA, intrinsic bioremediation and engineered treatment systems can be designed to work together to improve cleanup and reduce costs.

In conclusion, AMIBA can be used to:

- Improve Natural Attenuation by better demonstrating expressed capacity and by providing useful data for predictive modeling.
- Support RBCA by supplying defensible loading data for this analysis and by demonstrating the natural attenuation of any contaminants that remain onsite in concentrations that are not considered an immediate risk to human health.
- Support Engineered Remediation by supplying requisite data for remedial system design especially with respect to source control and post treatment degradation of residual contaminant mass.



For natural attenuation in general one must justify the increase in analytical, evaluation, and monitoring costs against the cost for remediation. Further, one must balance those tangible costs against the potential legal liabilities or environmental/personnel risks present when natural attenuation is selected in favor of a more aggressive engineered treatment system. Although AMIBA is more costly to perform than a typical aqueous natural attenuation it should reduce the risk that the natural attenuation option is improperly applied and provide valuable data for remediation should such action be required. Furthermore, used at many sites, AMIBA will justify natural attenuation at more sites, compared to aqueous only analyses. This has the potential to create significant savings by avoiding unnecessary active remediation. AMIBA could be impractical for small sites where remedial action is patently obvious.

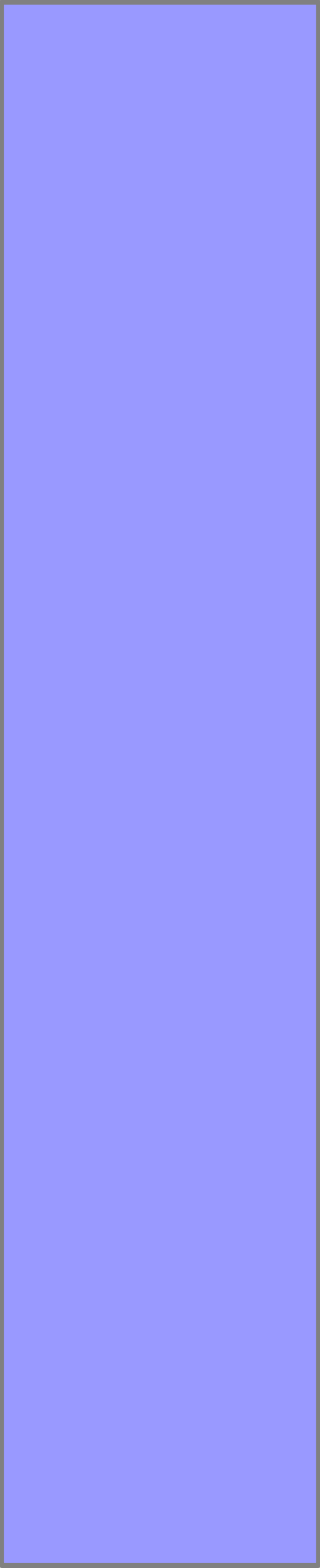
2. AMIBA THEORY AND BACKGROUND

This section is written to provide a general overview of natural attenuation processes. These processes are described more fully in Wiedemeier et al. (1999). Additional detail is provided here on microbial/mineral interactions, principally with respect to the iron and sulfur system. This section initially reviews the concepts behind redox development in organic rich subsurface systems. Possible sources for electron acceptors are described. Thermodynamic considerations of common redox reactions are examined including reactions involving solid phase Fe and S based electron acceptors. Observations are also made with respect to electron acceptor abundance in the environment. Special emphasis is given to the geomicrobiology of Fe and S reactions. Finally, examples are also shown of existing intrinsic bioremediation studies focusing on the apparent relationship between Fe^{3+} and SO_4^{2-} reduction and methanogenesis.

2.1. Microbial Environment

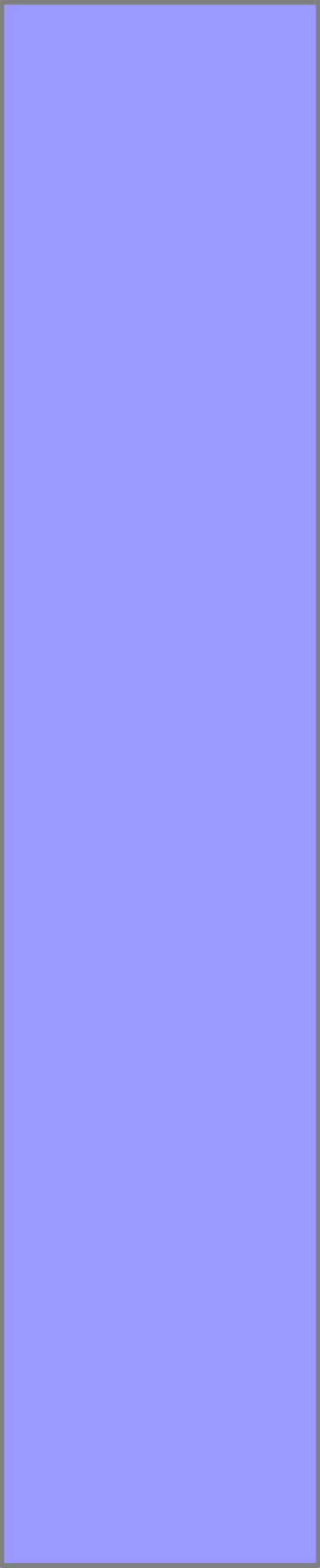
In simplest terms, the subsurface environment is comprised of multiple components, including water (with dissolved ions); organic matter (including biomass), gases, and minerals. In the absence of significant microbial processes, aquifer geochemistry can be remarkably stable with significant changes often measured in terms of decades or even centuries for regional flow systems. Alternatively, under certain conditions, bacteria play a pivotal role and dramatically alter the subsurface environment in short periods measured in days. Such rapid changes can occur when labile organic contaminants are released to a soil/aquifer system, causing a rapid increase in microbial growth and respiration.

Soil bacteria can play a central role in determining an aquifer's mineral, organic, dissolved ion, and gaseous contents. Under certain conditions, soil bacteria catalyze mass transfer between these phases. When an organic is introduced to the subsurface, bacterial processes facilitate a very complex sequence of events. Chemoheterotrophic bacteria oxidize organic carbon through the complimentary reduction of various dissolved and solid electron acceptors.



New organic substances are also created (e.g., biomass or fermentation products) while some carbon is converted to inorganic CO₂. Gases, such as O₂, H₂, CO₂, H₂S, CH₄ and N₂, can be both generated and/or removed. The geochemical system is also forced out of equilibrium, causing some minerals to dissolve while others are precipitated. This entire process occurs in a complex ecosystem where numerous microbial types interact with each other as well as with their surrounding inorganic environment.

Geochemical equilibrium studies have shown the importance of microbial processes on a regional scale (Thorstenson et al., 1979; Plummer, 1977; and Plummer et al., 1990). For example, Plummer et al. (1990) suggested that bacteria oxidized naturally occurring organics in the Madison aquifer of Wyoming and Montana. In that study, variations in water chemistry caused by microbial activity could be attributed to the dissolution of mineral gypsum (CaSO₄•2H₂O), dolomite (Ca•Mg(CO₃)), and goethite (FeOOH) with the concurrent precipitation of pyrite (FeS₂) and calcite (CaCO₃). Microbial activity was associated with organic consumption; biomass production; gas production



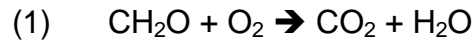
(H₂S and CO₂); and mineral dissolution and precipitation, which contributed significantly to changes in overall water chemistry. Evaluated on a regional scale, these microbially produced changes occur slowly because organic carbon is limited, keeping bacterial growth/reproduction minimal. However, many of these same changes can occur very rapidly on a local scale if labile organic contaminants are released to shallow soil/aquifers.

2.2. Bioremediation Processes/Redox Zone Development

Considerable information has been amassed in support of intrinsic bioremediation of many organic contaminants in the subsurface. With respect to fuels, bacteria capable of degrading hydrocarbons are ubiquitous in soils (Litchfield and Clark, 1973; and Ridgeway et al., 1990). Microbial degradation of organic substrates is accomplished through a complex series of enzymatically-mitigated fermentative and respiratory pathways, which ultimately can be described in terms of simple redox processes. Here, energy is generated by heterotrophic bacteria and used to make ATP by oxidizing an organic substrate. This redox reaction requires the

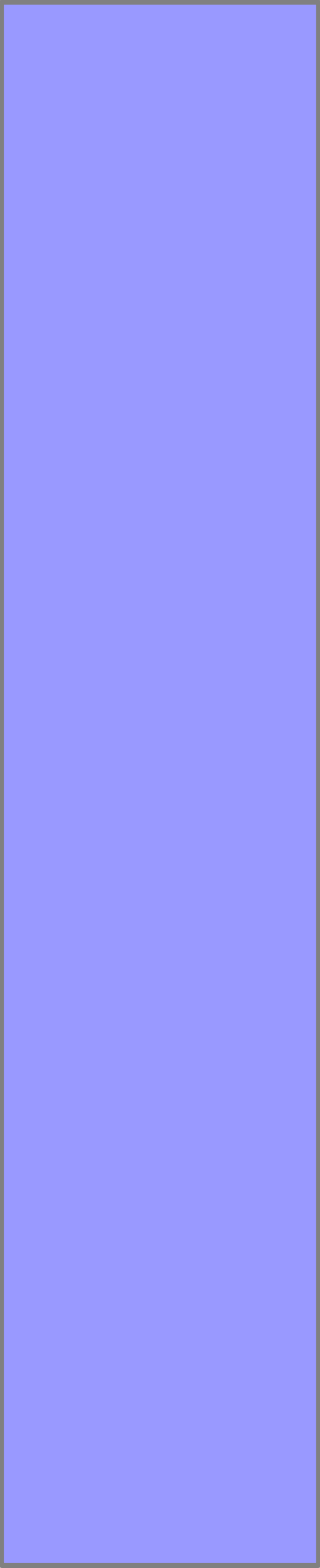
complimentary reduction of an electron acceptor compound.

For example, aerobic oxidation can be represented as:



Here, carbon (C^0) is oxidized to C^{4+} by transferring 4e^- to oxygen, which is reduced. Often it is necessary for complex organics to be fermented to create smaller carbon compounds, which may also be activated through the ultimate insertion of a carboxyl group (Gaudy and Gaudy, 1988). In some cases, a single bacterial strain is capable of accomplishing both fermentation and respiratory oxidation. However, many complex interspecies relationships occur between bacterial groups; one or more groups may accomplish fermentation while oxidation is done by others. Energy can be released as a result of some fermentation reactions; however, in many cases, a required fermentation step results in a loss of ATP energy. Respiratory oxidation, through the TCA cycle, usually results in the conservation of ATP forming energy.

In addition to oxygen, indigenous soil bacteria have the ability to oxidize organics using other electron acceptors.



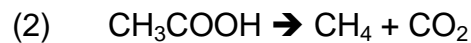
Alternative electron acceptors include nitrate (NO_3^-), manganese (Mn^{4+}), sulfate (SO_4^{2-}), and iron (Fe^{3+}) (Barbaro et al., 1992; Beller et al., 1992; Lovley and Phillips, 1986 and 1987; Lovley, 1990; and Hutchins et al. 1991 and 1992).

Electron acceptors are often limited in the subsurface. If a sufficiently large hydrocarbon spill occurs, carbon mass may greatly exceed electron acceptor supply and a redox series may develop as certain electron acceptor types are preferentially used (Berner, 1980; Norris et al., 1994; and Stumm and Morgan, 1996). Common convention holds that the order of utilization is $\text{O}_2 > \text{NO}_3^- > \text{Mn}^{4+} > \text{Fe}^{3+} > \text{SO}_4^{2-} >$ methanogenesis. Overall, this represents a redox change (pE) ranging from approximately +15 to -10. However, as discussed below, and observed in this research, mineral Fe^{3+} reduction may occur over a wide redox range through methanogenesis.

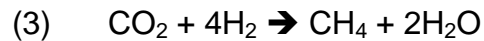
For complete mineralization, an organic is oxidized to CO_2 . In this case, organic removal is stoichiometrically balanced against a given mass of electron acceptor. A certain fraction of organic, however, may be biotransformed to intermediate organic products that are not fully oxidized. Additionally, some substrate can be converted to biomass

through anabolic processes with little or no oxidation. Therefore, the observed organic consumption is usually greater than that predicted from mass of electron acceptor consumed based on stoichiometry.

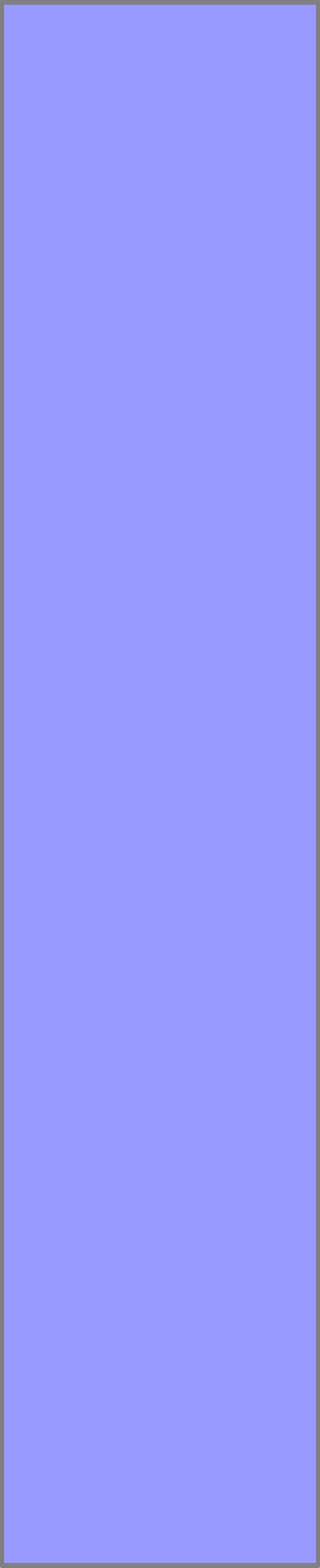
Given the exceptions above, reactions involving O_2 , NO_3^- , Mn^{4+} , Fe^{3+} , and SO_4^{2-} are often written in terms of redox processes involving an organic balanced with a specified mass of inorganic electron acceptors. However, this is not true with respect to methanogenesis. Acetoclastic methanogenesis involves the simultaneous oxidation and reduction of the organic compound (acetate) as:



Chemoautotrophic bacteria can also generate methane as:



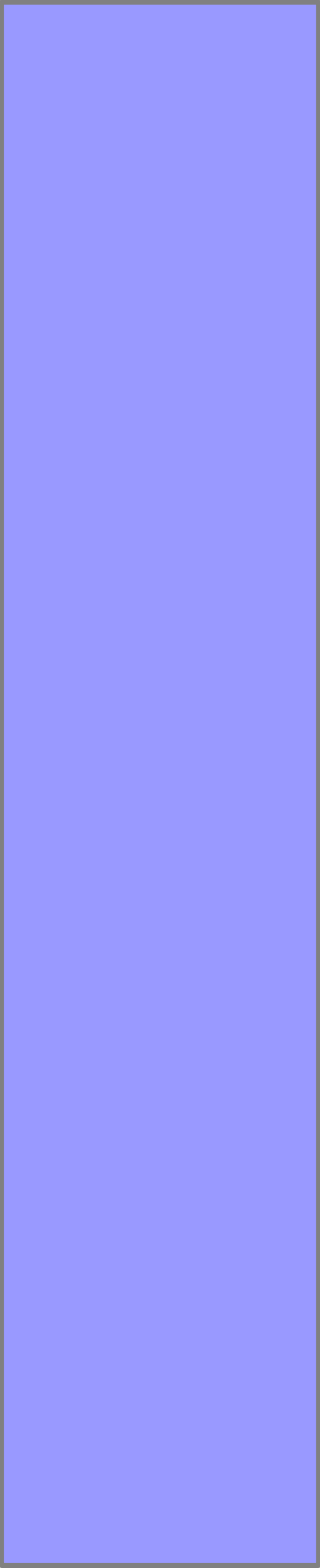
In Equation 2, the electron donor and acceptor is the organic substrate. For Equation 3, the reactants are both inorganic, CO_2 and H_2 gas, so an organic substrate is not directly oxidized. H_2 can, however, be generated through



organic substrate fermentation. In general, methanogenesis occurs in the relative absence of inorganic electron acceptors.

The electron acceptor redox succession is believed to be thermodynamically related (Berner, 1980 and Stumm and Morgan, 1996). The amount of free energy (ΔG) that can be generated for each of these oxidation/reduction reactions decreases for each successive electron acceptor couple. The bacterial type capable of deriving the most energy per unit organic oxidized/electron acceptor reduced has a natural advantage over other types and may dominate the local environment (McCarty, 1971). When an electron donor is in abundance, a lower energy yielding electron acceptor is utilized only if the electron acceptors of higher energy levels have been substantially depleted. This situation infers the secession of microbial species with changing redox conditions.

Numerous examples of redox zone development associated with hydrocarbon fuel spills are reported by Wiedemeier et al. (1999). Successively lower redox zones are thought to develop concentrically towards the center of the organic plume. Oxygen is depleted around the outer



edge of a plume followed by NO_3^- , $\sim\text{Fe}^{3+}$, and SO_4^{2-} consumption. In the center of the plume, methanogenic processes may dominate. However, as discussed below, this conceptualized view of redox zone distribution is perturbed because iron reduction may occur before sulfate reduction and/or concurrent with methanogenesis.

2.3. Electron Acceptor Occurrence In the Subsurface

Given favorable subsurface conditions, an excess of labile organic substrate, and reasonable reaction rates, the oxidative potential for each electron acceptor type is ultimately dependent upon its abundance. Though each aquifer is unique, certain generalities can be made concerning the natural electron acceptor mass, which are discussed in this section along with the development or origin of oxidized species.

2.3.1. Oxygen

The equilibrium concentration of oxygen in pure water is a function of the concentration in the surrounding atmosphere, as described by Henry's Law:

$$(4) \quad N_g = N_w * \frac{P_g}{H} * (1 - \frac{P_g}{H})^{-1}$$

Where:

N_g = Moles gas in solution at equilibrium

N_w = Moles of water per liter

H = Henry's law constant for gas (atm/mole fraction)

P_g = Percent gas (oxygen) at prevailing condition

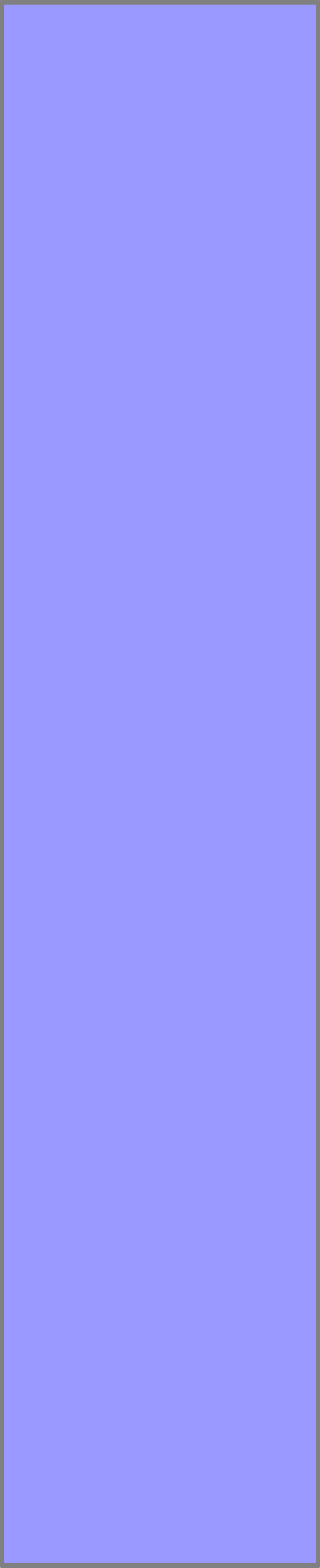
Using Equation 4 the dissolved oxygen content for surface water is calculated to be 9.76 mg/L assuming 20 C°, 1 atm, $N_w = 55.6$ moles/L, and $H = 4.01 \times 10^4$ atm/mole given an atmospheric O₂ concentration of 22%. The oxygen concentration in the vadose zone soil gas is, however, much lower. Soil oxygen content is depleted by aerobic bacteria and plant root respiration. Additionally, air exchange with the soil is greatly inhibited both by the solid matrix and soil water content. Under dry conditions there is limited gas exchange between the soil and atmosphere through soil macropores (fissures and cracks) and micropores (intergranular porosity). With increasing moisture, first micropores then macropores become blocked with water

and oxygen exchange becomes increasingly restricted. Consequently, concentrations of oxygen in shallow vadose zone soil (<120 cm) typically range from 15% when dry to 5% when wet (Brady, 1990).

Under typical soil conditions, non-contaminated groundwater would be expected to have between 6.6 mg/L to as little as 2.2 mg/l dissolved O₂. Obviously, even lower concentrations of oxygen can occur with increasing depth, soil moisture, and soil organic content. This range is consistent with the average 5.0 mg/L background O₂ found at several fuel-contaminated sites by Wiedemeier et al. (1999).

2.3.2. Nitrate

Nitrate salts are extremely soluble in water (e.g. 1.8 g/cm³ water for NH₄NO₃ (Weast et al., 1987)), so that the solubility limit is unlikely to be exceeded in groundwater; however, concentrations of NO₃⁻ are typically low. The drinking water standard is 10 mg/L (NO₃⁻) which is usually not exceeded in normal groundwater, though higher concentrations can be found, especially in agricultural regions where nitrogen based fertilizers are applied. There are no common mineral sources of NO₃⁻. Small amounts of



nitrogen oxides come by combustion of fossil fuels and oxidation of atmospheric nitrogen from lightning; however, naturally occurring nitrate is predominantly generated by microbial processes (nitrogen fixation and nitrification) (Pierzynski et al., 1994). Wiedemeier et al. (1999) found average NO_3^- concentrations of 23 mg/L for non-hydrocarbon fuel contaminated water at several air force bases.

2.3.3. Iron

Iron is the fourth most abundant element in the earth's crust and, in the broadest sense, all sediments are likely to be iron bearing (Pettijohn, 1975). As discussed further below, Fe is largely insoluble in water at normal pH and exists, for all practical purposes, as a solid mineral phase. Iron mineral content may exceed 80% in biogenically produced iron ore sediments. In more typical sediments, iron minerals average 4.56% in graywacke (feldspar rich) sand, 0.34% in quartz arenites, and 6% in shale sediments (Pettijohn, 1975). Based on this research and the authors' experience, Fe^{3+} in sandy sediments is generally in the range of 1%. As discussed below, only a fraction of this

(conservatively 0.01% or approximately 300 mg/Kg) is available for immediate bacterial reduction.

Simple iron minerals (hydroxides, oxides, sulfides, etc.) in shallow sedimentary rock are of greatest interest to natural attenuation. Originally, these simple iron minerals were formed from the weathering and diagenesis of primary (parent) Fe-bearing igneous/metamorphic minerals, the more common of which include hematite, ilmenite, and Fe-bearing silicates including amphiboles, pyroxenes, olivine, and biotite (Chesterman and Lowe, 1987).

There are numerous common Fe^{2+} and Fe^{3+} sedimentary minerals, as shown in Table 2.1. More than one species can be present in the same sediment, depending on sedimentary and post depositional (diagenetic) conditions. Although these minerals can exist as crystalline or amorphous particles, the oxides are often present as coatings on silicates. Simple Fe^{3+} rusts are more rare because they are unstable and tend to develop into more crystalline forms, such as hematite or goethite over time under geologic conditions (Huang and Schnitzer, 1987). The occurrence of Fe^{3+} minerals is probably greatest in

Table 2.1

shallow sediments where the concentration of oxygen is highest.

Oxidized Fe^{3+} can be incorporated during sedimentation or develop authigenically (formed in place after deposition) by the precipitation of dissolved Fe in groundwater. Iron cycling is relatively straightforward. Under alkaline to neutral conditions, Fe^{2+} is inherently unstable in the presence of O_2 and is oxidized spontaneously to Fe^{3+} . Microorganisms may have little chance to extract energy from the oxidation process. Under acidic conditions, spontaneous Fe^{2+} oxidation is greatly retarded and it is then used as the foundation for energy generation by chemolithotrophic acidophilic bacteria (Atlas and Bartha, 1993).

2.3.4. Sulfate

SO_4^{2-} can be generated by both biotic and abiotic means. Sources for reduced forms of S include elemental sulfur (S^0), hydrogen sulfide (H_2S), polysulfides, and various metal sulfides of which the iron sulfides shown in Table 2.1 are the most common. A combination of autoxidation and microbial sulfur oxidation of iron sulfide minerals produces

large amounts of acidic water or acid mine drainage (Evangelou and Zhang, 1995; and Fortin et al., 1994). At a neutral pH, oxidation by atmospheric oxygen occurs spontaneously and quite rapidly, but below pH 4.5, autoxidation slows drastically and acidophilic bacteria are responsible for continued oxidation. Reduced S forms are also oxidized by many bacterial species at the normal pH ranges typically found in groundwater (Atlas, 1993). Reduced S can also oxidize abiotically to SO_4^{2-} by the reduction of NO_3^- and possibly by Fe^{3+} (Postma et al., 1991; and Jorgensen, 1990).

Table 2.2

Sulfate occurs in certain igneous-rock minerals of the feldspathoid group, but the most extensive and important occurrences are in evaporite sediments (Hem, 1985). As shown in Table 2.2, there are thirteen common minerals containing SO_4^{2-} found in evaporitic deposits that can be sources for dissolved SO_4^{2-} in groundwater (Hardie, 1991). Of these, gypsum ($\text{CaSO}_4 \cdot 2\text{H}_2\text{O}$) and anhydrite (CaSO_4) are very common in some areas, where evaporite deposits can be hundreds of feet thick. As a practical matter, because gypsum and anhydrite are highly soluble, groundwater is rarely saturated with them unless mineral forms are present

in quantity. The concentration of SO_4^{2-} in groundwater is dictated by mass action principally controlled by Ca. In pure water, the total solubility for gypsum can be calculated by summing the amount of the mineral present in both ionic and complexed form. The solubility product for gypsum is:

$$(5) \quad (\gamma_{\text{Ca}^{2+}} * m_{\text{Ca}^{2+}}) * (\gamma_{\text{SO}_4} * m_{\text{SO}_4}) = 10^{-4.6}$$

and the stability constant for complexed gypsum is:

$$(6) \quad \frac{[\text{CaSO}_4^0]}{[\text{Ca}][\text{SO}_4]} = 10^{2.31}$$

For low ionic strength solutions, Equations 5 and 6 would yield SO_4^{2-} concentrations of approximately 1,400 mg/L at equilibrium (Hem, 1985). Increased Ca^{2+} content will reduce SO_4^{2-} concentrations, and accordingly, carbonate-type groundwater in gypsiferous aquifers actually contain lower SO_4^{2-} concentrations, often only several hundred mg/L. Conversely, up to 299,000 mg/L SO_4^{2-} has been measured in some unusual Ca^{2+} deficient brines (Hem, 1985). High SO_4^{2-} concentrations, however, make groundwater of poor quality and limited use. The SO_4^{2-} content in a good quality aquifer is usually much lower than the solubility limit. An average of 39 mg/L SO_4^{2-} was found by Wiedemeier et al.

(1999) in nonfuel contaminated groundwater from several U.S. Air Force bases.

2.3.5. Comparison of Electron Acceptor Abundance by Type

It is instructive to compare the amount of organic that could potentially be oxidized for each electron acceptor type in an aquifer with typical electron acceptor properties. To complete this analysis, a hypothetical aquifer is assumed to have 30% liquid filled porosity (300 L/m³) and have a bulk density of 1,876 Kg/m³. Electron acceptors are assigned concentrations based on the discussion above, as shown on Table 2.3. The following half reactions are observed:

Table 2.3

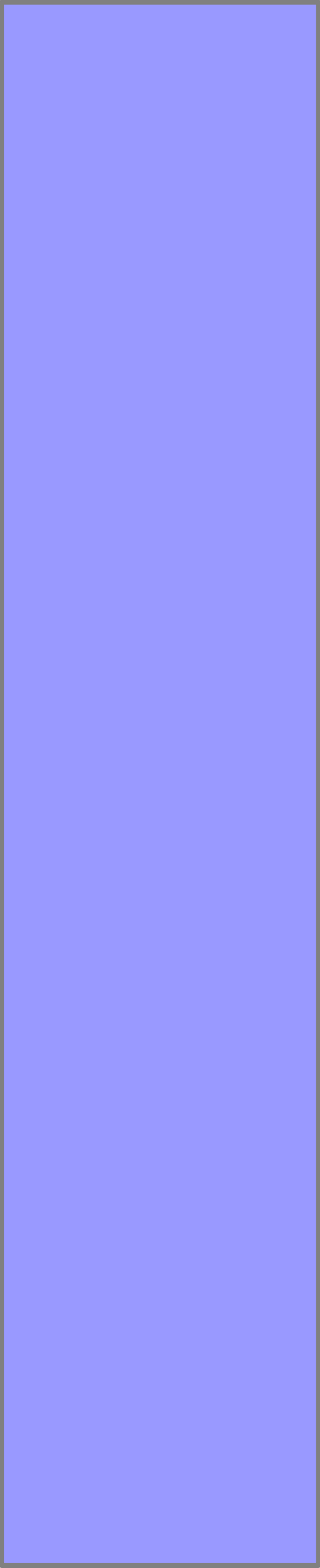
- (7) Oxygen $O_2 + 4H^+ + 4e^- \rightarrow 2H_2O$
- (8) Nitrate $NO_3^- + 6H^+ + 5e^- \rightarrow \frac{1}{2}N_2 + 3H_2O$
- (9) Sulfate $SO_4^{2-} + 10H^+ + 8e^- \rightarrow H_2S + 4H_2O$
- (10) Iron $Fe^{3+} + e^- \rightarrow Fe^{2+}$

Table 2.3 shows the calculated electron equivalent mass that could be accepted by each type. As shown, electron acceptance potential is lowest for O₂ and NO₃⁻ but becomes higher for SO₄²⁻ and Fe³⁺, respectively.

As discussed above, values for SO_4^{2-} and Fe^{3+} can be quite variable. Although concentrations can be lower than those used here they are often much higher. O_2 and NO_3^- concentrations, however, will usually not vary much from those used. This simple comparison illustrates that the amount of organic that could potentially be degraded by SO_4^{2-} and Fe^{3+} reduction may be much greater than the amount possible by O_2 or NO_3^- . It suggests that SO_4^{2-} and Fe^{3+} reduction processes may play a very significant role in the biodegradation of organic contaminants.

2.4. Iron Microbial Geochemical Processes

Fe^{3+} is functionally insoluble in the near neutral pH conditions usually found in groundwater. For example, Whitemore and Langmuir (1975) found groundwater in equilibrium with Fe-oxyhydroxides to have log iron activity products (IAP) ranging from -36 to -43 . Usually, little dissolved Fe^{3+} is found, although considerable solid phase Fe^{3+} may be present for bacterial use. Iron mineral forms, in ascending order of crystallinity (decreasing lattice disorder and specific surface area) include ferrihydrite rust ($\text{Fe}(\text{OH})_3$), lepidocrocite and akageneite (γ - & β - FeOOH), goethite (α - FeOOH), and hematite α -(Fe_2O_3) (Heron et al., 1994^a).



As discussed above, sediments and sedimentary rocks commonly contain about 1% by weight Fe minerals or 10,000 mg/Kg. Assuming this iron is Fe^{3+} and extending the mass calculations developed in the preceding section, this quantity of iron would equate to approximately 336,000 mMol/m^3 electron acceptance capacity. Assuming chemical redox balance, this mass of Fe^{3+} would be sufficient to oxidize 9,333- mMol/m^3 toluene or approximately 1 L toluene/ m^3 . With such great oxidizing potential, it is apparent that 1) only a fraction of the total Fe^{3+} is ordinarily utilized and/or 2) the kinetic rate for Fe^{3+} utilization is slow. It is, however, generally observed that only a portion of the total iron present in a given subsurface system, the *biologically available Fe^{3+}* fraction, is susceptible to direct enzymatic reduction at any one time.

The ability of bacteria to enzymatically reduce Fe^{3+} is dependent on many factors including:

- Variations in free energy for various iron forms.
- Available or reactive Fe^{3+} mineral specific surface area; and
- Reaction time or kinetics.

Based on free energy calculations, dissolved or chelated iron is thought to be more biologically reactive than solid forms Ehrlich (1996). Additionally, there is a tendency for decreasing thermodynamic (ΔG) energy available for the bacterium with increasing Fe^{3+} mineral crystallinity. Figure 2.1 shows the free energy calculations for a generalized organic (CH_2O) at standard conditions assuming reduction of various electron acceptors including several common Fe^{3+} mineral forms (modified after Lyon, 1995). Recall that a negative ΔG value indicates an exothermic (energy releasing) reaction favorable for the formation of microbial ATP. As discussed above, the order of diminishing thermodynamic benefit is O_2 then NO_3^- (-479.8 and -449.8 kJ/Mole CH_2O respectively). The energy yield for dissolved Fe^{3+} is quite high (-302.5 kJ/Mole CH_2O); however, Fe^{3+} is poorly soluble and usually does not exist in large amounts at normal pH ranges in an aquifer. Organic oxidation coupled with sulfate reduction or methanogenesis would produce -79.5 and -70.8 kJ/Mole CH_2O , respectively. Reactions involving solid Fe are thermodynamically poor compared to other redox reactions and have decreasing energy benefits with respect to increasing crystalline structure. These

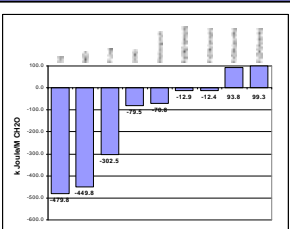
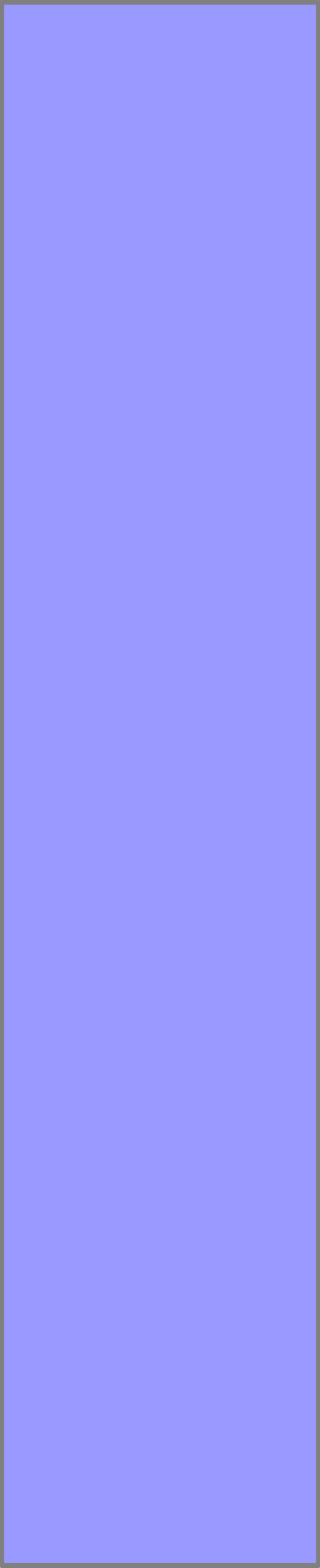
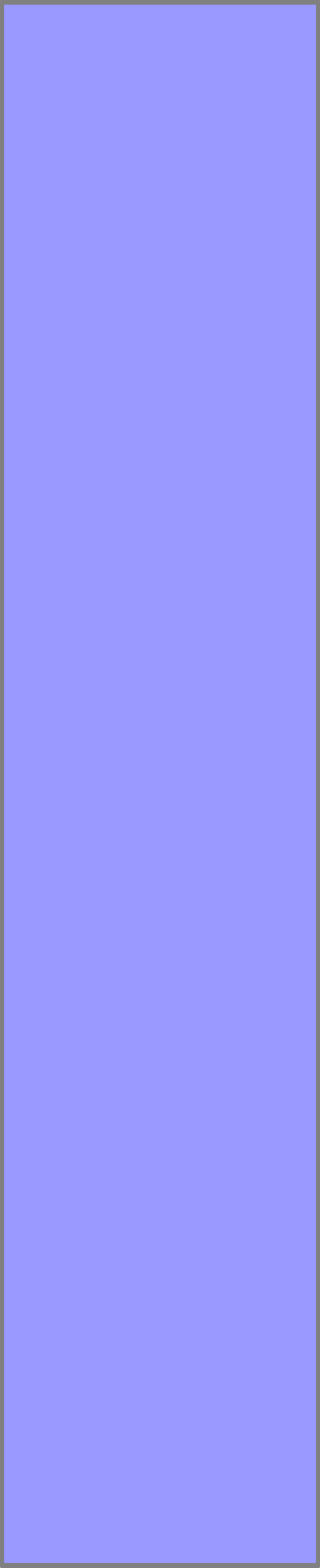


Figure 2.1



reactions range from -12.9 kJ/Mole CH_2O for amorphous $\text{Fe}(\text{OH})_3$ to +99.3 kJ/Mole CH_2O for Fe_2O_3 . Note that Berner (1980) reported -114 kJ/Mole CH_2O for $\text{Fe}(\text{OH})_3$ so there appears to be some controversy, presumably regarding thermodynamic constants at standard conditions. In any case, based on thermodynamic evidence, it appears that Fe^{3+} reduction could theoretically occur across a wide redox range, beginning after NO_3^- and extending beyond methanogenesis.

Munch and Ottow (1980 and 1983) observed decreasing bacterial Fe^{3+} utilization with increasing mineral crystalline structure and observed that direct, physical contact with the mineral was necessary. In general, there is a relationship between increasing specific surface area and decreasing Fe mineral crystalline structure. Taking these facts together, it is not surprising that Roden and Zachara (1996) found a relationship between increased Fe^{3+} mineral specific surface area and increased microbial utilization. The requirement for intimate microbial contact further suggests that only the outer layer or surface portion of the total Fe^{3+} mineral mass, to which the bacteria have access, can be immediately utilized.



The kinetics of microbial Fe^{3+} reduction are discussed in more detail below; however, evidence of active Fe^{3+} reduction has been found at contaminated sites that are many years or even decades old (Wiedemeier, 1999). This suggests that the rate of Fe^{3+} mineral utilization is slow and/or much time is required for bacteria to enzymatically attack more recalcitrant iron forms.

Based on thermodynamic estimates and specific surface area it appears that crystalline Fe^{3+} minerals are resistive to microbial reduction. Indeed, according to free energy calculations, at standard conditions, bacteria should not be able to reduce goethite and hematite at all. However, evidence of microbial reduction of these crystalline forms has been observed in many laboratory studies (Lovley, 1987). Further, direct evidence of crystalline Fe^{3+} microbial attack has been observed in the field both by the author and by others (Heron and Christensen, 1995 and Hiebert and Bennett, 1992). For example, scanning electron microscopy was performed on sediment samples taken from the gasoline fuel contaminated site (Kennedy et al., 1998). These images show complete removal of the hematite coating on some quartz sand grains in the contaminated

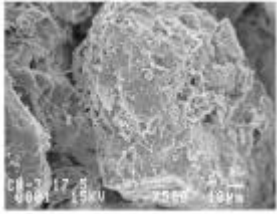


Figure 2.2

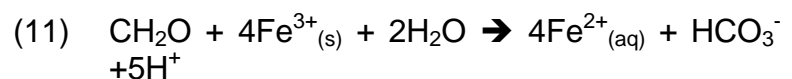
portion of the plume compared to grains taken from the non-contaminated portion of the study area (Figure 2.2).

It has been suggested that not all Fe^{3+} reducing bacteria gain energy in the process. For instance, Ghiorse (1988) and Lovley (1991) propose that a number of bacteria reduce ferric iron merely to dispose of excess reducing power via secondary respiratory pathways without generating energy, or that the iron reduction that was observed for these organisms was part of their iron assimilation process. Additionally, energy might be obtained during the reduction of mineral Fe^{3+} should the reaction be coupled with other respiratory or fermentative processes needed to meet the full energy demand (Ehrlich, 1996).

Finally, it is also possible that recalcitrant Fe^{3+} might be solubilized via chelation to an aqueous form with thermodynamically favorable properties. Fe solubility can be strongly controlled by chelation increasing stable aqueous concentrations to very high levels. Hematite dissolution in the presence of protons only is very slow; however, the dissolution process is accelerated many times in the presence of organic ligands like oxalate. Chelating agents can be directly produced by bacterium. Organic chelating

compounds could also be formed during petroleum hydrocarbon fermentation. Organic acids (e.g. keto- and hydroxy-acid anions) formed through microbial fermentation of hydrocarbons are thought to be responsible for increased mineral solubility and reaction kinetics found at the crude oil spill site examined by Bennett (1991) and Hiebert and Bennett (1992). Although recalcitrant crystalline Fe^{3+} minerals are still resistive to solubilization via chelation, this process provides a mechanism for microbial energy conservation via indirect enzymatic reduction, even for stubborn forms.

Due to mass action constraints, evidence of Fe^{3+} reduction is poorly represented by aqueous analyses alone. Direct enzymatic reduction of Fe^{3+} minerals may produce a certain amount of dissolved Fe^{2+} as:



There is, however, a strong tendency for produced Fe^{2+} to precipitate as several mineral forms, e.g., reacting with:

- Sulfides to form iron sulfides (FeS or FeS_2);
- Carbonate to form siderite (FeCO_3);

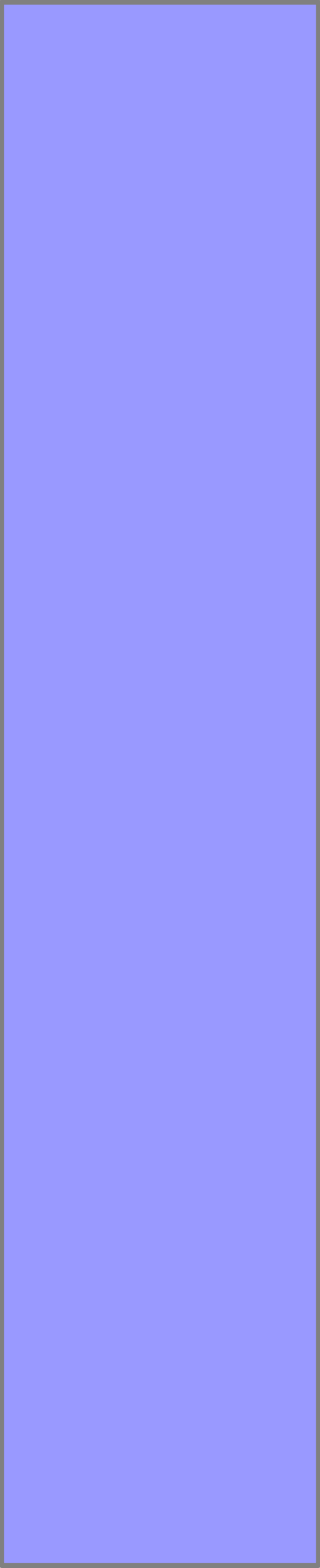
- Other Fe oxides/hydroxides to form magnetite (Fe_3O_4);
- Phosphates to create vivianite ($\text{Fe}_3(\text{PO}_4)_2 \cdot 8\text{H}_2\text{O}$); and others.

These biogenic minerals have been observed in field and laboratory studies where Fe^{3+} reduction occurred (Lovley et al., 1993; Baedecker et al., 1992; and Postma, 1981 and 1982). Geochemical equilibrium conditions constrain both the oxidized and reduced states of Fe to a mineral form. As a result, aqueous Fe (usually Fe^{2+}) may indicate that Fe^{3+} reduction is occurring, but is probably a poor indicator of microbially available Fe^{3+} and also inadequately measures the magnitude of reductive microbial activity represented by produced Fe^{2+} . This observation suggests that solid mineral analysis is a necessity in intrinsic bioremediation studies where Fe^{3+} reduction is suspected.

As discussed previously, based on thermodynamics, the generally accepted redox sequence is $\text{O}_2 > \text{NO}_3^- > \text{Fe}^{3+} > \text{SO}_4^{2-} > \text{methanogenesis}$. It is observed that SO_4^{2-} reduction often occurs in the presence of mineral Fe^{3+} (Lovely et al., 1991). SO_4^{2-} reduction may occur largely to the exclusion of, or possibly concurrent with, enzymatic Fe^{3+}

mineral reduction. It could also be assumed that the bioavailable Fe^{3+} fraction was consumed thereby allowing SO_4^{2-} reduction in the presence of residual, biologically recalcitrant Fe^{3+} . Other explanations are also possible, singularly or in combination.

One potential explanation for SO_4^{2-} reduction in the presence of Fe^{3+} is based on thermodynamics. The electron acceptor utilization sequence is typically calculated using a ΔG° based on aqueous Fe^{3+} . This results in a computed heat of reaction for Fe^{3+} that is greater than that of SO_4^{2-} . However, as pointed out by Ehrlich (1996) and Lyon (1995), the heat of formation (ΔG°) values for solid iron are high, resulting in thermodynamic calculations where SO_4^{2-} reduction is more energetic than that of Fe^{3+} . Further, thermodynamic benefits decrease with increasing crystallinity. This infers that Fe^{3+} reduction could happen over a wide redox range with some occurring before, during, or possibly after SO_4^{2-} reduction, depending on Fe^{3+} mineral species. In this case, biologically available Fe^{3+} is present as different mineral species that are consumed across a wide redox range due to variations in ΔG° potential.

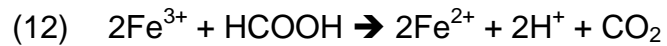


A second rationale for SO_4^{2-} reduction in the presence of Fe^{3+} is based on kinetic limitations. Fe^{3+} reducing organisms may slowly reduce crystalline Fe^{3+} forms, such as goethite and hematite, in systems that are otherwise dominated by sulfate reduction or even methanogenesis, as proposed by Lovley (1987). In this case, bioavailable Fe^{3+} is present but slowly used, permitting competitive SO_4^{2-} consumption, more or less independent of thermodynamic constraints.

Finally, Fe^{3+} and SO_4^{2-} reduction may occur simultaneously due to physical aquifer properties. Because Fe^{3+} is a solid, unlike the other electron acceptors, its distribution is fixed in the aquifer matrix. This inhibits mixing and may favor the creation of microenvironments where direct enzymatic Fe^{3+} and SO_4^{2-} reduction occur in close proximity, as suggested by Canfield (1988).

Nonenzymatic reduction of Fe^{3+} can occur. Fe^{3+} oxide minerals are stable in the absence of oxygen but reduce in the presence of a strong reducing agent. As discussed in detail below, HS^- produced by sulfate reducing bacteria can reduce Fe^{3+} . According to Ghiorse (1988), certain microbial organic metabolites can also act as a

reductant for Fe³⁺ including formate (formic acid), which is produced by a number of bacteria. Reduction of Fe³⁺ by formic acid can be represented as:



Fe³⁺ reduction, from reactions like Equation 12, are not the result of direct enzymatic processes, but may be considered an indirect form of organic oxidation via Fe³⁺ reduction. This type of reaction is favored by acid pH.

Based on the above discussion, sediment iron should be subdivided and classified for practical discussion. Such classifications are admittedly imprecise and the resulting terms tend to be operationally defined. Typical sediments may contain several percent mineral iron. For practical purposes, this bulk iron can be measured using an aggressive extraction with a strong acid solution (SAS) as described below, though other methods can be used that may result in higher or lower iron recovery. A fraction of the SAS Fe³⁺, the *Bioavailable Iron*, can potentially be easily used by bacteria under proper redox conditions with a labile substrate. Again, as described fully below, bioavailable iron is normally estimated by sediment extraction with a weak acid solution (WAS). Though an exhaustive survey has not

been performed, bioavailable or WAS Fe^{3+} comprised about 5 to 10% of the WAS Fe^{3+} in some shallow sediment samples (Kennedy et al., 1999). Bioavailable iron tends to have high surface area, low ΔG , and be located on the exterior sediment grains. “*Biogenic Fe^{2+}* ” is the amount of Fe^{2+} produced as a direct result of enzymatic Fe^{3+} reduction. This can also be estimated by weak acid extraction, though some of the produced Fe^{2+} mineral forms may be resistant or recalcitrant to acids. The Fe^{3+} remaining after bioavailable iron is used is defined here as “*Iron Reserve*”. This iron may be used as an electron acceptor but probably at a slower rate. Thus, Bulk Fe^{3+} is the total of Bioavailable iron + Iron Reserve.

An experiment was conducted by Kennedy and Everett (2000) examining aqueous, gas, and mineral interaction for iron and sulfate reducing systems using a mixture of labile fatty acids (C2 through C6) as a substrate in native sediments. $\text{Fe}(\text{OH})_3$ was added to one system to encourage Fe^{3+} reduction. Fe^{2+} was measured in both the sediment and in aqueous phase using the techniques described below. At the end of 12 weeks of monitoring, 1,120 mg/Kg mineral Fe^{2+} had been produced (Figure 2.3).

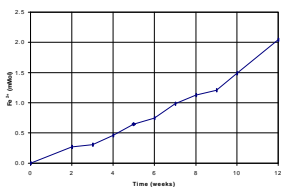


Figure 2.3

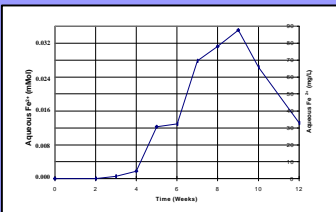


Figure 2.4

If the mineral Fe^{2+} were in solution, the equivalent concentration would be approximately 2,536 mg/L. Note also that each successive monitoring event showed consistent increases in the concentration of mineral Fe^{2+} . Figure 2.3 should be contrasted with Figure 2.4 showing the measured dissolved phase Fe^{2+} during the experiment. Dissolved Fe^{2+} concentrations did not show a consistent increase. Rather, concentrations increased then decreased over the course of the experiment as mineral species were formed, taking dissolved Fe^{2+} out of solution. The maximum recorded concentration of aqueous Fe^{2+} was 88 mg/L. That value is quite high for groundwater but it only represented 2.5% of the mineral Fe^{2+} . Furthermore, the ratio of dissolved Fe^{2+} to mineral decreased to 0.6% at the end of the experiment as progressively more aqueous Fe^{2+} precipitated to mineral form. This experiment demonstrates the tendency for Fe^{2+} minerals to be formed following Fe^{3+} reduction and the inability of aqueous analyses to monitor iron expressed capacity.

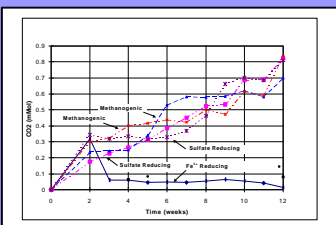


Figure 2.5

Figure 2.5 shows produced CO_2 from the same microcosm study. The rate of CO_2 production for the Fe^{3+} reducing system is compared to that of both SO_4^{2-} and

methanogenic systems. All systems had similar rates of organic removal and should produce equivalent amounts of CO_2 . Interestingly, the quantity of measured CO_2 in the Fe^{3+} reducing system was virtually nonexistent as CO_2 was consumed to form siderite (FeCO_3). Equation 12, shows two moles of Fe^{2+} is formed per mole of carbon oxidized or carbon dioxide produced. Thus, excess Fe^{2+} is produced relative to CO_2 and carbonate concentrations may decrease in Fe^{3+} reducing areas in contrast to all other redox zones.

Iron reduction experiments were also conducted with native sediment iron from river alluvium and a loosely consolidated sandstone. Figure 2.6 shows Fe^{3+} utilization in these sediments to be first order at about 0.1 week^{-1} . The rate of iron utilization may vary with sediment and contaminant type but the kinetic model is expected to remain first order.

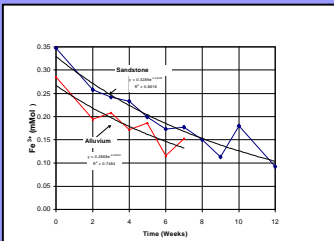


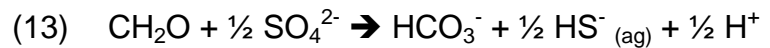
Figure 2.6

2.5. Sulfur Microbial Geochemical Processes

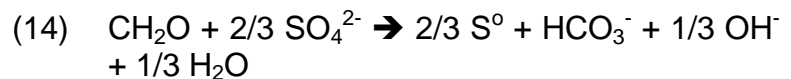
In many ways, microbial geochemical processes for S are considerably more complex than for Fe. Though not discussed in detail here, numerous oxidative states are possible for S species, ranging from 2^- to 8^+ and many complex intermediates (including thiosulfate and

polysulfides) are formed during cycling (Jorgensen, 1990). For simplification, this discussion is directed towards major S processes and end member species that are important with respect to natural attenuation.

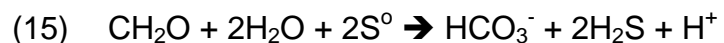
A general equation for sulfate reduction can be written as:



Equation 13 assumes complete reduction of SO_4^{2-} ; however, only partial reduction to an intermediate oxidation state may occur to form S^0 , for example as:

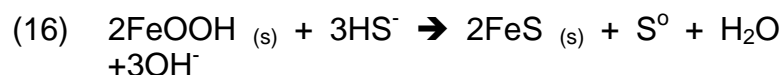


Additionally, S^0 can be used directly as an electron acceptor for the enzymatic oxidation of organic material as:

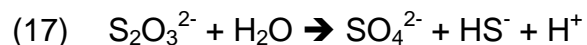


As part of a natural attenuation study, the detection of aqueous HS^- as a quantitative indicator of SO_4^{2-} reduction

is usually not feasible. This is due in part because Fe^{3+} minerals are a chemical sink for HS^- , reducing aqueous concentrations as (Appello and Postma, 1994):



Here, Fe^{3+} is reduced abiotically to Fe^{2+} with the simultaneous oxidation of S^{2-} to S^0 . This reaction demonstrates partial S cycling because 1/3 of the reduced HS^- is oxidized to S^0 that could be reused as an electron acceptor by heterotrophic bacteria. In tests performed by Pyzik and Sommer (1981), S^0 accounted for 86% of the oxidized product from Equation 16 with thiosulfate ($\text{S}_2\text{O}_3^{2-}$) comprising the balance. Jorgensen (1990) found that thiosulfate was used as an electron acceptor by heterotrophic bacteria and converted back to HS^- ; however, there is a potential disproportionation to form SO_4^{2-} and HS^- as:



As is apparent from Equation 17, the formation of thiosulfate could ultimately cycle SO_4^{2-} . Jorgensen (1990)

also suggests that thiosulfate could fully oxidize by reaction with Fe^{3+} minerals, however the degree to which this occurs is unknown.

Equation 16 represents non-enzymatic reduction of Fe^{3+} by HS^- during SO_4^{2-} reduction, which is well-documented (Lovely et al., 1991). Precipitated iron monosulfide mineral forms include amorphous iron sulfide, mackinawite ($\text{Fe}_{0.995 - 1.023}\text{S}$), greigite (Fe_3S_4), and pyrrhotite ($\text{FeS}_{1.1}$). These minerals are also known as acid volatile sulfides (AVS) because, in contrast with pyrite (FeS_2) and S^0 , they readily dissolve in hydrochloric acid.

The rate of AVS formation is rapid and has been described by Pyzik and Sommer (1981) as:

$$(18) \quad d(\text{FeS})/dt = k S_t(\text{H}^+)A_{\text{FeOOH}}$$

Where:

$d(\text{FeS})/dt$ = rate of AVS formation

k = rate constant $82 \pm 18 \text{ (L}^2/(\text{m}^2 \cdot \text{min})$

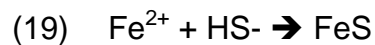
S_t = Molar sulfide concentration
(mol/L)

H^+ = Hydrogen ion activity

A_{FeOOH} = Surface area of goethite (m^2/L)

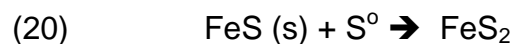
FeS formation is largely controlled by available Fe³⁺ mineral specific surface area. Initially high FeS formation is due to large unreduced Fe³⁺ surface area. According to Pyzik and Sommer (1981), successive AVS formation proceeds only after the surface Fe³⁺ mineral layer dissolves to expose additional surface area.

It is possible to form AVS by direct reaction with Fe²⁺ as:



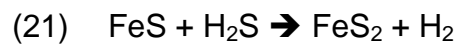
This reaction does not involve oxidation/reduction. Therefore, Fe³⁺ is not reduced and S⁰ is not formed.

Even under sulfidic conditions, AVS is a transient form in many environments. Monosulfides combine with elemental sulfur to form pyrite (Appello and Postma,1994) according to:



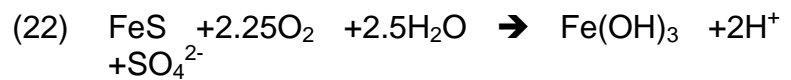
This second step involves the simultaneous oxidation and reduction of S so that S²⁻ and S⁰ produce 2S⁻. This reaction occurs spontaneously and abiotically. Therefore,

there is potential competition for S^0 which could be used either as an electron acceptor by bacteria or chemically bound as FeS_2 . It should also be noted that the direct formation of FeS_2 by H_2S was reported by Drobner et al. (1990) as:

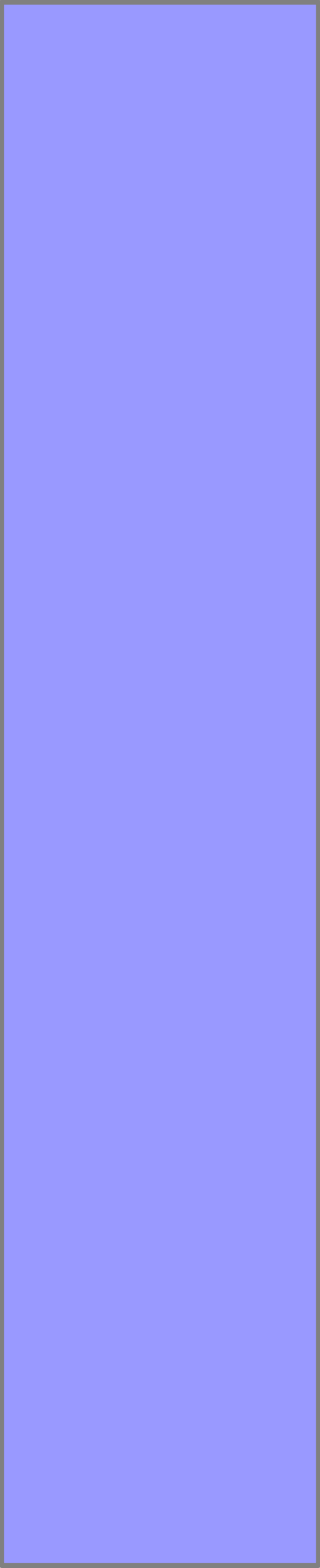


Most research and literature references for FeS_2 formation assume the reaction expressed in Equation 21. Drobner et al., (1990) used an incubation temperature of 100 °C to produce FeS_2 by direct H_2S reaction, so the importance of this reaction is unclear at typical aquifer temperatures. The reaction expressed in Equation 22 could be an important source of H_2 for chemolithotrophic bacteria in the deep subsurface.

In the presence of oxygen, AVS can be oxidized as:



This reaction may be microbially mediated, as in the case of acid mine drainage (Tuttle et al. 1969 and Evangelou and Zhang, 1995). AVS is reactive, both by oxidation and by



reduction/oxidation to form FeS_2 . Therefore, it is reasonable to assume that the presence of AVS is a general indicator of recent sulfate reduction. In marine sediments, AVS is found to disappear with time (depth) as it transforms to pyrite (Appelo and Postma, 1994). Environments rich in AVS relative to FeS_2 may indicate recent or on-going biological processes.

The rapid deposition of iron sulfide minerals has been noted in many natural organic rich environments, such as marine or lake sediments (Morse et al., 1987; Howarth and Jorgensen, 1984 and Howarth, 1979). Increases in iron sulfide mineral content have been documented in aquifers contaminated with organic rich landfill leachate (Heron, 1994; and Heron et al., 1994^a, 1994^b) but much less work exists on iron sulfide mineral deposition in hydrocarbon contaminated aquifers.

Although SO_4^{2-} is usually a dissolved ion in an aquifer, the reduced product of microbial respiration (HS^-) often precipitates as an iron sulfide. In an aquifer, evidence of SO_4^{2-} reduction can be inferred by its aqueous depletion. However, the respiratory products of SO_4^{2-} reduction (HS^-)

may largely be preserved in mineral form (AVS or FeS₂), which can only be quantified by mineral analysis.

It should be clear from the discussion above that many chemical routes can be taken in the formation of iron sulfides which may involve numerous partially oxidized/reduced sulfide intermediates and full or partial cycling. However, from a practical perspective, iron sulfide formation can be adequately summarize in terms of Equations 13, 16, and 20. In summary, the oxidation of labile organic contaminants via microbial sulfate reduction produces hydrogen sulfide. Hydrogen sulfide reacts spontaneously with naturally occurring Fe³⁺ minerals to form FeS and S⁰. Next, FeS and S⁰ combine to form FeS₂. As is intuitive from this discussion, given time, concentrations of CrES in the form of FeS₂ tend to accumulate at the expense of AVS as FeS.

As was described above, experiments were conducted to examine aqueous, gas, and mineral interactions for iron and sulfate reducing systems using a mixture of labile fatty acids as a substrate (Kennedy and Everett, 2000). Two microcosm sets were constructed to examine sulfate reducing conditions by adding SO₄²⁻ to two

different types of native sediments. Sediment “A” was river alluvium with 1,100 mg/Kg Fe^{3+} and sediment “B” was a crushed, friable sandstone that contained 4,700 mg/Kg Fe^{3+} . The test was conducted only over a 12 week period with equivalent amounts of organic oxidation and total sulfide reduction.

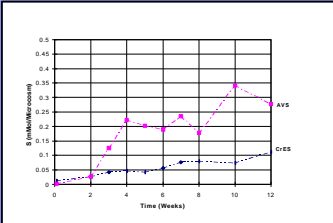


Figure 2.7

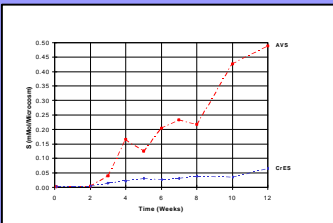
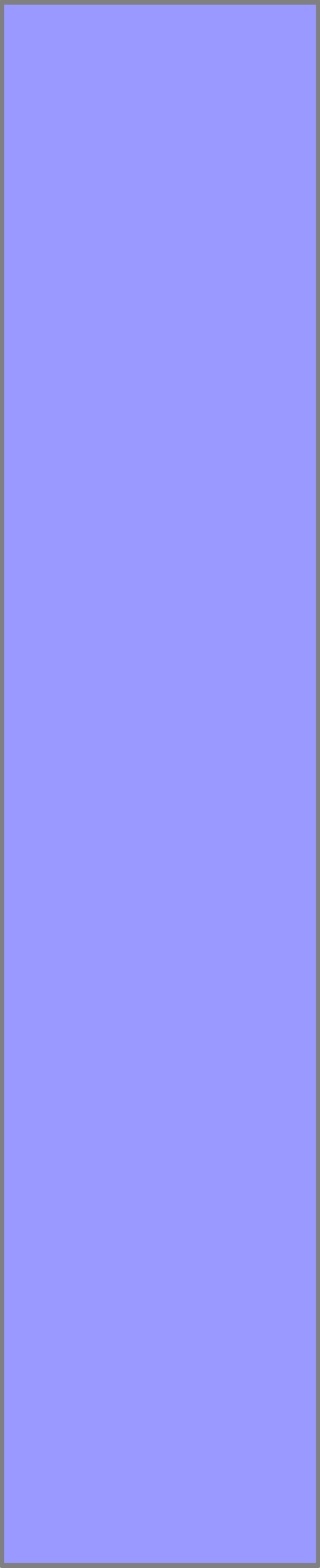


Figure 2.8

Quantities of measured mineral AVS and CrES for both the A and B microcosm sets are shown on s 2.7 and 2.8. These microcosms show the rapid formation of iron sulfide species, initially forming mostly AVS but with consistently increasing concentrations of CrES. For the two sets, higher concentrations of AVS were formed in sediment A than B but higher concentrations of CrES were formed in B over A. Thus, it appears that sediments with higher iron content favor the formation of iron monosulfide AVS whereas iron disulfide CrES tends to be formed in lower iron content soil.

2.6. Fe^{3+} and SO_4 Redox Zone Delineation from Prior Studies

As described above, based on thermodynamic and other considerations Fe^{3+} reduction could occur over a wide



range of redox conditions from before SO_4^{2-} extending through methanogenesis. Reviewing redox zone characterizations at past fuel contaminated sites can aid in further defining the nature of Fe^{3+} reduction. The presence of dissolved Fe^{2+} is a qualitative indicator of Fe^{3+} reduction commonly observed in prior natural attenuation studies.

A literature search was conducted to find examples of good natural attenuation studies from existing AFCEE natural attenuation projects. To qualify, the natural attenuation study must have evaluated O_2 , NO_3^- , Fe, SO_4^{2-} , and methanogenesis. Additionally, the hydrocarbon plume must have been fully delineated and could not intersect any natural or artificial barrier that prevented the full expression of redox zone development. These studies were conducted following the protocol of Wiedemeier et al. (1999) so all analytes were measured as aqueous phase from water samples taken from monitoring wells. Five sites were found that met the search criteria including:

- Hill Air Force Base (Wiedemeier et al., 1999 and Parsons Engineering Science, Inc., 1994);



Figure 2.9



Figure 2.10



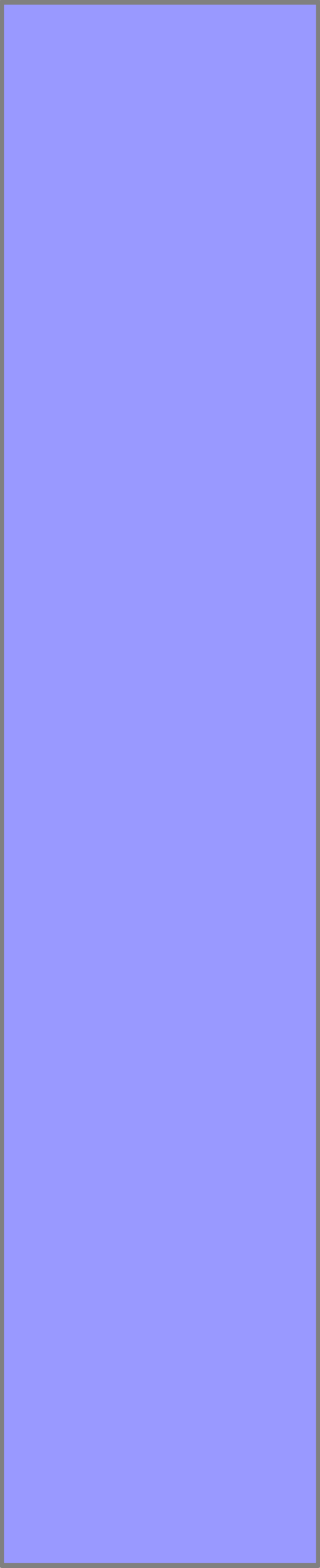
Figure 2.11



Figure 2.12

- George Air Force (International Technologies, 1996);
- Elmendorf Air Force Base Hanger 10 Site, (Parsons Engineering Science, Inc., 1995^a);
- Elmendorf Air Force Base Site ST-41, Anchorage, Alaska, (Parsons Engineering Science, Inc., 1995^b);

The redox zones for these natural attenuation sites are shown on s 2.9 through 2.12. Complete concentration contour maps were available for each analyte for each site listed above. However, only the boundary areas for dissolved contamination (total BTEX), aqueous Fe^{2+} production, SO_4^{2-} depletion, and CH_4 production are shown, combined on a single map for each site. The contaminant boundary was defined as total BTEX >1 mg/L. SO_4^{2-} reduction was determined as the region where concentrations of SO_4^{2-} first demonstrated depletion below background. The boundary for methanogenesis and Fe^{2+} were each defined as the areas where increases in those analytes were observed above their respective background values.



After examining all of the natural attenuation sites the following general observations are made:

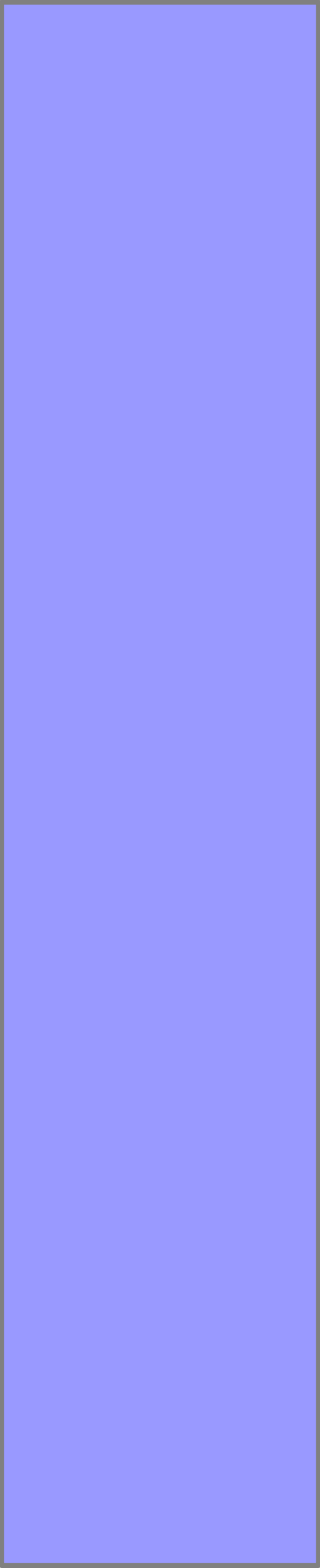
- The region of SO_4^{2-} depletion is generally larger than the region of aqueous Fe^{2+} and CH_4 ;
- Aqueous Fe^{2+} and CH_4 often occur together;
- Aqueous Fe^{2+} forms are found only in areas where SO_4^{2-} is greatly depleted.

These data indicate that Fe^{3+} reduction can occur concurrent with methanogenesis. Further, there is no evidence that Fe^{3+} reduction occurs before or inhibits SO_4^{2-} reduction. However, these contaminated sites are old; more labile forms of Fe^{3+} , which may have competitively excluded SO_4^{2-} reduction, may have been consumed in the past leaving no aqueous evidence at the time of sampling. Fe^{3+} reduction may occur concurrent with SO_4^{2-} reduction, but there is no indication of that process because produced Fe^{2+} will precipitate as an iron sulfide mineral where SO_4^{2-} reduction is significant.

2.7. Intrinsic Bioremediation Summary

Hydrocarbon can be oxidized through natural microbial processes in the subsurface. Soil bacteria have the ability to respire several common electron acceptor types including O_2 , NO_3^- , Fe^{3+} , and SO_4^{2-} . It is generally assumed that the order of utilization is $O_2 > NO_3^- > Fe^{3+} > SO_4^{2-} >$ methanogenesis based on thermodynamic analysis showing lower energy generation for each successive redox couple. This sequence may be correct for aqueous Fe^{3+} , which is rare at normal pH. There is much less thermodynamic benefit for solid Fe^{3+} . Therefore, Fe^{3+} reduction may occur across a broad redox range, possibly concurrent with SO_4^{2-} reduction and methanogenesis when mineral forms are considered. Evidence from natural attenuation studies supports the concept that Fe^{3+} reduction occurs concurrent with methanogenesis.

In the subsurface, the order of abundance (electron acceptor capacity), the common electron acceptors can be shown to be $Fe^{3+} \gg SO_4^{2-} > NO_3^- > O_2$, which is largely the opposite of the accepted microbial utilization sequence. This suggests that Fe^{3+} and SO_4^{2-} reducing bacteria may contribute greatly to intrinsic bioremediation. Acetoclastic



methanogenesis is functionally independent of electron acceptor mass.

Both the oxidized and reduced forms of Fe are usually found as solid minerals, so groundwater analysis alone may not adequately reflect Fe^{3+} reduction. Additionally, respiratory HS^- from SO_4^{2-} reduction can also be trapped in mineral form as AVS, S^0 or FeS_2 . Therefore, examining solid Fe and S minerals at sites contaminated with organic pollutants will be of great benefit in natural attenuation studies and compliment aqueous groundwater analyses. Based on the available literature, such analysis is theoretically sound. Inclusion of a mineral study will improve estimates of expressed and assimilative capacity and provide other insights supporting intrinsic bioremediation.



3. AMIBA SAMPLING AND LABORATORY PROTOCOL

3.1. Objective of Methods Development

Based on electron acceptor abundance, Fe^{3+} and SO_4^{2-} reduction by bacteria can play a dominant role in intrinsic bioremediation of some organic contaminants in the subsurface. Both Fe^{3+} and SO_4^{2-} reduction processes involve mineral phases and may not be properly understood by evaluating only groundwater concentrations. Fe and S mineral analyses should be incorporated in natural attenuation studies; however, inherent problems with sample collection and analysis have probably discouraged such efforts.

Whereas routine methods are available for aqueous Fe and S analysis, much of the present research hinges on the ability to measure these species in mineral phase. After a careful review of the problem, it was determined that methods were needed to determine the following mineral types:

- Bioavailable Fe^{3+} ;
- Biologically produced Fe^{2+} ;
- Bulk Fe^{2+} and Fe^{3+} ;
- Acid volatile sulfides (iron sulfide, mackinawite, etc.);
- Chromium reducible sulfides (FeS_2 and S^0)

As discussed below, methods for collecting and extracting some of these mineral analytes had previously been developed; however, many of those techniques are labor intensive and generally impractical for extensive use. Therefore, an emphasis was placed on developing methods that could be practically applied.

Finally, AMIBA is improved when key aqueous phase electron acceptors and respiratory products are measured in the aquifer from the same place that sediment samples are obtained. Important aqueous phase analytes include NO_3 , SO_4^{2-} , and Fe^{2+} (dissolved Fe total). As described below, these dissolved phase ions can be analyzed from pore water extracted from sediment, if the original sample is collected and preserved anoxically.

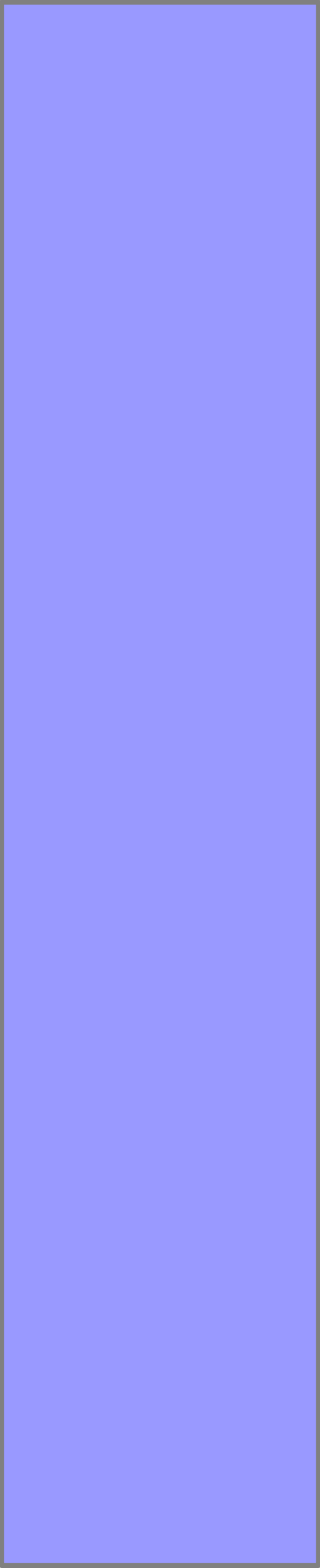


This chapter will:

- Discuss field sampling techniques,
- Describe mineral Fe and S extraction methods,
- Review the results of extraction tests performed using synthetic minerals under laboratory conditions, and
- Outline the method for pore water extraction/analyses.

3.2. Sample Planning and Boring Placement

AMIBA relies on the analysis of mineral and aqueous data spatially distributed in the subject aquifer. Ideally, a geostatistical analysis should be performed to verify that vertical sampling points and boring locations are of sufficient density so that correlation and interpolation is possible, as described below. Unfortunately, such analyses can only be performed after the data has been collected and analyzed, so some “guesstimation” is required for planning purposes. Obviously, sample planning can be improved with experience working in the same geologic media.



The required sample density is a functional attribute of variability with respect to distance. As a rule in geologic media, there is considerable change per unit distance in the vertical plane relative to the horizontal. Thus, many samples are required in the vertical plane for each soil boring/core hole. Further, rapid change is often observed in the meter above and below the water table. One meter below the water table, attribute concentrations change more gradually with depth. In the plume area, one should consider a sampling every 0.25 to 0.50 meters from the capillary fringe to a depth of one meter below the water table. As a practical matter, it may be wise to collect vertical samples at high density. One can initially analyze only part of the samples collected while holding the balance in reserve to be analyzed if data gaps are apparent during the evaluation phase. Refrigerated, sealed, anoxic sediment samples can be kept for several months before use.

The spatial distribution of both mineral and aqueous parameters is often a function of hydrocarbon distribution. Where hydrocarbon concentrations change quickly with distance, important aquifer/mineral characteristics change

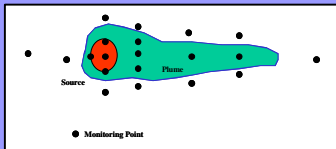


Figure 3.1

rapidly as well. Thus, observing hydrocarbon concentrations, even in a qualitative manner, can aid in determining the frequency and distribution of sediment and pore water samples. In the horizontal plane there should be increased soil boring density immediately up gradient of the source area and cross gradient but gradually increasing boring density down gradient as hydrocarbon concentrations diminish (Figure 3.1). Field screening of headspace soil gas can be used as a guide to sample frequency. Sample frequency may be increased as headspace gas readings decrease in the vertical plane. Similarly, fewer samples may be considered in redundant cross-gradient borings that are clearly pristine.

Sampling should be modified for lithologic variability in both the vertical and horizontal directions. Increased sample and boring density should be considered where lithology changes rapidly.

Establishing background conditions is extremely important for AMIBA. Background soil borings must be drilled up gradient. Though of lesser importance, down gradient and side gradient background samples are

recommended. For AMIBA “background” does not mean the absence of hydrocarbon rather, it is locations where hydrocarbon has never existed, so that the aquifer (aqueous and mineral phase) is fully oxidized. Typically, AMIBA background exists some distance beyond the observed hydrocarbon plume. That “distance” will tend to be shortest up gradient from the source area, intermediate in length cross gradient, but could be extremely long in the down gradient direction.

3.3. Field Observations

Some qualitative information concerning Fe and S mineral content can be observed in the field during drilling and sampling operations. It is recommended that a geologist or geological engineer add such observations to the lithology log. An example of a lithology log with Fe and S mineral notations is shown on Figure 3.2.

Many sediments are principally quartz, which is normally white to clear. Secondary minerals, often iron based, are thus responsible for much of the natural variations in sediment coloration commonly seen. Sediments containing oxidized iron minerals can range in

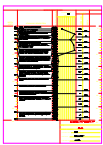


Figure 3.2



Figure 3.3

color from brown to red. Iron oxide ($\text{Fe}(\text{OH})_3$) is typically rusty brown to rust, goethite ranges from yellow to orange, and hematite red to maroon. Examination of oxidized sediment with a hand lens or binocular microscope will often reveal quartz or other primary mineral species coated with a rust-like oxidized iron coating or stain. Examples of oxidized sediment from cores are shown on Figure 3.3. There is generally a correlation between decreasing sediment grain size and increasing iron content. Thus, special consideration should be given towards identifying changes in lithology and grain size.



Figure 3.4

Sediment containing iron sulfide minerals can be especially distinctive. Where reduced, the typically oxidized colors described above can be replaced with a gray to charcoal black color indicating the presence of iron sulfide species (Figure 3.4). This coloration is often mistakenly identified as “hydrocarbon or fuel stain”. Examination of such sediment under a hand lens or binocular microscope will show that the oxidized iron coating has been removed so that quartz or other primary mineral grains can be clearly seen mixed with fine gray FeS particulates. Visually, FeS

and FeS_2 cannot be distinguished in the field. However, if a few grams of sediment containing FeS is placed in a small mouth bottle and several milliliters of acid are applied the “rotten egg” odor of H_2S can readily be detected. A 160 ml serum bottle and ~6 N HCl work well for this simple test. Covering the mouth of the bottle for half a minute or so permits off-gas to accumulate in the bottle and increases the odor if FeS is present. Care should be taken to avoid inhaling too much of the gasses produced by this test.

Sediments that undergo iron enzymatic iron reduction in the absence of sulfides are more difficult to distinguish visually. In laboratory studies where enzymatic iron reduction is encouraged, sediment can be seen to gradually darken. In some sediments, where documented iron reduction has occurred, the oxidized iron color appears faded or of a slightly grayish cast. An example of alluvial sediment that has undergone Fe^{3+} reduction is shown on Figure 3.5.

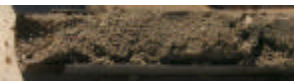


Figure 3.5

3.4. Field Sample Collection and Preservation

Many reduced Fe^{2+} and iron monosulfide minerals will oxidize when exposed to the atmosphere, so exposure to air should be minimized. Field portable gloveboxes or bags, while potentially minimizing air contact, are not practical for general applications. The alternative method described here is rapid, effective, and requires a minimum of specialized equipment.

Sediment samples can be obtained utilizing common drilling methods, including a continuously coring hollow stem auger equipped with a split spoon sampler or Shelby tube or a geocore/hydropunch drilling unit. In poorly consolidated, heaving sands, excellent sediment recovery (>90%) has been achieved using a hollow stem auger equipped with a clam-shell fitted auger head (Leach et al., 1988).

Anoxic conditions can be maintained by placing sediments in a N_2 gas atmosphere. A portable nitrogen gassing station can be purchased or built for use in the field similar to that shown on Figures 3.6 and 3.7. This station consists of a N_2 gas cylinder attached to a multiport manifold system. The manifold should consist of a gas regulator connected to a header pipe fit with four to eight individual

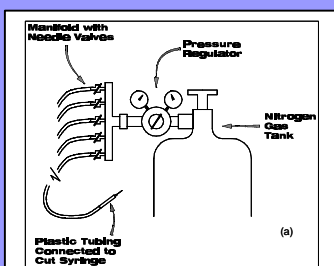


Figure 3.6



Figure 3.7

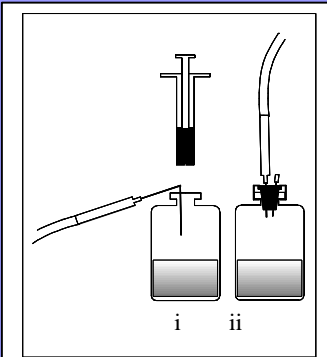


Figure 3.8



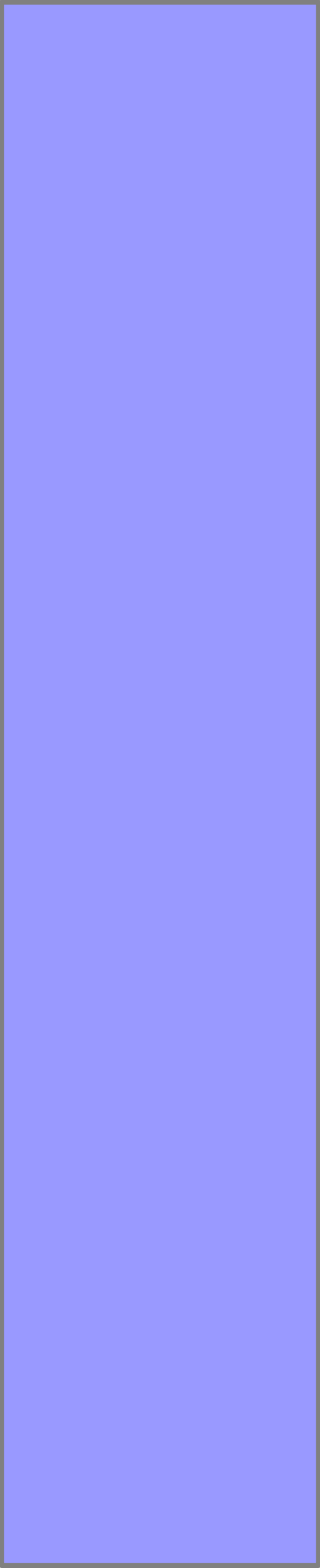
Figure 3.9



Figure 3.10

gas needle valves. Each needle valve is then fit with flexible hose (e.g. clear polyvinyl) with Luvier Lock fittings on the effluent end. Long, large diameter syringe needles can be attached to the end of the hose. These needles can be made flexible by heating under a gas flame and bent to a desired hook shape after cooling. This gassing station permits multiple samples to be nitrogen purged at once. For safety, the regulator should be set for a delivery pressure of no more than 10 psi.

Sediment samples can be transferred to storage bottles in the field. The tip of a 5 cc plastic syringe is cut to create a disposable piston-coring tool (3.8). This tool can be used to subsample a sediment core and inject it directly into a 160 ml N₂ purged serum bottle (Figure 3.9). The serum bottle can be stoppered, sealed using an aluminum crimp, and purged again with N₂ as shown on Figure 3.10. As above, after purging the vent needle should be withdrawn first followed by the purge needle to form positive atmospheric pressure in each storage bottle. All sediment samples should be refrigerated stored at 4°C while awaiting analysis. The total collection method is as follows:

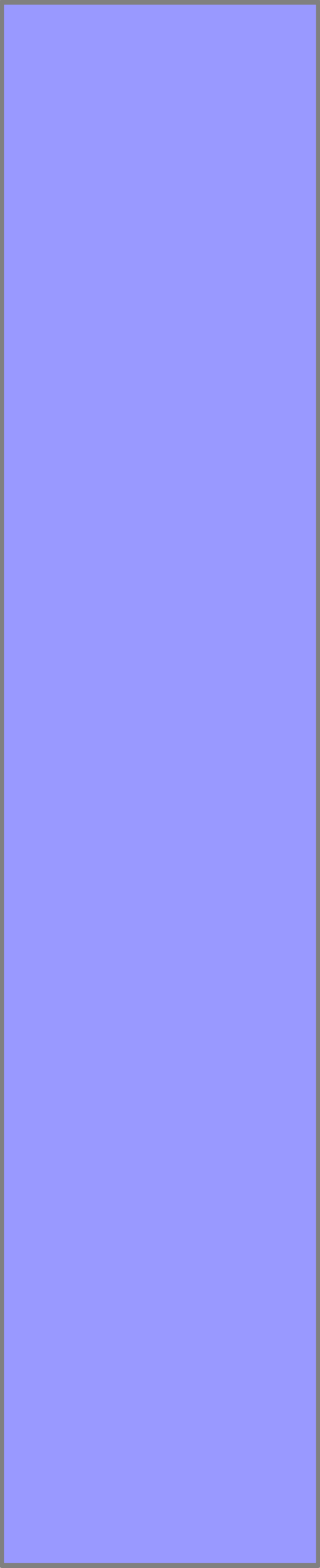


Step 1: Have at least two lines connected to the manifold system and flowing N₂ at the desired pressure. One line will be connected to a bent large diameter syringe needle (e.g. 8 gage) while the other will be connected to a smaller diameter syringe needle (e.g. 22 gage).

Step 2: Nitrogen purge an empty 160-ml serum bottle for 2 to 5 minutes using the large diameter syringe needle hooked over the lip of the serum bottle.

Step 3: Collect approximately a half bottle of sediment by successively subcoring the core at the desired depth and injecting the sample directly into the serum bottle while it continues to be purged with nitrogen.

Step 3: Hold a smaller syringe needle (e.g. 22 gage) over the open mouth of the serum bottle and remove the large gage needle. While holding the syringe needle in place slip a butyl rubber stopper into the neck of the bottle, then quickly remove the needle. Work the stopper completely into the mouth of the bottle if



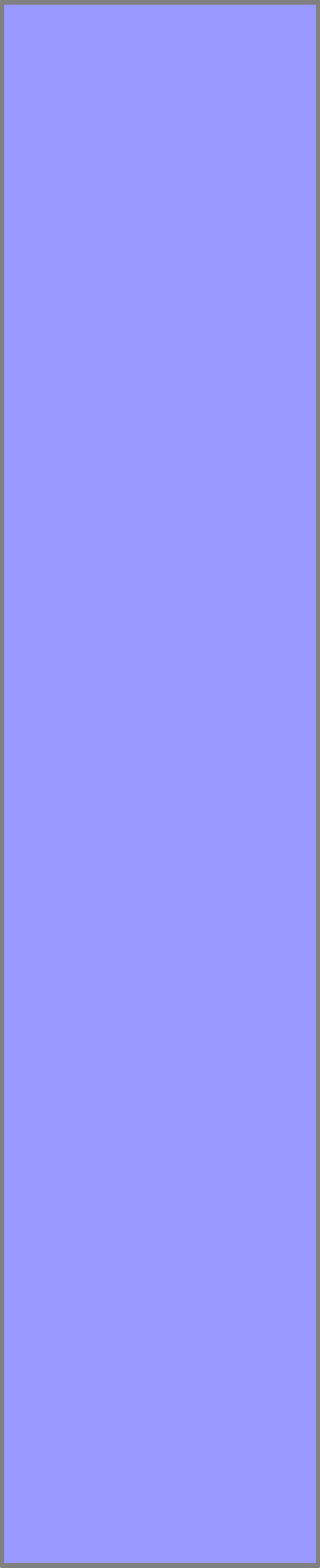
necessary and secure in place using a standard aluminum seal with crimping tool.

Step 4: Peel the removable tab off the aluminum seal. Pierce the rubber stopper with the small gage syringe to supply nitrogen to the inside of the sealed bottle. Pierce the rubber stopper again with one to three other plain small gage needles, which vent N₂ to the atmosphere. Continue to purge the sealed bottle with N₂ for 2 to 5 minutes. Early in this purging process lightly tap the bottle several times against the work surface so that gas pockets are eliminated.

Step 5: Once the purging is complete remove the vent needles. Wait 5 to 10 seconds then remove the remaining small gage N₂ gas needle. This will provide positive atmospheric pressure in the sample bottle.

Step 6: Place the bottle in a 4 C° cooler to await analysis.

This sampling procedure can be quite rapid, especially when the manifold system includes 4 to 8 individual gas lines. In that case, a sample can be collected



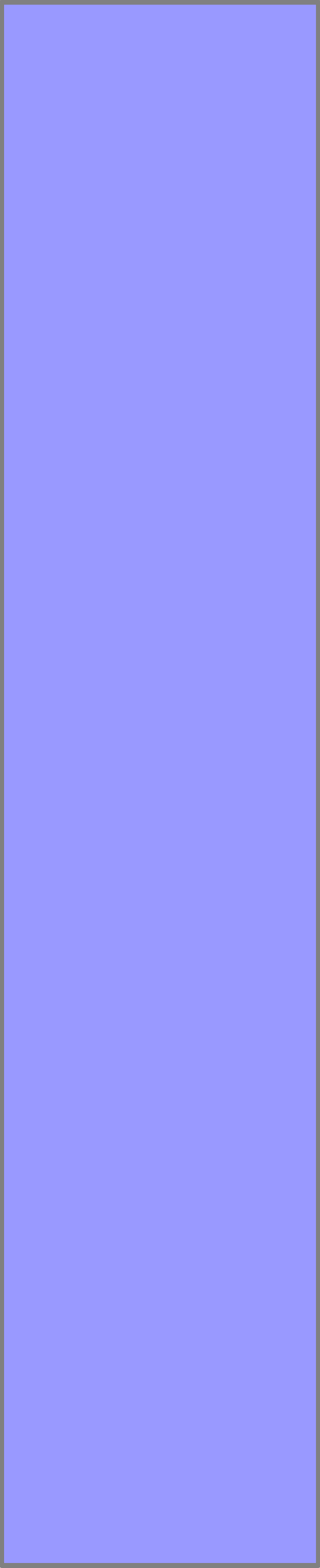
at the same time that one or more bottles are undergoing the final or initial N₂ purge.

Note: Extreme care should be exercised to avoid puncturing the skin with a N₂ pressurized syringe needle. Although N₂ is not directly toxic, if injected below the skin it could potentially cause coronary failure or diver's bends.

3.5. Weak Acid Solution (WAS) Iron Analysis

3.5.1. WAS Method Background

Fe minerals of interest are generally either so finely particulate or poorly crystalline that identification by direct X-ray diffraction is difficult (Jenne, 1977). Consequently, various chemical extractions are used for mineral speciation; however, many of these demonstrate inconsistent selectivity (Robinson, 1984). Chemical extraction scenarios have also been employed to try to quantify biologically available Fe³⁺ and biogenically produced Fe²⁺ iron minerals in sediments. Therefore, in addition to the requirement for a certain level of mineralogical speciation, for an intrinsic bioremediation study



there is an additional requirement that the analyses identify minerals associated with biological processes.

Microbial/mineral interactions tend to be surface phenomena. The Fe^{3+} that is reduced is on the outer exposed portion of the sediment grain. Alternatively, Fe^{2+} can be deposited on sediment surfaces as a coating, as discrete particulates, or exchange with clay ions. The chemical extraction procedures for Fe speciation normally employ a weak acid solution extractant that dissolves only a small fraction of the total iron present in the sediment. The goal of the mild acid extraction is to distinguish small quantities of those microbially important iron forms (e.g. bioavailable Fe^{3+} or biogenic Fe^{2+}) from a much larger bulk mass of Fe inherently present in abundance in many sediments. As described below, many techniques have been proposed for this purpose. All of these are semiquantitative due to the nonspecific nature of the extraction process.

Many iron extractants have been proposed, including 0.5N HCl, 0.2 M ammonium oxalate, dithionite-citrate-bicarbonate, and 0.008 M Ti(III) / 0.05 M EDTA, as

summarized by Heron et al. (1994^b). For biologically available Fe^{3+} , Lovley and Phillips (1987) recommend a one-hour extraction employing 0.5 N HCl and hydroxylamine hydrochloride. For reactive biogenically produced Fe^{2+} species, Heron et al. (1994), used an extraction time of 24 hours, also using 0.5N HCl.

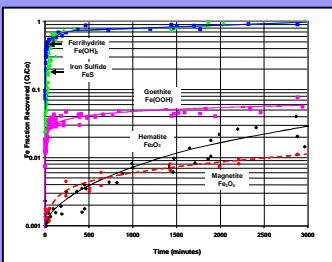
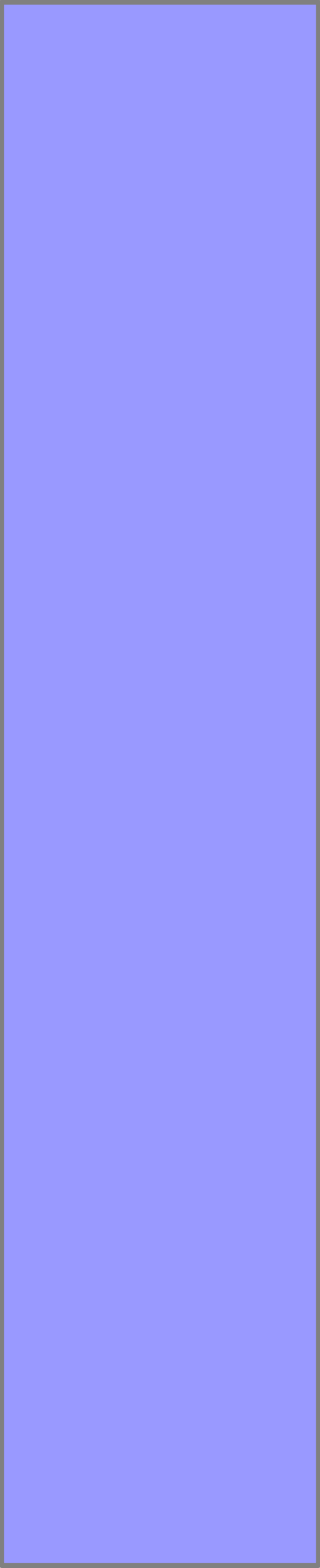


Figure 3.11

Iron extraction tests using 0.5 N HCl were conducted by Kennedy et al., 1999. Figure 3.11 shows the results of those tests, expressed fractionally as (Ct/Co) where Ct is the measured iron mass in solution and Co is the total amount of solid iron present initially. For all iron species, varying Co did not change the extraction rate significantly. Approximately 85 to 90% of the easily extractable Fe^{2+} and Fe^{3+} species (FeS and $\text{Fe}(\text{OH})_3$) were extracted in 24 hours, with the remainder recovered in 48 hours. Of the poorly extractable iron forms, the rate of extraction was $\text{Fe}(\text{OOH}) > \text{Fe}_2\text{O}_3 > \text{Fe}_3\text{O}_4$. Significantly, Fe_2O_3 and crystalline Fe_3O_4 , common iron forms in mature sediments, had average maximum recoverable concentrations of less than 3%. Approximately 6% of $\text{Fe}(\text{OOH})$ was extracted. Similar dissolution tests using 0.5 N HCl were conducted by Sidhu



et al., 1981, who performed experimentation on the isomorphic varieties of Fe(OOH) for periods up to 100 hours. There is reasonable correlation with respect to extraction rates for minerals common to both studies.

These extraction test results indicate that reactive iron species are almost entirely extracted in 24 to 48 hours of exposure to 0.5N HCl. Crystalline Fe³⁺ species (principally hematite, goethite, and magnetite), which usually comprise much of the background bulk iron species, are not extracted to any significant extent. This suggests that a reaction time between 24 to 48 hours should maximize the measurement of reactive, biologically important, iron species while minimizing the contribution of bulk iron typically found in sediments from primary deposition or abiotic diagenesis. Siderite (FeCO₃) was not tested here, however, Heron (1994) reports fifty percent recovery of abiotically produced crystalline mineral FeCO₃ in 0.5 N HCl extractions conducted over 24 hours. Additionally, the form of magnetite (Fe₃O₄) digested above was highly crystalline. Freshly precipitated magnetite from microbial activity may be much more easily solublized in mild acid.

3.5.2. Weak Acid Iron Mineral Extraction

Method Description

The suggested method for weak acid solution (WAS) extraction of bioreactive Fe^{3+} and biogenic, HCl extractable Fe^{2+} minerals is as follows. Approximately 0.6 to 0.8 g of sediment is placed inside 25 ml serum tubes, which are N_2 purged using a gassing station and stoppered. After all samples are prepared, they are uncorked and 15 ml 0.5 N HCl is immediately added. Each tube is recorked to prevent evaporation and gently shaken for 48 hours on a rotary shaker table. Each tube is then centrifuged or filtered to remove suspended solids and a portion of the extractant analyzed for total Fe and Fe^{2+} spectrophotometrically. Fe^{2+} and total Fe can be determined with a HACH spectrophotometer using HACH reagents 1,10 Phenanthroline and 3-(2-pyridyl)-5, 6-bis (4-phenylsulfonic acid)-1,2,4-triazine, monosodium salt (FerroZine) (Stookey, 1970; Eaton et al., 1995). Results are converted to dry weight per unit soil mass. Sediment moisture content is

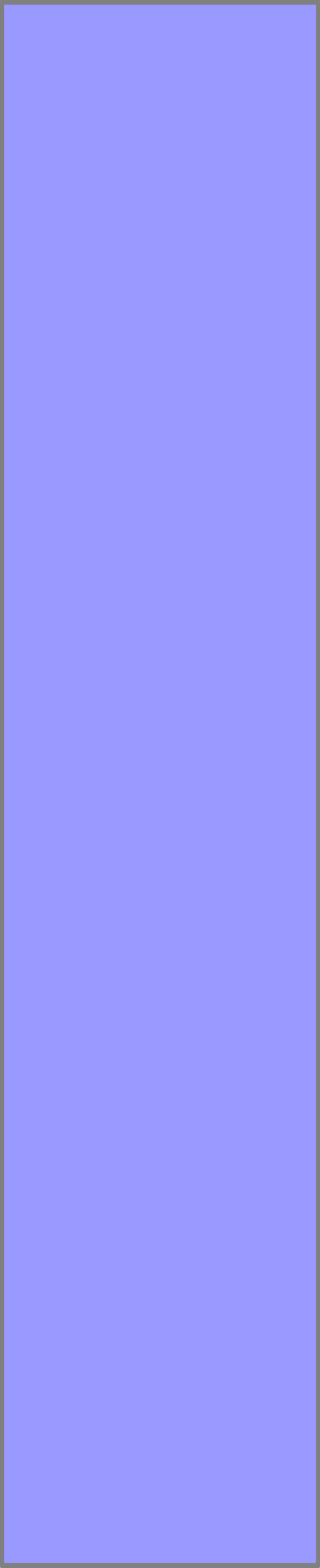
determined by drying ~10 g wet sediment from each sample interval for approximately 48 hr at 95 C°.

Note that the Fe²⁺ reagent requires near normal pH conditions for full color development, but some Fe²⁺ may rapidly oxidize to Fe³⁺ if the sample pH is adjusted before adding the reagent. As an alternative, the Fe²⁺ reagent can be added to the acidified sample solution, swirled in the bottle to mix, then buffered to the proper pH by the direct addition of NaHCO₃ power to saturation (i.e. until a small amount of power does not dissolve). NaHCO₃ is the buffer actually used in the standard HACH power pillow reagent. As verified by tests, this technique produces full color development and accuracy without oxidizing the Fe²⁺. Concentrations of Fe³⁺ can be determined by subtracting the Fe²⁺ values from Fe total.

3.6. Strong Acid Solution (SAS) Fe and Extended Sulfide Analysis

3.6.1. Method Background

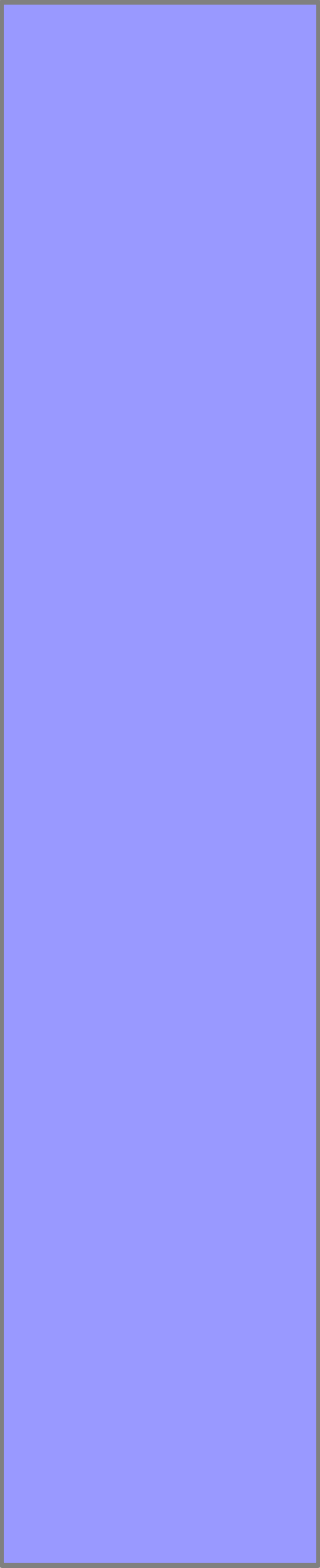
Crouzet et al. (1994); Wicks (1989); Rice et al. (1993); and Herlihy (1987) have all described extended sulfide extraction techniques. Chemically, these techniques are



based on the ability of Cr(II) to extract FeS_2 , S^0 , and AVS; acetone to extract S^0 ; and HCl to extract AVS. By subtraction, concentrations of FeS_2 , S^0 , and AVS are determined. Here, the technique is simplified using only HCl for AVS analysis followed by a Cr(II) attack on the same sediment sample to determine S^0 and FeS_2 (Canfield et al., 1986), which are referred to here as chromium extractable sulfides (CrES).

The first strong acid solution (SAS) extraction step (6 N HCl) used for AVS can also be used to determine bulk Fe^{3+} and Fe^{2+} . The stronger acid extracts a greater quantity of native iron in sediments than the weak acid method and approximates the total bulk iron in the sediment. If more aggressive extraction techniques are employed (e.g. increased acid concentration or heating) then greater quantities of iron could be extracted, however, such methods are not necessary.

Whereas complete mineral S speciation may be required for some purposes, for natural attenuation studies the division of S into AVS and CrES is adequate. AVS is used as a general indicator of recent sulfate reduction. As



shown below, *Total Sulfide* (S^- from AVS + CrES) must be used for expressed capacity mass determinations. The speciation of AVS is required because Fe^{3+} is spontaneously and abiotically reduced to Fe^{2+} in the presence of HS^- to form FeS. The Fe^{2+} from FeS is unfortunately readily eluded by the mild (0.5 N HCl) acid extraction described above and cannot be determined by direct measurement. Thus, to correct biogenic Fe^{2+} , the equivalent mole mass of Fe^{2+} associated with S^- in AVS is subtracted from the mole mass of Fe^{2+} determined from the mild acid extraction.

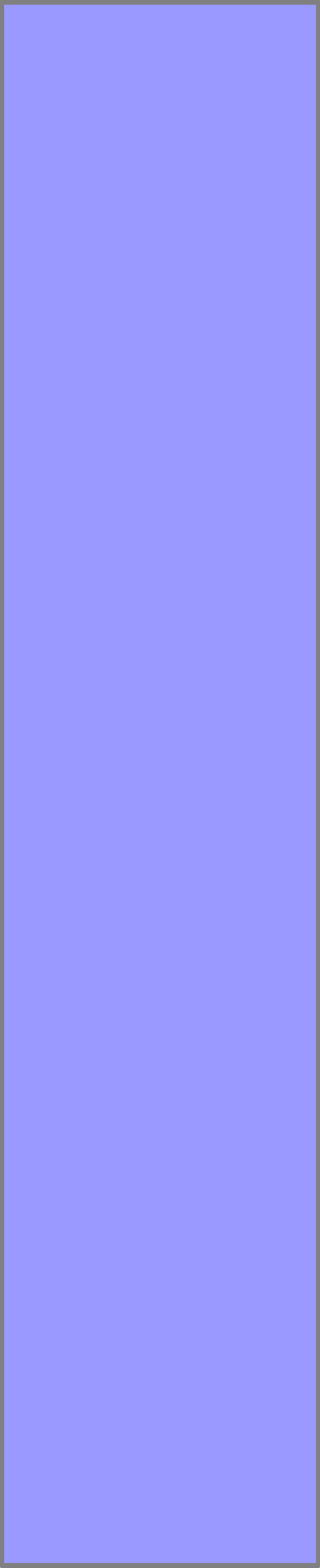
The sulfide extraction described by earlier workers (Crouzet et al., 1994; Wicks, 1989; Rice et al., 1993; and Herlihy, 1987) used a retort converter technique. The process described here uses a single test tube, can be run in batch, and requires little specialized equipment. It is based on a well-tested, closed vessel method developed by Ulrich et al. (1997) and modified as per Kennedy et al., (1999).

3.6.2. Method Description

3.6.2.1. Reagent Preparation

To prevent H₂S oxidation during extraction, all aqueous reagent solutions are deoxygenated by bringing to boil (near boil for acids) for 20 minutes while sparging with N₂ in a boiling flask to maintain a N₂ atmosphere. While hot, the liquid can be immediately transferred using an electric pipetter to nitrogen purged 160 ml serum bottles, sealed with butyl rubber stoppers, and secured with aluminum seals. A gassing station is used to inject N₂ into each sealed serum bottle to obtain a positive pressure of approximately 15 psi. Using this technique, quantities of 10% zinc acetate Zn(CH₃COO)₂•2H₂O, 6 and 12 N reagent grade HCl, and a supply of deoxygenated deionized water are produced using nano-pure water. Solutions prepared in this manner remain anoxic for long periods of time. During use, solutions are withdrawn via syringe and pressure maintained in the storage bottles by injection of N₂.

A 1N solution of Cr³⁺ is produced similar to Canfield et al. (1986) as follows. A large (1 L) aspirator bottle is filled with zinc chips, which are immersed in 0.5 N HCl for



approximately 15 minutes. This acid is drained and the procedure repeated again until the zinc has a shiny, silver finish. A large diameter syringe is inserted into the base of the zinc chips and connected to a gassing station to provide N₂ sparging and headspace. A 1N Cr (III) chloride hexahydrate (CrCl₃•6H₂O) solution is added to near the top of the zinc chips. After ~15 minutes the green colored Cr³⁺ solution changes to a blue color, indicating that the solution is reduced to Cr²⁺. Approximately 100 ml fluid is transferred under a nitrogen head using an electric pipetter to 160 ml nitrogen purged serum bottles, which are sealed with butyl rubber stoppers and secured with aluminum seals. Excess pressure may build inside the storage bottles over time so additional N₂ is not added to the headspace and some gas may, in fact, need to be bled after a few days (check with a syringe tip pressure gauge). The Cr³⁺ solution produced in this manner can remain in a reduced form for at least three months.

3.6.2.2. *Sample Preparation*

For each sample, approximately 0.8 to 1 g sediment is placed in weighed 25-ml nitrogen purged, serum tubes.

Nitrogen is supplied to each tube continuously during sediment transfer through a six-inch long syringe attached to polyvinyl hose connected to a nitrogen gassing station. The actual sediment weight is then determined for each sample. A small diameter rubber o-ring (approximately 3-mm dia.) is placed around a smaller 4-ml test tube, approximately 1 cm from the top. The serum tubes are reopened, and the smaller 4-ml test tube is placed inside each larger serum tube while maintaining an anoxic head by continuously flooding with N_2 (Figure 3.12). Using a syringe, 2.5 ml of zinc acetate solution is extracted from a sealed serum bottle and placed into the 4-ml test tube. The serum tube is then sealed with a butyl rubber stopper and secured with an aluminum seal. Using a syringe, approximately 8-ml nitrogen gas is withdrawn from the headspace of the sealed test tube to create a slight vacuum. Using a syringe, 3 ml of 6N HCl is withdrawn from a sealed serum bottle. This acid is carefully injected through the stopper against the inner wall of the serum tube so that it immerses the sediment without entering the 4-ml tube containing the acetate solution. The tube is then placed in a rotary shaker for 3 days. The shaker

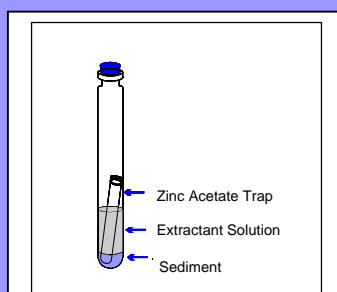
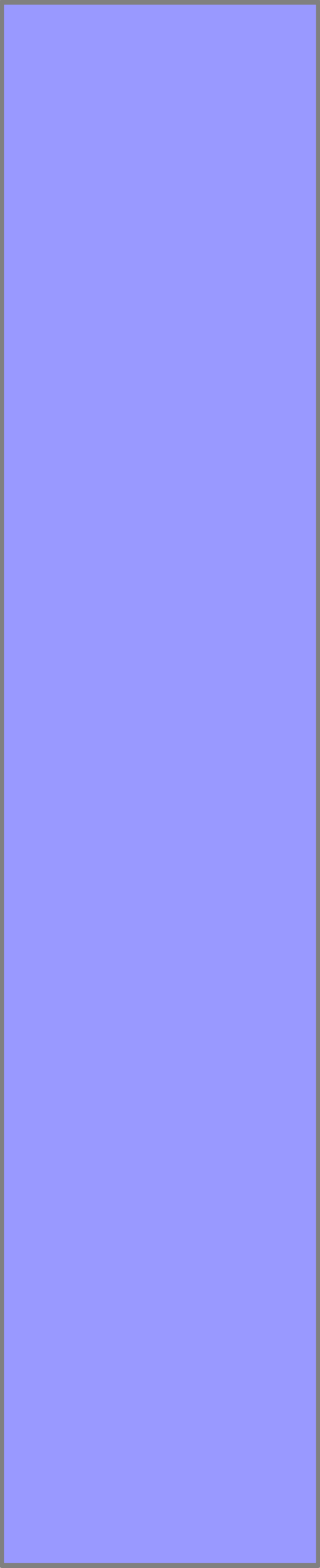


Figure 3.12



rotates the tubes sufficiently to provide good mixing without spilling the acetate solution.

For this first step, the 6N HCl acid 1) dissolves bulk Fe^{3+} and Fe^{2+} minerals, and 2) eludes H_2S , from AVS minerals, which is subsequently trapped in the Zn acetate solution as ZnS. Following the extraction period, the serum tubes are unsealed but kept under a constant nitrogen gas flow. The Zn acetate traps are removed and analyzed for sulfide spectrophotometrically using the methylene blue technique (Eaton et al., 1995). Five milliliters deoxygenated deionized water is added to the 6N HCl/sediment solution. Each tube is restoppered, vigorously shaken by hand, and then centrifuged to settle suspended solids. Again, the tubes are unsealed but kept under nitrogen flow. Samples of the extractant are withdrawn and evaluated for total Fe and Fe^{2+} spectrophotometrically, as above.

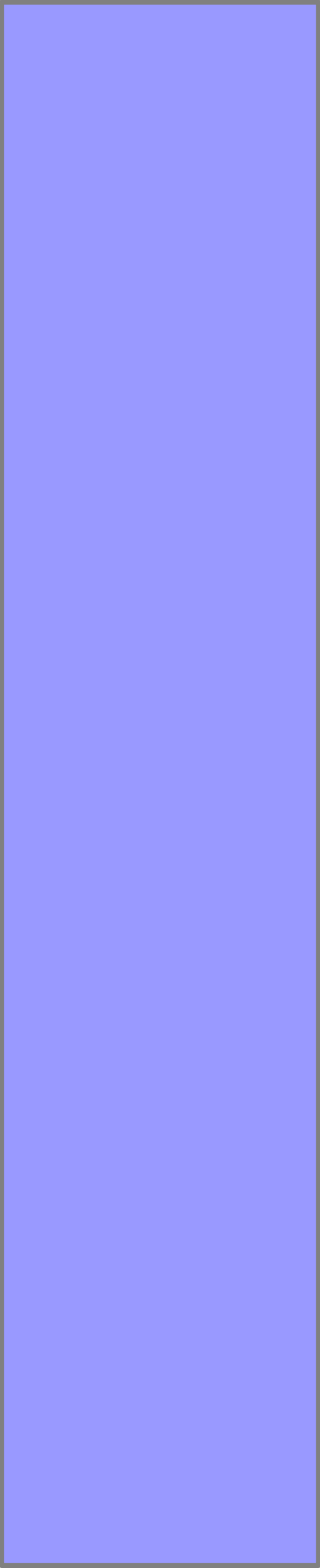
To begin the second extraction, most of the HCl solution is carefully decanted from the serum tubes, under a N_2 atmosphere, and discarded. A fresh Zn acetate trap is inserted into the seal tube. The steps involved in the first extraction are repeated, using 2.5 ml 1N Cr^{3+} and 1 ml 12 N

HCl instead of 6 N HCl. Again, the serum tubes are placed in the rotary shaker for 3 days. Sulfide, from pyrite (FeS_2) and S^0 (CrES), are eluted during this extraction and trapped in Zn acetate. At the end of this time, the serum tubes are unsealed and the Zn acetate traps analyzed for sulfide, as above. Solid phase Fe and S data are typically presented on a dry weight basis.

3.6.3. Laboratory Testing and Discussion

Tests were performed to verify the efficacy of the method used here. Test samples were made using a crushed glass matrix mixed with 0.5% FeS and FeS_2 and 1% Fe_2O_3 (Alpha Aesar) in quadruplicate lots. Using the methods described above, the average recoveries were FeS = 99.6%, FeS_2 = 105.4%, and Fe_2O_3 = 100.0%. These tests also showed that negligible FeS_2 was extracted during the initial HCl phase.

As above, it should be noted that synthetic and/or crushed minerals used in extraction testing may or may not extract like natural sediment samples. However, some natural sediment samples tested were originally bright red

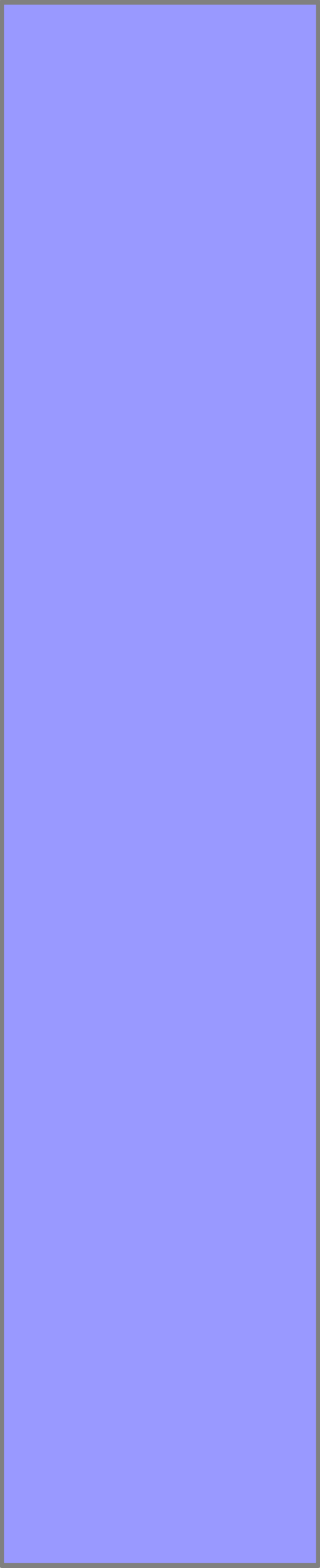


from abundant Fe^{3+} minerals, but at the conclusion of the HCl acid extraction phase they were usually completely white or very light gray, indicating near complete Fe removal. After this extraction, residual iron may remain in some sediments, which may only be extracted by heating the sample. Complete Fe removal, however, is probably not necessary for the analyses, as discussed below. Rice et al. (1993) warns that during the acid extraction phase some eluded H_2S may become oxidized by Fe^{3+} minerals to create S^0 . Therefore, measured AVS may be under-reported in some conditions. In the author's experience, the Cr solution maintains a bluish color throughout the second extraction process; indicating sufficient quantity of the reagent was used.

3.7. Pore Water Extraction

3.7.1. Method Background

Although the emphasis in this document is on mineral phase analyses, aqueous analysis of key natural attenuation indicators is implicit. Groundwater samples taken from monitoring wells will probably lack sufficient detail and may not be fully representative of actual groundwater conditions



where sediment samples are taken. Clustered monitoring wells improve detail and chemical representation but are expensive and difficult to install and sample. As an alternative, pore water can be extracted directly from the core material used for mineral analysis. This technique is rapid, inexpensive, and represents groundwater conditions at the core sample point. The targeted analytes for pore water extraction are NO_3^- , dissolved Fe, and SO_4^{2-} . Oxygen cannot be reasonably determined from pore water analyses and should be measured in the field as described by Wiedemeier et al., (1999).

3.7.2. Sample Collection

A number of 160-ml serum bottles should be preweighed, with rubber stopper, before going out into the field. Using the techniques described above, approximately one-half bottle of sediment should be collected into a nitrogen purged bottle (~100 g wet weight). As above, this bottle should be sealed and undergo a final N_2 purge before being cooled to 4 C° for storage.

3.7.3. Laboratory Analysis

In the laboratory, sediment can be tarred by removing the aluminum seal and reweighing the sample with stopper, then subtracting the empty bottle and stopper weight. Each bottle can then be opened but maintained under a N₂ atmosphere again using a large hooked syringe attached to polyvinyl hose connected to a nitrogen gassing station (Figure 3.13). Approximately 10 g sediment should be removed, weighed, dried, and reweighed to determine moisture content. To increase fluid volume, 50 ml deoxygenated, deionized water should be added to each bottle using an electric pipetter. Each bottle should be shaken for fifteen minutes on a shaker table. For gravel through silt size sediments, the entire contents of the bottle can be then filtered through a 0.45 μm vacuum filter. Samples containing large amounts of clay can be centrifuge filtered. Upon filtering, a 15 ml sample should be immediately acidified to pH<3 to inhibit iron precipitation and preserve dissolved Fe²⁺/Fe total ratios until they can be spectrophotometrically analyzed as above. It is not strictly necessary to differentiate between dissolved Fe²⁺ and Fe³⁺

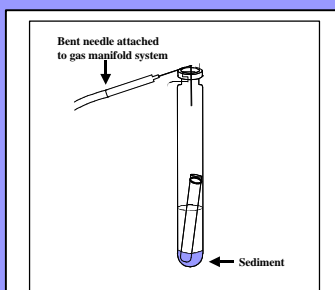


Figure 3.13

species as it can normally be assumed that all dissolved Fe at normal pH is in a Fe^{2+} form. Thus, total iron need only be evaluated. The remaining unpreserved sample should be immediately analyzed for NO_3^- , SO_4^{2-} or other dissolved ions using ion chromatography or other approved methods.

3.8. Field Examples of Fe and S extraction

In addition to the natural attenuation example from Westover AFB shown below, the Fe and S mineral extraction methods described were tested on several other sites with different organic contaminants as described in Kennedy et al., (1999). A couple of examples are shown here for instructive purposes.

Figure 3.14 is a profile from a core hole near a fuel leak at a former underground storage tank site in Oklahoma City. The chart shows mineral iron concentrations from both 0.5 N and 6 N HCl acid extractions at various depths. Iron mineral data were calculated on a mass/mass basis (e.g., mg/Kg). For this location, fuel was present for approximately 2 m below the water table but not above it, except as a vapor phase. The aquifer at this site consists of rather

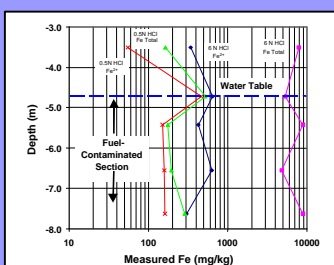
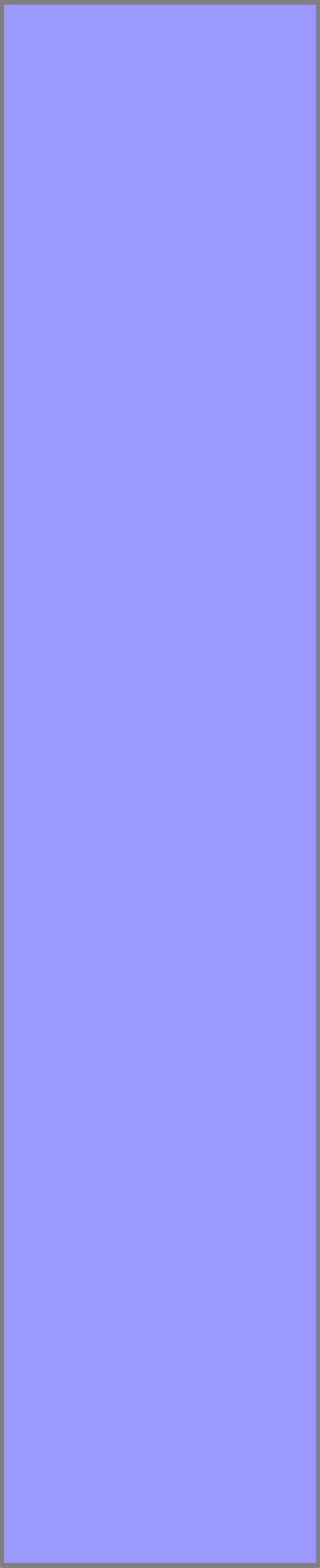


Figure 3.14



homogeneous, very poorly consolidated sandstone that was a maroon to red color from iron mineral staining.

As is typical, there was considerably more Fe extracted using the strong acid as compared with the weak acid technique. This tendency has been found for virtually all sediment samples analyzed at any site studied to date. For this sample set the SAS Fe was more than 10 times the WAS Fe amount. The SAS extraction provides an estimate of bulk iron in the sediment, which approaches 1% by weight. The estimate of bioavailable iron is calculated by subtracting WAS Fe²⁺ from WAS Fe total on a point-by-point basis. Biogenic Fe²⁺ is estimated as measured WAS Fe²⁺ less background and abiotically produced Fe²⁺ (from FeS). Finally, Fe³⁺ reserve can be calculated as SAS Fe³⁺ minus bioavailable Fe³⁺.

Data presented on a mass basis is needed for calculation purposes to properly estimate available or expressed capacity for Fe³⁺ reduction in natural attenuation studies (Kennedy et al., 1998). However, determining which zones have had significant iron reduction can be difficult by just examining mass/mass (e.g. mg/Kg) iron data. Observing

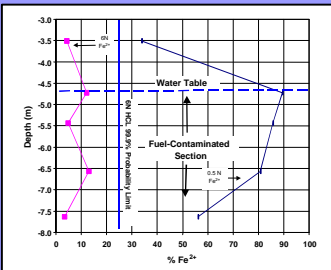


Figure 3.15

the ratio of Fe^{2+} to total Fe can aid in identifying zones of significant Fe^{3+} reduction. Figure 3.15 uses the exact same data set as in Figure 3.14 but Fe^{2+} is shown as a percent of the Fe total for both the WAS and SAS extractions. For WAS data this ratio shows the amount of easily extractable iron (~bioavailable iron) that has been converted to Fe^{2+} by direct enzymatic reduction or secondary abiotic reduction with sulfides. For the SAS data, this ratio approximates the amount of Fe^{2+} inherent in the sediment. As shown, data from the SAS ratio can be used to calculate a 99.9% statistical cutoff, forming a baseline for examining the Fe^{2+} % in the WAS extraction as:

$$(23) \quad \hat{x}_p = \bar{x} + Z_p * s$$

Where:

\hat{x}_p = 99.9% percentile of the 6N HCl Fe^{2+} %

\bar{x} = 6 N HCl Fe^{2+} sample average

Z_p = 99.9% percentile of the standard normal distribution; and

s = Sample standard deviation

The 99.9% percentile establishes a limit value which a sample could only be expected to exceed by random chance 1:1,000 times.

As shown on Figure 3.15 the fraction of WAS Fe^{2+} to total Fe increased from about 34% to approximately 90% below the water table, indicating probable Fe^{3+} reduction occurred in that area for the mild acid extraction data. Alternatively, the SAS Fe^{2+} ratio averaged only 7.5% (not exceeding 15%) for the same interval. Thus, only a small fraction of the bulk iron in this system is in the Fe^{2+} form.

SAS Fe^{2+} is comprised in part by any precontamination event Fe^{2+} (background) and all WAS Fe^{2+} produced directly or indirectly by microbial activity in response to the contaminant. Thus, the SAS Fe^{2+} ratio will increase in iron reducing portions of a plume, making the apparent background concentrations of Fe^{2+} and the statistical baseline more conservative. Where possible, it is advisable to examine Fe^{2+} ratios from non-contaminated portions of the aquifer to aid in establishing background conditions. Note that obtaining such sediment samples from different geographic areas of an aquifer is not necessarily

ideal, because true background conditions may not be represented due to spatial heterogeneity in mineralogical composition inherent in any aquifer. Also, subsequent interpretation is still required to discriminate Fe^{3+} reduction from naturally occurring soil organics versus reduction brought on as a result of organic contamination.

Figure 3.16 shows an example of mineral sulfide speciation for a single core hole taken near the base of a landfill. The drilled section was typical fluvial consisting of unconsolidated coarsening downward sediments. Low-density organics were present near the top of the water table and higher density organics were confined to an area near the base of the aquifer above a bedrock confining layer.

As shown, the technique presented here can discern independent trends for AVS and CrES using actual sediments. Both AVS and CrES concentrations are low (< 1 mg/Kg) above the water table. Concentrations of both AVS and CrES peak below the water table. Deeper in the aquifer, AVS decreases to background levels, except through the basal gravel zone, where concentrations increase again. CrES levels remain high above the clay zone, but drop to

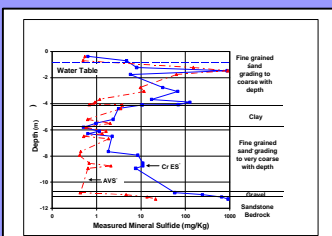
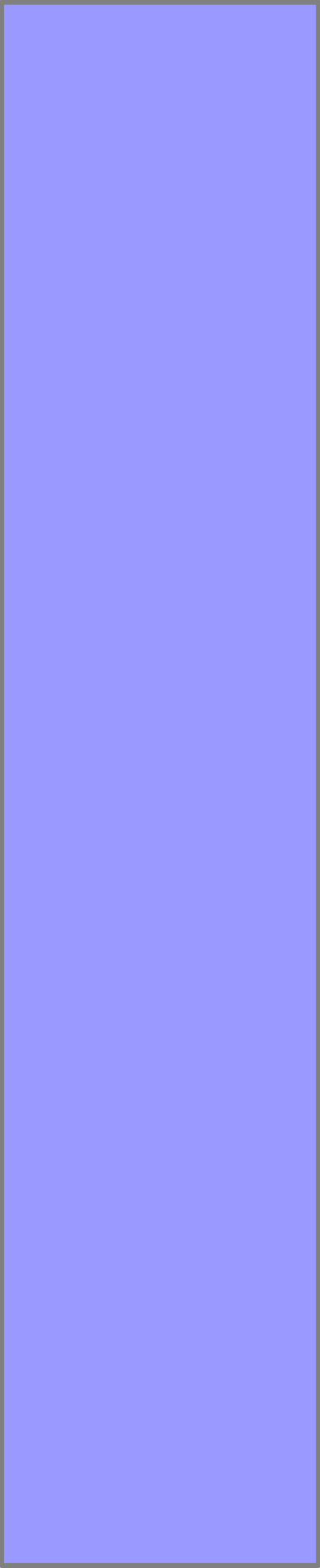


Figure 3.16

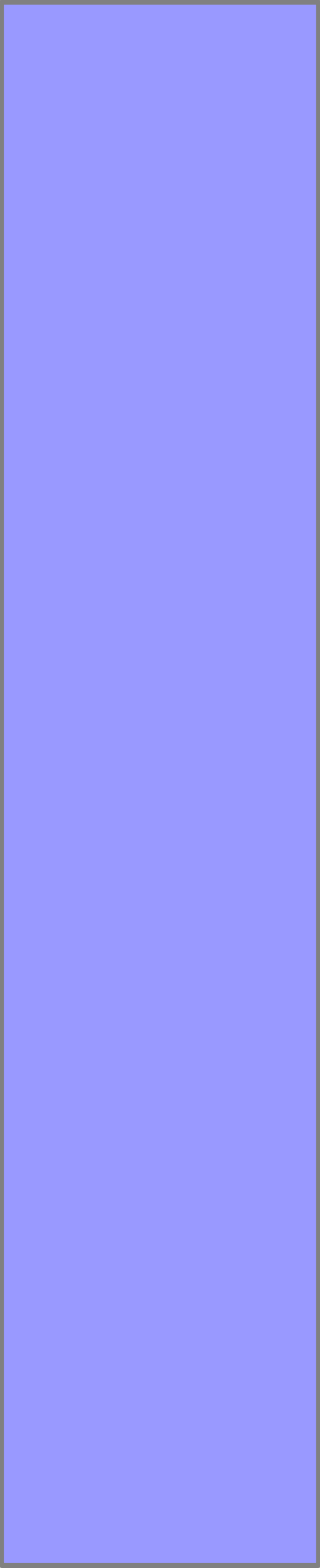


background in the clay. Below the clay layer, CrES levels increase again, reaching a peak in the gravel layer.

The pattern of AVS suggests recent SO_4^{2-} reduction just below the water table and at the base of the aquifer. The pattern of CrES infers past geologic control of SO_4^{2-} reduction and/or organic contaminant migration. High levels of CrES above the clay zone may have been caused by preferential leachate migration in porous sand across the top of the clay layer. Little SO_4^{2-} reduction occurred in the clay layer; however, below that zone CrES levels increased correlative to aquifer grain size. Increased grain size usually equates to increased permeability, which probably enhanced advective mass transport of SO_4^{2-} and/or organic leachate. That condition undoubtedly promoted SO_4^{2-} reduction, which caused increased CrES mineral deposition over time.

3.9. Fe and S Extraction Summary

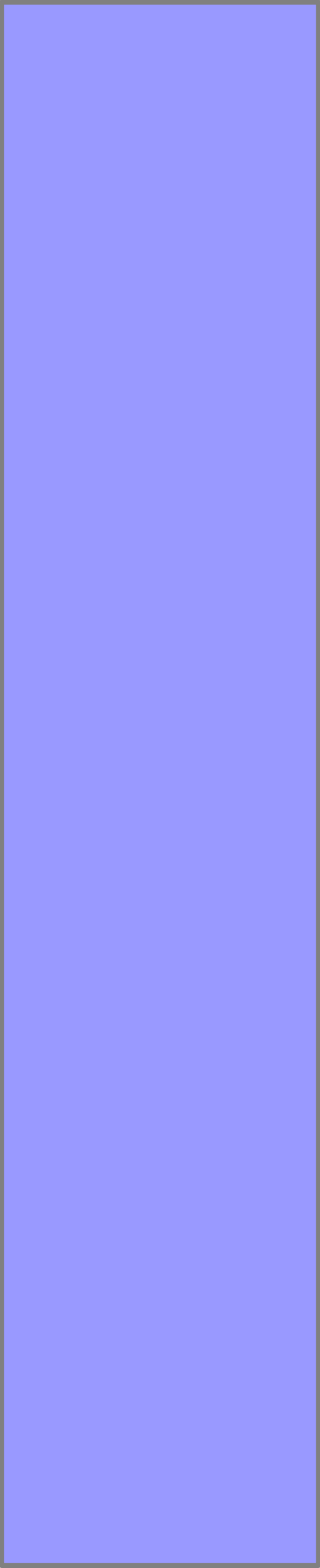
Due to geochemical constraints, many of the microbial processes associated with natural attenuation involving Fe and S are expressed in mineral form. Although SO_4^{2-} is usually aqueous, its reduction often results in the deposition of AVS or CrES solids. Little Fe^{3+} is aqueous at



normal pH and much produced Fe^{2+} precipitates in mineral form. Therefore, it is logical that natural attenuation studies should include mineral Fe and S analysis to determine expressed and assimilative capacity. Difficulties in mineral sample collection and analyses have probably inhibited routine mineral Fe and S evaluation and simplified methods were needed.

The methods presented to collect and preserve sediment samples for subsequent Fe and S mineral analysis are practical and effective. Grab samples can be more easily preserved in the field by transferal to serum bottles. These bottles can be sealed and purged with nitrogen to prevent further exposure to oxygen.

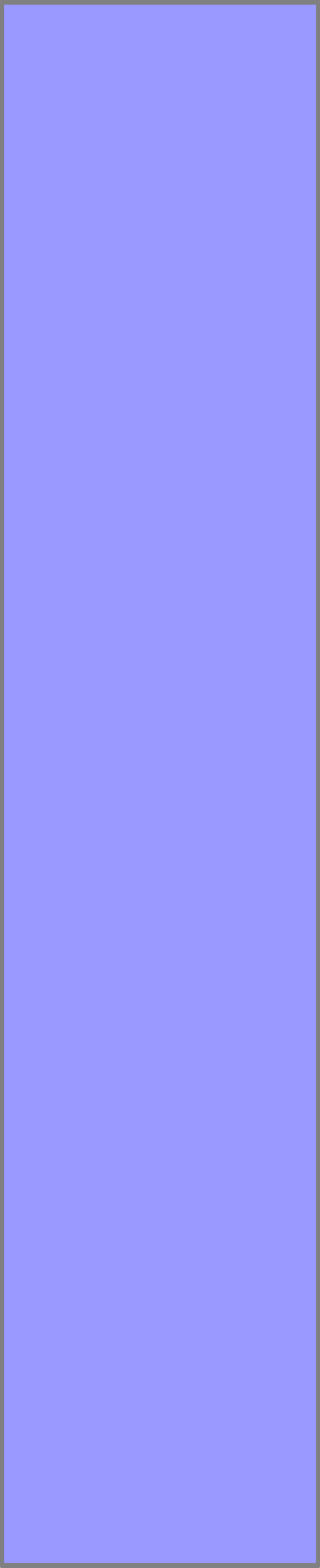
Laboratory testing with pure mineral forms using WAS, suggests substantial extraction of the primary reactive iron forms between 24 to 48 hours without extracting a large percent of the more crystalline Fe minerals that commonly constitute bulk iron mass in sediments. Due to the nonspecific nature of the extraction process, and many other factors, a chemical determination of the biologically available Fe^{3+} or biogenically produced Fe^{2+} minerals is largely



subjective. However, Fe^{3+} minerals that are prone to microbial reduction are more easily extracted by weak acid attack. Additionally, certain biologically precipitated Fe^{2+} minerals can also be extracted..

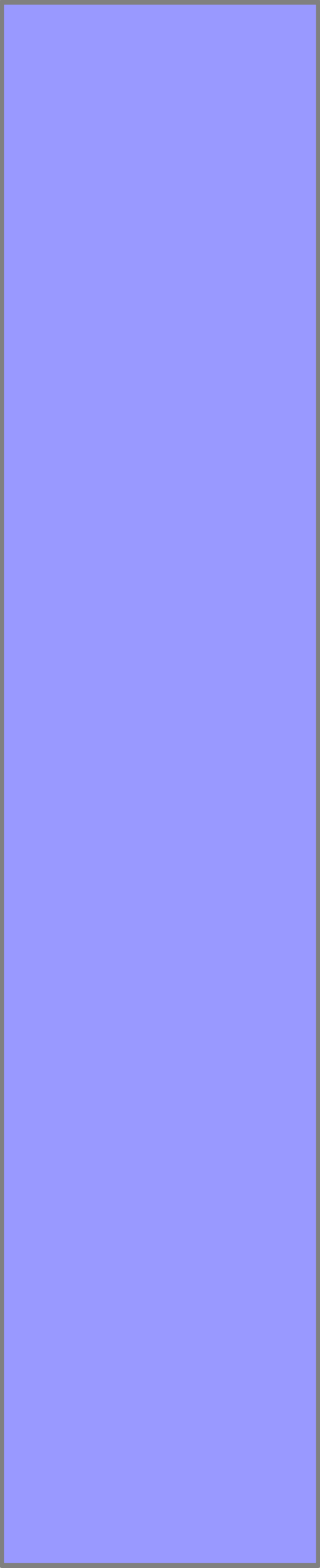
Identifying areas where Fe^{3+} reduction occurred can be difficult when examining mass concentration data, such as mg/Kg, although data presented in that form is often important for an intrinsic bioremediation study. Evaluating the ratio of Fe^{2+} to Fe total can aid in identifying areas where significant Fe^{3+} reduction occurred. Tests on actual samples commonly showed Fe^{2+} to total Fe ratios less than 50% in noncontaminated areas but between 80 to 100% in contaminated areas.

Data from field tests suggests that the WAS extraction technique used on these sediments recovered the biogenically produced Fe^{2+} mineral species without overly extracting background iron, which is largely comprised of Fe^{3+} species. Had the extraction time been too long, lower WAS Fe^{2+} to total Fe ratios would be expected, reflecting unwanted dissolution of background Fe^{3+} . The fact that the Fe^{2+} ratio approaches 100% in these contaminated areas



also suggests that the WAS extraction procedure described here is a reasonable approximation of the biologically available Fe^{3+} fraction.

Comparing the Fe^{2+} to Fe total ratios between the SAS and WAS extractions may aid in differentiating zones where Fe^{3+} reduction has occurred. Microbial Fe^{3+} reduction often only converts a small amount of the total Fe present in a sediment to Fe^{2+} . In non-contaminated areas the Fe^{2+} to Fe total ratios are approximately the same for both the strong and weak acid extractions for the same sediment. However, in contaminated areas, where Fe^{3+} reduction has occurred, the Fe^{2+} ratios increase for WAS extractions but remain about the same for SAS. Therefore, SAS data can be used to develop a statistical probability limit. This limit can serve as a benchmark to evaluate the significance of WAS Fe^{2+} ratio data. Interpretation is still required, however, to discriminate between Fe^{3+} reduction from naturally occurring organics versus that occurring as a result of organic contamination. Also, this comparative technique may not work in Fe limited sediments where the amount of Fe total extracted using SAS and WAS are similar.



Background conditions could also be established by comparing WAS values from contaminated and noncontaminated areas; however, spatial variability may make such analyses difficult.

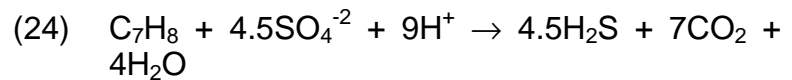
The extended sulfide analysis method proposed here is simplified in that it only quantifies AVS and CrES; however, for most natural attenuation studies this level of discretion is adequate. The room temperature, closed system method of sulfide trapping is greatly simplified over previous methods and permits many samples to be prepared and evaluated per day. The resulting AVS data is used as a general indicator of recent SO_4^{2-} reduction, whereas high CrES concentrations suggests older microbial activity. AVS plus CrES yields a total Fe sulfide mass number that can be used to determine expressed capacity in natural attenuation studies.

4. AMIBA DATA ANALYSES

4.1. Expressed and Assimilative Capacity

Expressed capacity (EC) is a measure of the amount of contaminant degraded by past biodegradation, based on electron acceptor (EA) reduction or expressed product (EP) buildup in and downgradient of a plume. Assimilative capacity (AC) is a measure of the amount of contaminant that can potentially be degraded via a given EA, based on EA concentrations within or downgradient of a plume. Functionally, AC only has significance if contaminant oxidation is limited by electron acceptor availability or arrested if a required electron acceptor is unavailable. Otherwise, kinetic degradation rates govern contaminant decay. EC, however, is a direct measurement of the amount of contaminant that has been degraded by microbial processes (excluding methanogenesis) and is a general indicator of past degradation efficiency. Both EC and AC are described in terms of the amount of contaminant required to balance a specified amount of EA or respiratory EP

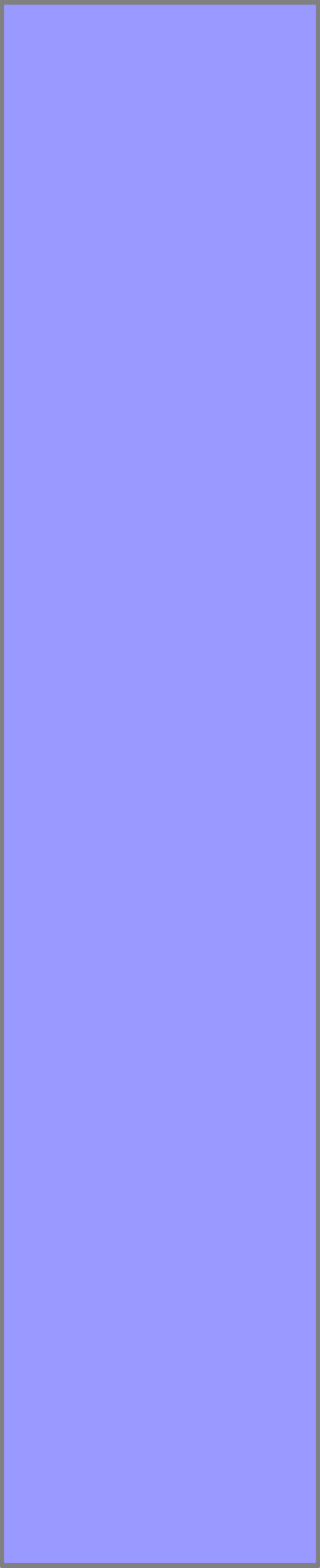
according to chemical stoichiometry. The chemical balance for common fuel components with respect to common subsurface electron acceptors are shown in Wiedemier et al., 1999. By way of example, regard the following equation:



By stoichiometry it can be seen that for every 4.5 moles of SO_4^{2-} one mole of toluene (C_7H_8) could theoretically be degraded. Thus, the moles of sulfate found in groundwater divided by 4.5 yields the assimilative capacity of sulfate for toluene. Conversely, every 4.5 moles of S^- found in the environment could represent one mole of toluene that has been degraded. Thus, the moles of S^- found in a system divided by 4.5 equals the equivalent amount of toluene degraded and is the expressed capacity of sulfate for toluene.

4.2.Expressed and Assimilative Capacity – Aqueous Compounds

To calculate EC based on aqueous EAs (O_2 , NO_3^- , or SO_4^{2-}) or aqueous EPs (Fe^{2+}), the mass of contaminant degraded via compound i is estimated as:


$$(25) \quad C_i = \frac{MR_i}{MW_i} \sum_{j=1}^J (A_{ij} V_j n_j)$$

Where:

- C_i = Expressed capacity or assimilative capacity as moles of contaminant degraded via a redox reaction involving electron acceptor i ;
- A_{ij} = Effective concentration of electron acceptor compound i in volume j , mg/L;
- V_j = Descretized unit volume j (i.e., a unit cell) of the subsurface and where the sum of V_j over all j is the total volume of interest under the study area, (convert volume in m^3 to L);
- n_j = Porosity of volume j (a single porosity will often be used for an entire site making this term constant);
- MR_i = Molar ratio of the contaminant to an electron acceptor or expressed product i , as determined by stoichiometry; and

MW_i = Formula weight of electron acceptor or expressed product i, mg/mole.

To determine EC, A_{ij} is calculated as the absolute value of the background concentration minus the concentration in volume j or:

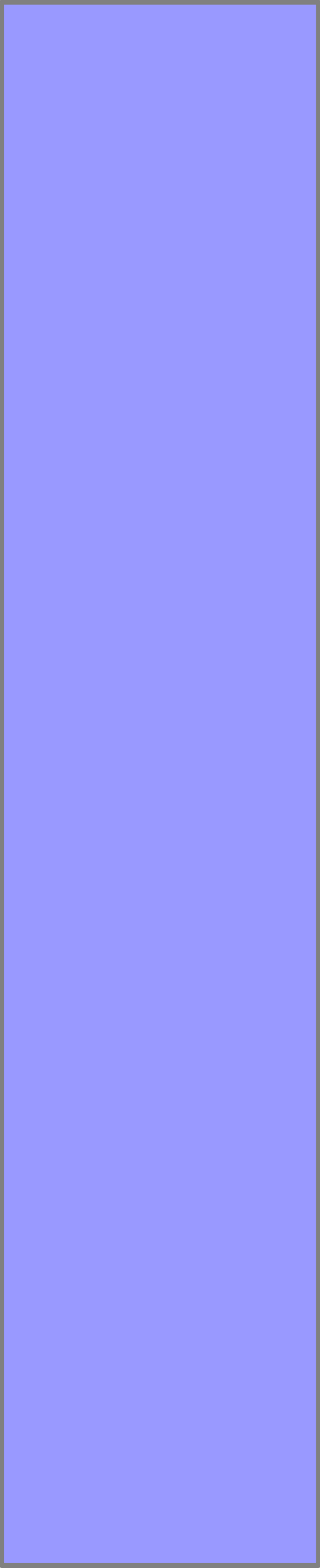
$$(26) \quad A_{ij} = |\bar{m}_j - B_i|$$

Where:

\bar{m}_{ij} = Average concentration of EA or EP i in cell j

B_i = Background concentration of Ea or EP i

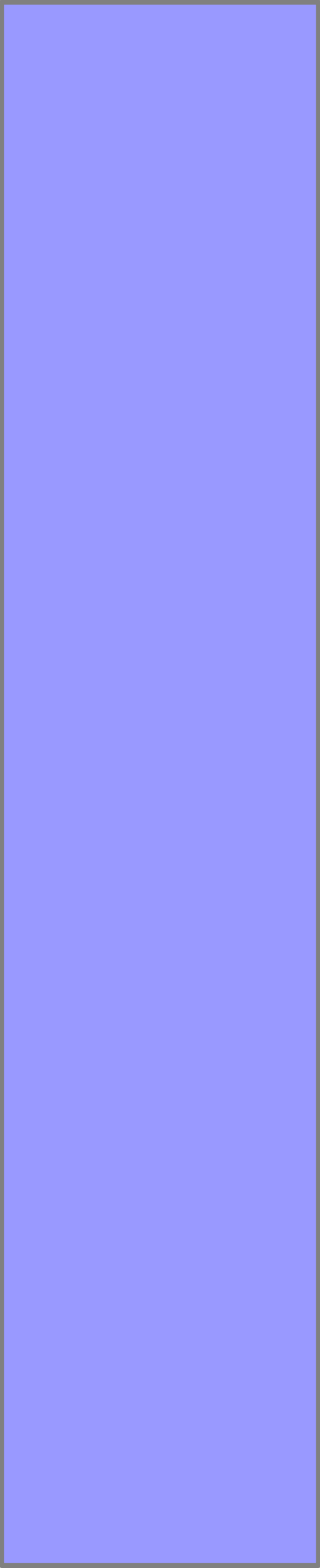
Thus for EC calculation, A_{ij} is the concentration of aqueous EA consumed by biodegradation processes. However, for O_2 , NO_3^- and SO_4^{2-} the EA concentrations will decrease in the plume whereas; dissolved Fe will increase. Thus, using aqueous data the decrease in Fe^{3+} is indirectly measured as the increase in dissolved Fe^{2+} . Similarly, AC is determined where A_{ij} is the concentration of the EA in the cell minus the minimum concentration found in any cell giving the EA available for potential microbial use. The



background concentration is often estimated from one or more up gradient monitoring well(s).

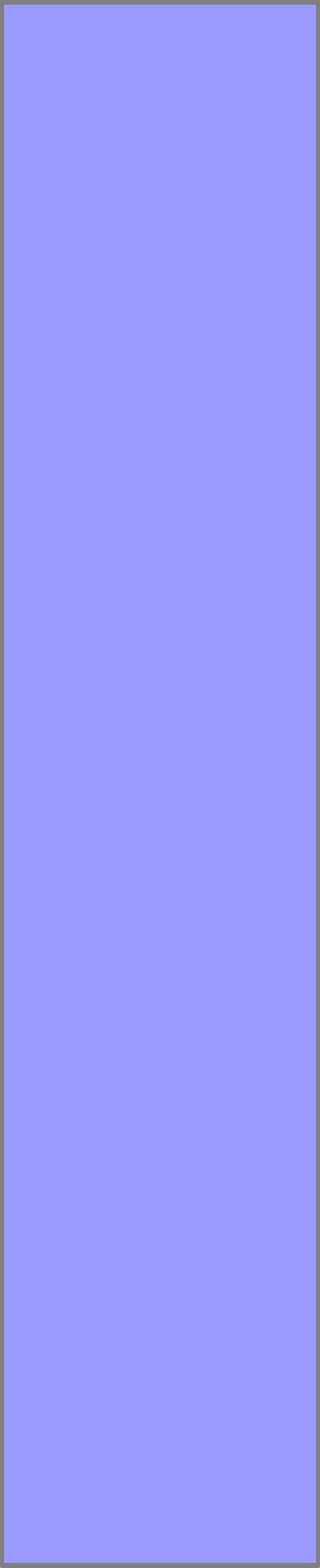
Simply stated then, the expressed capacity or assimilative capacity for an aqueous electron acceptor can be determined by dividing the aquifer into discrete units of known volume, normally m^3 is calculated then converted to L. Each cell is assigned an average estimated effective concentration of an electron acceptor. Porosity times cell volume yields the liquid water volume in the cell, typically expressed in terms of liters. Liquid water volume times effective concentration (mg/L) yields the mass of electron acceptor consumed. This is then converted into the equivalent amount of contaminant consumed by multiplying by the stoichiometric ratio of electron acceptor consumed to organic destroyed divided by the formula weight of the electron acceptor. This process is then repeated for all the cells in the study area, which are then subsequently summed to produce the Ci.

EC estimation methods based on aqueous compounds rely on the EA depletion zone or EP plume created by biodegradation. As groundwater passes through



a contaminated zone, aqueous EAs are consumed and aqueous products generated. This consumption and generation can be observed down gradient, in groundwater that passed through the contaminated zone. However, EA depletion zones and EP plumes are not complete reflections of past biodegradation. For EAs, diffusion and dispersion will replace some of the EAs down gradient. Precipitation of S and Fe minerals will reduce the dissolved EP concentrations down gradient for Fe^{3+} and SO_4^{2-} reduction. The EPs for O_2 and NO_3^- (principally CO_2 and N_2) are also transient and nonspecific in groundwater. In all cases, aqueous data will tend to underestimate EC and past biodegradation. As discussed below, evaluation of EP precipitants should be used to document much more EC for Fe^{3+} and SO_4^{2-} reduction directly, and indirectly for O_2 and NO_3^- . **Thus, Equation 25 should not be used for EC calculation when solid mineral data are available.**

Equation 25 can be used to estimate AC for O_2 , NO_3^- , and SO_4^{2-} ; however, such estimates are inherently conservative, because the effects of ongoing advection and diffusion are ignored. This problem can be corrected by



including the amount of aqueous EA contained in the volume of water that will pass through the plume volume during some future period of interest. If such a dynamic approach is desired then the use of a reactive mass transport model such as Bioplume III (Rafai et al., 1997) may be appropriate.

Equation 25 should never be used to calculate Fe^{3+} AC because Fe^{3+} is practically insoluble at normal pH.

Thus, in summary, aqueous data from groundwater sampling is of limited utility in directly calculating EC or AC.

This approach:

- Can yield a highly conservative estimate of expressed capacity but is not strongly recommended;
- Should not be used to calculate EC if mineral data are available;
- Can yield a highly conservative estimate of assimilative capacity but a reactive mass transport model should be considered for this function;
- Should never be used to calculate AC of Fe^{3+}

4.3.Expressed and Assimilative Capacity – Solid Compounds

Precipitated EPs represent a cumulative record of past biodegradation. Thus, for SO_4^{2-} and Fe^{3+} reduction, EC is best calculated using the solid EPs including AVS, CrES,

and WAS Fe²⁺. The EC and AC for Fe³⁺ and the EC for SO₄²⁻ based on mineral analyses can be determined using:

$$(27) \quad C_i = \frac{MR_i}{MW_i} \sum_{j=1}^J (S_{ij} V_j \rho_{dj})$$

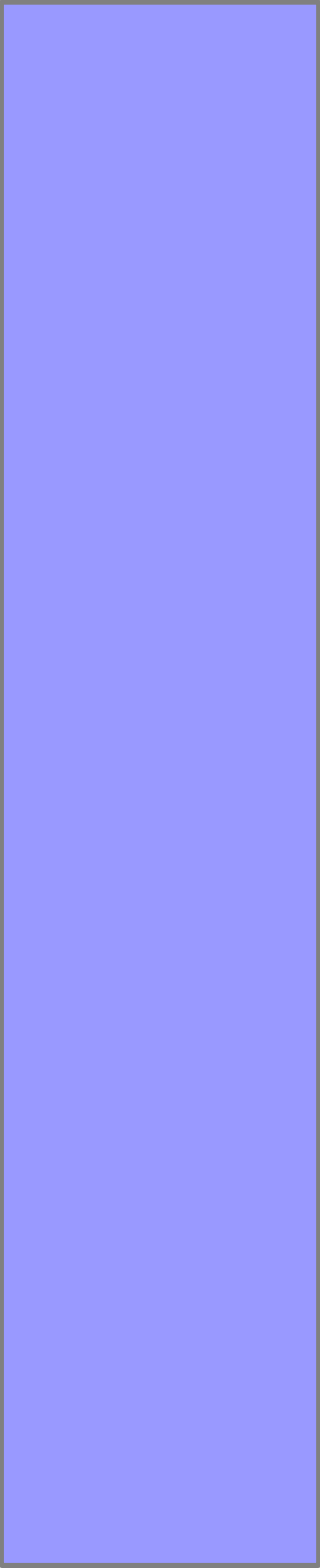
Where:

S_{ij} = Effective concentration of solid EP or EA compound i in volume j, mg/kg.

V_j = Volume of unit cell (m³)

ρ_{dj} = Dry density of volume j (mass of dry sediment per volume of j), kg/m³. A single dry density is often used for an entire site and this density includes the effect of porosity.

For Equation 27 the aquifer system is divided into n discrete cells of known height, width, and depth to calculate a defined volume. Cell volume times the density yields sediment mass. The cell average of effective EA and/or EP times sediment mass yields EA or EP mass per unit cell. EA



or EP mass is then transformed to AC or EC, respectively, by simple units conversion. The AC or EC for each cell is then added to calculate the total for the study area.

C_i is in terms of assimilative capacity (AC) if oxidized WAS Fe^{3+} concentrations are used for S_{ij} and C_i is expressed capacity (EC) if EPs are used for S_{ij} (AVS, CrES, and WAS Fe^{2+}). Also, as above, S_{ij} for EC must be determined as the measured EP minus the reduced background concentration for that electron acceptor (Equation 26). Background concentrations of S as FeS will normally be zero in oxidized, uncontaminated sediments. Usually, there is zero background S as FeS_2 and S^0 , however, these minerals are more stable in the subsurface than FeS and could be present naturally. If S as FeS_2 and S^0 is present, a typical background concentration can be determined by averaging results from a number of up gradient locations. Thus, S_{ij} for sulfur minerals is determined by subtracting the concentration in volume j from the average background concentration.

Determining S_{ij} for iron EP can be slightly more difficult. Both Fe^{2+} and Fe^{3+} minerals are naturally present in many subsurface environments, contaminated and pristine. Their concentrations, total and relative, may vary greatly based on depositional or diagenic factors that predate the contamination event. Because the kinetics of Fe^{3+} reduction is typically first order, the mass of Fe^{3+} consumed, or Fe^{2+} produced, is a function of the initial concentration or mass of Fe^{3+} present in the system and the reaction rate, or:

$$(28) \quad C_t = C_o * e^{-k*t}$$

Where:

- C_o = Initial concentration of Fe^{3+} , assumed to be equivalent to Fe total.
- C_t = Concentration of remaining Fe^{3+} at time t or Fe^{2+} produced as $(C_o - C_t)$.
- k = Rate constant for Fe^{3+} reduction.
- t = Time

Thus, given Fe^{3+} reduction occurs for the same period of time, two areas with different initial concentrations of Fe^{3+}

will have different absolute concentrations of Fe^{2+} or residual Fe^{3+} . Then, if C_o is variable, it becomes difficult to observe where significant iron reduction has occurred using concentration data alone. But if Equation 28 is rewritten as:

$$(29) \quad C_t / C_o = e^{-k^*t}$$

then the ratio of Fe^{2+}/Fe total (C_t/C_o) is independent of the initial concentration and is a function only of the rate constant and time. Regions where significant Fe^{3+} reduction has occurred can then be readily identified as being where the ratio approaches 100% (usually between 60 and 90%) and background conditions also can be more easily recognized as values normally between 50% and 5% depending on local conditions.

Based on this concept, a normalization and filtering technique is proposed that can aid in discerning areas where Fe^{3+} reduction in response to contaminant oxidation has occurred. To normalize the data, calculate F_j , the ratio of Fe^{2+} to Fe Total from WAS extraction for each sample point. F_j shows the fractional part of the total iron that exists as Fe^{2+} . It is usually recommended that a map or model of F_j

be generated. Determine B, the typical up gradient F_j value, which is usually less than 50% and often in the 10 to 30% range. Within the plume, F_j ratios will generally be higher than 50% if iron reduction has occurred. Determine S_{ij} using the equations:

$$(30) \quad S_{ij} = 0 \quad \text{if } F_j \leq B$$

$$(31) \quad S_{ij} = (F_j - B)Fe_T \quad \text{if } F_j > B$$

Where:

F_j = The ratio of Fe^{2+} to Fe Total from WAS in volume j;

B = The typical up gradient F_j value, and

Fe_T = Fe Total, mg/kg from WAS.

Selection of B should be based on background ratios from a number of up gradient locations. The authors have used values ranging from 30 to 50 %. Higher values of B are more conservative.

There is one final wrinkle in determining the EC for Fe. The objective in determining EC is to calculate the total

amount of organic contaminant destroyed based on the observed mass of EP. It has been demonstrated that Fe^{3+} can be reduced abiotically to Fe^{2+} through reaction with HS^- (Equation 16) giving the appearance of enzymatic Fe^{3+} reduction where none has occurred. To correct for this, the mass of Fe associated with measured AVS must be subtracted from the measured Fe^{2+} mass. If measured S_{ij} for iron (determined as above) and AVS are converted to mmoles (divide by 55.85 and 32.1 mg/mMol respectively), then the molar mass of AVS can be subtracted directly from the molar mass of Fe^{2+} to provide the necessary correction.

Finally, the assimilative capacity of Fe^{3+} is easily determined. The S_{ij} is simply the measured Fe^{3+} from WAS extraction. Equation 25 is then directly applied.

4.4. Sulfide Indexing of Aqueous EC

The EC for oxygen and nitrate can be calculated using an alternative method, called *sulfide indexing*. This method is based on the concept that a fixed ratio of oxygen:sulfate and nitrate:sulfate occurs in up gradient

groundwater. As groundwater is mixed with the contaminate via advection, all aqueous electron acceptors are consumed, but only evidence of cumulative sulfate EC remains (as reduced S minerals). The cumulative EC for oxygen and nitrate can be estimated as their respective up gradient sulfate ratios times sulfate EC. The equation is simply:

$$(32) \quad IC_i = C_s * R_i$$

Where:

IC_i = Indexed expressed capacity for compound i, oxygen or nitrate;

C_s = Expressed capacity of from total sulfides (AVS+CrES) calculated using Equation 27 above; and

R_i = Mole ratio of oxygen/sulfate or nitrate/sulfate in background groundwater.

This analysis should provide satisfactory results provided groundwater mass transfer is advection dominated or alternatively where mass transfer via dispersion is not

significantly different between the electron acceptor species of concern.

4.5. Total Expressed Capacity

Total EC is the sum of all expressed capacity (C_i) for all four electron acceptor types or:

$$(33) \quad EC = \sum_{i=1}^n C_i$$

Where i = each electron acceptor class evaluated (usually O_2 , NO_3^- , SO_4^{2-} , and Fe^{3+}). For AMIBA, EC should normally be calculated as:

$$(34) \quad EC = C_s + C_{Fe} + IC_o + IC_n$$

Where:

C_s = Expressed capacity of total sulfide mineral sulfide (AVS + CrES) from Equation 25.

C_{Fe} = Expressed capacity of WAS Fe^{2+} from Equation 27.

IC_o = Sulfide indexed expressed capacity for oxygen from Equation 32.

IC_n = Sulfide indexed expressed capacity for nitrate from Equation 32.

As described above, C_i can be determined from aqueous data using Equation 25, but this typically will result in greatly underestimating total EC.

4.6. Hydrocarbon Mass Calculations

One advantage of performing an AMIBA analysis is that hydrocarbon can be more fully characterized with respect to mass and distribution. Such information can then be used in support of natural attenuation or for remediation design, should it be required. For AMIBA, an objective evaluation of expressed capacity must include an evaluation of existing hydrocarbon mass. Total hydrocarbon mass (HC) is simply:

$$HC = HC_s + HC_a$$

Where:

HC_s = Sorbed or oily phase hydrocarbon measured in sediment samples (moles or mmoles).

HC_a = Dissolved phase hydrocarbon measured in aqueous samples (moles or mmoles).

HC_s and HC_a can be determined using:

$$(35) \quad HC_s = \frac{1}{MW} \sum_{j=1}^J (A_j V_j n_j)$$

$$(36) \quad HC_a = \frac{1}{MW} \sum_{j=1}^J (S_j V_j r_{dj})$$

Where:

MW = Molecular weight of hydrocarbon

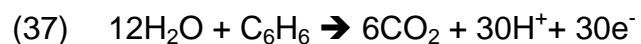
A_j = Aqueous concentration of hydrocarbon (mg/L)

S_j = Sorbed and oil phase concentration of hydrocarbon (mg/Kg)

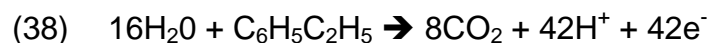
The term MW defines the hydrocarbon in terms of mole mass. MW is simply the molecular weight of the constituent of concern, where only one hydrocarbon constituent exists. However, where a mixture of organics is

present an “average” molecular weight should be considered for MW. For example, toluene ($C_7H_8 = 92 \text{ g/mol}$), as a seven-carbon compound represents a reasonable average carbon compound considering the C5 to C12 range typically quantified in total petroleum hydrocarbon and the C6 to C8 composition for BTEX. Recommendations for average fuel composition are found in Wiedemeier et al., 1999.

AMIBA results are not strongly influenced by the selection of an average hydrocarbon compound because the consumption of electron acceptors with respect to hydrocarbon oxidized is fundamentally dependent on the oxidation state of carbon, which does not vary much for most fuel constituents. For example, observing the half cell reactions for benzene:



and ethyl benzene:



one observes that an average of 5.0 and 5.25 electrons per carbon atom are transferred, respectively, to fully oxidized each compound. This constitutes only a 5% error difference between the two extreme endpoints.

4.7. Index of Expressed Capacity

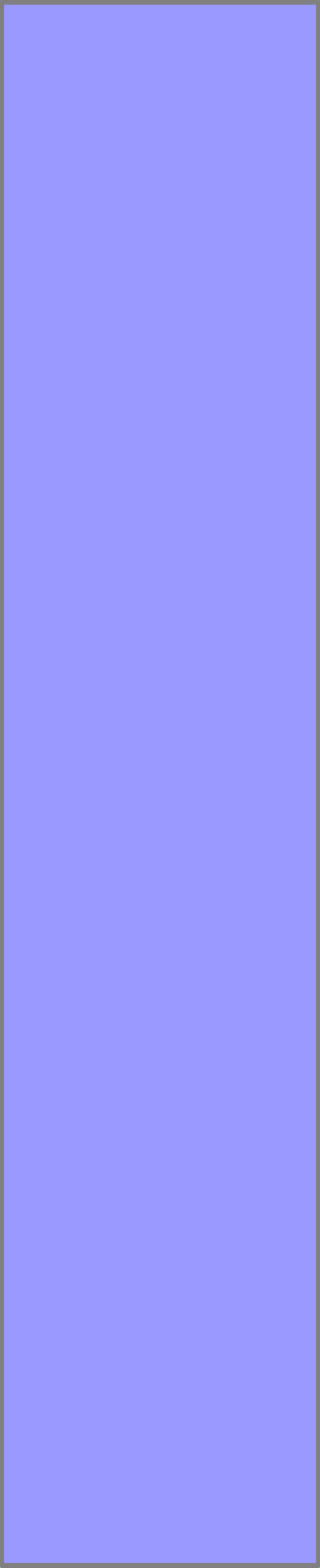
With the incorporation of mineral data, EC can be determined with reasonable accuracy, then used to generate an index of overall biodegradation efficiency. For practical purposes, EC is less than or equal to the mass of total hydrocarbon constituent degraded by biological processes. The total amount of fuel spilled at many sites is unknown; however, the original hydrocarbon mass can be estimated by adding the current hydrocarbon mass to the hydrocarbon mass estimated from the EC equations. An index of expressed capacity (ECI) can then be determined as:

$$(39) \quad ECI = 1 - \frac{EC}{HC + EC} * 100$$

Where:

ECI = Index of expressed capacity, fraction;

EC = Total expressed capacity;



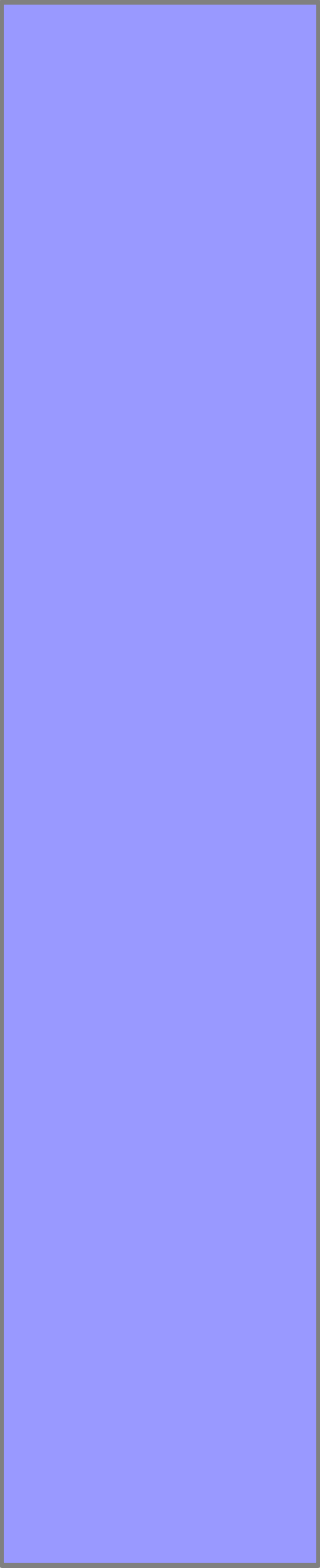
HC = Current hydrocarbon amount, estimated from sediment and groundwater analysis.

EC and HC can be expressed in any consistent units (moles, kg, lb, L, gallons).

Any EC estimation based on EAs and EPs is conservative because it does not take into account incorporation of contaminants into cell mass, degradation to recalcitrant intermediate metabolites, or methanogenesis. EC estimation based on aqueous EAs is also conservative because AEs diffuse and disperse into the AE plume. EC estimation based on EPs is also conservative because it does take into account any loss of EP to the environment or cycling processes.

4.8. Geostatistical Approach

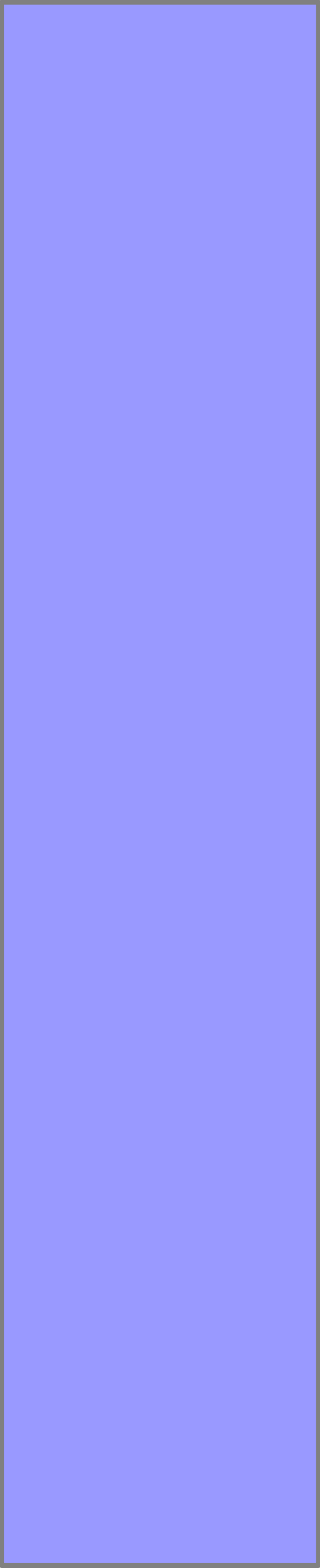
AMIBA relies on spatially distributed mineralogical and aqueous data. To be useful, this data set must be interpolated across a defined region of the aquifer. There are two fundamental methods of data interpolation, deterministic and geostatistical. Deterministic methods include hand contouring and certain mathematical methods



including inverse distance or minimum curvature. With the deterministic approach, one assumes a relationship exists between the data. If a computer contouring program is used, the data are interpolated based on a single arbitrarily assigned weighting function. The results of deterministic modeling are assumed to represent reality and cannot be described probabilistically.

Geostatistics is a relatively new mathematical discipline largely brought to the forefront by Matheron (1971). Its main contribution is that it suggests how to weight the data, compute best estimates, and place error bounds on those estimates. Before interpolation, the data are examined to ascertain if there is a spatial relationship and if so, what is the best mathematical function to describe that relationship. That unique function is used for interpolation. The output is expressed in terms of the “most probable” value and can be described probabilistically with, for example, error boundaries.

Advances in geostatistics and subsurface visualization have been realized in the early to middle



1990's. Much of this progress has been focused on the petroleum industry, where substantial fiscal resources make research and development in advanced computer software economically feasible. However, the analysis of environmental data can be directly benefited from this technology. Sophisticated geostatistical programs were initially written almost entirely for high-end, and unfortunately, expensive workstations. However, rapid advances in personal computers make operation of such software on inexpensive desktop systems possible. As such, advanced geostatistical software resides no longer in the exclusive domain of a relatively few financially endowed companies but is increasingly becoming widespread and less expensive.

Geostatistics has been aptly described as a guide to the unknown. It is an approach for utilizing observations to make inferences about an unmeasured quantity. Though extremely practical, even a cursory discussion of geostatistical theory is beyond the scope of this document. Rather, this section is written to generally describe and

identify the utility of the approach. Many texts exist on the subject, including Chiles and Delfiner (1999) and Kitanidis (1997).

In traditional mapping approaches, such as hand contouring or deterministic algorithms such as *inverse distance*, one makes the prior assumption that the data distributed in space are in some way correlated. For example, a contour map could certainly be drawn using one water sample taken at random from each state in the U.S. But what does such a map mean if the data are not in fact related? We implicitly understand that an estimated value next to a data point is probably more accurate than one far away, but is there any way to qualify that estimate?

In contrast, a rigorous examination of data are implicit to the geostatistical approach before data interpolation begins. The basis of the Kriging method is variogram analysis (Figure 4.1). A variogram is a graph of the mean square variance of the data as a function of distance or:

$$(40) \quad I(h) = \frac{1}{2N_h} \sum_{x_b - x_a} [z(x_b) - z(x_a)]^2$$

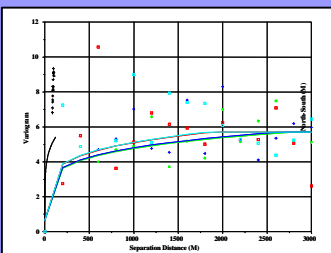
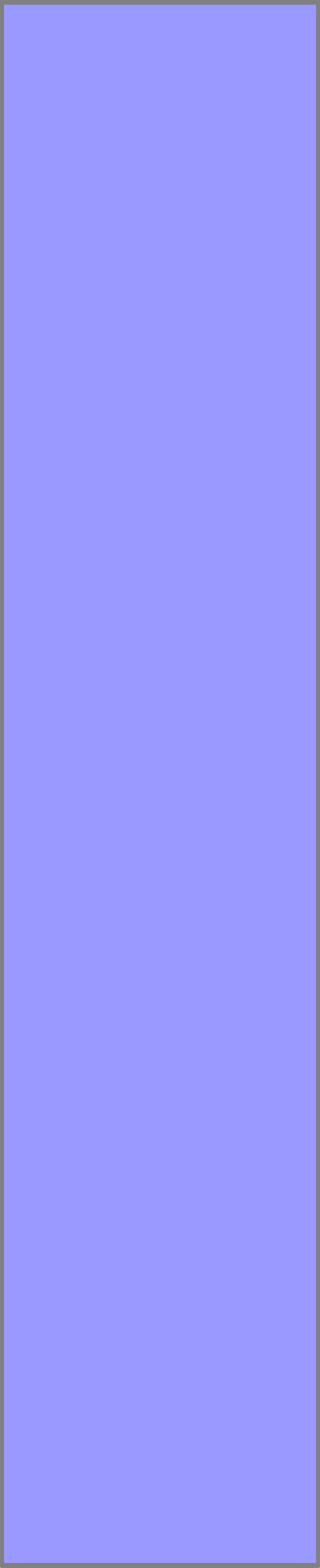


Figure 4.1



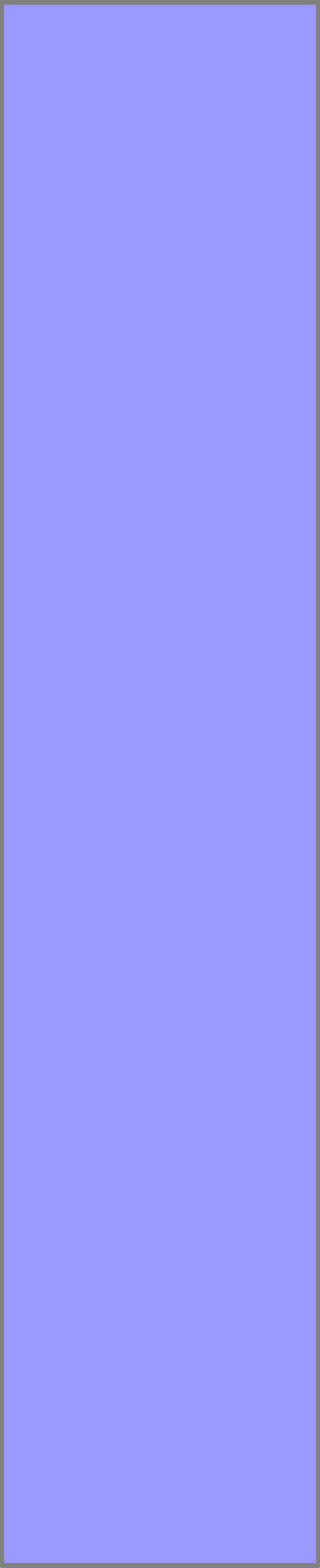
Where

$\lambda(h)$ = Mean square error variance taken for all sample points a given distance or lag h apart.

N_h = Number of data points separated by a distance or lag h .

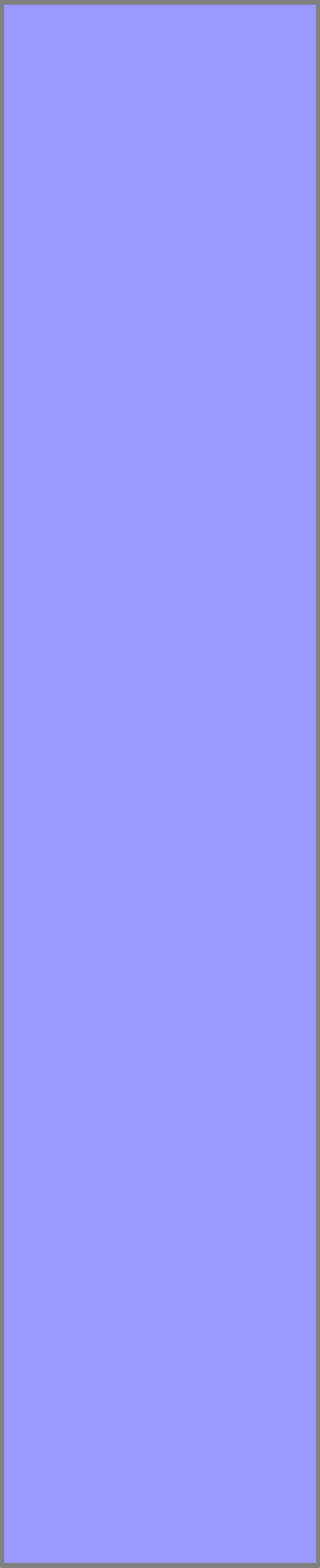
h = Distance between two data points within a range or window of separation $x_\beta - x_\alpha$ apart.

For most spatially distributed geologic data, sampling points that are close together tend to be more similar than points that are progressively farther apart. Therefore, the variance (or difference) between respective data values tends to increase as a function of separation distance. Normally, the variance of geologic data increases as a function of distance up to a certain point known as the *range*. Beyond the range distance, data no longer have spatial correlation to one another and cannot be used to aid in interpolation analyses. The variance for all points beyond



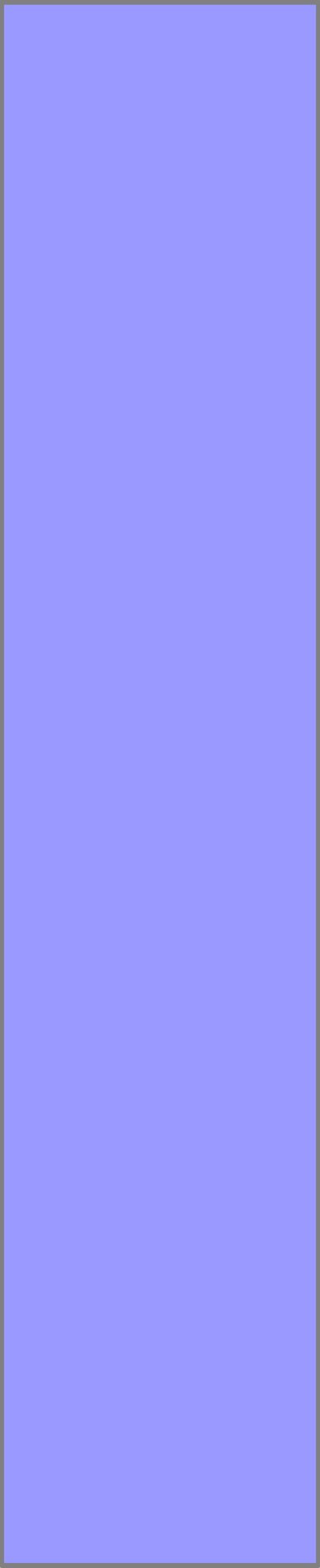
the range is known as the *sill* and is equivalent to the standard sample variance (σ^2) of traditional statistics.

When variance is examined with respect to orientation it can often be seen that there is greater change in one direction as compared to another. This *geometric anisotropy* can readily be seen when vertical and horizontal data are compared. Large changes in data often occur in short distances in vertical geologic section but changes that are more gradual occur in the horizontal plane. Geometric anisotropy can also occur in the horizontal plane alone. For example, in a groundwater plume there is normally less change in concentration with respect to distance along-flow-gradient as opposed to the transverse direction. Many geostatistical software packages automatically generate a series of variograms for cardinal orientations (N-S, E-W, NE-SW, and NW-SE) and vertically. Examination of those variograms can be used to interpret data exhibiting spatial anisotropy.



Solid geologic media is typically heterogeneous, often resulting in seemingly poor analytical repeatability and laboratory QA/QC. Variogram analysis can be used to quantify the quality of spatially distributed data. As mentioned above, variance between geologic data values normally increases as a function of distance. Conversely, for perfect data, as the separation distance decreases to nothing the variance should similarly approach zero. However, when there is variance at a separation distance of zero it indicates sample error. Such error (known as the *nugget*) can be caused by measurement error including laboratory error, spatial location variability, sample variability, or other inaccuracies.

The presence of nugget does not infer that the data cannot be used; rather, such error (if it exists) is implicitly incorporated in the Kriging procedure and influences interpolated results. The data becomes unusable for geostatistical modeling in two cases. The first case is when the nugget approaches the sill, which indicates that the data contains too much error to map. In this case,



review the data or analytical methods to see if errors can be identified and corrected or outliers removed. The second case is when the theoretical variogram is essentially horizontal. This indicates that spatial correlation occurs at a distance less than the minimum sampled interval. In this situation increasing the sample density by, for example, adding additional soil borings may rectify the problem. In either case, the data can only be generally described in terms of standard population statistics, unless a correction can be made. It should be noted that variogram analysis can readily identify problems with sample precision, but not necessarily accuracy, if the causal error is consistent from sample to sample (i.e. if all samples have consistently high or low error).

Data can be interpolated across the study area using the theoretical variogram as the mathematical model to weight the observed data as a function of distance. Two geostatistical methods can be used for this purpose, kriging and conditional simulation. The kriging approach produces a single model or “realization” that minimizes the

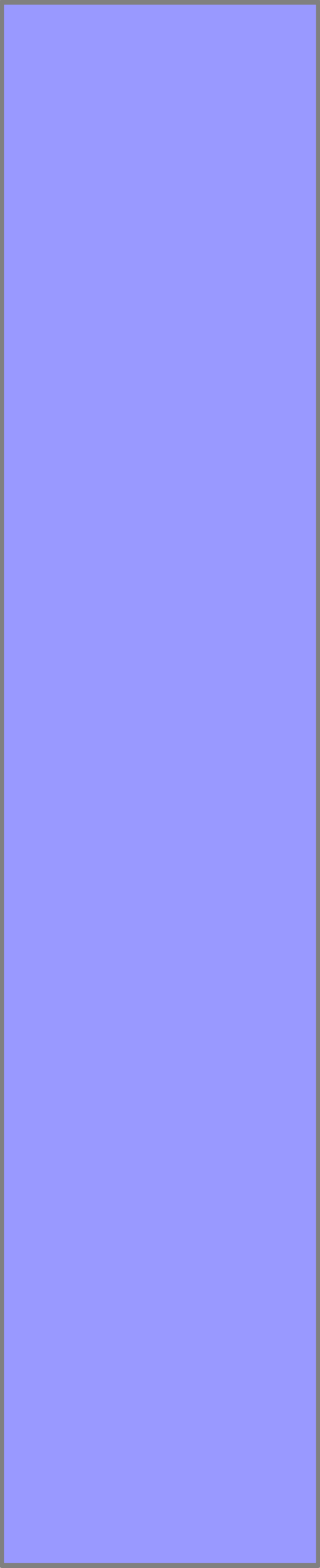
error variance of the estimation. The result is a weighted average representing the most probable realization; however, attribute variability is not preserved. Conditional simulation is a slightly more rigorous approach, where a number of equiprobable realizations are generated, the average of which approximates the kriging estimate. However, using the conditional simulation approach, attribute variability is preserved and probabilistic analyses can be performed.

Although deterministic methods can be used, a geostatistical approach is recommended for AMIBA analyses. Geostatistical analyses require the use of computer software, some of which are referenced on Table 4.1.

4.9. Data Distribution and Dimensional Analyses

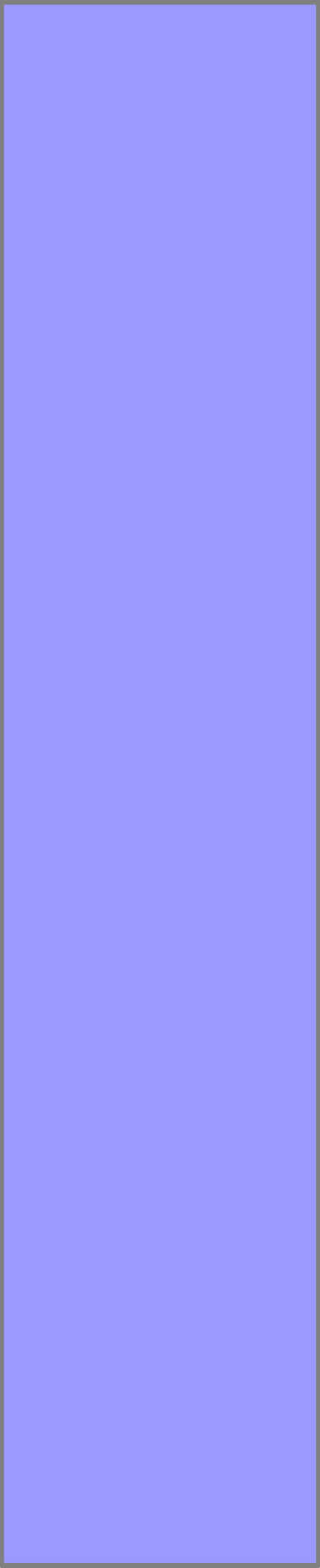
AMIBA analyses are spatial and technically require evaluation of data through a three-dimensional unit of aquifer with components of length, width, and depth. However, within reason, the region of analysis can be user defined and can range from a rigorous evaluation of the entire affected

Table 4.1



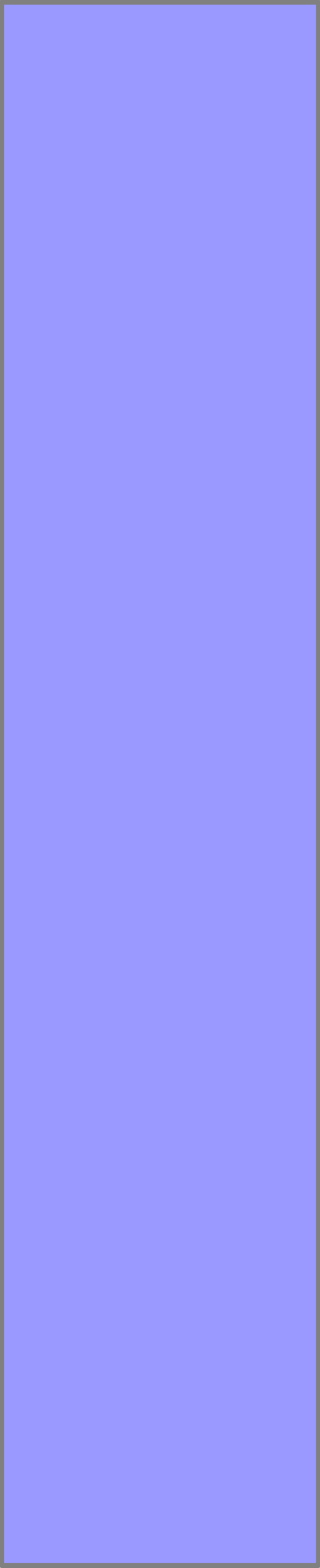
area (as presented below) to a small area immediately around individual bore holes. Input data can be mapped or modeled prior to evaluation in three, two, or one dimensions. Here, the term “model” refers to the physical representation of a spatially distributed attribute that is fixed in space as opposed to a simulation model depicting, for example, contaminant mass transport.

For three-dimensional analyses, the sample frequency and distributed in the x, y, and z plane must be sufficient to allow interpolation throughout the study area, which normally would include all or most of the contaminated geologic section plus background areas. Ideally, geostatistical variogram analysis of the data should be performed to determine data range, sill, and the proper spatial model. When good quality data are properly distributed, spatial interpolation can be performed in three-dimensions. Typically, such analyses cannot be done by hand and require the aid of a geologic modeling program. Such programs can use either a geostatistical or deterministic approach. These programs create a



mathematical framework representing the structural configuration of the aquifer as a series of contiguous cubes, which are then assigned interpolated attribute values.

Three-dimensional modeling provides the maximum potential for data analyses and has the most flexibility and overall utility. A modeled attribute can be visualized in virtual 3D to show subsurface distribution. EC can easily be determined by the direct application of Equations 25 and 27 as the summation of expressed mass calculated on a cell-by-cell basis where A_{ij} or S_{ij} are the modeled concentrations for each individual cell. Most geostatistical modeling programs will export grid values in ASCII format, so evaluation with a spreadsheet program can be done. Normally, 3D modeling software includes the ability to slice the modeled area in any plane to create 2D attribute cross-sections or structural profiles. Because the study area is modeled in all dimensions, the resulting interpolated matrix can be sampled vertically, in a column-wise manner, to calculate attribute average or isopach values that can be represented as 2D maps in the x-y plane. Finally, one-



dimensional point values or column averages also easily be determined for any location in the model domain. Thus, average EC and ECI per column of cells can be presented in a graphical format as concentration vs. distance through the centerline of the contaminant plume. A 3D evaluation can provide a single comprehensive EA and ECI value that can describe the overall status of intrinsic bioremediation for the entire site.

Three-dimensional analysis can be used, provided there is a sufficient density of bore holes and vertical sampling points to warrant interpolation across the model area based on variogram analyses. Many high-end computer programs can perform three-dimensional geostatistical analysis including EarthVision, Property 3D, Geographix, and RSM (Table 4.1). These programs, while certainly robust, may be cost prohibitive. GridStat is also a very versatile three-dimensional geostatistical program. Applied Computer Engineering offers an inexpensive “Student Version” which is fully adequate for most environmental applications.

AMIBA data can also be evaluated with a two-dimensional mapping approach. Two-dimensional analysis in the x-y plane is recommended when:

- Sufficient borehole density exists to provide spatial correlation in the horizontal plane but there is insufficient data in the vertical direction, or
- Sufficient data exists in the x, y, and z planes but a three-dimensional modeling program is not available.

For the two-dimensional modeling approach, all data obtained along each vertical well/boring profile must be averaged to provide a single value representative of the entire soil/aquifer thickness at that point. A weighted average can be calculated using representative vertical packet(s) of strata as:

$$(41) \quad W_{avg} = \sum_{s=1}^n \left(\frac{h_s}{L} \cdot P_s \right)$$

Where:

W_{avg} = Weighted average of vertical sample points for a single soil boring.

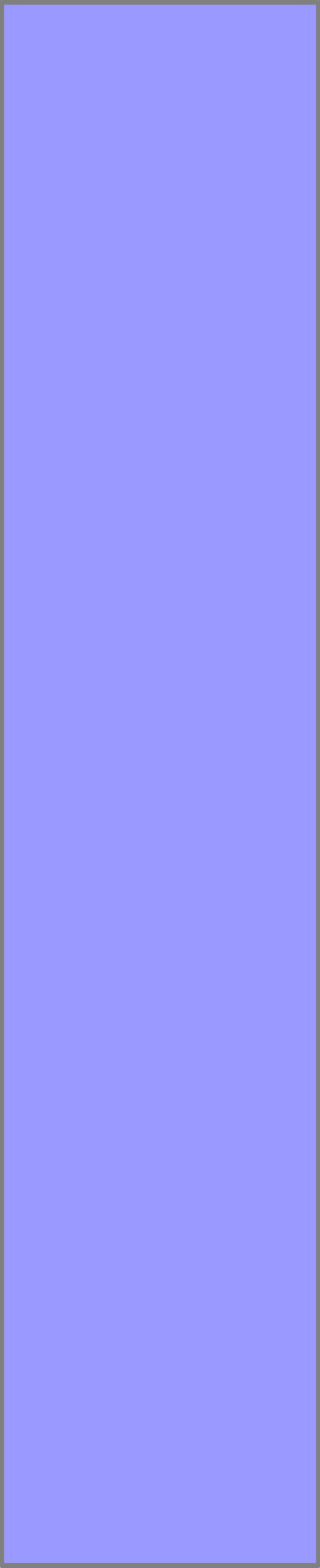
n = Number of sample points in a single vertical soil boring.

L = Total vertical distance over which average is taken which is the sum of the h_s from $s = 1$ to n .

h_s = Thickness of vertical section containing the point sample near the center. For $s = 1$ h_s is equal to the distance from the surface to the midpoint between P_1 and P_2 . For $1 < s < n$, h_s can be taken as the distance between respective mid points P_{s-1} and P_s and P_s and P_{s+1} respectively. Finally, h_n can be taken as the midpoint distance between sample points for P_n and P_{n-1} and the maximum depth of L .

P_s = Point concentration value.

Equation 41 will result in a single “average” concentration value for each soil boring through a user defined thickness that must be the same for all monitoring points in the x-y plane. If samples are taken at equal distances then a simple average can be used. For water samples from monitoring wells, the observed value is

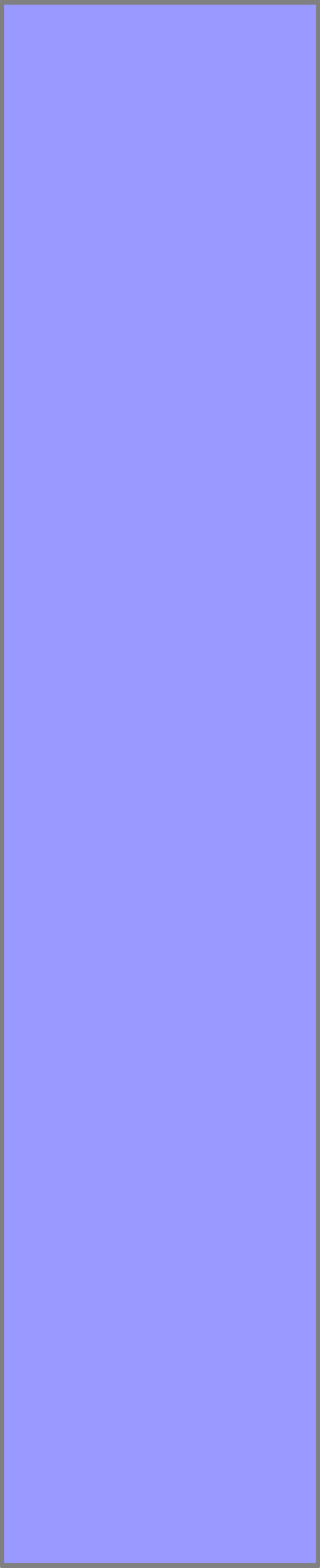


assumed to represent the average value (W_{avg}) across the saturated thickness, which is taken as L .

As the next step, W_{avg} for each monitoring well/boring are then interpolated (mapped) across the horizontal (x,y) plane of the study domain. Any of the 3D modeling programs listed above can make D2 maps, however, simpler mapping programs, such as Surfer or Geo-EAS can also be used. It is also possible to perform such mapping by hand. All of the software programs generate a 2D grid over the mapping domain.

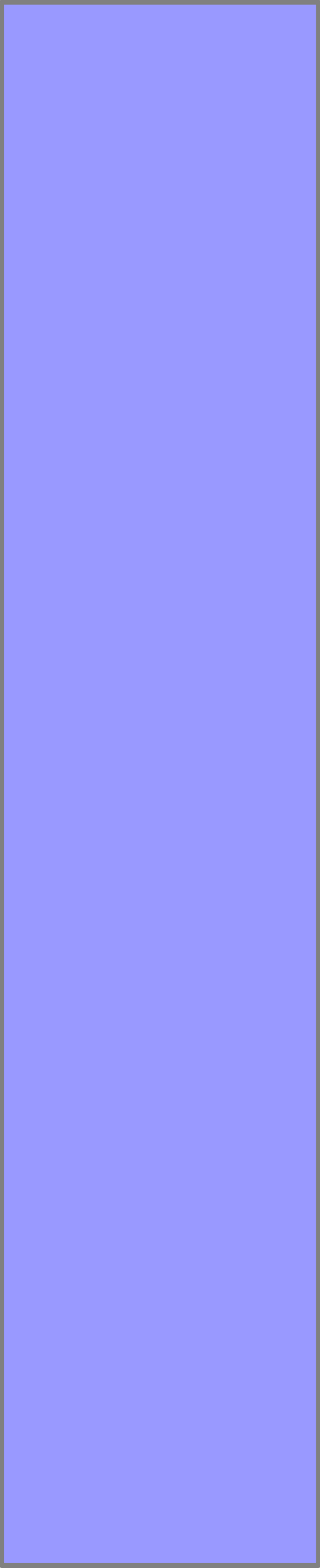
As the final step, Equations 25 or 27 are used. The interpolated cell concentration is used for A_{ij} or S_{ij} and volume (V) is the cell horizontal length \times width multiplied by cell vertical length (L) over which the vertical well/borehole samples were averaged.

Obviously, 3D visualization of the attribute distribution cannot be attained using the 2D approach and concentration profiles are not fully integrated with data outside of the line of section. The 2D approach, however, can show the averaged distribution of the attribute in a map plan perspective.



Concentration profiles must be made individually as cross-sections through soil borings along defined lines-of-section. The 2D analysis, as with a 3D evaluation, will produce a single value for EA and ECI that describes the overall status of intrinsic bioremediation for the site.

Finally, EA can be evaluated one dimensionally around a single monitoring well/bore hole. This option should only be used when the frequency or distribution of monitoring wells/borings is insufficient to reasonably interpolate data two- or three-dimensionally. As above, the average or weighted average of data from the vertical profile of each monitoring well/soil boring must be calculated for A_{ij} and S_{ij} using Equation 27. Interpolation of data along a well profile is possible using mapping/modeling or graphing software or can be performed by hand. As for the 2D case, the length component (L) must be constant for all monitoring wells/soil borings. However, the horizontal length and width components are, within reason, arbitrary. For example, the length and width components of V_j can be calculated based on a meter square or foot square or even a radial area

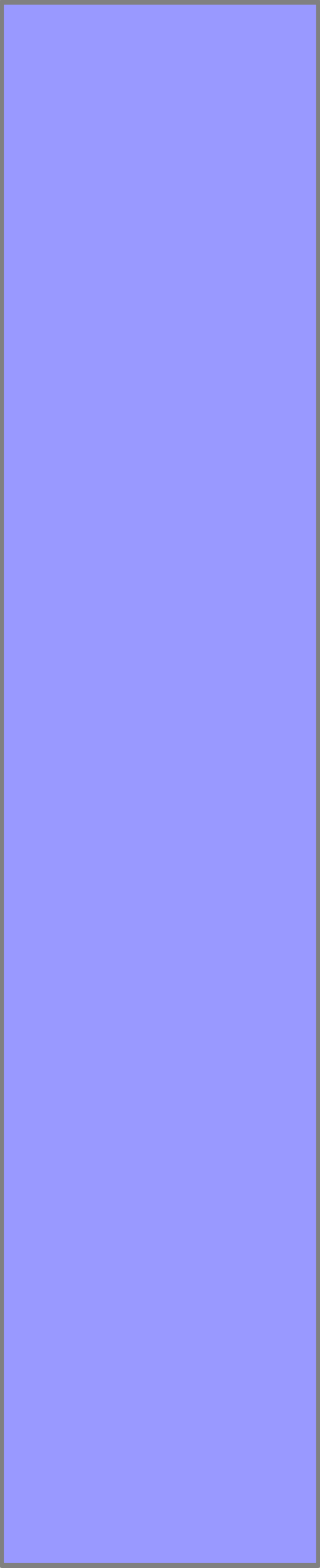


around the well bore, so long as the same dimensional relationship is applied to all monitoring wells/soil borings under consideration in the project.

The total EC and ECI for the site in question cannot normally be determined from a one-dimensional analyses. Rather, EC and ECI must be determined as a local average on a well-by-well basis. EC and ECI can be presented in a graphical format as concentration vs. distance, preferably through the centerline of the contaminant plume. A one-dimensional analysis provides the least amount site information but requires fewer monitoring wells/soil borings, so assessment costs can be reduced.

4.10. Plume Footprint

The usual evidence for a shrinking or stable contaminant plume is two or more sampling events demonstrating that contaminants of concern are not migrating, and that concentrations at the leading edge of the plume are decreasing. The geomicrobial processes described here indicate that reduced sulfide and iron products of microbial processes precipitate near their



generation point, providing a record of past activity. Thus, the spatial distribution of reduced Fe minerals delineates the down-gradient extent of past intrinsic bioremediation processes. As a plume retreats, it can leave behind a trail of reduced mineral species demarking its past location.

When the contaminant distribution is considerably smaller than that of the reduced Fe minerals it may indicate that the plume has reduced in size. This conclusion is subject to site-specific consideration. First, it must be possible to rule out the past presence of contamination from other sources. Second, concentrations of reduced iron in the path of the contaminate plume must be significantly higher than background levels. Finally, it must be possible to rule out the presence of reduced iron through advection as an aqueous species followed by precipitation. This could occur in the absence of precipitating anions or the presence of chelating agents.

4.11. Rate Constant Determination

Several methods are available to estimate biodegradation rates for dissolved compounds including

Buscheck and Alcantar (1995) and the TMB tracer technique outlined in Wiedemeier et al., (1999). Although dissolved phase degradation is important, the estimation of site cleanup is often dependent on the rate of source decay. Determination of a source decay term can be achieved using AMIBA data. Assuming first order kinetics it can be shown that:

$$(42) \quad k = -\ln(C_t/C_o) \cdot 1/t$$

Where:

- k = First order rate constant
- C_t = Concentration mass at time t
- C_o = Original concentration mass at time zero.
- t = Time

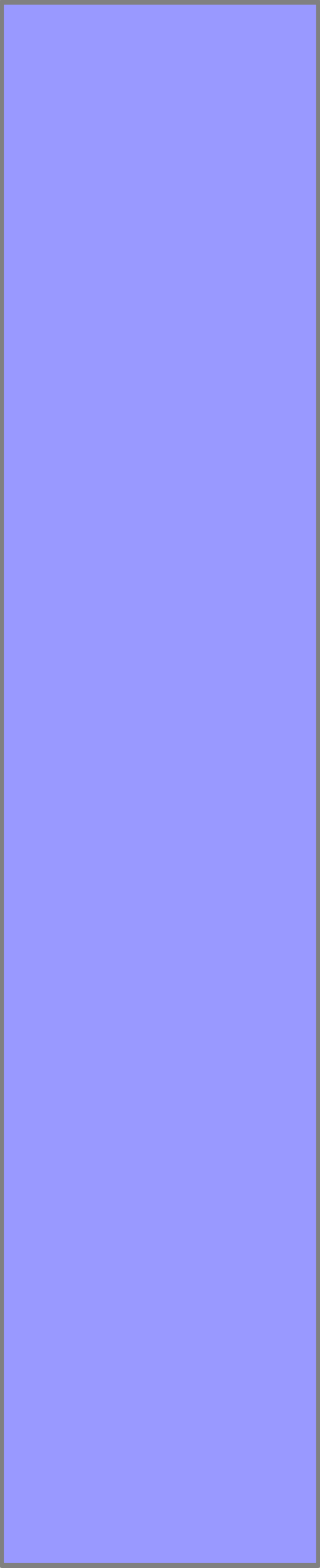
By definition,

$$(43) \quad C_t/C_o = 1 - ECI$$

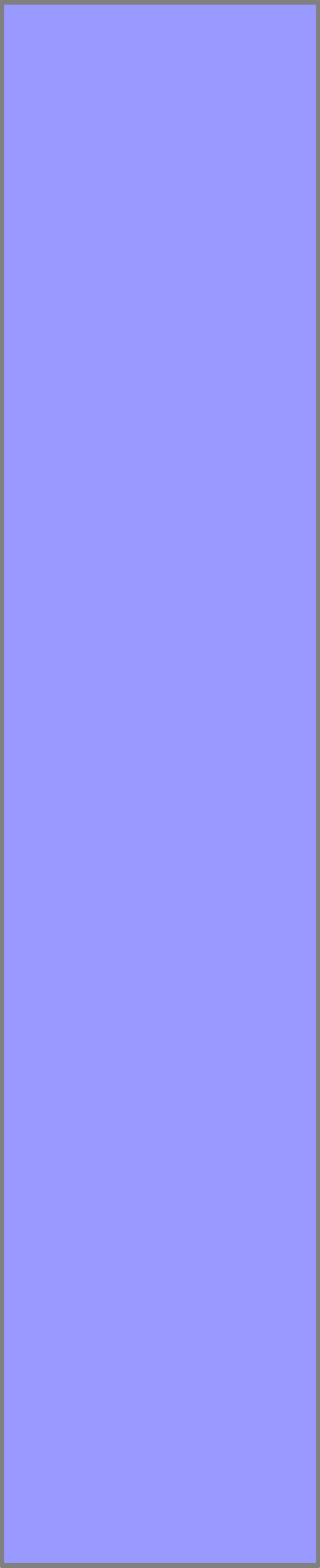
Thus,

$$(44) \quad k = -\ln(1-ECI) \cdot 1/t$$

Often there is considerable uncertainty with regards to the value for *t*. Using a smaller *t* will result in a higher rate



constant. Normally, it is recommended values of t range from the years after the last source loading (e.g. date tank removed – current date) or the average years source loading (date tank remove – current date + average years leaking).

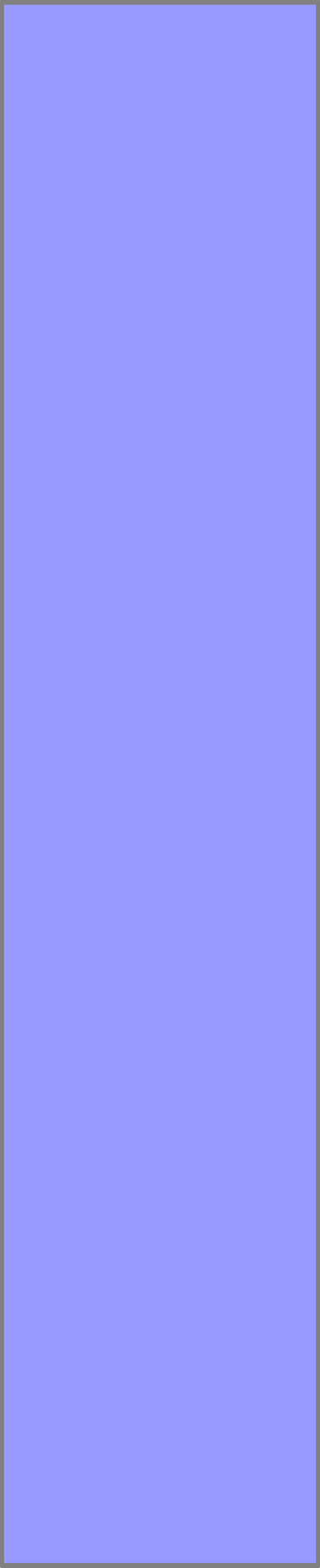


5. AMIBA EXAMPLE AT WESTOVER AIR FORCE BASE

5.1. Executive Summary

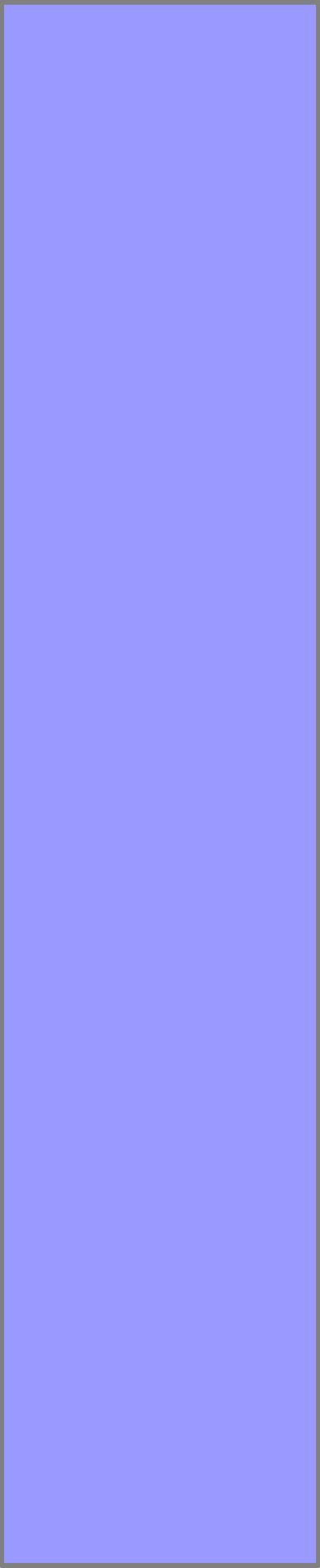
An aqueous and mineral intrinsic bioremediation study (AMIBA) was performed at Westover Air Reserve Base, in Chicopee, Massachusetts at the Fire Training Area (FT-08). Groundwater and soils on this site were found to contain elevated concentrations of fuel hydrocarbons with small amounts of chlorinated solvents. Source areas included a burn pit and an underground storage tank.

Several prior site investigations were done including one natural attenuation study, which principally used aqueous data from monitoring wells. The current study relied heavily on Fe and S mineral analyses as well as aqueous data using the pore water extraction technique. Where possible, data from preexisting studies was used. Eighteen new soil borings were drilled to depths ranging from 14 to 36 feet. These borings were full hole cored and



were sampled for Fe and S minerals and pore water at intervals ranging from two to four feet. Data were evaluated for WAS Fe²⁺, WAS Fe Total, AVS, CrES, pore water Fe and SO₄²⁻. Soil samples were also analyzed for fuel and volatile organic components using EPA Method 8260. Existing monitoring wells were sampled for dissolved O₂, NO₃⁻, SO₄²⁻, Fe, and fuel/organic components.

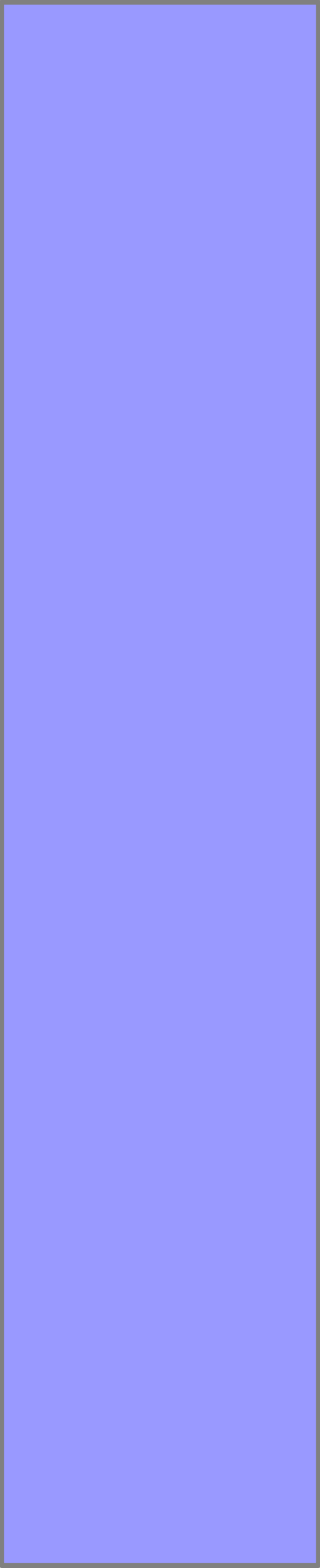
The spatial distributions of the data were evaluated using the geostatistical program GridStat (1997). Three-dimensional static models of soil/aquifer attributes were developed. The geostatistical method interpolated values for hydrocarbon, important Fe and S minerals, and pore water Fe and SO₄²⁻ for the site onto a three-dimensional grid. Using values from the geostatistical grid allowed the direct calculation of the existing fuel mass, expressed capacity (EC) for Fe³⁺ and SO₄²⁻, and the assimilative capacity (AC) for Fe³⁺. The EC for O₂ and NO₃⁻ were estimated using the sulfate indexing method. The geostatistical modeling showed a clear pattern of Fe³⁺ and SO₄²⁻ depletion and



corresponding mineral sulfide and Fe^{2+} deposition associated with the microbial degradation of fuel.

Existing hydrocarbon was found to have a mass of 2,395 moles (~67 gallons) of which 85% was associated with sediments. Total EC hydrocarbon was 52,773 moles (~1480 gallons). These data result in an expressed capacity index (ECI) that demonstrates at least 96% of the released fuel mass was destroyed by microbial processes. Iron footprint analyses show the depletion of Fe^{3+} and the deposition of Fe^{2+} minerals well down gradient of the existing dissolved phase hydrocarbon plume. That footprint demonstrates that the plume reached maximum extent in the past and is shrinking in aerial extend.

For evaluation purposes a comparison was made between EC from the aqueous analyses as compared with the mineral based assessment. For SO_4^{2-} , 2.5 times more EC was found in mineral form than from aqueous analyses. However, for Fe^{3+} over 300 times more EC was in mineral form than aqueous data would indicate alone. The most important microbial process in fuel degradation is via Fe^{3+}



reduction, which is completely marginalized using only aqueous data. Using AMIBA more than 13 times more EC can be documented above that observable with aqueous data alone.

With data from AMIBA, estimates of source degradation rates were developed. Those rates were used in subsequent flow and mass transport modeling. Model results suggest that complete cleanup with natural attenuation alone will require an additional 50 years. If the source is removed, residual hydrocarbon can be naturally attenuated in approximately 20 years. Most common in-situ treatment techniques will be hampered due to the high concentration of reduced mineral species present in the soil system. Thus, direct excavation followed by soil treatment is recommended if source removal is desired. Spatial analyses of fuel show that this option is feasible.

5.2. Introduction

5.2.1. Scope and Purpose

The site of concern here is the 'Current' Fire Training Area, FT-08, at Westover Air Reserve Base, in Chicopee, Massachusetts (Figure 5.1). This project is predominantly a demonstration project for the AMIBA approach to intrinsic natural attenuation evaluation. Although small quantities of chlorinated solvents were found at this site, the emphasis is on the natural attenuation of fuel hydrocarbons by incorporating data from Fe and S mineral phase EAs and EPs.

For cost efficiency and resource conservation, any AMIBA study should incorporate to the fullest extent possible the data and results from prior investigations, as is the case here. The objective is not to duplicate prior work but, rather, to add to the body of knowledge already existing so that the contribution of intrinsic bioremediation towards site restoration can be fully appreciated. Specifically, the role of SO_4^{2-} and Fe^{3+} reducing bacteria may have been significantly under estimated because these electron

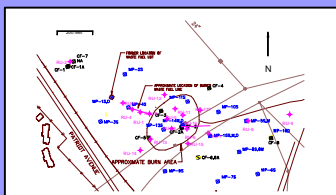
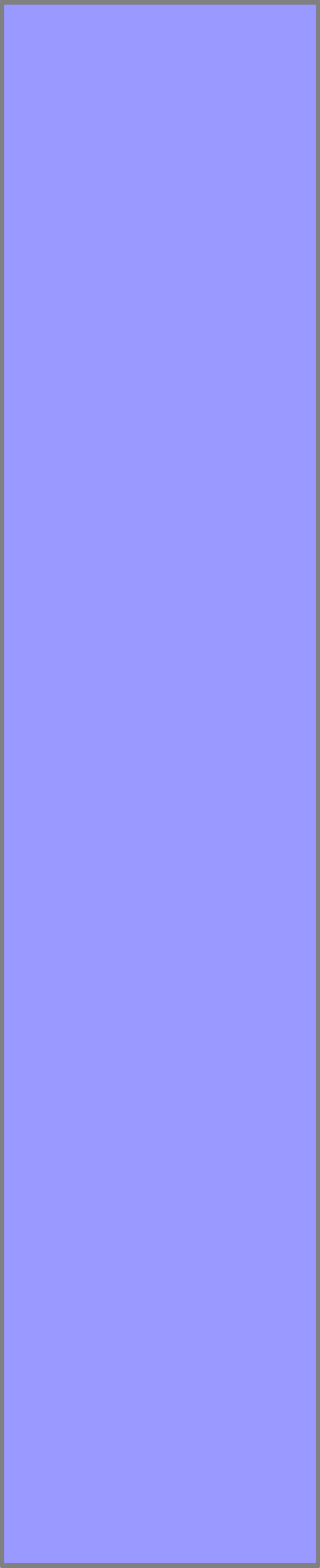


Figure 5.1

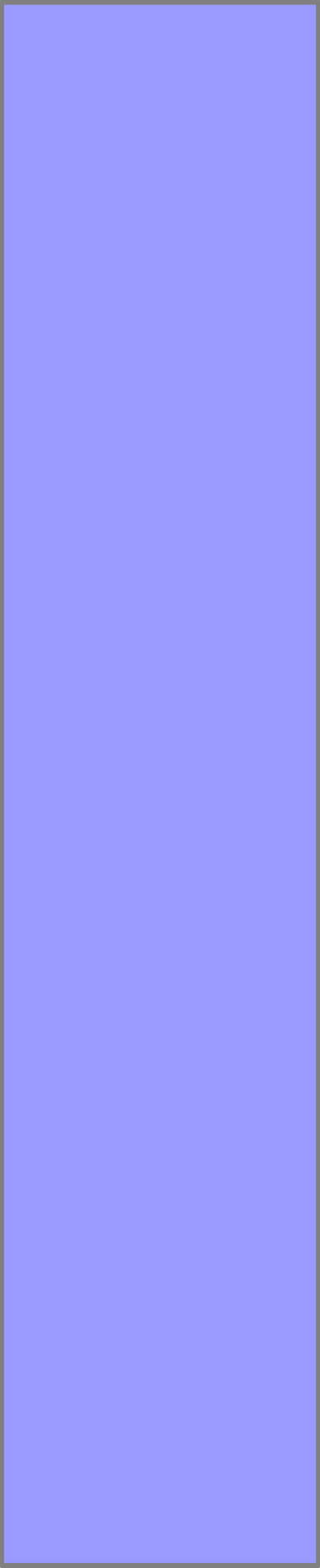


acceptor species and their reduced products may involve mineral species that are not observable with the typical groundwater analyses used in standard natural attenuation assessment.

An earlier intrinsic bioremediation study was conducted on this site (Parsons Engineering Science, 1997) using the methods outlined in Wiedemeier (1999). For that study, aqueous electron acceptors (EAs) and expressed products (EPs) from groundwater analyses were used almost exclusively. This approach:

- Emphasizes the qualitative identification of active redox processes,
- Estimates a dissolved phase biodegradation rate constant which is used to create a fate and transport computer simulation,
- Relies on long term monitoring of natural attenuation to verify degradation, possibly in conjunction with an engineered remediation solution.

AMIBA differs in its objectives. By examining mineral phase EPs, the AMIBA approach used here emphasizes the quantitative analysis of expressed capacity. This method will quantify the efficiency with which intrinsic bioremediation has destroyed labile fuel components. Redox zones are better

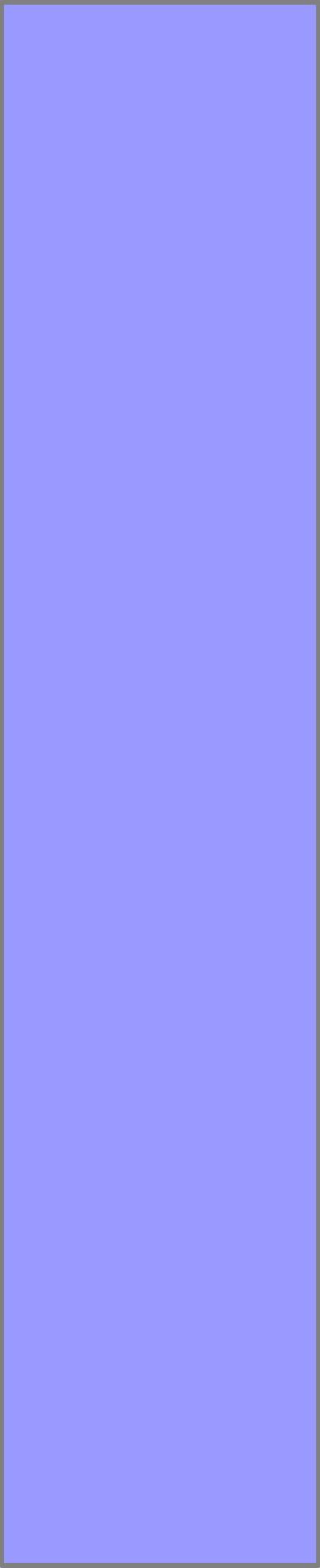


identified, especially with respect to Fe^{3+} reduction. The distribution of mineral Fe^{2+} provides a footprint of prior plume extent and helps verify plume retreat. This method better characterizes the distribution and mass of residual fuel and provides a method of measuring the overall rate constant for source degradation that can be used for improved mass transport modeling.

In conclusion, natural attenuation is an operative remediation system that was in service almost as soon as fuel was released on the site. The goal of AMIBA is to provide a “Remediation Progress Report” for natural attenuation in the same manner that such a report would be generated for any engineered treatment system. It identifies the quantity of fuel that has been removed and estimates the time required for continued treatment.

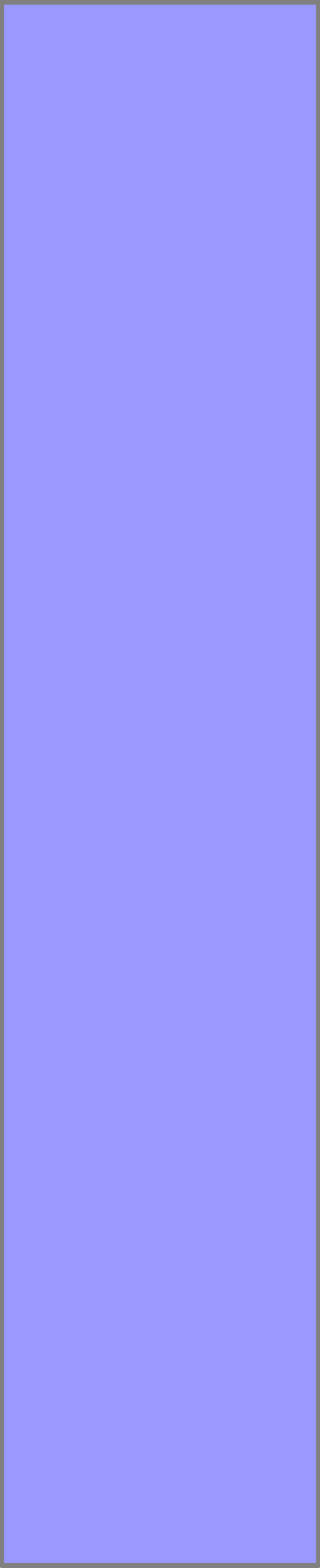
5.2.2. Site Background

There are two source areas consisting of a fire-training pit and under ground storage tank (Figure 5.1). The site was used between 1964 and 1986 as a fire training exercise area. Exercises included igniting fuels poured over



a mockup aircraft fuselage. Fuel volumes used before 1974 are unknown. After 1974 approximately 125 gallons of jet fuel (LP-4) was spread over the mock fuselage for monthly exercises. This fuel was ignited, so it is uncertain as to the quantity that remained in the soil after burning. An underground storage tank used for the storage of waste fuel was removed in 1986. The buried fuel line from the tank was abandoned in place. The site is an approximate ellipse, measuring 300 feet by 250 feet. It is surrounded by open space and accessible by a road entering from the east. There are storm sewers in the site vicinity. No soil remediation technologies have been implemented at the site.

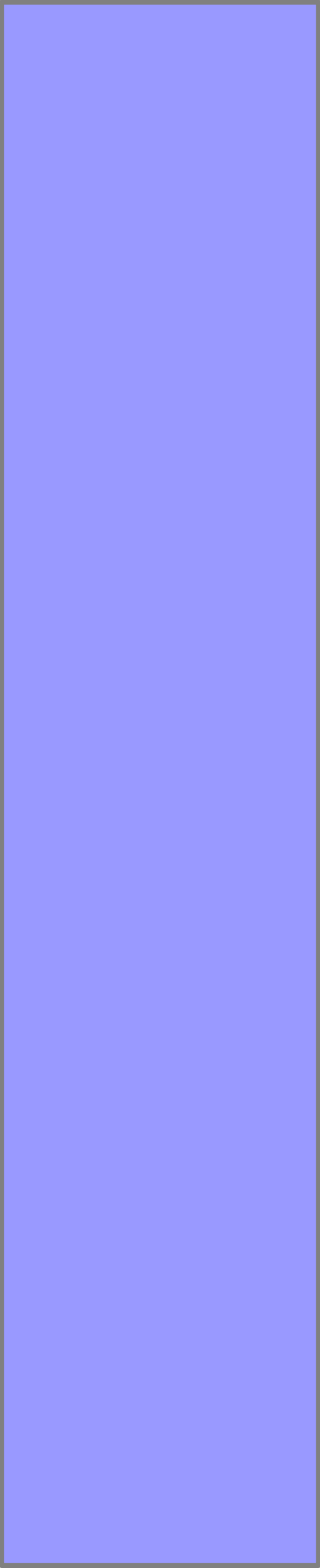
Several previous characterization studies have been performed. Engineering Sciences completed a geophysical survey, installed and sampled monitoring wells, and sampled and tested sediment from three shallow boreholes. Low levels of chlorinated and non-chlorinated hydrocarbons were identified in groundwater. Groundwater samples contained high levels of fuel and low levels of various chlorinated hydrocarbons. Benzene, toluene and TPH were identified in



sediment samples, benzene and TPH at high concentrations.

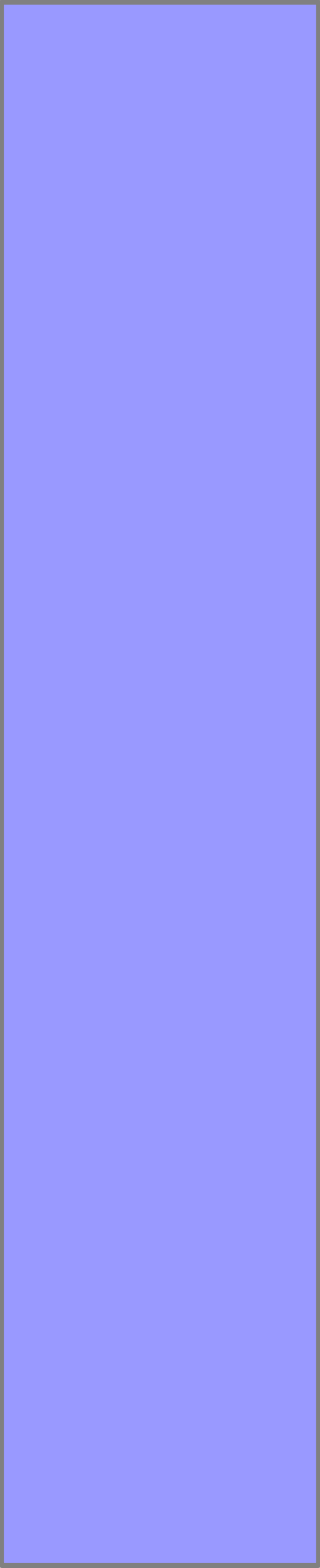
UNC Geotech completed a geophysical and soil gas survey, installed and sampled more monitoring wells and collected and analyzed soil samples from 25 shallow boreholes. Sediment samples contained high concentrations of grease, oil, and total chromatographable organics. Groundwater samples contained BTEX (benzene, toluene, ethylbenzene, and xylenes), naphthalene, and trichloroethene (TCE), none at high concentration.

O'Brien and Gere Engineers, Inc. installed and sampled 12 more shallow soil test boreholes and installed one groundwater well. Soil contamination was detected near and down gradient of the site. However, neither volatile nor semi-volatile compounds were detected at concentrations above 6 ug/kg. Low levels of metal concentrations were identified. Groundwater concentrations of volatile and semi-volatile compounds in the contaminated area ranged from 1.4 ug/L to 5,400 ug/L. No dissolved groundwater contamination was detected down gradient of the site. Light



non-aqueous phase liquid was not detected at the site. The recommended alternative for the site was capping with asphalt (with an Activity and Use Limitation) and natural attenuation of groundwater. A risk assessment identified two state-listed avian species as ecological sensitive biotic receptors.

Parsons Engineering (1997) completed an intrinsic remediation treatability study. Comparison of BTEX, chlorinated solvent, EA, and biodegradation byproduct isopleth maps from two sampling events provided strong qualitative evidence of BTEX and chlorinated solvent biodegradation at the site. It appeared that both aerobic and anaerobic biodegradation processes were occurring at the site. Bioplume II was used to model chemical fate and transport at the site. Model results indicated that natural attenuation would reduce BTEX and chlorinated solvents to levels below current regulatory limits before potential downgradient receptors could be adversely affected. However, significant levels would persist in the groundwater at the site for at least 60 years.



Montgomery Watson collected and analyzed more soil and groundwater samples, identifying petroleum hydrocarbons and BTEX compounds in surface soil, subsurface soil, and groundwater. Risk assessments, conducted following methods prescribed by the Massachusetts Department of Environmental Protection, determined that a condition of “No Significant Risk” had not been achieved at the site. Furthermore, the site was found to present a potential risk to ecological receptors.

5.2.3. Hydrogeology

The bedrock of Westover AFB consists of Triassic “redbeds” consisting of arkosic sandstone, conglomerates, siltstones, and occasional gray shales belonging to the Portland Formation. Uplift and erosion of the Triassic formations resulted in an unconformity between the Portland Formation and Pleistocene glacial sediments forming the surficial deposits.

The Pleistocene glacial advance reshaped the landscape and deposited poorly sorted gravel, sand, silt, and clay mixtures as moraines and till sheets. During the glacial

retreat, melt waters impounded by glacial deposits and existing topography formed several large glacial lakes. The largest of the Pleistocene lakes in the region was glacial Lake Hitchcock, which extended from Hartford, Connecticut to Lyme, New Hampshire. The lake was as much as 250 feet deep in the Chicopee area (Thomas, 1987). The resulting sedimentation deposited thick, gray, varved lacustrine clays with silt and fine sand laminations. Overlying the lacustrine sediments are fine to coarse sands with traces of gravel and silt that were deposited as deltaic outwash deposits when glacial Lake Hitchcock drained and filled with sediment. These outwash deposits comprise the uppermost, unconsolidated sedimentary sequence and contain the unconfined aquifer system.



Figure 5.2

Onsite, groundwater is typically five to eight feet below ground surface across the majority of the site. The groundwater direction is generally towards the east but curves across the site reflecting a convergent flow path (Figure 5.2). The average gradient is 0.034 with an average hydraulic conductivity of 7.2 ft/day.

5.2.4. Known Fuel Distribution

From Parsons Engineering Science (1997) areal distributions of total dissolved BTEX in groundwater for May 1995 and July 1996 are presented on 5.3. For May 1995, as indicated by the 10 ug/L isopleth, the BTEX plume is approximately 750 feet long and 350 feet wide. The estimated area of the plume is about 244,800 square feet (5.6 acres). The July 1996 observed BTEX plume is approximately the same length but is only 250 feet wide with an area of 140,000 square feet (3.2 acres). Values in excess of 10,000 ug/L were observed for both sampling events.

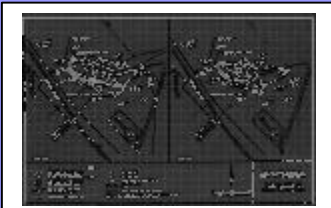


Figure 5.3

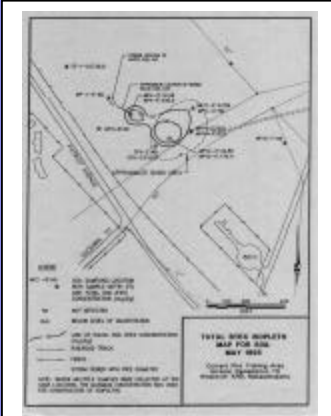


Figure 5.4

In May, 1995, fourteen soil samples were collected from nine borings at depths of 2 and 4 feet below ground surface (Figure 5.4). The maximum observed concentration was 176.1 mg/Kg at MP-12. With the exception of borehole MP-4, soil samples outside of the known burn pit area did not contain quantifiable levels of BTEX.

5.2.5. Review of Prior Natural Attenuation Studies



Figure 5.5



Figure 5.6



Figure 5.7

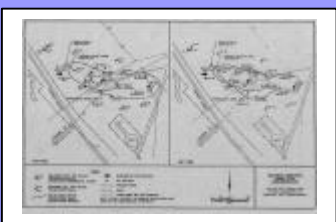


Figure 5.8



Figure 5.9

As described above, a prior natural attenuation study was conducted Parsons Engineering Science (1997) in which all existing monitoring wells were analyzed for soluble electron acceptors and expressed products. The study relied almost exclusively on soluble electron acceptors and reduced products from monitoring well samples of groundwater. The microbial oxidation of fuel was correctly reported to have been due to O_2 (5.5), NO_3^- (Figure 5.6), Fe^{3+} (Figure 5.7), SO_4^{2-} (Figure 5.8) reduction and methanogenesis (Figure 5.9). This observation was based on the increase in dissolved Fe^{2+} and methane in groundwater and virtual removal of all dissolved electron acceptors. Methanogenesis was reported as being an active removal mechanism, but only one well (MP-14) contained significant concentrations greater than 1 mg/L. Thus, methanogenesis appears to be minimally active at this site. As stated in the report, natural attenuation measurements were used only in a qualitative manner to demonstrate that

common microbial intrinsic remediation processes were active. Redox areas could be generally identified in map plan but not vertically.

As part of the Parsons Engineering Science (1997) natural attenuation study, the reactive mass transport model Bioplume II (Rifai et al,1987) was used to predict fate and transport of BTEX. A dissolved phase biodegradation rate constant of $1.5E-3 \text{ day}^{-1}$ was estimated using the method described by Buscheck and Alcantar, 1995). A source decay term of 5% per year was used to represent fuel source weathering but little long-term field data were available to concretely justify the selection of this value. Without source removal, the modeling results indicated that the plume would increase in size by approximately 10% over the next 30 years, then reduce in size and be completely remediated in 65 years (Figure 5.10). The maximum predicted plume length to the 20 mg/L isopleth was 1,000 feet.

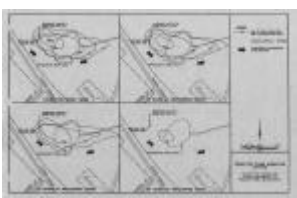


Figure 5.10

5.2.6. Overview of Approach

The current study uses the aqueous and mineral intrinsic bioremediation assessment approach (AMIBA). The approach is more rigorous than the standard protocol for natural attenuation in that it evaluates aqueous data from monitoring wells, pore water taken from cores, and mineral Fe and S electron acceptors and expressed products. The following major steps are presented below:

- Field, laboratory, and evaluation methods are briefly reviewed
- Dissolved and adsorbed/oily phase BTEX distribution and mass are determined.
- Mineral sulfides from AVS and CrES species are evaluated to determine SO_4^{2-} EC.
- Mineral and aqueous iron species are evaluated to determine the iron EC and AC.
- The Fe footprint is discussed to evaluate past plume position and verify plume retreat.
- The contribution to EC by oxygen and nitrate is evaluated using the sulfide indexing technique.
- Total EC and the expressed capacity index (ECI) are determined to estimate intrinsic bioremediation efficiency.
- Overall rate constants for bioremediation are estimated.
- The fate and transport of BTEX is simulated using a flow and mass transport model.
- Recommendations are given for site restoration.

5.3. Methods

5.3.1. Sample Planning

Sediment samples were obtained from boreholes completed during August 1999. Eighteen soil borings were completed as shown on Figure 5.11. The majority of these sampling locations were situated in the immediate vicinity of known source areas to provide spatial analysis of fuel and solvent concentrations and for mass analysis. Many soil borings were also intentionally located in nearby clean areas. This was done to evaluate reduced Fe and S minerals that could have been deposited in the past when the source/plume size was larger. RU-2 was located far up the groundwater flow gradient from the source area, for use as a background control point. Similarly, RU-9 was located to provide a down-gradient control. A series of soil borings were positioned parallel to the groundwater flow gradient through the centerline of the fuel plume so that a good cross-sectional view of subsurface conditions could be generated. Listed from up-flow-gradient to down these soil borings were

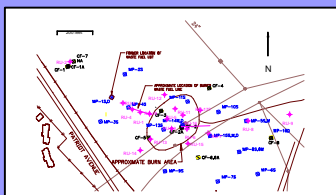
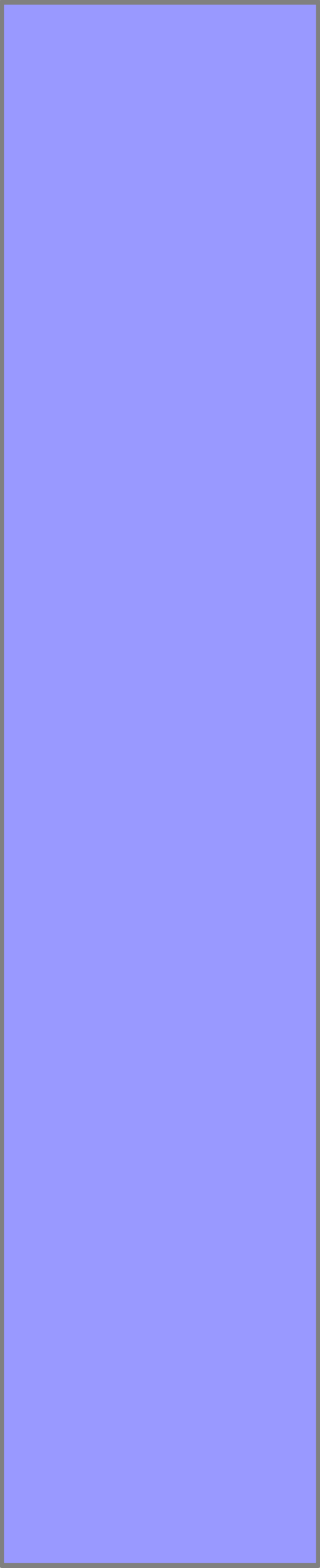


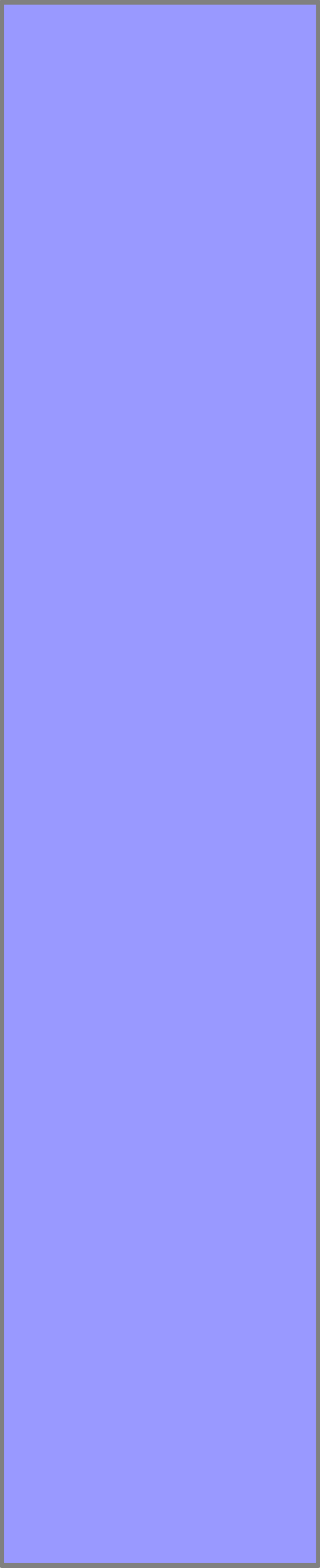
Figure 5.11



RU-2, RU-3, RU-4, RU-1, RU-18, RU-5, RU-10, RU-6, RU-7, RU-8, and RU-9.

Vertical sampling frequency was determined using the semi-quantitative results obtained from PID analysis of sediment carried out as boreholes were drilled. Approximately 200 g wet sediment was collected across a 1 or 2 foot section of core interval for organic vapor analysis in the field using a photo-ionizing detection unit (PID). This sediment was sealed in zip-lock plastic bags and allowed to stand for approximately 15 minutes to permit volatile organic vapors to achieve equilibrium with the container headspace. Organic vapor was then measured by piercing the plastic bag with a large diameter needle connected via plastic tubing to the PID unit. The PID device was calibrated daily and checked periodically for accuracy with the appropriate span gas (100 ppm isobutylene).

In contaminated areas, individual borings were extended to a depth at least four feet below any PID reading exceeding 10 ppm. Where PID readings were elevated sample density was generally set to 2.0 feet, particularly

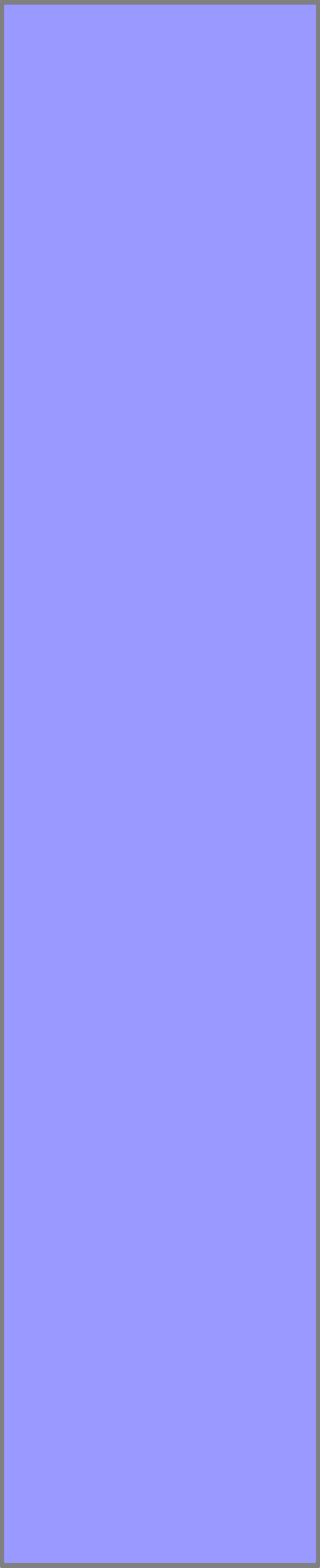


immediately above and below the water table. Where PID values diminished, sample frequency was selectively increased to 4.0 feet.

The location of aqueous sampling locations was limited to existing monitoring wells and monitoring points. Groundwater samples were obtained using standard operating procedures. Seven groundwater samples were collected to supplement groundwater data obtained on previous investigations. Some monitoring points could not be sampled, as they had been installed to a depth above the current water table.

5.3.2. Drilling and Lithologic Logging

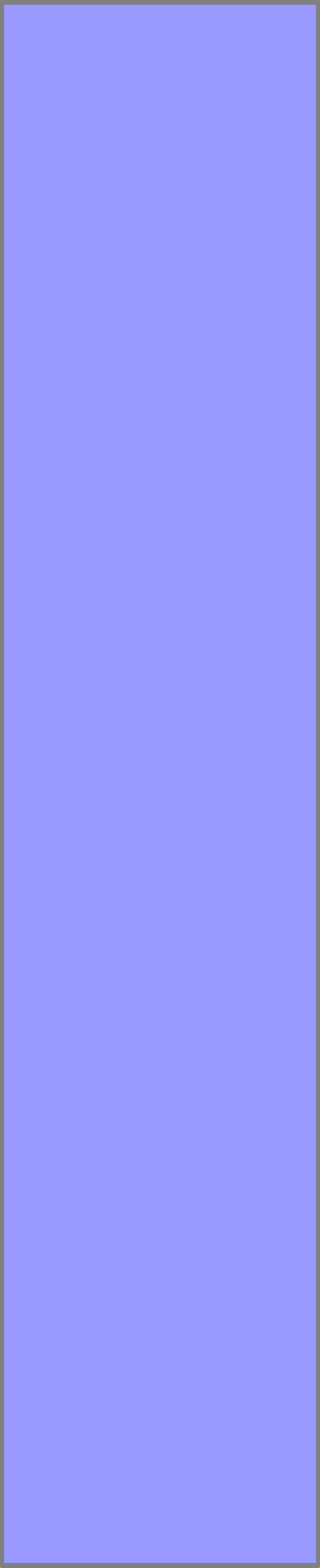
Soil boring depth ranged from 14 to 36 feet. Drilling was completed with a standard hollow stem auger. Each boring was cored from surface to total depth with a 2- or 3-inch split spoon sampler. The smaller size sampler was used in areas where sediment recovery was more difficult; otherwise, the 3-inch diameter was used. To improve sediment recovery, cores were extracted in two-foot



increments. Overall, sediment recovery was good with missing cores occurring only rarely. A hydrogeologist logged core lithology during sediment collection/preservation. Sediment was examined using a binocular microscope and described. The resulting geologic logs and accompanying PID analyses are shown in Appendix I.

5.3.3. Sediment and Pore Water Collection

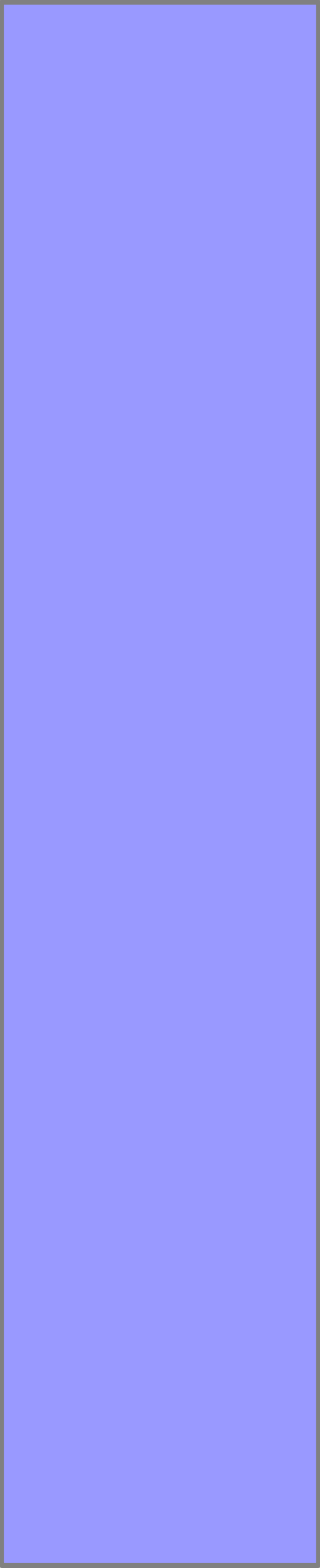
Because some sulfide and Fe(II) minerals are prone to oxidation, sediment samples were immediately transferred to nitrogen purged 125 mL serum bottles, which were sealed with anaerobic bungs and crimped with aluminum seals. The procedure is as follows. Before a sediment sample is brought to the surface, two serum bottles are purged with nitrogen. Once the sediment sample is brought to the surface, approximately 100 g of sediment is quickly transferred to each serum bottle by subcoring using 5cc syringes with the needle tip cut off. Once the sediment transfer is complete, the serum bottles are stoppered and crimped. Three needles are inserted into the stopper. The



first is connected to a pressurized nitrogen source and the other two are bleed needles. The serum bottle is purged again with nitrogen. At the end of the purge, all three needles are removed, leaving the sediment sample isolated in an anaerobic environment. All sediment samples were immediately cooled to 4 C° until used. One of the serum bottles was used for the pore water analysis, the other was used for the sediment analyses. Additional sediment samples were obtained for the organics analysis, described below.

5.3.4. Monitoring Well Sampling

For each monitoring well the depth to water and total depth to shoe was measured using a decontaminated water level indicator. New plastic tubing was then inserted to near the base of the well. At the surface this tubing was connected to a peristaltic pump and setup to discharge water into a 1 L plastic graduated cylinder. Into this cylinder was placed a calibrated pH/conductivity meter, dissolved oxygen probe, and pE meter. The well was then pumped, filling the cylinder while overflow water was collected in a separate 1 L

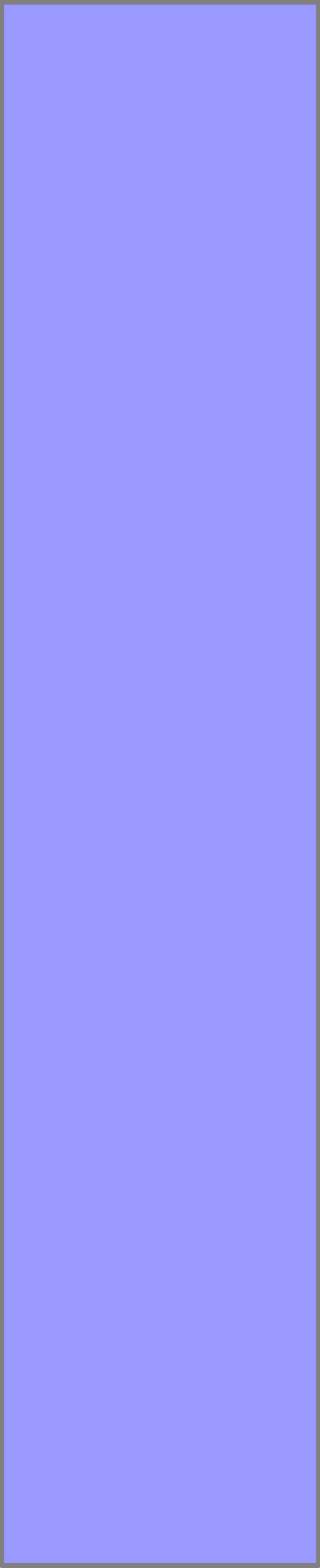


container to determine total volume purged. Each well was pumped in this manner until conductivity readings stabilized, indicating that the well was completely purged. At that time measurements of conductivity, pH, pE, and dissolved oxygen were recorded (Appendix 2).

After purging, water samples were collected for volatile organic constituents (EPA 8260). Eleven groundwater samples were collected for that analysis. Separate samples were also collected, filtered (10 μm syringe filter), and evaluated for dissolved iron and sulfide in the field. A Hach DR2100 was used with Hach reagents. Dissolved Fe total was measured using FerroZine, Fe 2^+ with 1,10 Phenanthroline, S- with Methylene Blue. Analytical results are listed in Appendix 3.

5.3.5. Laboratory Analytical

Where available, analytical methods followed AFCEE recommended procedures. Oxygen in groundwater from monitoring well was analyzed in the field using a YSI DO probe. Fe $^{2+}$ in groundwater from monitoring well was



analyzed in the field with a HACH DR2100 spectrophotometer using Hach Method 8146, recommended by AFCEE.

Groundwater samples from monitoring wells were analyzed for nitrate and sulfate at Rowan University using a Dionex DX-500 ion chromatograph (EPA method SW9056). Pore water samples were analyzed for sulfate and Fe^{2+} at Rowan University using the same methods as for groundwater. Laboratory spectrophotometric methods used a Hach DR4000 spectrophotometer. The method for extracting pore water is as follows: approximately 100 g sediment, under nitrogen, is mixed with 50 mL of oxygen-free DI water, then centrifuged and filtered.

Sediments were analyzed at Rowan University for acid volatile sulfides (AVS), chromium extractable sulfides (CES), 0.5N HCl Fe^{2+} and 0.5N HCl Fe Total. AVS is S as FeS, while CES is S as FeS_2 and S^0 . All sulfide analyses used Hach Method 8131, EPA Approved. Fe^{2+} analyses used Hach Method 8146, recommended by AFCEE. Fe

Total analyses used Hach Method 8147, adopted from Standard Methods for Water and Wastewater.

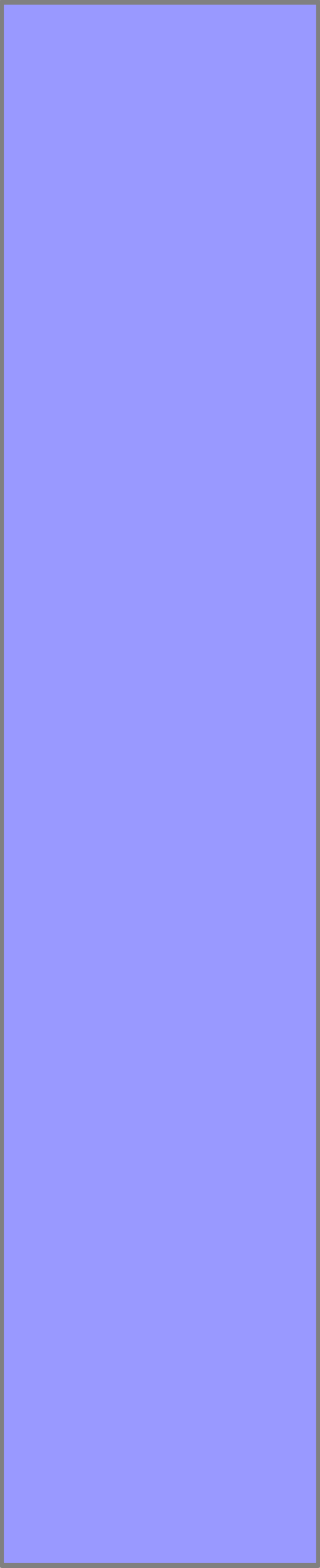
Solid phase reduced sulfides were digested and separated from sediment using 6 N HCl for AVS and 1 N Cr^{2+} / 12 N HCl for CES, in each case using zinc acetate as a trap. Reactive Fe^{2+} and Fe Total were extracted from sediment using weak acid solution (WAS) 0.5 N HCl. This method removes only a portion of the iron on any given sediment, a portion that includes bioavailable Fe^{3+} and Fe^{2+} of recent biological origin, called biogenic Fe^{2+} . Bioavailable Fe^{3+} is estimated by subtracting Fe^{2+} from Fe total.

Groundwater and sediment samples were analyzed for fuel and volatile organic components using EPA Method 8260. Analyses were carried out by Con-test Analytical Laboratory (East Longmeadow, MA), a MADEP certified laboratory.

5.4. Data Analyses Methods

5.4.1.1. Data Interpolation and Modeling

Subsurface data were evaluated using GridStat (Applied Computer Engineering, 1997). Texaco originally



developed GridStat for use in the petroleum industry to model spatially distributed geologic data. The program allows spatial data to be modeled in two or three-dimensions using a Kriging procedure. Once a model is constructed the program can:

- Permit the dynamic viewing of the model as a spatial object that can be viewed from any angle;
- Successively slice the model along any axial plane or make cross-sections across any user defined traverse;
- Sample the model to generate two-dimensional attribute isopleth maps;
- Generate geobody models according to user designated cutoff parameters; and
- Calculate attribute mass and volume.

With respect to Westover, all sediment and pore water data were initially evaluated using four horizontal and one vertical variogram. The horizontal variograms related to the principal compass directions (N-S, NE-SW, E-W, SE-NW). In general, based on variogram analysis, the vertical data was sufficiently abundant and of good quality for excellent spatial analysis. In some cases nugget error was evident, however, in other instances little or no nugget was found. Viewed horizontally the data was usable but it was

observed that additional sample borings nearer together would have improved interpretation.

For all geostatistical analyses of soil data a three-dimensional grid was established representing the study area. This grid had dimensions of 1,300 feet in the x-direction (east-west), and 550 feet in the y-direction (north-south). This region was divided into 25 by 25 foot unit cells. For modeling purposes, the vertical (z-direction) extended to a depth of 30 feet and was divided into 1-foot units. In total there were 37,789 individual 25 x 25 x 1 foot cells constituting the entire study block. This grid size and density was used for actual modeling.

5.4.1.2. *Expressed Capacity Calculations*

For EA and EC mass calculations only a portion of the model area was evaluated; the area of highest data density. This consisted of a 1000 by 500-foot subregion, ranging from 350 to 1300 feet in the x-direction and 50 to 350 in the y-direction (Figure 5.12). The interpolated attribute grid generated by GridStat was exported in ASCII format, which preserved the x, y, z coordinate and cell values. These data

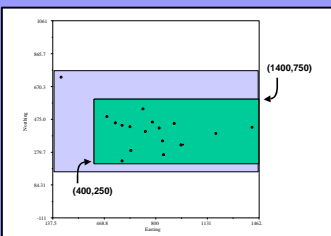


Figure 5.12

Table 5.1

Table 5.2

were imported into a spreadsheet program where Equations 25 or 27 were employed. The total EC for each electron acceptor is generated by summing the product of all cells after performing the necessary math to calculate EC or AC on a cell-by-cell basis. Toluene was assumed to represent the average fuel component. The chemical stoichiometry shown on Table 5.1 was used to calculate the mass of BTEX destroyed based on the ratio of moles of electron acceptors consumed or expressed products produced.

The data used in EC mass calculations by electron acceptor type are shown on Table 5.2. EA mass was calculated on a cell by cell basis using the appropriate values shown on Table 5.2, given a unit cell size of 25 x 25 x 1 feet. R_i 's were based on background concentrations for oxygen, nitrate, and sulfate of 9.5, 13.3, and 25.5 mg/L, respectively. A constant porosity of 0.35 and dry density of 48.78 kg/ft³ was assumed.

5.5. AMIBA Results

Modeling results are presented in three and two-dimensional perspective for each attribute. Three-dimensional models can be rotated and sliced by clicking on the appropriate image. Two-dimensional images include concentration profiles in the x and z plane and average attribute maps in the x and y plane (map plan) perspective. Attribute average maps were created by merely averaging each cell through each vertical column of the three-dimensional model (an automatic function of GridStat). Unless otherwise noted, all concentration profiles shown are taken through the same line of section ranging from the most up gradient (RU-2) to the most down gradient soil boring (RU-9) as shown on Figure 5.13.

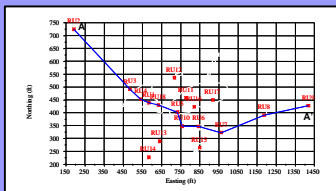
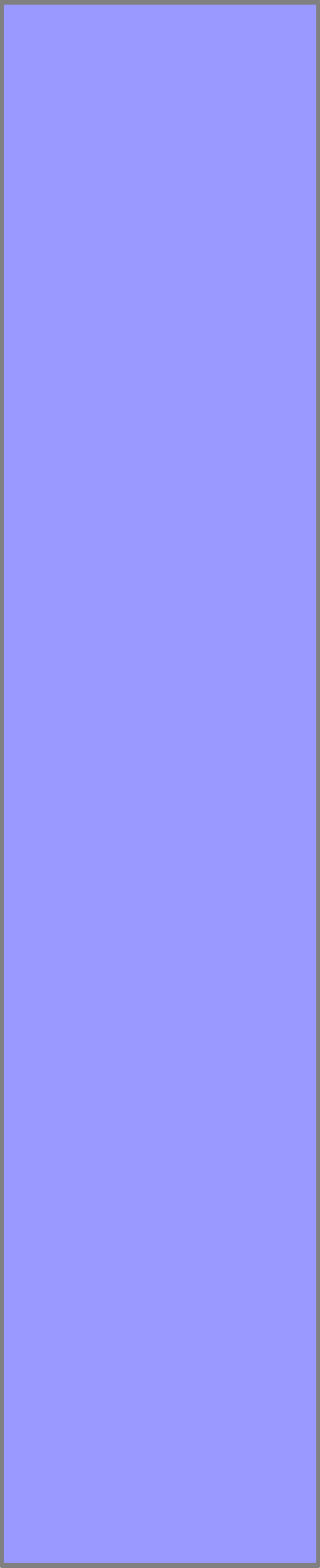


Figure 5.13

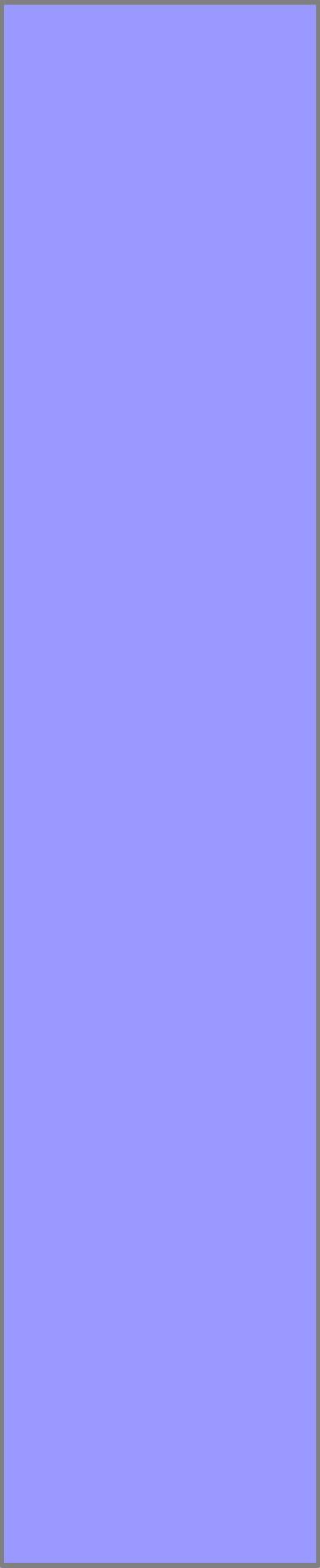
5.5.1. Geologic Observations

The drilled stratigraphic section can be classified into three broad geologic units which include surface soils/fill and two stacked alluvial sand sequences. The soil section extends to approximately 1.5 feet in undisturbed areas and consists of brown or tan fine sand or silt loam. The soil



section may be partially or totally removed to a depth of 3.5 feet by fill material in the burn pit area. This fill consists of olive gray to black native soils mixed with gravel. The black coloration is presumably due to ash generated during fire training exercises where fuel was burned.

The upper alluvial section extends to a depth of approximately 20 feet. In general, alluvial deposition typically consists of a courting downward grain size sequence. Here, the fine-grained sediment extended to about 8 ± 4 feet below the surface. The transition to medium or coarse-grained material is abrupt. The base of the zone is comprised of alternating medium-fine or coarse-fine sediments. Three to possibly 10% pebbles, sometimes over 1-inch in length, are found in intermittent bands of increasing frequency with depth. In non-contaminated areas, this upper alluvial unit ranges in color from rusty tan to rust, indicating a moderate to rather high concentration of iron oxide (Fe^{3+}) coating the primary matrix. In contaminated areas this color is replaced by light gray or grayish rust as



Fe^{3+} is converted to Fe^{2+} . Where high concentrations of FeS or FeS_2 are present, the color is gray to dark gray.

There is an abrupt change in grain size demarking the contact between the first and second alluvial sand sequence. The second sequence begins with very fine sand and silt layer which is about 8 ± 4 feet thick. This unit is typically light grayish rust colored in non-contaminated areas. This unit was not completely penetrated during drilling for this study, however, medium to coarse-grained sediments were found in deeper borings with the same lithology as in the first alluvial sequence.

No clay layers were observed in either the upper or lower alluvial sequences. Therefore, there appears to be no significant impediments to horizontal or vertical fluid movement at this site.

5.5.2. BTEX Mass and Distribution

5.5.2.1. *Dissolved Hydrocarbons*

Eleven existing monitoring wells were sampled for hydrocarbon fuels. A few of the existing monitoring wells could not be found; several of the ones that were located were dry due to low water tables at the time of sampling. To supplement our data, dissolved fuel concentration information from the 1996 sampling event (Parsons Engineering Science, 1997) was used. Specifically, 1997 concentration values from MP11S, MP4S, MP3S, MP9S, MP8S, MP6S, and MP2S were used, however, the fuel concentrations at those wells were not detectable (ND). Thus, those wells were used only to establish the plume boundary and not for plume concentration.

Two-dimensional Kriging was used to create the BTEX plume distribution map shown on Figure 5.14. The plume extends as far down gradient as monitoring well MP5S, which is just short of RU-8. The existing dissolved phase plume stops well short of RU-9, the down-gradient

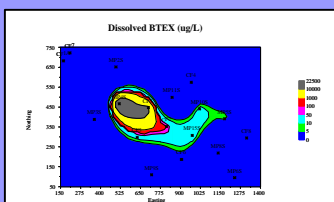


Figure 5.14

background well and is quite remote from RU-2, the up-gradient background well.

5.5.2.2. *Adsorbed/Oily Phase Hydrocarbons*

One hundred and thirty soil samples were collected for volatile organic analysis according to EPA Method 8260. Laboratory results are shown in Appendix 3. Soil samples were collected throughout the stratigraphic interval deemed most likely to contain hydrocarbon fuel as determined by PID analysis. Fewer samples were taken at depths typified by low PID readings.

The maximum concentration found was 720 mg/kg at eight feet below the surface in RU-5. Where present, fuel was concentrated in the upper 10 feet of aquifer material which including the capillary fringe and extending a few feet below the water table as shown on Figure 5.15. Very small concentrations of BTEX extend to as deep as 30 feet around the burn pit area.

Soil BTEX was evaluated using three-dimensional geostatistical analyses. The three-dimensional distribution

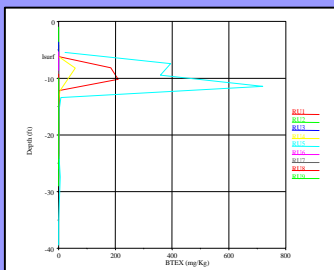


Figure 5.15

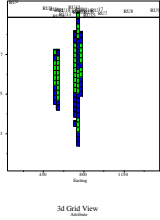


Figure 5.16 3D (mg/Kg)

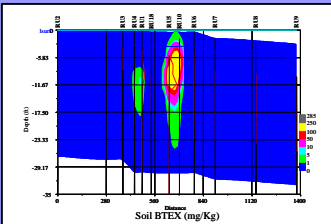


Figure 5.17

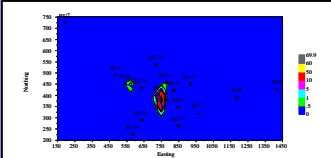


Figure 5.18

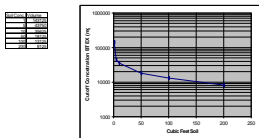
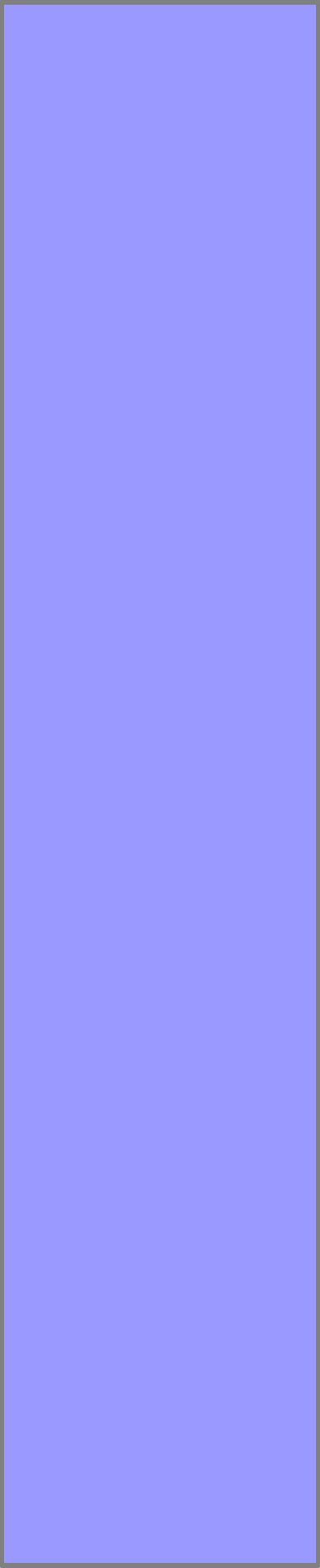


Figure 5.19

of BTEX is shown on Figure 5.16 and a cross-section through traverse A to A' is shown on Figure 5.17. An average of BTEX data was calculated from the three-dimensional grid (Figure 5.18). Spatially, soil BTEX is isolated in the two source areas, the burn pit and fuel tank area. In the horizontal plane, soil hydrocarbon extends no farther down gradient than an area between RU-5 and RU-10, which is clean.

Although soil phase BTEX extends deep into the aquifer, potentiometric surface measurements from nested monitoring wells on this site indicate some small vertical groundwater advection. It is likely that the observed hydrocarbon distribution is also a function of fuel being “pulled” to depth by chlorinated solvents, which could solublize BTEX, then transport it via density flow.

Soil volume was calculated based on various cutoff criteria ranging from 1 mg/Kg to 200 mg/Kg (Figure 5.19). All soils containing 1 mg/Kg or greater BTEX have a total volume of 143,125 ft³, but this volume decreases rapidly



should the cutoff criteria be increased to only 10 mg/Kg resulting in 35,625 ft³.

As discussed above, one recommended remediation option from prior investigations of the site was for capping with asphalt (with an Activity and Use Limitation) and natural attenuation of groundwater. That recommendation was based on limited soil sampling, suggesting that the fuel source was predominantly above the water table. However, this study demonstrates that significant soil phase hydrocarbons extend into the saturated portions of the aquifer. Thus, capping the site will probably not significantly reduce BTEX loading to groundwater.

5.5.2.3. *Hydrocarbon Mass Analysis*

Toluene was selected as the average BTEX compound with a density of 0.87 g/cm³ and a molecular weight of 92 g/Mol. Dissolved hydrocarbon mass was based on aqueous data from monitoring wells, which was assumed to represent the average concentration through 10 saturated feet of aquifer to generate A_{ij} . Ten feet represents the

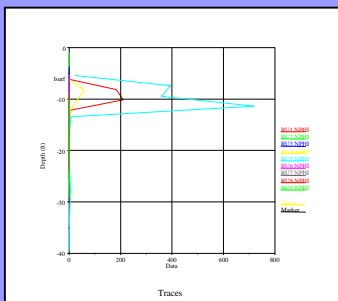


Figure 5.15

Table 5.3

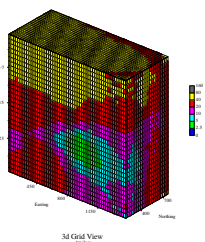


Figure 5.20 3D (mg/L)

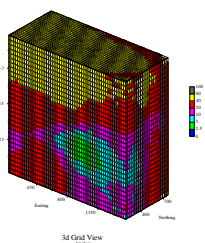


Figure 5.21 3D (mg/L)

thickness of aquifer containing the significant dissolved phase hydrocarbon mass, based predominately on the depth distribution of source materials (Figure 5.15).

Table 5.3 is used to present information on the distribution of BTEX compounds, based on samples collected in August 1999. Approximately 67 gallons of BTEX compounds remained at the site. Approximately 85% of the residual hydrocarbon was associated with sediments. BTEX compounds are located in two source areas, one corresponding to the location of an underground storage tank used to store fuels for the fire training exercises, the other corresponding to the fire training area.

5.5.3. Sulfate Analyses

5.5.3.1. *Sulfate Removal*

The distribution of SO_4^{2-} from pore water analysis is shown in three-dimensions on Figure 5.20, a series of slices through the study area on Figure 5.21 and a concentration profile on Figure 5.22. The background concentration is more than 40 mg/L near the surface of SO_4^{2-} , but decreases

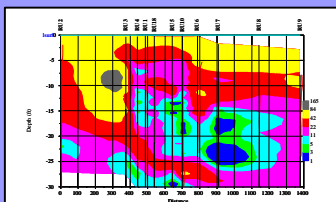


Figure 5.22

with depth to approximately 10 mg/L in the bottom of the sampled zone. This phenomenon is especially evident on Figure 5.21. There is a sharp decrease in SO_4^{2-} concentrations at the interface of the two source areas, followed by a long plume of SO_4^{2-} depleted groundwater down gradient as shown on the average SO_4^{2-} map (Figure 5.21). In the contaminated section of the study area, SO_4^{2-} is depleted to <2.5 mg/L. Up gradient areas where SO_4^{2-} was first removed correspond to the deposition of both CrES and AVS minerals, as can be seen below. Based on the removal of SO_4^{2-} , the oxidation of fuel via sulfate reduction is currently ongoing and aggressive.

SO_4^{2-} concentrations increase somewhat in an isolated area around RU-6, which is down gradient of both source areas in an area that should be strongly reduced. As will be seen on almost all successive electron acceptor types, the area around RU-6 appears to be more oxidized. This effect is probably a function of aquifer heterogeneity resulting in an isolated area with less fuel.

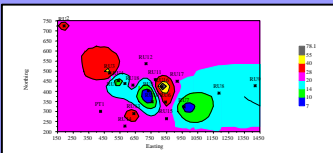


Figure 5.23

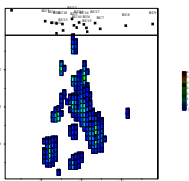


Figure 5.24 3D (mg/Kg)

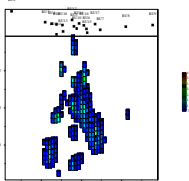


Figure 5.25 3D (mg/Kg)

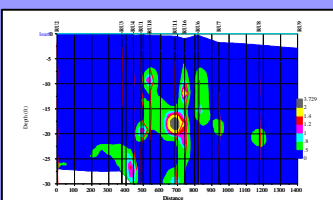


Figure 5.26

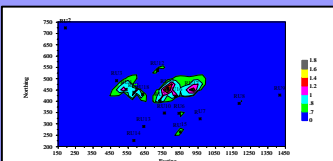


Figure 5.27

With AMIBA, SO_4^{2-} analysis is not required for EC calculations, but is shown here for instructive purposes. The average background concentration for SO_4^{2-} is 25.5 mg/L (Figure 5.23). A_{ij} was calculated by subtracting the interpolated cell values from Kriging analysis from the background concentration. Equation 25 was then employed to determine the theoretical mass of expressed SO_4^{2-} from aqueous analysis, which was 8,060 moles or 258 Kg S. Typically, EC for sulfate is better determined by examining mineral species AVS and CrES as shown below.

5.5.3.2. AVS Sulfide

AVS (FeS) distribution is shown in three-dimensions on Figure 5.24 and as a series of slices through the model on Figure 5.25. A concentration profile of AVS through line of section B to B' is shown on Figure 5.26 and the vertical concentration average on Figure 5.27. Overall, the concentration of AVS was found to be slight, with a maximum concentration of only 6.1 mg/Kg. AVS was principally found in and around the hydrocarbon source areas. Because the site is old, it is likely that most AVS has

been converted to CrES in the form of FeS_2 , which is not extracted by the strong acid solution used for AVS.

Very little sulfide can be found in the background area and background concentration of AVS was taken as 0.4 mg/Kg. That value was subtracted from the interpolated cell values from Kriging to calculate the effective concentration (A_{ij}) for AVS sulfide. The estimated mass of sulfide from AVS was 570 moles or 18 Kg S.

5.5.3.3. CrES Sulfide

At this site, most mineral sulfides were found to be in the form of CrES, probably mostly in the form of FeS_2 . The best indication of CrES distribution can be seen on the three-dimensional concentration model on Figure 3.28 and the sliced section on Figure 5.29. CrES is concentrated around both source areas, especially immediately above and below the water table. However, CrES extends deep in the burn pit area around RU-5. The maximum concentration observed was 262 mg/Kg. In map plan, the average concentration shows CrES deposition around the source areas but shows a northeastern trend with deposition around RU-11 and RU-

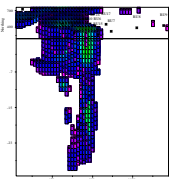


Figure 5.28 3D (mg/Kg)

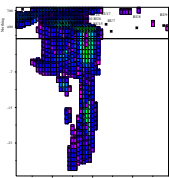


Figure 5.29 3D (mg/Kg)

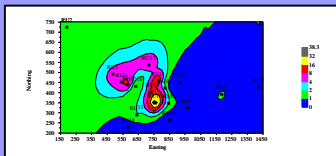


Figure 5.30

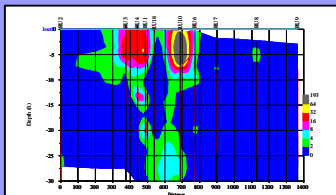


Figure 5.31

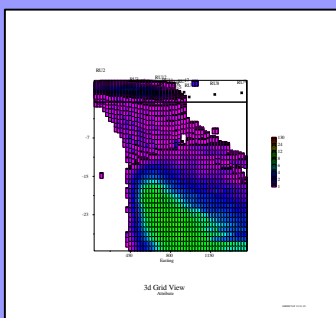


Figure 5.32 3D (mg/L)

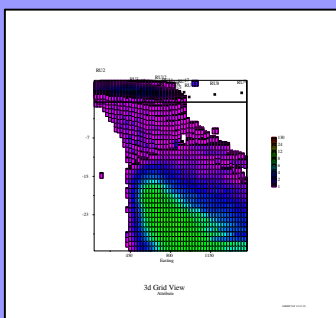


Figure 5.33 3D (mg/L)

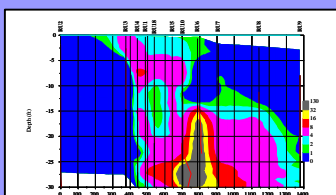


Figure 5.34

12 (Figure 30). A simple CrES concentration profile view along line of section A to A' can be seen on Figure 5.31.

There is little CrES deposited up gradient from the source area. Background concentrations were taken as 1.4 mg/Kg. That value was subtracted from all interpolated cell concentrations to calculate A_{ij} in Equation 27. The calculated EC sulfide from CrES was 18,540 moles or 593 Kg S. Thus, there is 33 times the amount of sulfide as CrES compared to AVS at this site. This observation is consistent with the age of contamination at the site, which permits AVS to be converted to CrES according to Equation 20.

5.5.4. Iron Reduction

5.5.4.1. 4.3.4.1 Dissolved Phase Iron

Dissolved iron from pour water analyses was mapped in three dimensions using a geostatistical approach as seen on Figures 5.32 and 5.33. The three dimensional model was then used to construct a concentration profile of dissolved iron through transact A - A' as shown on Figure 5.34.

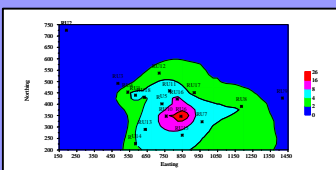


Figure 5.35

Similarly, by sampling the grid along the vertical profile for each column the average dissolved iron concentration was calculated as shown on Figure 5.35.

Dissolved Fe^{2+} is low in background areas, averaging 0.8 mg/L. However, concentrations greatly increase in plume area to as much as 194 mg/L. In profile view, concentrations of aqueous Fe^{2+} show the tendency for vertical distribution. Presumably, increases in Fe^{2+} with depth are in response to vertical hydrocarbon movement. As is demonstrated below, distribution of dissolved Fe^{2+} is small in contrast to the distribution and total mass of mineral phase Fe^{2+} . Based on the abundance of aqueous Fe^{2+} , the oxidation of fuel via iron reduction processes is currently ongoing and quite aggressive.

The calculation of EC for dissolved iron is not recommended but is presented here for instructive purposes. Equation 25 was employed to calculate EC for dissolved Fe^{2+} based on A_{ij} from modeled data, where the background concentration (0.8 mg/L) was subtracted on a cell-by-cell

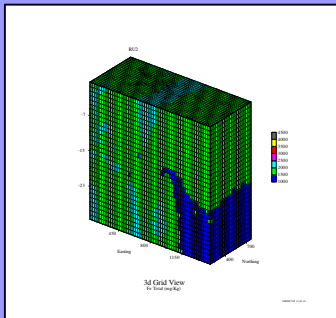


Figure 5.36 3D (mg/Kg)

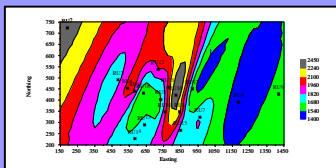


Figure 5.37

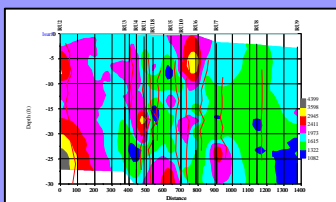


Figure 5.38

basis. Using this approach a total EC for aqueous Fe^{2+} of only 5,270 moles or 294 Kg Fe was estimated.

5.5.4.2. WAS Fe Total

WAS Fe total ($Fe^{2+} + Fe^{3+}$) was modeled in three-dimensions. Slices through the model can be seen on Figure 5.36. Average Fe concentrations can be seen on Figure 5.37. Finally, a concentration profile through line of section A to A' is shown on Figure 5.38.

It should be noted that the distribution of Total Fe is not related in any way to the presence or absence of fuel. This distribution is in response to deposition in an alluvial channel system. Concentrations are quite variable. Often, increasing Fe content is associated with decreasing sediment grain size or the presence of fines. Fine geologic materials have increased surface area facilitating more Fe, which commonly exists as a mineral coating. The increase in Fe around RU-6 suggests increased fines in that area which would reduce permeability, locally inhibit fuel migration, and result in a zone that is slightly more oxidized in the top of the aquifer system.

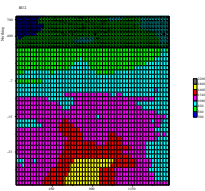


Figure 5.39 3D (mg/Kg)

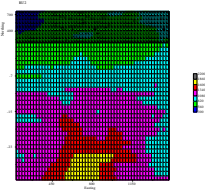


Figure 5.40 3D (mg/Kg)

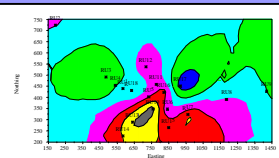


Figure 5.41

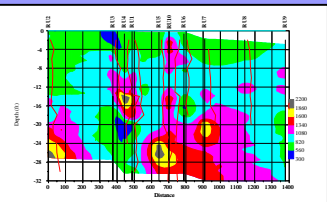


Figure 5.42

5.5.4.3. WAS Mineral Fe^{2+}

Statistical analysis of WAS Mineral Fe^{2+} was performed to generate a three-dimensional model shown on Figure 5.39 and sliced on Figure 5.40. Average mineral Fe^{2+} is shown on Figure 5.41. Finally, a concentration profile through line of section A to A' is shown on Figure 5.42. These graphics show a significant increase in mineral Fe^{2+} in the source area and down gradient. Mineral Fe^{2+} distribution mirrors that of dissolved Fe^{2+} but occupies a larger aerial extent.

The model of mineral Fe^{2+} is not directly used in EC calculation. Because the concentration of total WAS Fe is variable it is difficult to differentiate quantitatively the mineral Fe^{2+} generated in response to fuel oxidation. Therefore, the approach described in Section 4.3 was used for EC calculation. As an initial step, the ratio of Fe^{2+}/Fe total was calculated for all data then modeled in three dimensions (Figure 5.43). From this model the concentration profile through line of section A to A' is shown on Figure 5.44 which can be compared against Figure 5.42 to see the improved

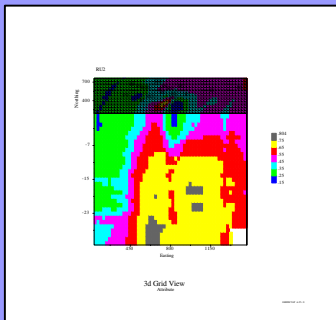


Figure 5.43 3D (unitless)

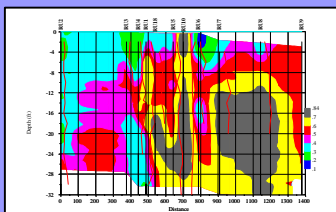


Figure 5.44

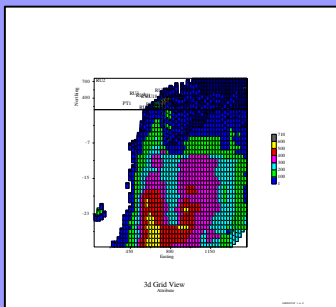


Figure 5.45 3D (mg/Kg)

discretion of Fe^{2+} reduction zones. This ratio analysis allows areas that have undergone significant Fe^{3+} reduction in response to the enzymatic reduction of fuel to be more clearly seen.

The background ratio of $\text{Fe}^{2+}/\text{Fe Total}$ of 0.50 was used for the term B in Equations 31 and 32. The average background value for B is 0.33. However, there are a few small, noncontaminated zones where the ratio of $\text{Fe}^{2+}/\text{Fe Total}$ was 0.5. So, the higher value was used to be conservative. Thus, for this site, the mineral fraction of Fe^{2+} from the oxidation of fuel is only the observed iron times the observed ratio of $\text{Fe}^{2+}/\text{Fe Total}$ less 0.50. Where the ratio of $\text{Fe}^{2+}/\text{Fe Total}$ is below 0.5 no biological reduction of Fe^{3+} was attributed to EC.

Equations 30 and 31 were applied by taking F_j from the model of $\text{Fe}^{2+}/\text{Fe total}$ and Fe_t from the model of WAS Fe Total on a cell by cell basis. This generated a new three-dimensional grid of expressed Fe^{2+} from the reduction of fuel. That three-dimensional model is shown on Figure 5.45

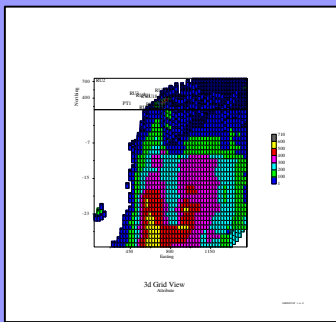


Figure 5.46 3D (mg/Kg)

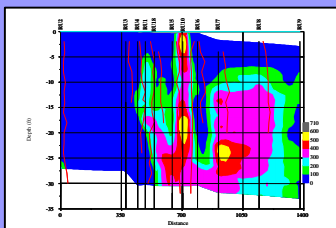


Figure 5.47

and is sliced on Figure 5.46. A concentration profile is shown on Figure 5.47 through line of section A to A'.

As can be seen from the above referenced figures, by applying the normalization and filtering technique virtually all background concentrations of mineral Fe²⁺ are eliminated. This results in the appearance of expressed Fe²⁺ only in the areas that currently or once contained fuel components down gradient of the fuel source. A maximum concentration of 700 mg/Kg Fe²⁺ was observed. Both the width and length of expressed mineral Fe²⁺ exceeds the size of the known BTEX distribution suggesting that the plume at one time covered a much larger aerial extent.

Total Fe³⁺ EC was calculated by applying Equation 27 using data from the expressed Fe²⁺ model. In this case, background Fe²⁺ has already been removed by the filtering process described above so the value for expressed Fe²⁺ is used directly for A_{ij}. Using the AMIBA technique 1,584,350 moles (88,500 Kg) Fe³⁺ has been produced as a direct or indirect response to the microbial oxidation of fuel at this site. However, some of the reduced Fe²⁺ may be from the

abiotic reduction of Fe^{3+} by H_2S occurring from the formation of AVS according to Equation 16. The Fe^{2+} from abiotic processes can be removed by subtracting the moles of observed AVS. Thus, Fe^{2+} expressed capacity strictly from the enzymatic reduction of fuel is equal to the net Fe^{2+} (1,584,350) minus the moles AVS (570) resulting in a net total EC Fe^{2+} of 1,583,780 moles. Note that although the AVS fraction was insignificant here it can constitute a very high amount of the reduced Fe^{2+} fraction at other sites.

5.5.4.4. WAS Fe^{3+}

A geostatistical model of mineral WAS Fe^{3+} was made and can be seen as a series of slices and in cross-section on Figures 5.48 and 5.49 respectively. These images distinctly illustrate the removal of bioavailable Fe^{3+} from the aquifer system. Background concentrations of Fe^{3+} , generally greater than 1000 mg/Kg, are reduced to less than 200 mg/Kg down gradient from the source area.

Obviously, the inverse of the Fe^{2+}/Fe Total ratio yields the remaining fraction of Fe^{3+} . Then, as can be seen from Figure 5.43, approximately 15% WAS Fe^{3+} remains even in

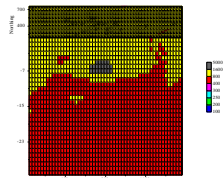


Figure 5.48 3D (mg/Kg)

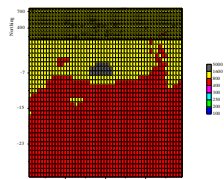


Figure 5.49 3D (mg/Kg)

areas that have experience the maximum Fe^{3+} reduction. The presence of high concentrations of dissolved Fe in pore water indicates that Fe^{3+} reduction is currently on going. As is shown below under the section for ECI, the percentage of hydrocarbon remaining on-site is much less than the percentage of bioavailable Fe^{3+} that has been removed. Thus, the assimilative capacity of Fe^{3+} is easily sufficient to meet the reductive demands of residual hydrocarbons. As a result, Fe^{3+} reduction will likely continue as long as labile hydrocarbons are present in the system.

5.5.4.5. *Iron Footprint*

Because the deposition of mineral Fe^{2+} is rapid, its presence can mark the position of the current or past hydrocarbon plume extent. For comparison, Figure 5.50 shows a chart of the concentration of dissolved BTEX through the same line of section as the net mineral Fe^{2+} concentration profile. Increased levels of mineral Fe^{2+} precipitates were identified significantly down gradient of BTEX compounds. This is evidence that, at some time past,

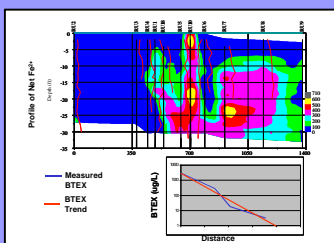


Figure 5.50

BTEX compounds were farther downstream than present and suggests that the plume is shrinking in extent.

It can be argued that under some conditions, small quantities of Fe^{2+} remain soluble long enough for advection to occur. Thus, Fe^{2+} may migrate into areas where no Fe^{3+} reduction has occurred leaving a false footprint of prior plume extent. However, Figure 5.51 shows that Fe^{3+} has been significantly depleted in down gradient areas where BTEX currently does not exist. As described in Section 2.33, it has been demonstrated that Fe^{3+} reduction cannot occur without the direct contact of active iron reducing bacteria and that the solubility of Fe^{3+} is such that spontaneous dissolution at normal pH can occur only on a more geologic time scale. Thus, in the absence of bacterial processes Fe^{3+} cannot be removed by either by reduction or by dissolution. Therefore, the area of depleted Fe^{3+} down gradient of the current BTEX plume conclusively shows the footprint of the historic plume extent and proves that the plume is retreating.

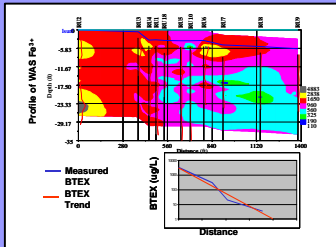


Figure 5.51

5.5.5. Oxygen and Nitrate Reduction

The reduced products of O_2 and NO_3^- reduction are transient in an open, dynamic aquifer system. Thus, the EC from direct measurement of aqueous O_2 and NO_3^- is often underestimated to the point of being useless. Using the AMIBA method, the EC of oxygen and nitrate are not calculated directly. Better estimates of O_2 and NO_3^- EC can be determined using the sulfide indexing technique used here (See Section 4.4).

As measured at well CF-1A, background concentrations of O_2 and NO_3^- (as N) were 3 mg/L (0.214 moles/L) and 5.16 mg/L (0.297 moles/L) respectively. Those electron acceptors were essentially exhausted in the BTEX plume area (0.2 mg/L O_2 and 0.41 mg/L NO_3^-). The continuing depletion of oxygen and nitrate is evidence for ongoing fuel degradation via microbial oxidation using those electron acceptors.

The background sulfate concentration was 25.5 mg/L (0.265 moles/L). Thus, the ratio of O_2/SO_4^{2-} and NO_3^-/SO_4^{2-} entering the fuel source area is $0.297/0.265 = 1.12:1$ and

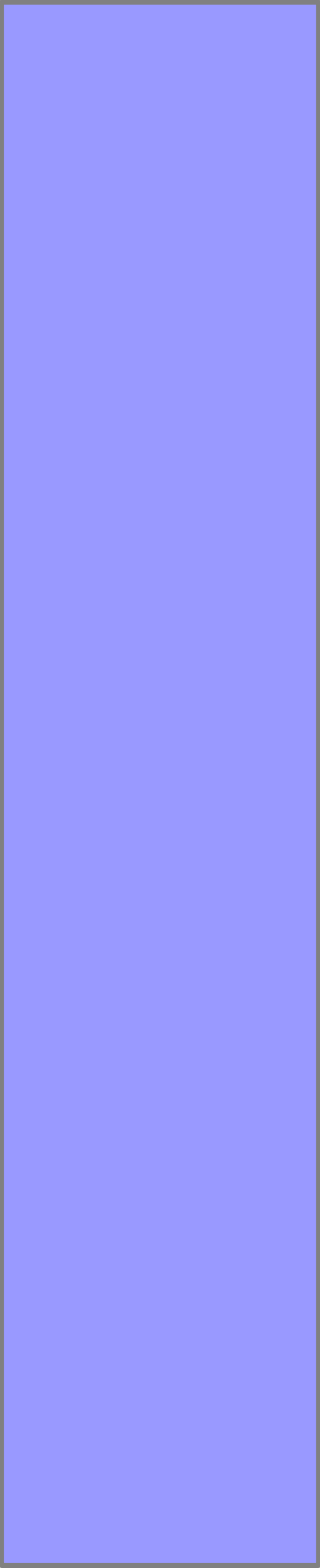
0.214/0.265 = 0.81:1 respectively. Honoring the redox reaction series, sulfate is used as an electron acceptor after oxygen and nitrate. Thus, for every mole of sulfide present at least 1.12 moles oxygen and 0.81 moles nitrate must have been consumed. From above, total sulfides from AVS (570 moles) + CrES (18,540 moles) is 19,110 moles. Thus, the EC of oxygen is 19,110 x 1.12 = 21,403 moles. Similarly, the EC of nitrate is 19,110 x 0.81 = 15,479.

5.5.6. Expressed Capacity Index

A summary of calculated EC values by electron acceptor type is shown on Table 5.4. As described in the succeeding sections, aqueous analyses were not used to derive any EC values. EC for SO_4^{2-} and Fe^{3+} were derived by direct mineral analysis. The EC for O_2 and NO_3^- was from the sulfide indexing technique.

Calculation of the quantity of fuel degraded by biological processes is straightforward; the mole mass of EC for each electron acceptor is divided by the stoichiometric ratio from the balanced chemical equations from Table 5.1. The oxidized fuel mass by electron acceptor type is shown

Table 5.4



on Table 5.4. AMIBA analysis demonstrates that approximately 53,000 moles of BTEX compounds have been biodegraded at the site, or about 1480 gallons. This assessment is conservative because it does not account for fuel destroyed by methanogenesis, assimilative reduction, or loss due to physical processes (advection, hydrolysis, volatilization, etc.). As described above, the total mass of residual hydrocarbon from water and soil analyses is 2,395 moles or approximately 67 gallons.

The estimate of total fuel released on-site is the sum of destroyed fuel plus existing fuel (1,480 gal + 67 gal = 1,547 gal). This value appears to be reasonable considering approximately 125 gallons of fuel were placed in the burn pit each month for fire training exercises from 1974 to 1986. Thus, the total amount of fuel applied was 144 months x 125 gal/month = 18,000 gal. Thus the measurable fuel from AMIBA is $1,547 \text{ gal} / 18,000 \text{ gal} \times 100 = 8.5\%$ of the total fuel used; a logical value considering that the fuel was burned in the pit.

Any engineered remediation system would normally be evaluated to determine operational efficiency by comparing the mass of fuel removed to the initial quantity. This concept is extended to intrinsic bioremediation through the calculation of the expressed capacity index (ECI). Using Equation 31, the ECI is:

$$(45) \quad ECI = 1 - \frac{EC}{HC + EC} \times 100 = 1 - \frac{1,480}{67 + 1,480} = 96\%$$

Therefore, at least 96% of the measured hydrocarbon has been removed due to biological processes alone; a respectable value for any form of treatment. Based on this value it can be stated that bioremediation has been highly effective at this site.

5.5.7. Comparison of AMIBA EC to Prior Protocol

Based on the AMIBA method, it can be seen that most of the expressed capacity is via Fe^{3+} reduction, 83% followed by SO_4^{2-} (9%), O_2 (4.5%), and NO_3^- (4.1%) (Table 5.4, Figure 5.52). The EC for each of the electron acceptor

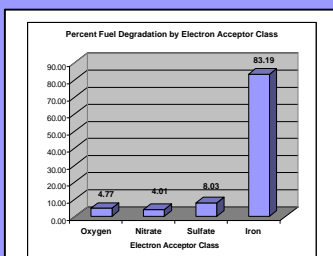
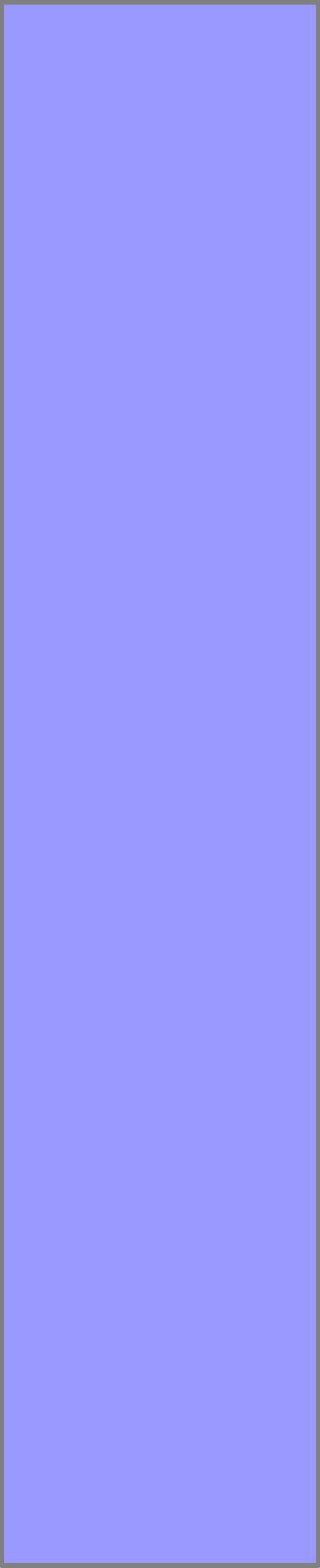


Figure 5.52

Table 5.5

types was also calculated using Equation 25 for aqueous data similar to the existing protocol (Wiedemeier et al., 1999). Although calculation of EC using aqueous data is not required by the AMIBA protocol it is performed here for comparative purposes. The resulting aqueous EC values are shown on Table 5.5.

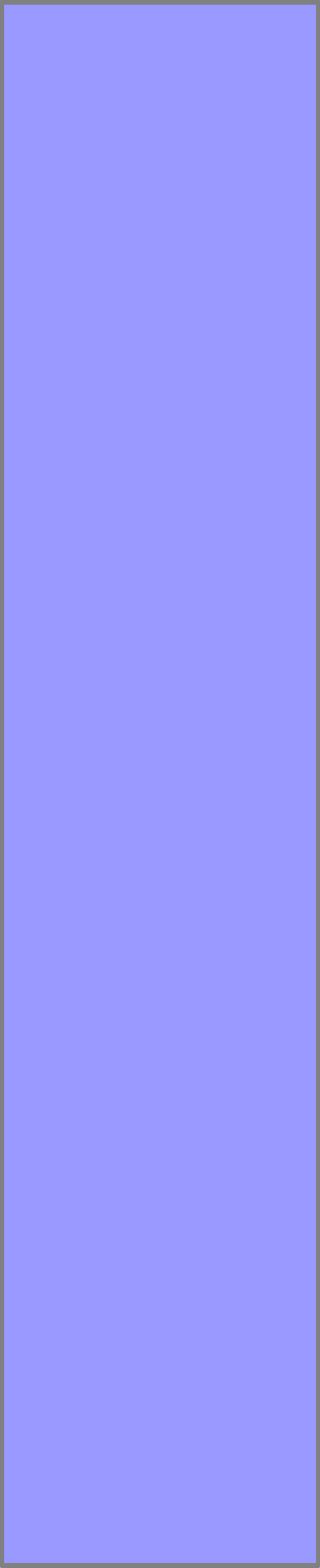
The aqueous analysis can be used to demonstrate biodegradation of only 3,900 moles of BTEX compounds, or 109 gallons as opposed to AMIBA where 53,000 moles of BTEX, or about 1480 gallons, can be documented. The aqueous method would indicate that most of the aqueous expressed capacity is via SO_4^{2-} reduction (46%) followed by O_2 (27%), NO_3^- (23%). Significantly, only 4% of the EC would be attributed to Fe^{3+} reduction. Thus, ignoring mineralogical data completely changes our understanding of redox processes at this site. With AMIBA, Fe^{3+} reduction is shown to be the dominant microbial process but with aqueous data alone this important remediation pathway appears to be insignificant.



For SO_4^{2-} reduction, 2.4 times more EC can be observed at this site using AMIBA mineral sulfide analysis (19,110 moles) as compared with an analysis using only aqueous data (8,060 moles). For iron, the error when using only aqueous data is extreme. Aqueous analysis demonstrates only 5,270 moles as compared with AMIBA (1,584,350 moles): a correction of over 300 times.

Using aqueous data yields a calculated ECI of only 63% compared to 96% with the AMIBA technique. Thus, aqueous analysis would indicate that intrinsic bioremediation has been rather ineffective. As a whole, AMIBA analysis was able to demonstrate over 13 times more biodegradation (53,000 moles/3,900 moles).

The improvement in EC when applying AMIBA will vary from site to site depending on geologic conditions. Where O_2 and/or NO_3^- reduction processes absolutely dominate, AMIBA may not contribute greatly. However, as described in Section 2.3.5, the AC of SO_4^{2-} and Fe^{3+} are often significantly higher than O_2 and NO_3^- in typical sediments so AMIBA will likely provide a significant enhance



the understanding of intrinsic bioremediation at the majority of fuel contaminated sites.

5.5.8. Rate Constant Analysis

Using AMIBA, data estimates of the source decay rates were made according to Equation 44. Being conservative, active source loading could have occurred from 1964 through 1998 with the removal of the UST system. Thus, acceptable values for time (t) range from 13 to 25 years. Using those dates and given an ECI of 96% will result in an estimated k value ranging from 0.13 to 0.24 year⁻¹.

As is shown below, these source decay values can be used in dynamic fate and transport groundwater simulations. However, simple analytical methods can be employed to estimate the time for site cleanup. Given that, semi-steady state conditions exist for a monitoring well, decreases in contaminant concentrations are directly proportional to decreases in source loading. Thus, site cleanup can be estimated by applying first order decay to the observed

concentration in a monitoring well near the source area using the k derived from AMIBA.

The procedure above was applied to monitoring well CF-3 as is shown on Figure 5.53. The estimated time for cleanup is then dependent on the concentration limit. For a regulatory limit of 10 mg/L total BTEX the required cleanup time would range from 25 to 45 years depending on the rate constant used.

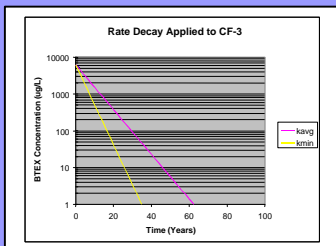


Figure 5.53

5.5.9. Groundwater Modeling

The fate of the BTEX plume was simulated using the groundwater flow and mass transport model Bioplume III (Rafai et al., 1997). Standard groundwater modeling procedures were used. AMIBA data contributed to the modeling effort in two distinct ways:

- Based on iron footprint analysis it could be ascertained that the plume was shrinking in extent so modeling could be simplified with respect to the initial plume calibration;
- Source rate constants could be defined and applied to the simulation definitively.

5.5.9.1. *Model Definition and Flow Simulation*

A model domain of 1500 feet in the x direction and 950 feet in the y direction was established over the project site. This area was divided into $x = y = 50$ foot unit cell size. No flow boundaries were set around the entire parameter of the model area. From slug test data, hydraulic conductivity ranged from $1e-5$ to $3.5e-4$ ft/sec (Figure 5.54). Based on the observed water table maps high hydraulic conductivity was set along the 48-inch sewer line and in certain portions of the source area. The model thickness was defined as 35 feet with an average porosity of 0.25. and average density of 1.75 g/cm^3 .

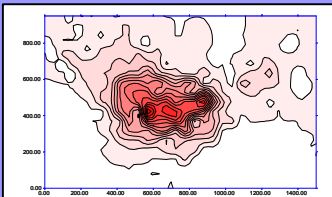


Figure 5.54

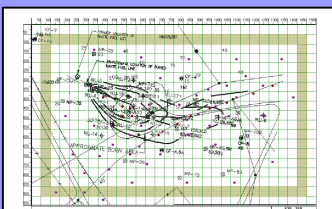


Figure 5.55

To achieve proper simulated head distribution, water was withdrawn from the simulation from eight cells located along the 48-inch sewer line that is below the water table surface. A constant withdraw rate of 0.002 to $.0002 \text{ ft}^3/\text{sec}$ was applied. The location of those points is shown on Figure 5.55. The model was run as a steady state simulation.

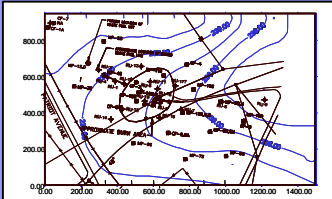


Figure 5.56

The resulting calibrated potentiometric surface map from modeling is shown on Figure 5.56. The simulated surface compares within tolerance with the observed water table surface (Figure 5.2).

5.5.9.2. Mass Transport Definition and Initial Steady State Simulation

Because the plume was known to be retreating, the initial calibration step for hydrocarbon mass transport was simplified. Five injection wells were located on the site to provide source loading. Four were located in the vicinity of the burn pit and one in the UST area. These wells were given extremely low injection rates ($1\text{e-}6 \text{ ft}^3/\text{sec}$) so they did not impact the water table surface. A first order decay rate for dissolved hydrocarbon of 0.0015 day^{-1} was used in all simulations. This value was calculated using the method of Buscheck and Alcantar (1995) and was originally developed for this site by Parsons Engineering Science, Inc. (1997). A K_d value of 0.09 was used creating a retardation factor of 1.63. A dispersivity value of 8 was used with a lateral/transverse ratio of 0.3. By iteration, successive

simulations were conducted wherein the injected concentration of hydrocarbon was varied in each well until the concentrations in the source area approximated observed concentrations from the last sampling event (>10,000 mg/L).

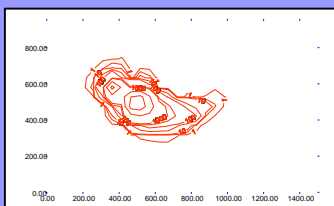


Figure 5.57

Using the above defined input values a satisfactorily calibrated steady state mass transport simulation was developed. This simulation was set for a 20-year duration. Steady state was achieved after 15 years. Beyond that time, modeled plume concentrations were approximately the same for each time step. The steady state plume distribution is shown on Figure 5.57 and correlates well with the observed concentrations on Figure 5.3. Although a rate constant for the dissolved solute was used in this simulation, the plume size cannot decrease below the steady state area until a source decay term is applied.

5.5.9.3. *Natural Attenuation Simulation*

After the steady state simulation was completed, two separate models were developed to simulate plume fate with source decay. These simulations respectively used the

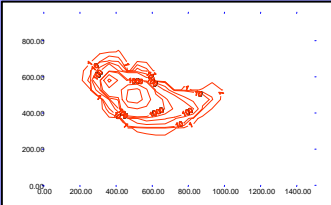


Figure 5.58

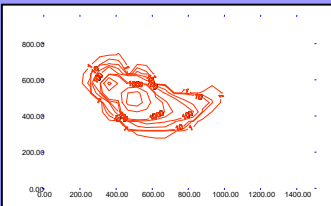


Figure 5.59

average and high first order rate constants developed by AMIBA of 0.13 to 0.24 year⁻¹. To reflect source decay, the source cells in the simulation were allowed to run at steady state for 15 years to permit full plume development. After that time, source concentration was decreased according to the specified rate constant in step increments of five years over an additional 50-year simulation period. Simulation results for the average and fast source decay rates can be seen as time animation on Figures 5.58 and 5.59.

With a source decay of 0.13 year⁻¹ the site does not achieve a minimum concentration of 10 mg/L until approximately 50 years. For the 0.24 year⁻¹ decay rate the site is projected to be at the 10 mg/L cutoff in about 30 years. Both simulation values correlate well to the estimated cleanup times calculated analytically above (Figure 5.56).

5.5.9.4. *Source Removal Simulation*

Natural attenuation has been active at this site and has contributed significantly towards cleanup. However, both analytical and numerical analyses indicate a fairly long time period is required for complete restoration using natural

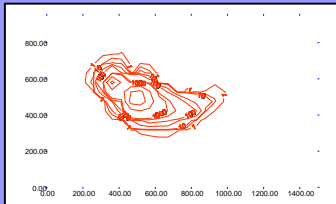


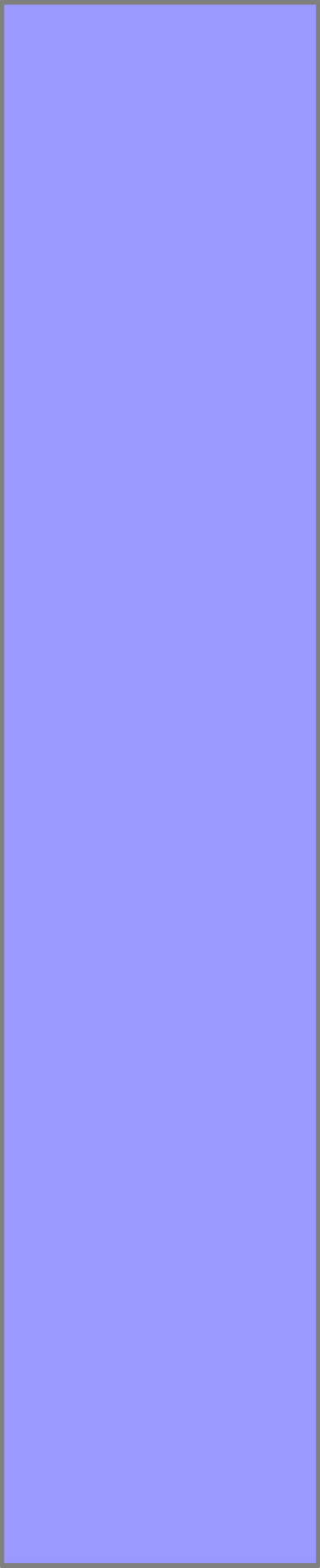
Figure 5.60

attenuation alone. An alternative is for source removal relying on natural attenuation to ameliorate residual fuel. This option was simulation by permitting the source wells to run at steady state for the obligatory initial 15 years followed by 5 years of source decay, then a cessation of source loading through the remaining term of the simulation.

The results of this final simulation can be seen on Figure 5.60. This approach will result in the complete restoration of the site in approximately 20 years.

5.6. Discussion and Recommendations

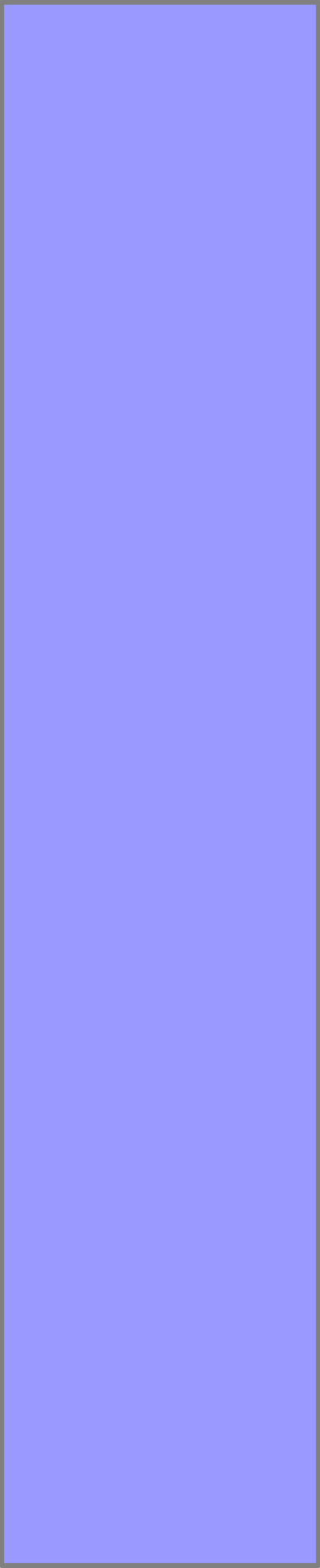
AMIBA has demonstrated aggressive intrinsic bioremediation processes have been active on this site. The primary redox pathway has been via Fe^{3+} reduction. Approximately 88% of the released hydrocarbon was attenuated through this process. In this case, an examination of mineral phase was necessary because aqueous data would indicate Fe^{3+} reduction was insignificant. AMIBA recovered 300 times more Fe^{3+} AC than aqueous methods alone. Similarly, SO_4^{2-} reduction was found to be the second largest oxidative pathway.



Mineralogical analysis improved EC estimates for SO_4^{2-} by over 2.5 times. Finally, using the sulfide indexing method facilitated much better analysis of O_2 and NO_3^- expressed capacity.

Using aqueous data only, the prior natural attenuation study could only generally identify the active redox processes on-site. AMIBA permitted a quantitative assessment of natural attenuation. It was determined that approximately 67 gallons of fuel are currently present on site. Of that mass 85% is in the soil phase. From mineral analysis it was determined that approximately 1,480 gallons of fuel had been destroyed by microbial processes. Thus, 96% of the original release has been remediated by in-situ biological processes. AMIBA accounted for over 13 times more expressed capacity than estimation methods relying only on aqueous data.

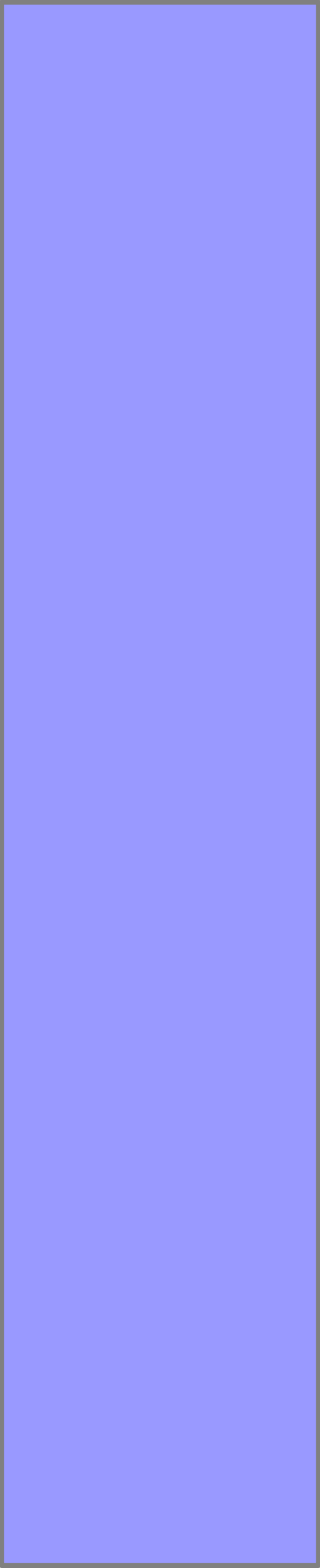
The soluble electron acceptors are continually supplied to this site via advection. Therefore, there is no reason to believe that redox those processes will be inhibited in the future. However, the supply of Fe^{3+} is finite in the



aquifer matrix. Mineral evaluation shows that a minimum 15% Fe^{3+} remains in the most depleted sections of the aquifer. Observing that only 4% of the original hydrocarbon mass remains suggests that the bioavailable Fe^{3+} assimilative capacity of is easily sufficient. Thus, Fe^{3+} reduction will continue as a dominant microbial pathway for contaminant oxidation.

Under proper redox conditions, microbial Fe^{3+} reduction and Fe^{2+} deposition occur in close proximity to the electron donor hydrocarbon. At this site, significant mineral Fe^{3+} depletion and Fe^{2+} deposition occur down gradient of the known hydrocarbon area. That mineralogical condition marks the prior plume extent and indicates that this plume has reduced in size. Thus, one need only be concerned with potential receptors within the current boundary of the plume.

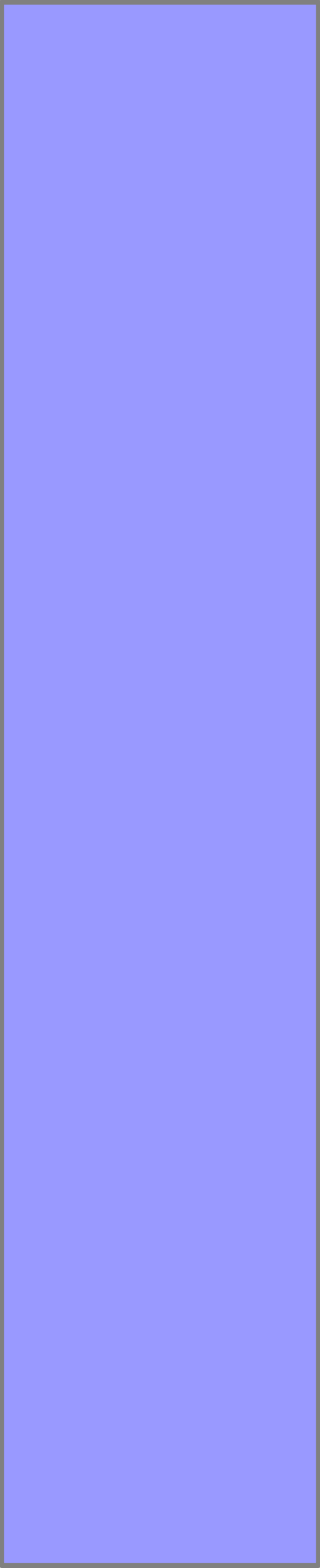
The prior natural attenuation study had estimated the dissolved hydrocarbon phase rate constant of 0.0015 day^{-1} (0.54 year^{-1}); however, estimates for source decay could not be verified from site data. Predictions of site cleanup cannot be developed without that term. Using data from AMIBA, the



calculation of a source decay term ranging from 0.13 to 0.24 year⁻¹ was possible.

A series of groundwater flow and mass transport computer simulations were performed. If a dissolved phase decay term is only available the resulting simulated plume can only achieve a steady state condition. However, the rate constants from AMIBA analysis were introduced for source decay facilitating the simulation of plume collapse over time. This permitted an estimate of total site restoration under various scenarios. These simulations indicate that with natural attenuation alone, the site will attain complete cleanup in a period ranging from 30 to 50 years.

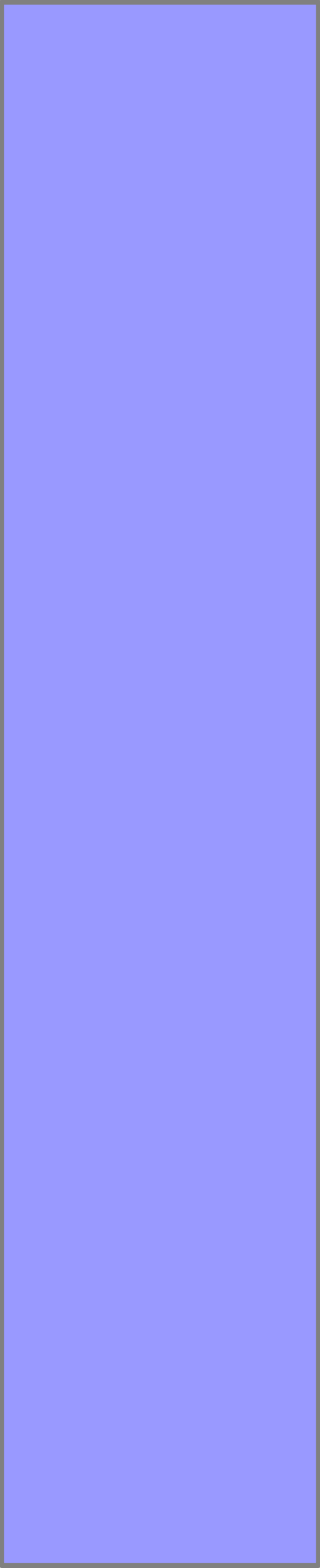
It was demonstrated that intrinsic bioremediation has been very aggressive at this site and will completely address the problem. However, the time required for complete restoration using natural attenuation alone may be undesirable. Therefore, a computer simulation was conducted assuming substantial source removal followed by natural attenuation of the residual BTEX mass. The



modeled results indicate that the site would be completely remediated in approximately 20 years.

If source removal is selected, the results of the AMIBA assessment should strongly be considered. One prior study suggested capping the site with asphalt as a treatment option. However, as has been demonstrated here, most of the residual hydrocarbon is on or below the water table. Thus, capping will be ineffective. A second proposed treatment, bioventing, will also be of limited use due to the same problem.

Many of the common in-situ treatment techniques including sparging or ORC application will be significantly hampered by the presence of large amounts of mineral Fe^{2+} . Although only 67 gallons of BTEX remain onsite, over 18 times that amount of oxidizable Fe^{2+} exists in mineral form. Thus, a significant amount of the oxygen supplied to this system will potentially be used for iron oxidation rather than being used as an electron acceptor for aerobic bacteria. Further, the addition of oxygen in any form will be severely

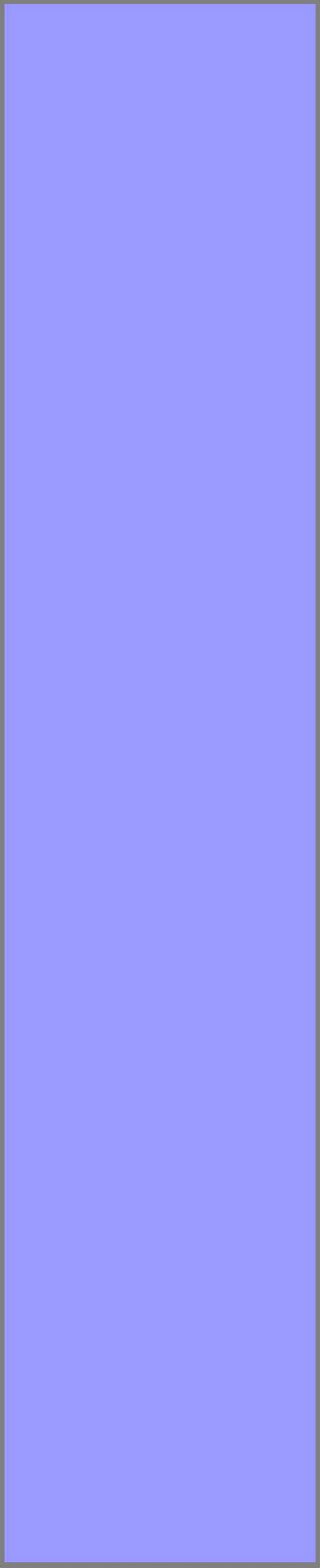


complicated by iron fowling through mineral precipitation and biomass from chemoautotrophic iron oxidizing bacteria.

The best technical option for source removal may be direct excavation followed by soil treatment or landfill emplacement. The excavation area can planned by examining the three-dimensional model of soil BTEX distribution shown on Figure 5.16. Estimates of requisite soil removal volumes can be seen on Figure 5.19.

5.7. Conclusions

In summary, the AMIBA approach demonstrated that significant biodegradation of fuel has occurred on this site. The plume is shrinking in arial extent. The natural in-situ remediation processes will continue and can fully achieve site restoration; however, the duration for that cleanup may be unacceptable. Source removal will significantly decrease the time required for natural attenuation to treat any residual hydrocarbons. Most of the common in-situ treatment technologies will be significantly impaired by the large quantity of reduced mineral species present. Thus, direct



excavation followed by ex-situ treatment of contaminated soils is recommended should this option be desired.

6. REFERENCES

- Appelo, C., and D. Postma, 1994. Geochemistry, groundwater and pollution; A.A. Balkema, Rotterdam, p. 536.
- ASTM, 1995. Standard guide for risk-based corrective action applied at petroleum release sites; Designation: E 1739-95, West Conshohocken, PA., p. 51-68.
- ASTM, 1996. Standard guide for remediation by natural attenuation at petroleum release sites (DRAFT).
- Atlas, R. and R. Bartha, 1993. Microbial ecology, fundamentals and applications; Benjamin/Cummings, N.Y., NY.
- Barbaro, J., J. Barker, L. Lemon, and C. Mayfield, 1992. Biotransformation of BTEX under anaerobic denitrifying conditions: Field and laboratory observations, *Journal of Contaminant Hydrology*, 11:245-272.
- Baedecker, M., I. Cozzarelli, J. Evans, and P. Hearn, 1992. Authigenic mineral formation in aquifers rich in organic material; In: *Water-Rock Interaction, Proc. 7th International Symp. on Water Rock Interaction*, Yousif K. Kharaka and Ann S. Maest eds., A.A. Balkema Pub., p. 257-261.
- Beller, H., D. Grbic-Galic, and M. Reinhard, 1992. Microbial degradation of toluene under sulfate-reducing conditions and the influence of iron on the process; *Applied & Environmental Microbiology*, 58:786-793.
- Bennett, P., 1991. Quartz dissolution in organic-rich aqueous systems. *Geochimica Cosmochimica Acta*, 49:1781-1797.
- Berner, R., 1980. Early diagenesis, Princeton University Press, Princeton, NJ., p. 241.
- Brady, C., 1990. The nature and properties of soils, Macmillian Pub. Co., N.Y.
- Buscheck, T.E., and Alcantar, C.M., 1995. Regression techniques and analytical solutions to demonstrate intrinsic bioremediation, In: *Proceedings of the 1995 Battelle International Symposium on In Situ and On-Site Bioreclamation*.
- Canfield D., 1988. Reactive iron in marine sediments; *Geochimica et Cosmochimica Acta*, 53:619-632.
- Canfield D., R. Raiswell, J. Westrich, C. Reaves, and R. Berner, 1986. The use of chromium reduction in the analysis of reduced inorganic sulfur in sediments and shales; *Chemical Geology*, 54:149-155.
- Chiles, J.P. and Pierre Delfiner, 1999. *Geostatistics: modeling spatial uncertainty*, John Wiley, N.Y., N.Y., pp. 695.
- Chesterman, C., and K. Lowe, 1987. Field guide to north American rocks and minerals; Audobon Society Press, N.Y., NY.
- Crouzet, C., R. Altmann, and A. Bourg, 1994. Sulfur speciation in aquifer sediments contaminated by landfill leachate: Methodology and application of the Vejen landfill, Denmark; Dept. of Geochem. and Phys. Chem., BRGM, 45060 Orleans Cedex 2, France (unpublished), pp. 27.

- Drobner, E., H. Huber, G. Wächtershäuser, D. Rose, and K. Stetter, 1990. Pyrite formation linked with hydrogen evolution under anaerobic conditions; *Nature*, 346:742-744.
- Eaton, A., L. Clesceri, and A. Greenberg, eds, 1995. Standard methods for the examination of water and wastewater, American Water Works Association, Denver, CO.
- Ehrlich, H., 1996. Geomicrobiology, Marcel Dekker, N.Y, pp. 719.
- Evangelou, V., and Y. Zhang 1995. A review: pyrite oxidation mechanisms and acid mine drainage prevention; *Critical Reviews in Environmental Science and Technology*; 25(2):141-199.
- Fortin, D., B. Davis, G. Southam, and T. Beveridge 1994 Biogeochemical phenomena induced by bacteria within sulfidic mine tailings; *Journal Industrial Microbiology*.; 14:178-185.
- Gaudy, A. and E. Gaudy, 1988. Elements of bioenvironmental engineering; Engineering Press, Inc., San Jose, CA.
- Ghiorse, W., 1988. Microbial reduction of manganese and iron. In: A.J.B. Zehnder, ed. Biology of Anaerobic Microorganisms. Wiley, New York, N.Y.
- GridStat, 1997. GridStat Users Manual, Applied Computer Engineering, Houston TX.
- Hardie, L., 1991. On the significance of evaporites. *Annual Review of Earth and Planetary Science*, 19:131-168.
- Hach, 1992. Water quality handbook; Hach Company, Loveland CO.
- Hiebert F. and P. Bennett, 1992. Microbial control of silicate weathering in organic-rich groundwater. *Science*, 259:278-281.
- Herlihy, A., 1987. Sulfur dynamics in an impoundment receiving acid mine drainage; Ph.D. Dissertation, Univ. Virginia.
- Heron, G., 1994. Redox buffering in landfill leachate contaminated aquifers; M.S. Thesis, Institute of Environmental Science and Engineering, Technical University of Denmark.
- Heron, G. and T. Christensen, 1995. Impact of sediment-bound iron on redox buffering in a landfill leachate polluted aquifer (Vejen, Denmark); *Environmental Science and Technology*, 29:187-192.
- Heron, G., C. Catherine, A. Bourg, and T.H. Christensen, 1994^a. Speciation of Fe II and Fe III in contaminated aquifer sediments using chemical extraction techniques; *Environmental Science and Technology*, 28:1698-1705.
- Heron, G., T. Christensen, and J. Tjell, 1994^b. Oxidation capacity of aquifer sediments; *Environmental Science Technology*, 28:153-158.
- Hem, J., 1985. Study and interpretation of the chemical characteristics of natural water; 3ed ed., U.S. Geological Survey, Water Supply Paper No. 2254., Alexandria, VA.
- Howarth, R., 1979. Pyrite: its rapid formation in a salt marsh and its importance in ecosystem metabolism; *Science*, 203:49-51.
- Howarth, R., B. Jørgensen, 1984. Formation of ³⁵S-Labelled elemental sulfur and pyrite in coastal marine sediments (Limfjorden and Kysing Fjord, Denmark) during

- short-term $^{35}\text{SO}_4^{2-}$ reduction measurements; *Geochimica et Cosmochimica Acta*, 48:1807-1818.
- Huang, P. and M. Schnitzer, 1986. Interactions of soil minerals with natural organics and microbes; Soil Science Society of America No 17., Madison, WA.
- Hutchins, S., W. Downs, G. Smith, J. Wilson, D. Hendrix, D. Fine, D. Kovacs, R. Douglass, 1991. Effect of nitrate addition on bioremediation of fuel-contaminated aquifer: field demonstration, *Groundwater*, 29(4):571-580.
- Hutchins, S., S. Moolenaar, and D. Rhodes, 1992. Column studies on BTEX biodegradation under microaerophilic and denitrifying conditions, *Journal Hazardous Materials.*, 32:195-214.
- International Technologies, 1996. George Air Force Base draft natural attenuation monitoring treatability study report operational unit 2; Air Force Center for Environmental Excellence, San Antonio, TX.
- Jenne, E., 1977. Trace element sorption by sediments and soils – sites and processes; in: W.R. Chappell and K.K. Peterson (Editors), *Molybdenum in the Environment*, Vol. 2. Marcel Dekker, New York, NY. pp. 425-553.
- Jorgensen, B., 1990. A thiosulfate shunt in the sulfur cycle of marine sediments; *Science* 249: 152-154.
- Kennedy L.G., J.W. Everett, K. J. Ware, and V. Green, 1999. Methods for analyzing iron and iron sulfide, minerals for natural attenuation assessment with field examples; *Bioremediation Journal*, 3:259-275
- Kennedy, L.G., and J. W. Everett, 2000. Microbial Degradation of Simulated Landfill Leachate: Solid Iron/Sulfur Interactions, *Advances in Environmental Research*, In Press.
- Kennedy, Lonnie G., Jess W. Everett, Thomas Dewers, William Pickins, and David Edwards, 1998. Application of Mineral Iron and Sulfide Analysis to Evaluate Natural Attenuation at a Fuel Contaminated Site; *Journal of Environmental Engineering*, ASCE, 125
- Kitanidis, P.K., *Introduction to geostatistics: applications in hydrology*, Cambridge University Press, Cambridge, pp. 249
- Leach, L., F. Beck, J. Wilson, and D. Kampbell, 1988. Aseptic subsurface sampling techniques for hollow-stem auger drilling; *Proceedings of the 2ed National Outdoor Action Conference on Aquifer Restoration, Groundwater Monitoring and Geophysical Methods*; Association of Groundwater Scientists and Engineers, Las Vegas, NV, 1:2-24.
- Litchfield, J., and L. Clark, 1973. Bacterial activities in groundwaters containing petroleum products, *Pub. 4211, Am. Petrol. Inst., Washington, D.C.*, p. 43
- Lovley, D., and E. Phillips, 1986. Organic matter mineralization with reduction of ferric iron in anaerobic sediments, *Applied and Environmental Microbiology*, 51(4):683-689.
- Lovley, D., 1991. Dissimilatory Fe(III) and Mn(IV) reduction; *Microbiology Review*; 55:259-287.

- Lovley, D., and E. Phillips, 1987. Rapid assay for microbially reducible ferric iron in aquatic sediments; *Applied and Environmental Microbiology*.; 53(7):1536-1540.
- Lovley, D., 1987. Organic matter mineralization with the reduction of ferric iron: a review, *Geomicrobiology Journal*, 5(3/4):375-399.
- Lovley, D. 1990. Dissimilatory Fe(III) and Mn (IV) reduction. *Microbiology Review*, 55:259-287.
- Lovley, D., Phillips, E. and Lonergan, D. J., 1991. Enzymatic versus nonenzymatic mechanisms for Fe (III) reduction in aquatic sediments. *Environmental Science Technology*, 25:1062-1067.
- Lovley, D., E. Roden, E. Phillips and J. Woodward, 1993. Enzymatic iron and uranium reduction by sulfate-reducing bacteria; *Marine Geology*, 113:41-53.
- Lyon, W., 1995. Assessment of redox categories in soils and sediments monitoring iron minerals and hydrogen; Internal report, Robert S. Kerr Laboratory, National Environmental Risk Management Laboratory, Ada, OK. pp. 7.
- Matheron, G., 1971. The theory of regionalized variables and its applications, Ecole de Mines, Fontinbleau, France, pp. 212.
- McCarty, P. 1971. Energetics and bacterial growth, In: Organic Compounds and Aquatic Environments, Samuel J. Faust and Joseph V. Hunter eds., Marcell Dekker, Inc. Pub., N.Y., Ch 10, 495 - 531
- Morse, J., F. Millero, J. Cornwell, and D. Rickard, 1987. The chemistry of the hydrogen sulfide and iron sulfide systems in natural waters; *Earth Science Review*, 24:1-42.
- Munch, J. and J. Ottow, 1980. Preferential reduction of amorphous to crystalline iron oxides by bacterial activity; *Soil Science*, 129(1):15-21.
- Munch, J. and J. Ottow, 1983. Reductive transformation mechanism of ferric oxides in hydromorphic soils; *Environmental Biogeochemistry*, 35:383-394.
- Moses, C., and J. Herman, 1989. Pyrite oxidation at circumneutral pH; *Geochimica et Cosmochimica Acta*, 55:471-482.
- Munch, J. and J. Ottow, 1980. Preferential reduction of amorphous to crystalline iron oxides by bacterial activity; *Soil Science*, 129(1):15-21.
- Munch, J. and J. Ottow, 1983. Reductive transformation mechanism of ferric oxides in hydromorphic soils; *Environmental Biogeochemistry*, 35:383-394.
- Parsons Engineering Science, Inc. 1994. Intrinsic remediation engineering evaluation/cost analysis for ST-29, Air Force Center for Environmental Excellence, San Antonio, TX.
- Parsons Engineering Science, Inc., 1995a. Treatability study in support of intrinsic remediation for the Hangar 10 Site, Elmendorf Air Force Base, Anchorage, Alaska, Air Force Center for Environmental Excellence, San Antonio, TX.
- Parsons Engineering Science, Inc., 1995b. Treatability study in support of intrinsic remediation for site ST-41, Elmendorf Air Force Base, Anchorage, Alaska, Air Force Center for Environmental Excellence, San Antonio, TX.

- Parsons Engineering Science, Inc., 1997. Treatability Study in Support of the Intrinsic Remediation Option at the Current Fire Training Area, Westover Air Reserve Base, Chicopee, Mass., Air Force Center for Environmental Excellence, Technology Transfer Division, Brooks Air Force Base, San Antonio, TX.
- Pettijohn, F., 1975. Sedimentary rocks; 3ed ed., Harper and Row, New York, NY.
- Plummer, L. 1977. Defining reactions and mass transfer in part of the Floridan aquifer; *Water Resources Research* 13:801-812.
- Plummer, L., J. Busby, R. Lee, and B. Hanshaw, 1990. Geochemical modeling of the Madison aquifer in parts of Montana, Wyoming, and South Dakota; *Water Resources Research* 26(9):1981-2014.
- Pierzynski, G., J. Sims, and G. Vance, 1994. Soils and environmental quality; CRC Press, Boca Raton, FL.
- Postma, D., C. Boesen, H. Kristiansen, and F. Larsen, 1991. Nitrate reduction in an unconfined sandy aquifer: Water chemistry, reduction processes, and geochemical modeling; *Water Resources Research*, 27:2027-2045.
- Postma, D., 1981. Formation of siderite and vivianite and the pore-water composition of a recent bog sediment in Denmark; *Chemical Geology*, 31:225-224.
- Postma, D., 1982. Pyrite and siderite formation in brackish and freshwater swamp sediments; *American Journal Science*, 282:1151-1183.
- Pyzik, A., and S. Sommer, 1981. Sedimentary iron monosulfides: kinetics and mechanism of formation; *Geochimica et Cosmochimica Acta*, 45:687-698.
- Rifai, H., P. Bedient, R. Borden, J. Haasbeek, 1987. Bioplume II, computer model of two-dimensional contaminant transport under the influence of oxygen limited biodegradation in groundwater; Rice Univ. Houst. Tx.
- Rafai, H., S., C. Newell, J. Gonzales, S. Dendrou, L. Kennedy, and J. Wilson. 1997. Bioplume III: Natural attenuation decision support system, ver 1.0; Air Force Center for Environmental Excellence, San Antonio, TX.
- Rice, C., M. Tuttle, and R. Reynolds, 1993. The analysis of forms of sulfur in ancient sediments and sedimentary rocks: Comments and cautions; *Chemical Geology*, 107:83-95.
- Ridgeway, H., J. Safarik, D. Phipps, P. Carl, and D. Clark, 1990. Identification and catabolic activity of well-derived gasoline degrading bacteria from a contaminated aquifer; *Applied Environmental Microbiology*. 56(11):3565-3575.
- Roden, E. and J. Zachara, 1996. The reduction of Fe Iron (III) Oxides: Measure of oxide surface area and potential for cell growth; *Environmental Science and Technology*, 30(5):1618-1628.
- Robinson, G., 1984. Sequential chemical extractions and metal partitioning in hydrous Mn-Fe-oxide coatings: Reagent choice and substrate composition affect results, *Chemical Geology*, 47:97-112.
- Sidhu, P., R. Gilkes, R. Cornell, A. Posner, and J. Quirk, 1981. Dissolution of iron oxides and oxyhydroxides in hydrochloric and perchloric acids; *Clays Clay Miner.* 29(4)269-276.

- Stumm, W., and J. Morgan, 1996. Aquatic chemistry an introduction emphasizing chemical equilibrium in natural waters, John Wiley & Sons, N.Y., p. 1022.
- Stookey, L., 1970. Analytical Chemistry, 42(7):779.
- Thorstenson, D., D. Fisher, and M. Croft, 1979. The geochemistry of the Fox Hills-Basal Hell Creek aquifer in southwestern North Dakota and northwestern South Dakota; Water Resources Research 15:1479-1498.
- Thomas, G.M., 1987. Sedimentation in a proglacial lake: Glacial Lake Hitchcock, Rutgers University.
- Tuttle, J., P. Dugan, C. Macmillan, and C. Rand, 1969. Microbial dissimilatory sulfur cycle in acid mine water; Journal of Bacteriology; 97:594-602.
- Ulrich, G. A., L. Krumholdz, and J. Suflita, 1997. A rapid and simple method for estimating sulfate reduction activity and quantifying inorganic sulfides; Applied Environmental Microbiology, 63(4):1627-1629.
- Weast, R., A. Melvin, and B. William eds., 1987. CRC handbook of chemistry and physics; 67th ed., CRC Press, Inc., Boca Raton, FL.
- Wicks, C. M., 1989. Early diagenesis of iron and sulfur in sediments of lakes that receive acid mine drainage; Masters Thesis, University of Virginia.
- Wiedemeier, Todd H., J. Wilson, D. Kampell, R. Miller, J. Hansen, 1999. Technical protocol for implementing intrinsic remediation with long-term monitoring for natural attenuation of fuel contamination dissolved in groundwater, Vol 1 and 2, Air Force Center for Environmental Excellence, Brooks Air Force Base, San Antonio, TX.
- Whittemore, D. and Langmuir, D., 1975. The solubility of ferric oxhydroxides in natural waters; Groundwater, 13:360-365.

Appendix 1: Geologic Logs

BORING RECORD

DEPTH (FEET)	LITHOLOGIC DESCRIPTION	GRAPHIC SYMBOL	PID ORGANIC VAPOR PPM X 45.0										SAMPLE				
			2	4	6	8	10	12	14	16	18	20	PID READING	DEPTH			
0.3	TOPSOIL: DARK BROWN, ABUNDANT ROOTS																0
1.9	SAND: LIGHT TAN, FINE-VERY FINE GRAINED, PARTIAL GRADING, 5% FELD, DRY	•••••													66	2.0	
	ORGANIC CLAY: DARK BROWN	•••••													812	4.0	
	SAND: DARK TANK, VERY FINE GRAINED, HIGHLY ORGANIC, 2% FELD, SLIGHT FeOx STAINS, DRY	•••••													770	6.0	5
5.5	SAND: GRAY, MEDIUM-FINE GRAINED WITH 2% PEBBLES, MOST FeOx IS GONE, SAMPLE IS MOIST	•••••													770	8.0	
7.0	SAND: GRAY, WITH SLIGHT RUST MOTTLING, COARSE-VERY FINE GRAINED, WELL GRADED, 2% PEBBLES, 1% RUTIL, 5% FELD, WET, SOME Fe STAINING, RED IN ZONE OF FeOx REMAINING	•••••													32	10.0	10
9.0	SAND: DARK GRAY, VERY COARSE-FINE GRAINED, 5% GRANET, NO FeOx, PROBABLE ABUNDANT FeS, WET	•••••													68	12.0	
9.5	SAND: VERY FINE GRAINED, LIGHT RUSTY GRAY, COARSE-MEDIUM GRAINED, 3% PEBBLES, SLIGHT FeOx STAIN, POSSIBLE SLIGHT FeS, 2% RUTIL, 10% CLAY CHIPS	•••••													16.4	14.0	
12.0	SAND: LIGHT RUSTY GRAY WITH SLIGHT FeOx MOTTLING, FINE-VERY FINE GRAINED, MEDIUM GRADING, 3% PEBBLES, 15% BIOTITE, 1% RUTIL, MOSTLY WITH FeOx WITH SOME MOTTLED REDUCED ZONES, WET	•••••													34.5	16.0	15
15.5	SAND: GRAY, COARSE-FINE GRAINED, WELL GRADED, SUBANGULAR, 3% FELD, 10% BIOTITE, MOST FeOx MOVED WITH SOME MOTTLING, PROBABLE HIGH FeS, WET	•••••													15	18.0	
16.0	SAND: LIGHT GRAY BROWN, FINE-VERY FINE GRAINED, PARTIALLY GRADED, SUBANGULAR, ABOUT 70% FeOx REMOVED IN MOTTLED AREAS, 15% BIOTITE, 64% SHALE, 1% ZEOLITE, 1% RUTIL, WET	•••••													11.9	20.0	20
18.5	SAND: RUSTY BROWN, VERY COARSE TO FINE GRAINED, WELL GRADED, SUBANGULAR, 3% FELD, 5% BLACK BASALT??, 1% ZEOLITE, VERY HIGH FeOx STAIN	•••••													12	22.0	
20		•••••													17.3	24.0	
25		•••••													20.3	26.0	25
		•••••													4.5	28.0	
		•••••													8.8	30.0	30
30.0	TOTAL DEPTH: 30.0 FEET																

WESTOVER AFB BURN PIT

SITE _____

BORING NUMBER **RU-1**

DATE DRILLED 8/2/99

DRILLED BY ROWAN UNIVERSITY

LOGGED BY L. KENNEDY

BORING RECORD

DEPTH (FEET)	LITHOLOGIC DESCRIPTION	GRAPHIC SYMBOL	PID ORGANIC VAPOR										SAMPLE	
			PPM X <u>45.0</u>										PID READING	DEPTH
			2	4	6	8	10	12	14	16	18	16		
0	TOPSOIL, BROWN SANDY LOAM: WITH ABUNDANT ROOTS, DRY													
0.8	FILL, ALTERNATING TAN AND BLACK FILL SAND AND GRAVEL: WITH BLACK BURNED SAND												42	2.0
3.0	SILT: BLACK, 40% CLAY, SLIGHTLY MOIST, BURNED												39.5	4.0
3.5	SILT: OLIVE GRAY, 40% CLAY, PROBABLE Fe RED, LITTLE FeOx, MOIST, GRADES TO FINE SAND IN BASE												884	6.0
5.0	SAND: LIGHT GRAY, MEDIUM TO FINE GRAINED WITH 3% PEBBLES, SUBANGULAR, WELL GRADED, 8% BASALT, MOIST FeOx WITH SOME Fe REDUCTION, WET												650	8.0
8.5	SAND: LIGHT YELLOWISH GRAY, MEDIUM TO VERY FINE GRAINED, WELL GRADED, SUBANGULAR, 8% BLACK BASALT, LIGHT FeOx WITH SOME Fe REDUCTION, WET												180	10.0
9.5	SAND: GREY TO SLIGHTLY YELLOWISH GRAY, COARSE TO FINE GRAINED WITH 8% PEBBLES, WELL GRADED, SUBANGULAR, 4% BASALT, ALMOST ALL FeOx REDUCED												17.8	12.0
11.0	SAND: AS ABOVE WITH 10% GRAVEL AND 10% PEBBLES, 5% ZEOLITE, 10% BASALT												28.5	14.0
13.0	SAND: ORANGE RUST, COARSE GRAINED, 5% PEBBLES, PARTIALLY GRADED, SUBANGULAR, 8% BASALT, VERY HIGH FeOx												7.5	16.0
13.5	SAND: VERY LIGHT ORANGE GRAY, FINE TO VERY FINE GRAINED, PARTIALLY GRADED, SUBANGULAR, 10% BASALT, 8% BIOTITE, SLIGHTLY EVEN FeOx COATING, WET												24	18.0
14.0	SAND: AS ABOVE BUT SOLID GRAY WITH VERY SLIGHT FeOx												9.7	20.0
15	SAND: VERY LIGHT RUSTY GRAY, WITH ONE STREAK OF RUST, MEDIUM TO VERY FINE GRAINED, PARTIALLY GRADED, SUBANGULAR TO ANGULAR, 5% BASALT, 3% BIOTITE, LIGHT TO MODERATE EVEN FeOx STAINING, WET												8.3	22.0
16.5	SAND: GE GRAY, FINE TO VERY FINE GRAINED, SUBANGULAR, PARTIALLY GRADED, 10% BASALT, 5% BIOTITE, VERY SLIGHT EVEN FeOx												3.5	24.0
17.5	TOTAL DEPTH: 19.0 FEET													

WESTOVER AFB BURN PIT

SITE _____

BORING NUMBER **RU-4**

DATE DRILLED 8/8/99

DRILLED BY ROWAN UNIVERSITY

LOGGED BY L. KENNEDY

BORING RECORD

DEPTH (FEET)	LITHOLOGIC DESCRIPTION	GRAPHIC SYMBOL	PID ORGANIC VAPOR PPM X 50.0										SAMPLE			
			2	4	6	8	10	12	14	16	18	20	PID READING	DEPTH		
0	TOPSOIL - BROWN SILT LOAM: WITH ABUNDANT ROOTS	[Symbol]														0
0.5	FILL SAND: TAN, VERY FINE GRAINED	[Symbol]													255	2.0
1.0	FILL SILTY CLAY: BLACK, BURNED	[Symbol]														
2.0	FILL SAND: DARK RUSTY BROWN, MEDIUM TO FINE GRAINED, MIXED WITH GRAVEL	[Symbol]													935	4.0
3.3	SAND: DARK RUST, COARSE TO VERY FINE GRAINED, 5% GRAVEL, WELL GRADED, SUBROUNDED, 4% BASALT, VERY HIGH FeOx, VERY SLIGHTLY MOIST	[Symbol]													707	6.0
4.5	SAND: AS ABOVE, RUSTY BROWN, HIGH FeOx	[Symbol]														
6.0	SAND: LIGHT RUSTY TAN, COARSE TO VERY FINE GRAINED, SUBROUNDED, WELL GRADED, 10% BASALT, 2% ZEOLITE, LIGHT EVEN FeOx, SLIGHTLY MOIST	[Symbol]													880	8.0
8.5	SAND: VERY LIGHT RUSTY GRAY, COARSE TO VERY FINE GRAINED, SUBANGULAR, WELL GRADED, 10% BASALT, 2% ZEOLITE, LIGHT FeOx COATING, PROBABLE Fe REDUCTIONS, SLIGHTLY MOIST	[Symbol]													924	10.0
10	SAND: VERY LIGHT RUSTY GRAY TO GRAY, 3% PEBBLES, MEDIUM TO VERY FINE GRAINED, WELL GRADED, SUBANGULAR, 5% BASALT, 2% ZEOLITE, VERY LIGHT FeOx STAIN, PROBABLE Fe REDUCTION, FeOx REMOVAL INCREASE WITH DEPTH	[Symbol]													30.8	12.0
12.0	SAND: GRAY TO VERY SLIGHT RUSTY GRAY, COARSE TO FINE GRAINED, SUBANGULAR, WELL GRADED, 5% BASALT, 5% FELD, 2% ZEOLITE, ALMOST ALL FeOx REMOVED, WET	[Symbol]													64.4	14.0
14.0	SAND: GRAY, FINE GRAINED, PARTIALLY GRADED, SUBANGULAR, 12% BASALT, 5% BIOTITE, 2% ZEOLITE, VERY LIGHT EVEN FeOx STAINS, WET AT 16'-18', HAD ONLY 10% RECOVERY, NO SAMPLES COLLECTED	[Symbol]													32.7	16.0
15	SAND: AS ABOVE, MEDIUM TO FINE GRAINED, NOTE 20'-22' NO SAMPLE	[Symbol]													26.7	18.0
18.0	SAND: AS ABOVE, FINE GRAINED, VERY POOR RECOVERY	[Symbol]													24.8	20.0
20	SAND: GRAY, FINE TO VERY FINE GRAINED, SUBANGULAR, PARTIALLY GRADED, 12% BASALT, 5% BIOTITE, VERY POOR FeOx TO NO FeOx, POSSIBLE Fe REDUCTION	[Symbol]													10.1	24.0
22.0	SAND: VERY LIGHT RUSTY GRAY, FINE TO VERY FINE GRAINED, PARTIALLY GRADED, SUBANGULAR, 15% BASALT, VERY LIGHT EVEN FeOx STAIN	[Symbol]													12	26.0
24.0	SAND: VERY LIGHT RUSTY GRAY, MEDIUM TO VERY FINE GRAINED, PARTIALLY GRADED, SUBANGULAR, 12% BASALT, 5% FELD, LIGHT EVEN FeOx	[Symbol]													8.0	28.0
25		[Symbol]													14.9	30.0
26.0		[Symbol]													4.6	32.0
30		[Symbol]													4.4	34.0
32.0		[Symbol]													4.3	
34.5		[Symbol]														

WESTOVER AFB BURN PIT

SITE

BORING NUMBER **RU-5**

DATE DRILLED 8/4/99

DRILLED BY ROWAN UNIVERSITY

CHECKED BY L. KENNEDY

BORING RECORD

DEPTH (FEET)	LITHOLOGIC DESCRIPTION	GRAPHIC SYMBOL	PID ORGANIC VAPOR PPM X 50.0								SAMPLE					
			2	4	6	8	10	12	14	16	18	PID READING	DEPTH			
35 36.0	SAND: ORANGE TAN, COARSE TO FINE GRAINED, SUBANGULAR, WELL GRADED, 8% BASALT, 5% FELD, MODERATE TO HIGH FeOx COATING, WET TOTAL DEPTH: 38.0 FEET	•••••												36.0	35	
40																40
45																45
50																50
55																55
60																60
65																65

WESTOVER AFB BURN PIT

SITE _____

BORING NUMBER **RU-5**

DATE DRILLED 8/4/99

DRILLED BY ROWAN UNIVERSITY

CHECKED BY L. KENNEDY

70

BORING RECORD

DEPTH (FEET)	LITHOLOGIC DESCRIPTION	GRAPHIC SYMBOL	PID ORGANIC VAPOR PPM X 1.0										SAMPLE		
			2	4	6	8	10	12	14	16	18	PID READING	DEPTH		
0	SAND FILL: BROWN SAND AND GRAVEL MIXED, DRY, NO ROOTS	[Symbol]													
0.8	SAND FILL: BLACK BURNED SAND AND SLAG, DRY	[Symbol]											10.9	2.0	
1.0		[Symbol]													
2.5	SAND FILL: BROWN FINE SAND AND GRAVEL MIXED	[Symbol]											10.1	4.0	
	SAND: OLIVE TAN, FINE-VERY FINE GRAINED, 35% SILTY CLAY, MODERATE-HIGH FeOx COATING, POSSIBLE Fe RED, MOIST	[Symbol]											11.2	6.0	
5	SAND: LIGHT ORANGE TAN, COARSE-FINE GRAINED, WELL GRADED, SUBANGULAR, 8% BASALT, MODERATE FeOx STAINING, SLIGHTLY MOIST	[Symbol]											4.0	8.0	
7.0	SAND: LIGHT RUSTY GRAY-GRAY, FINE-VERY FINE GRAINED, SUBANGULAR, PARTIALLY GRADED, 10% BASALT, 3% BIOTITE, LIGHT FeOx COATING, SLIGHTLY MOIST	[Symbol]											5.8	10.0	
7.5		[Symbol]											3.2	11.0	
9.0	SAND: RUSTY TAN, COARSE-VERY FINE, WELL GRADED, GRAINED, 10% FELD, 8% BASALT, 3% BIOTITE, MODERATE FeOx WITH A FEW BANDS OF VERY HIGH FeOx, SLIGHTLY MOIST, GRAY Fe RED MOTTLED ZONES WITH DEPTH	[Symbol]											4.6	12.0	
10.3		[Symbol]											6.4	13.0	
12.0	SAND: LIGHT ORANGE GRAY, MEDIUM-VERY FINE GRAINED, SUBANGULAR, PARTIALLY GRADED, 2% FELD, 12% BASALT, 2% ZEOLITE, LIGHT FeOx WITH SOME Fe RED POSSIBLE	[Symbol]											6.5	14.0	
15	SAND: GRAY, COARSE-VERY FINE GRAINED, 15% LAYERS OF COBBLES AND PEBBLES, WELL GRADED, SUBANGULAR, 8% BASALT, 2% FELD, 2% ZEOLITE, ALMOST ALL FeOx REMOVED, WET	[Symbol]											5.4	16.0	
15.5		[Symbol]											5.4	18.0	
15.8	SAND: GRAY, MEDIUM-VERY FINE GRAINED, SUBANGULAR, PARTIALLY GRADED, 10% BASALT, 2% BIOTITE, SLIGHT FeOx, A 0.25" THICK HIGH FeOx ZONE IN BASE	[Symbol]											5.9	20.0	
16.0		[Symbol]													
17.5	SAND: VERY LIGHT RUSTY GRAY, FINE-VERY FINE GRAINED, SUBANGULAR, PARTIALLY GRADED, 14% BASALT, 3% ZEOLITE, VERY SLIGHTLY FeOx STAINING, WET	[Symbol]													
20	SAND AS ABOVE: BUT COARSE-VERY FINE GRAINED	[Symbol]													
	GRAVEL: LIGHT YELLOW BLACK AND RED, PEBBLE TO COARSE SAND, 5% FELD, 10% BASALT, LIGHT-MODERATE FeOx COATING, WET	[Symbol]													
	SAND: LIGHT ORANGE GRAY, MEDIUM TO VERY FINE GRAINED, 8% BASALT, 2% ZEOLITE, VERY LIGHT FeOx COATING	[Symbol]													
25	SAND: AS ABOVE BUT FINE-VERY FINE GRAINED	[Symbol]													
	TOTAL DEPTH: 20.0 FEET	[Symbol]													

WESTOVER AFB BURN PIT

SITE _____

BORING NUMBER **RU-6**

DATE DRILLED 8/4/99

DRILLED BY ROWAN UNIVERSITY

CHECKED BY L. KENNEDY

BORING RECORD

DEPTH (FEET)	LITHOLOGIC DESCRIPTION	GRAPHIC SYMBOL	PID ORGANIC VAPOR PPM X 1.0										SAMPLE			
			2	4	6	8	10	12	14	16	18	20	PID READING	DEPTH		
0	TOPSOIL AND CEMENT FILL: DRY															
0.5	SAND SOIL: BROWN AND TAN, SANDY LOAM, DRY	•••••													4.1	2.0
2.0	SAND FILL: ORANGE TAN, FINE GRAINED WITH 10% GRAVEL, DRY-SLIGHTLY MOIST, EVEN FeOx COATINGS-CHUNKS OF CEMENT AND GRAVEL	•••••													6.5	3.0
4.0	NO SAMPLE: ONLY SMALL AMOUNT OF SAND WITH CHUNK OF CEMENT BLOCKING BOTTOM	•••••													7.3	4.0
5																
6.0	SAND: RUSTY TAN, COARSE-FINE GRAINED, WELL GRADED, SUBANGULAR, 8% BASALT, 5% ZEOLITE, HIGH FeOx, SLIGHTLY MOIST	•••••													6.7	
7.5	SAND: ORANGE TAN, MEDIUM-FINE GRAINED, PARTIALLY GRADED, SUBANGULAR, 8% BASALT, 3% BIOTITE, EVEN FeOx COATING, WET	•••••														8.0
8.3	SAND: LIGHT RUSTIC TAN WITH RUST STREAK, FINE-VERY FINE GRAINED, 8% BASALT, MODERATE-HIGH EVEN FeOx, VERY MOIST	•••••													0.3	9.0
9.3	SAND: LIGHT ORANGE TAN, COARSE-VERY FINE GRAINED, WELL GRADED, SUBANGULAR, 8% BASALT, 4% ZEOLITE, LIGHT EVEN FeOx, POSSIBLE Fe RED, WET, A FEW STREAKS OF ORANGE WITH DEPTH WITH GRAY Fe RED MOTTELING	•••••													0.4	10.0
10															0.8	11.0
11.3	SAND: LIGHT ORANGE TAN, COARSE-VERY FINE GRAINED, WELL GRADED, SUBANGULAR, 8% BASALT, 4% ZEOLITE, LIGHT EVEN FeOx, POSSIBLE Fe RED, WET, A FEW STREAKS OF ORANGE WITH DEPTH WITH GRAY Fe RED MOTTELING	•••••													0.5	12.0
12.5															0.4	13.0
13.0															0.5	14.0
14.8	SAND: LIGHT RUSTY TAN, MEDIUM-FINE GRAINED, PARTIALLY GRADED, SUBANGULAR, 8% BASALT, 3% FELD, 2% ZEOLITE, LIGHT EVEN FeOx	•••••													0.4	15.0
15.8															0.4	16.0
18.0	SAND: LIGHT RUSTY TAN WITH 12' RUST BAND IN BASE, COARSE-FINE GRAINED WITH 10% PEBBLES IN LAYERS, WELL GRADED, SUBANGULAR, 8% BASALT, 2% BIOTITE, LIGHT TO HIGH FeOx STAIN, WET	•••••													0.7	17.0
18.5															0.7	18.0
20	SAND: LIGHT ORANGE TAN, FINE GRAINED, SUBANGULAR, PARTIALLY GRADED, 15% BASALT, 5% ZEOLITE, LIGHT EVEN FeOx, WET	•••••													0.6	19.0
	SAND: RUSTY TAN, COARSE TO FINE GRAINED, SUBANGULAR, WELL GRADED, 8% BASALT, TRACE ZEOLITE, MODERATE FeOx, WET	•••••													0.5	20.0
	SAND: LIGHT RUSTY GRAY, AND GRAY WITH SLIGHT STREAKS, RUST, FINE-VERY FINE GRAINED, PARTIALLY GRADED, SUBANGULAR-ANGULAR, 10% BASALT, 6% BIOTITE, MOSTLY HIGH FeOx BUT STREAK MODERATE, WET	•••••														
25																
	SAND: RUSTY GRAY TAN, COARSE-VERY FINE GRAINED, SUBANGULAR-ANGULAR, WELL GRADED, 8% BASALT, 4% ZEOLITE, LIGHT EVEN FeOx COATING	•••••														
	SAND: VERY LIGHT ORANGE GRAY, FINE-VERY FINE GRAINED, PARTIALLY GRADED, 10% BASALT, 5% BIOTITE, VERY LIGHT EVEN FeOx, WET	•••••														
30	TOTAL DEPTH: 20.0 FEET															

WESTOVER AFB BURN PIT

SITE _____

BORING NUMBER **RU-7**

DATE DRILLED 8/5/99

DRILLED BY ROWAN UNIVERSITY

CHECKED BY L. KENNEDY

BORING RECORD

DEPTH (FEET)	LITHOLOGIC DESCRIPTION	GRAPHIC SYMBOL	PID ORGANIC VAPOR PPM X 1.0										SAMPLE			
			2	4	6	8	10	12	14	16	18	18	PID READING	DEPTH		
0	TOPSOIL: DARK BROWN SANDY LOAM WITH ABUNDANT ROOTS														0.3	1.0
0.8	SAND: ORANGE BROWN, VERY FINE GRAINED, TRACE ROOTS, HIGH FeOx COATING														0.5	2.0
3.8	SAND: ORANGE, COARSE-VERY FINE GRAINED, WELL GRADED, SUBANGULAR-SUBROUNDED, <1% BASALT, HIGH FeOx														0.4	3.0
4.5															0.4	4.0
5.3	SAND: MEDIUM ORANGE TAN, AS ABOVE BUT LESS FeOx														2.5	5.0
5															3	6.0
5.3	SAND: YELLOW TAN, FINE-VERY FINE GRAINED														0.8	8.0
9.0	SAND: ORANGE GRAY WITH ORANGE STREAK IN TOP, COARSE-VERY FINE GRAINED, 2% PEBBLES, SUBANGULAR, WELL GRADED, 10% BASALT, LIGHT EVEN FeOx, SLIGHTLY MOIST, INCREASING PEBBLES IN BOTTOM 1' TO 8' ALSO BOTTOM ZONE IS MORE ORANGE WITH HIGHER FeOx, WET AT ABOUT 8'														0.6	10.0
10															0.3	12.0
12.0	SAND: LIGHT ORANGE TAN, MEDIUM-FINE GRAINED, SUBANGULAR, PARTIALLY GRADED, 6% BASALT, TRACE OF ZEOLITE, LIGHT EVEN FeOx COATING, WET														0.4	14.0
13.0															0.5	16.0
13.1	SAND GRADING TO GRAVEL: LIGHT RUSTY TAN, SAND IS COARSE TO FINE GRAINED, BOTTOM 0.5' IS GRAVEL MIXED WITH COARSE SAND, WELL GRADED, SUBANGULAR, 6% BASALT, 2% FELD, MODERATE FeOx, WET														0.5	18.0
14.0															0.5	18.0
15	SAND: LIGHT ORANGE GRAY, MEDIUM-FINE GRAINED, SUBANGULAR, PARTIALLY GRADED, 5% BASALT, 5% FELD, TRACE BIOTITE, LIGHT FeOx COATING, WET														0.7	20.0
17.0																
18.0	SAND: AS ABOVE ONLY RUST WITH HIGH FeOx															
18.0	SAND: LIGHT RUSTY GRAY, COARSE-VERY FINE GRAINED, WELL GRADED, SUBANGULAR, 6% BASALT, LIGHT FeOx STAIN															
19.3																
20	SAND: VERY LIGHT ORANGE GRAY, FINE-VERY FINE GRAINED, SUBANGULAR, PARTIALLY GRADED, 10% BASALT, 5% ZEOLITE, VERY SLIGHT FeOx COATING															
20																
20	SAND: LIGHT RUSTY GRAY, COARSE TO FINE GRAINED, 6% BASALT, 2% ZEOLITE, VERY SLIGHT EVEN FeOx COATING, WET															
20																
20	SAND: AS ABOVE BUT MEDIUM TO FINE GRAINED															
20																
20	SAND: AS ABOVE BUT COARSE TO FINE GRAINED WITH 10%-15% PEBBLES, WET															
20																
20	TOTAL DEPTH: 20.0 FEET															

WESTOVER AFB BURN PIT

SITE _____

BORING NUMBER **RU-8**

DATE DRILLED 8/5/99

DRILLED BY ROWAN UNIVERSITY

CHECKED BY L. KENNEDY

BORING RECORD

DEPTH (FEET)	LITHOLOGIC DESCRIPTION	GRAPHIC SYMBOL	PID ORGANIC VAPOR PPM X 1.0										SAMPLE			
			2	4	6	8	10	12	14	16	18	PID READING	DEPTH			
0	TOPSOIL: BROWN SANDY LOAM WITH ABUNDANT ROOTS, DRY														8.5	0
0.8	SAND: MEDIUM ORANGE TAN, COARSE-FINE GRAINED, WELL GRADED, SUBANGULAR, 3% BASALT, TRACE ZEOLITE, MODERATE-HIGH FeOx, DRY, 0.1' STREEK VERY HIGH FeOx IN BASE														2.0	
4.5	SAND: ORANGE TAN, FINE GRAINED, PARTIALLY GRADED, SUBANGULAR, 4% BASALT, MODERATE FeOx, WET														0.5	4.0
5.5	SAND: AS ABOVE BUT COARSE-VERY FINE GRAINED, STILL MODERATE FeOx														0.4	6.0
9.8	SAND: RUSTY TAN, VERY COARSE-FINE GRAINED, 3% PEBBLES, SUBANGULAR, WELL GRADED, 8% BASALT, MODERATE FeOx, WET														0.5	8.0
10.75	GRAVEL: MEDIUM RUSTY TAN, GRAVEL WITH COARSE-FINE SAND, 6% BASALT, SUBANGULAR, PARTIALLY GRADED, MODERATE FeOx														0.5	10.0
11.0	SAND: LIGHT RUSTY TAN, MEDIUM-FINE GRAINED WITH 5% PEBBLES, 8% BASALT, MODERATE FeOx, WET														0.9	12.0
13.0	SAND: LIGHT ORANGE GRAY, COARSE-FINE GRAINED, SUBANGULAR, WELL GRADED, 6% BASALT, MODERATE FeOx, WET														0.5	14.0
13.5	SAND: LIGHT ORANGE GRAY, MEDIUM-FINE GRAINED, 12% BASALT, 1% ZEOLITE, MODERATE-LIGHT FeOx, WET														0.4	16.0
13.75	SAND: AS ABOVE BUT COARSE-FINE GRAINED WITH 10% PEBBLES														0.6	18.0
14.0	SAND: LIGHT ORANGE TAN, FINE GRAINED, GRADING TO COARSE GRAINED IN BASE WITH 10% GRAVEL, 8% BASALT, MODERATE FeOx COATING, WET														1.1	20.0
15	SAND: LIGHT ORANGE TAN, MEDIUM-FINE GRAINED, 10% GRAVEL IN BASE, SUBANGULAR, PARTIALLY GRADED, 8% BASALT, 3% BIOTITE, MODERATE FeOx, WET															
16.0	SAND: LIGHT ORANGE TAN, COARSE-FINE GRAINED, WELL GRADED, SUBANGULAR, 8% BASALT, MODERATE FeOx, WET															
18.0	TOTAL DEPTH: 20.0 FEET															
20																
25																
30																
35																

WESTOVER AFB BURN PIT

SITE _____

BORING NUMBER RU-9

DATE DRILLED 8/5/99

DRILLED BY ROWAN UNIVERSITY

CHECKED BY L. KENNEDY

BORING RECORD

DEPTH (FEET)	LITHOLOGIC DESCRIPTION	GRAPHIC SYMBOL	PID ORGANIC VAPOR PPM X 35.0										SAMPLE			
			2	4	6	8	10	12	14	16	18	PID READING	DEPTH			
0.3	TOPSOIL: BROWN SANDY LOAM WITH ROOTS, DRY	•••••												2.1	1.0	0
1.9	SANDY GRAVEL FILL: LIGHT GRAYISH TAN	•••••												344	2.0	
	SILT: BLACK, BURNED WITH 30% CLAY, SLIGHTLY MOIST	•••••												555	3.0	
	SAND: DARK OLIVE BROWN, VERY FINE GRAINED, 30% CLAY, FeOx BUT POSSIBLY SLIGHTLY REDUCED, VERY SLIGHTLY MOIST-MOIST AT 3.5'	•••••												638	4.0	
		•••••												853	5.0	
5	SAND: OLIVE, COARSE-VERY FINE GRAINED, SUBANGULAR, WELL GRADED, 6% BASALT, MODERATE FeOx WITH SOME REDUCTION, SLIGHTLY MOIST	•••••												354	6.0	5
6.3	SAND: SLIGHT ORANGE GRAY TO GRAY, COARSE-VERY FINE 3% PEBBLES GRAINED, SUBANGULAR, WELL GRADED, 3% BASALT, 4% ZEOLITE, SLIGHT FeOx WITH MUCH REDUCTION, VERY MOIST, WET AT 8.5', A FEW SMALL MOTTLED AREAS OF RUST	•••••												644	7.0	
8.0	SAND: SLIGHT ORANGE GRAY TO GRAY, COARSE-VERY FINE 3% PEBBLES GRAINED, SUBANGULAR, WELL GRADED, 3% BASALT, 4% ZEOLITE, SLIGHT FeOx WITH MUCH REDUCTION, VERY MOIST, WET AT 8.5', A FEW SMALL MOTTLED AREAS OF RUST	•••••												580	8.0	
		•••••												94.1	9.0	
10.0	SAND: AS ABOVE BUT MEDIUM TO FINE GRAINED WITH 5% PEBBLES, STILL MOSTLY REDUCED AND WET	•••••												38.8	10.0	10
11.3	SAND: AS ABOVE BUT ORANGE TAN, MORE FeOx REMAINING	•••••												52.4	11.0	
		•••••												21.3	12.0	
13.5	SAND: LIGHT ORANGE GRAY, VERY COARSE-VERY FINE GRAINED, 15% PEBBLES, SUBANGULAR, WELL GRADED, 6% BASALT, 2% FELD, VERY SLIGHT FeOx MOSTLY REMOVED, WET, THERE IS A 2' ZONE WITH HIGH FeOx IN THE BASE	•••••												19.8	13.0	
15		•••••												10.8	14.0	
15.5		•••••												11.7	15.0	15
16.5	SAND: GRAY, FINE-VERY FINE GRAINED, SUBANGULAR, PARTIALLY GRADED, 10% BASALT, 3% BIOTITE, VERY LIGHT NO FeOx, APPARENTLY REDUCED	•••••												8.8	16.0	
		•••••												6.4	17.0	
20	SAND: GRAY AND ORANGE GRAY, MEDIUM-FINE GRAINED, SUBANGULAR, PARTIALLY GRADED, 10% BASALT, 4% ZEOLITE, SLIGHT FeOx, POSSIBLE Fe RED, WET	•••••												7.8	18.0	
		•••••												9.0	19.0	
	SAND: GRAY, FINE-VERY FINE GRAINED, PARTIALLY GRADED, SUBANGULAR, 12% BASALT, VERY LITTLE FeOx	•••••												8	20.0	20
		•••••												6.4	21.0	
	SAND: AS ABOVE BUT COARSE-FINE GRAINED	•••••												6.1	22.0	
		•••••												6.0	23.0	
	SAND: GRAY, MEDIUM-FINE GRAINED, PARTIALLY GRADED, SUBANGULAR, 10% BASALT, 3% BIOTITE, 2% ZEOLITE, LITTLE TO NO FeOx, WET	•••••												5.7	24.0	
24.5		•••••												5.8	25.0	25
25	SAND: LIGHT RUSTY GRAY TAN, COARSE-FINE GRAINED, WELL GRADED, SUBANGULAR, 8% BASALT, 2% ZEOLITE, LIGHT EVEN FeOx, WET	•••••												4.0	26.0	
26.0	SAND: LIGHT ORANGE TAN WITH ORANGE RUST STREAKS, VERY COARSE-FINE GRAINED WITH 8% GRAVEL AND PEBBLES, SUBANGULAR, PARTIALLY GRADED, 10% BASALT, 3% FELD, 3% ZEOLITE, MODERATE TO LIGHT FeOx	•••••												3.8	28.0	
29.0		•••••												2.6	30.0	30
29.5	SAND: AS ABOVE BUT MEDIUM-FINE GRAINED	•••••														
30	SAND: LIGHT ORANGE TAN, COARSE-FINE GRAINED, SUBANGULAR, WELL GRADED, 12% BASALT, 2% ZEOLITE, SLIGHT TO MODERATE FeOx, WET	•••••												2.5	32.0	30
32.0	TOTAL DEPTH: 32.0 FEET	•••••														

WESTOVER AFB BURN PIT

SITE _____

BORING NUMBER **RU-10**

DATE DRILLED 8/5/99

DRILLED BY ROWAN UNIVERSITY

CHECKED BY L. KENNEDY

BORING RECORD

DEPTH (FEET)	LITHOLOGIC DESCRIPTION	GRAPHIC SYMBOL	PID ORGANIC VAPOR PPM X 60.0										SAMPLE		DEPTH	
			2	4	6	8	10	12	14	16	18	PID READING	DEPTH			
0	TOPSOIL: TAN, SANDY LOAM, ABUNDANT ROOTS, DRY															0
0.8	SAND FILL: OLIVE TAN, VERY FINE GRAINED, 25% CLAY, EVEN FeOx BUT POSSIBLE Fe REDUCTION, DRY													2.5	1.0	
2.0	SAND: OLIVE BROWN, VERY FINE GRAINED, 30% SILT AND CLAY, PARTIALLY GRADED, SUBANGULAR, MEDIUM FeOx BUT SOME PROBABLY REDUCED, SLIGHTLY MOIST													8.5	2.0	
	SAND: OLIVE BROWN, VERY FINE GRAINED, 30% SILT AND CLAY, PARTIALLY GRADED, SUBANGULAR, MEDIUM FeOx BUT SOME PROBABLY REDUCED, SLIGHTLY MOIST													27.8	3.0	
	SAND: OLIVE TAN, MEDIUM-VERY FINE GRAINED, SUBANGULAR, WELL GRADED, 8% BASALT, MODERATE FeOx, POSSIBLE Fe REDUCTION, SLIGHTLY MOIST													49.2	4.0	
5	SAND: OLIVE TAN, MEDIUM-VERY FINE GRAINED, SUBANGULAR, WELL GRADED, 8% BASALT, MODERATE FeOx, POSSIBLE Fe REDUCTION, SLIGHTLY MOIST													81.5	5.0	
5.3	SAND: OLIVE TAN, VERY COARSE-VERY FINE GRAINED WITH 10% PEBBLES, SUBANGULAR, WELL GRADED, 8% BASALT, MODERATE FeOx WITH MOTTLED AREAS REDUCED, VERY MOIST													1108	6.0	5
6.5	SAND: LIGHT RUSTY GRAY WITH RUST BANDS, FINE-VERY FINE GRAINED, PARTIALLY GRADED, 20% CLAY, 6% BASALT, MODERATE TO POOR FeOx IN REDUCED BANDS													847	7.0	
7.0	SAND: LIGHT RUSTY GRAY WITH RUST BANDS, FINE-VERY FINE GRAINED, PARTIALLY GRADED, 20% CLAY, 6% BASALT, MODERATE TO POOR FeOx IN REDUCED BANDS													206	8.0	
	SAND: ORANGE TAN GRAY, COARSE-FINE GRAINED, SUBANGULAR, POED, 3% BASALT, 1% ZEOLITE, MODERATE FeOx WITH SOME REDUCED MOTTLED AREAS, MOIST, STREAKS REST AND REDUCED GRAY LAYERS, WET AT ABOUT 8.5'													843	9.0	
10	SAND: LIGHT RUSTY GRAY-GRAY, VERY COARSE-FINE GRAINED 15% PEBBLES, WELL GRADED, SUBANGULAR, 8% BASALT, 2% ZEOLITE, MODERATE-LIGHT FeOx, SOME REDUCTION BUT MUCH FeOx REMAINING													174	10.0	10
10.3	SAND: LIGHT RUSTY GRAY-GRAY, VERY COARSE-FINE GRAINED 15% PEBBLES, WELL GRADED, SUBANGULAR, 8% BASALT, 2% ZEOLITE, MODERATE-LIGHT FeOx, SOME REDUCTION BUT MUCH FeOx REMAINING													56.8	11.0	
11.0	SAND: LIGHT RUSTY GRAY-GRAY, VERY COARSE-FINE GRAINED 15% PEBBLES, WELL GRADED, SUBANGULAR, 8% BASALT, 2% ZEOLITE, MODERATE-LIGHT FeOx, SOME REDUCTION BUT MUCH FeOx REMAINING													29.6	12.0	
12.0	SILT: BROWN, 40% CLAY													27.9	13.0	
13.3	SAND: RUSTY TAN-RUSTY GRAY, VERY COARSE TO VERY FINE GRAINED, SUBANGULAR, WELL GRADED, 3% BASALT, 1% ZEOLITE, VERY HIGH FeOx WITH MOTTLED AREAS REDUCED													29.7	14.0	
15	SAND: GRAY, COARSE-FINE GRAINED, SUBANGULAR, PARTIALLY GRADED, 6% BASALT, 2% ZEOLITE, ALMOST ALL FeOx REMOVED, PROBABLE Fe REDUCTION, WET													54.7	15.0	15
15.8	SAND: RUSTY DARK GRAY, COARSE-FINE GRAINED, SUBANGULAR, PARTIALLY GRADED, 8% BASALT, 2% FELD, MODERATE FeOx WITH MOTTLED REDUCED ZONES, WET													81.7	16.0	
16.3	SAND: RUSTY DARK GRAY, COARSE-FINE GRAINED, SUBANGULAR, PARTIALLY GRADED, 8% BASALT, 2% FELD, MODERATE FeOx WITH MOTTLED REDUCED ZONES, WET													39.5	17.0	
16.5	SAND: RUSTY DARK GRAY, COARSE-FINE GRAINED, SUBANGULAR, PARTIALLY GRADED, 8% BASALT, 2% FELD, MODERATE FeOx WITH MOTTLED REDUCED ZONES, WET													23.5	18.0	
18.3	SAND: DARK GRAY, FINE-VERY FINE GRAINED, PARTIALLY GRADED, SUBANGULAR, 15% BASALT, NO FeOx ALL REDUCED, VERY HIGH FeS													15.3	19.0	
20	SAND: DARK GRAY WITH SLIGHT RUSTY GRAY MOTTLEING, COARSE TO FINE GRAINED, SUBANGULAR, PARTIALLY GRADED, 12% BASALT, 3% ZEOLITE, SLIGHT FeOx WITH MUCH REDUCTION, PROBABLE FeS													18.1	20.0	20
20.0	SAND: DARK GRAY WITH SLIGHT RUSTY GRAY MOTTLEING, COARSE TO FINE GRAINED, SUBANGULAR, PARTIALLY GRADED, 12% BASALT, 3% ZEOLITE, SLIGHT FeOx WITH MUCH REDUCTION, PROBABLE FeS													20.3	21.0	
20.5	SAND: MEDIUM VERY SLIGHT RUSTY GRAY, FINE-VERY FINE GRAINED, SUBANGULAR, PARTIALLY GRADED, 8% BASALT, 2% FELD, VERY SLIGHT FeOx, PROBABLE Fe REDUCTION WITH FeS, WET													12.0	22.0	
21.5	SAND: AS ABOVE BUT COARSE TO FINE GRAINED													10.7	23.0	
22.5	SAND: AS ABOVE BUT MEDIUM-VERY FINE GRAINED, STILL VERY LITTLE FeOx WITH APPARENTLY MUCH Fe REDUCTION AND POSSIBLE FeS													7.4	24.0	
23.5	SAND: AS ABOVE BUT MEDIUM-VERY FINE GRAINED, STILL VERY LITTLE FeOx WITH APPARENTLY MUCH Fe REDUCTION AND POSSIBLE FeS													4.6	25.0	
24.0	SAND: AS ABOVE BUT MEDIUM-VERY FINE GRAINED, STILL VERY LITTLE FeOx WITH APPARENTLY MUCH Fe REDUCTION AND POSSIBLE FeS													5.7	26.0	
25	SAND: VERY SLIGHT ORANGE GRAY, MEDIUM-FINE GRAINED, PARTIALLY GRADED, SUBANGULAR, 10% BASALT, 4% ZEOLITE, VERY SLIGHT FeOx BUT MOSTLY REDUCED													9.1	28.0	25
25.5	SAND: AS ABOVE BUT COARSE-VERY FINE GRAINED															
26.0	SAND: AS ABOVE BUT COARSE-VERY FINE GRAINED															
28.0	SAND: VERY LIGHT RUSTY GRAY, MEDIUM-FINE GRAINED, SUBANGULAR, PARTIALLY GRADED, 12% BASALT, 5% ZEOLITE, 2% FELD, SLIGHT EVEN FeOx BUT MOSTLY REDUCED															
	SAND: LIGHT GRAYISH RUSTY TAN, MEDIUM-FINE GRAINED, SUBANGULAR, WELL GRADED, MODERATE-LIGHT FeOx, BASICALLY SAMPLE IS AS ABOVE BUT WITH INCREASED FeOx, GRADES TO COARSE TO VERY FINE GRAINED IN BASE 0.5'															
30	SAND: LIGHT RUSTY GRAY, MEDIUM TO FINE GRAINED, WELL GRADED, SUBANGULAR, 12% BASALT, 5% ZEOLITE, VERY SLIGHT EVEN FeOx WITH MUCH REDUCTION															30
	SAND: ORANGE AND GRAYISH TAN, COARSE TO FINE GRAINED, SUBANGULAR, WELL GRADED, 8% BASALT, MODERATE-POOR FeOx, LESS RED, WET															
	SAND: AS ABOVE BUT LIGHT RUSTY TAN, MOST FeOx PRESENT, LITTLE Fe REDUCTION															
35	SAND: RUSTY TAN, VERY COARSE-VERY FINE GRAINED WITH 10% PEBBLES, 6% BASALT, 5% ZEOLITE, MODERATE-HIGH FeOx, WET															35
	SAND: LIGHT RUSTY TAN, MEDIUM TO FINE GRAINED, SUBANGULAR, WELL GRADED, 4% BASALT, 2% FELD, MODERATE EVEN FeOx, WET															

TOTAL DEPTH: 28.0 FEET

WESTOVER AFB BURN PIT

SITE _____

BORING NUMBER **RU-11**

DATE DRILLED 8/6/99

DRILLED BY ROWAN UNIVERSITY

CHECKED BY L. KENNEDY

BORING RECORD

DEPTH (FEET)	LITHOLOGIC DESCRIPTION	GRAPHIC SYMBOL	PID ORGANIC VAPOR PPM X 2.0										SAMPLE			
			2	4	6	8	10	12	14	16	18	PID READING	DEPTH			
0	TOPSOIL: BROWN SANDY LOAM WITH ABUNDANT ROOTS														5.3	1.0
0.5	SAND FILL: TAN, FINE SANDY LOAM														3.7	2.0
1.5	SILT: BLACK BURNED, 30% CLAY														5.1	3.0
2.0	SILT: DARK BROWN, 30% CLAY, MODERATE FeOx, NO APPARENT REDUCTION, SLIGHTLY MOIST														5.2	4.0
4.3	SAND: RUSTY BROWN GRADING TO OLIVE WITH DEPTH, FINE-VERY FINE GRAINED, 20% CLAY, AND SILT, HIGH FeOx TOP WITH INCREASED REDUCTION WITH DEPTH, SLIGHTLY MOIST														5.1	5.0
5															5.4	6.0
7.5	SAND: LIGHT RUSTY TAN, COARSE TO FINE GRAINED, SUBANGULAR, WELL GRADED, 8% BASALT, 3% FELD, MODERATE FeOx, SLIGHTLY MOIST														26.5	7.0
7.5	SAND: AS ABOVE BUT FINE-VERY FINE GRAINED														6.9	8.0
9.5															7.3	9.0
10	SAND: ORANGE TAN, VERY COARSE TO FINE GRAINED, SUBANGULAR TO SUBROUNDED, WELL GRADED, 3% BASALT, 1% ZEOLITE, MODERATE TO HIGH FeOx, POSSIBLE LESS FeOx WITH DEPTH														5.6	10.0
12.0															5.4	11.0
12.0	SAND: LIGHT ORANGE GRAY, MEDIUM-FINE GRAINED, SUBANGULAR, PARTIALLY GRADED, 10% BASALT, 1% ZEOLITE, VERY SLIGHT FeOx, POSSIBLE Fe REDUCTION, WET														4.4	12.0
15															4.5	13.0
15															4.5	14.0
15															3.7	15.0
15															3.7	15.0
15															4.3	16.0
15															4.0	18.0
15															3.5	20.0
20	TOTAL DEPTH: 20.0 FEET															

WESTOVER AFB BURN PIT

SITE _____

BORING NUMBER **RU-12**

DATE DRILLED 8/6/99

DRILLED BY ROWAN UNIVERSITY

CHECKED BY L. KENNEDY

BORING RECORD

DEPTH (FEET)	LITHOLOGIC DESCRIPTION	GRAPHIC SYMBOL	PID ORGANIC VAPOR PPM X 1.5										SAMPLE				
			2	4	6	8	10	12	14	16	18	PID READING	DEPTH				
0	TOPSOIL: BROWN SANDY LOAM WITH ROOTS, DRY													1	0.5	1	0
0.5	FILL: DARK BROWN AND TAN MIXED SAND SOIL AND BURNED CHARCOAL, DRY													2	0.5	2	1.0
1.8	SAND: ORANGE TAN, VERY FINE GRAINED, PARTIALLY GRADED, MODERATE TO HIGH FeOx, TRACE ROOTS, SLIGHTLY MOIST													3	1.1	3	2.0
2.5	SAND: MEDIUM ORANGE TAN, FINE TO VERY FINE GRAINED, PARTIALLY GRADED, 10% CLAY, MODERATE FeOx, SLIGHTLY MOIST													4	1.2	4	3.0
5.3	SAND: RUSTY ORANGE TAN, COARSE TO FINE GRAINED, WELL GRADED, SUBANGULAR, 6% BASALT, MODERATE TO HIGH FeOx, SLIGHTLY MOIST													5	1.3	5	4.0
5.3	SAND: RUSTY ORANGE TAN, COARSE TO FINE GRAINED, WELL GRADED, SUBANGULAR, 6% BASALT, MODERATE TO HIGH FeOx, SLIGHTLY MOIST													6	1.2	6	5.0
7.5	SAND: LIGHT ORANGE TAN, VERY COARSE TO VERY FINE GRAINED, SUBANGULAR, PARTIALLY GRADED, WELL GRADED, SUBANGULAR, 8% BASALT, 2% FELD, MODERATE FeOx, MOIST													7	0.9	7	6.0
7.5	SAND: LIGHT ORANGE TAN, VERY COARSE TO VERY FINE GRAINED, SUBANGULAR, PARTIALLY GRADED, WELL GRADED, SUBANGULAR, 8% BASALT, 2% FELD, MODERATE FeOx, MOIST													8	1.2	8	7.0
8.5	SAND: LIGHT ORANGE GRAY, MEDIUM TO VERY FINE GRAINED, GRADING TO COARSE TO FINE GRAINED WITH DEPTH, 6% BASALT, 2% ZEOLITE, SLIGHT TO MODERATE FeOx, WET													9	1.3	9	8.0
8.5	SAND: LIGHT ORANGE GRAY, MEDIUM TO VERY FINE GRAINED, GRADING TO COARSE TO FINE GRAINED WITH DEPTH, 6% BASALT, 2% ZEOLITE, SLIGHT TO MODERATE FeOx, WET													10	1.3	10	9.0
9.5	SAND: LIGHT ORANGE GRAY, MEDIUM TO VERY FINE GRAINED, SUBANGULAR TO ANGULAR, 8% BASALT, SLIGHT TO MODERATE FeOx, WET													11	0.9	11	10.0
11.0	SAND: LIGHT ORANGE GRAY, MEDIUM TO VERY FINE GRAINED, SUBANGULAR TO ANGULAR, 8% BASALT, SLIGHT TO MODERATE FeOx, WET													12	0.7	12	11.0
12.0	SAND: LIGHT ORANGE GRAY, VERY COARSE TO VERY FINE GRAINED WITH 10% PEBBLES, 8% BASALT, 2% ZEOLITE, LIGHT FeOx, WET													13	4.3	13	12.0
12.5	SAND: LIGHT ORANGE GRAY, VERY COARSE TO VERY FINE GRAINED WITH 10% PEBBLES, 8% BASALT, 2% ZEOLITE, LIGHT FeOx, WET													14	8.5	14	13.0
13.3	SAND: LIGHT ORANGE GRAY, COARSE TO VERY FINE GRAINED, SUBANGULAR, WELL GRADED, 3% BASALT, 3% ZEOLITE, 1% FELD, VERY SLIGHT FeOx, WET													16	22.1	16	14.0
14.0	SAND: LIGHT ORANGE GRAY, COARSE TO VERY FINE GRAINED, SUBANGULAR, WELL GRADED, 3% BASALT, 3% ZEOLITE, 1% FELD, VERY SLIGHT FeOx, WET													17	3.5	17	15.0
15.0	SAND: VERY LIGHT ORANGE GRAY, VERY COARSE TO FINE GRAINED, SUBANGULAR, WELL GRADED, 8% BASALT, 1% FELD, SLIGHT FeOx, WET													18	2.2	18	16.0
15.0	SAND: VERY LIGHT ORANGE GRAY, VERY COARSE TO FINE GRAINED, SUBANGULAR, WELL GRADED, 8% BASALT, 1% FELD, SLIGHT FeOx, WET													20	2.0	20	17.0
15.0	SAND: VERY LIGHT ORANGE GRAY, COARSE TO VERY FINE GRAINED, WELL GRADED, SUBANGULAR, 2% BASALT, 1% ZEOLITE, VERY SLIGHT FeOx, WET													22	2.0	22	18.0
19.5	SAND: GRAY, VERY COARSE TO FINE GRAINED, 10% PEBBLES, WELL GRADED, 8% BASALT, LITTLE FeOx, MOSTLY REDUCED, WET													24	4.0	24	20.0
20.0	SAND: GRAY, VERY COARSE TO FINE GRAINED, 10% PEBBLES, WELL GRADED, 8% BASALT, LITTLE FeOx, MOSTLY REDUCED, WET													28	7.8	28	21.0
21.0	SAND: GRAY TO SLIGHTLY ORANGE GRAY, COARSE TO FINE GRAINED, 3% PEBBLES, SUBANGULAR, WELL GRADED, 6% BASALT, VERY SLIGHT FeOx, PROBABLE Fe REDUCTION, WET													30	1.5	30	22.0
21.0	SAND: GRAY TO SLIGHTLY ORANGE GRAY, COARSE TO FINE GRAINED, 3% PEBBLES, SUBANGULAR, WELL GRADED, 6% BASALT, VERY SLIGHT FeOx, PROBABLE Fe REDUCTION, WET													32	0.9	32	23.0
21.5	SAND: LIGHT VERY SLIGHT RUSTY GRAY, FINE TO VERY FINE GRAINED, SUBANGULAR, PARTIALLY GRADED, 12% BASALT, 1% BIOTITE, VERY SLIGHT FeOx, WITH POSSIBLE Fe REDUCTION, WET													32	1.0	32	24.0
23.0	SAND: LIGHT VERY SLIGHT RUSTY GRAY, FINE TO VERY FINE GRAINED, SUBANGULAR, PARTIALLY GRADED, 12% BASALT, 1% BIOTITE, VERY SLIGHT FeOx, WITH POSSIBLE Fe REDUCTION, WET													32	1.0	32	25.0
25.0	SAND: VERY SLIGHT RUSTY GRAY, COARSE TO VERY FINE GRAINED, SUBANGULAR, PARTIALLY GRADED, 8% BASALT, 3% FELD, 1% ZEOLITE, VERY SLIGHT FeOx, WET													32	1.0	32	26.0
25.5	SAND: VERY SLIGHT RUSTY GRAY, COARSE TO VERY FINE GRAINED, SUBANGULAR, PARTIALLY GRADED, 8% BASALT, 3% FELD, 1% ZEOLITE, VERY SLIGHT FeOx, WET													32	1.0	32	27.0
26.0	SAND: GRAY TO VERY SLIGHT ORANGE GRAY, FINE TO VERY FINE GRAINED, PARTIALLY GRADED, SUBANGULAR, 10% BASALT, 1% ZEOLITE, 1% BIOTITE, VERY SLIGHT FeOx, WET													32	1.0	32	28.0
28.0	SAND: AS ABOVE BUT MEDIUM-FINE GRAINED													32	1.0	32	29.0
28.0	SAND: AS ABOVE BUT MEDIUM-FINE GRAINED													32	1.0	32	30.0
30.0	SAND: GRAY, FINE TO VERY FINE GRAINED, PARTIALLY GRADED, 10% BASALT, 5% BIOTITE, NO TO VERY SLIGHT FeOx, WET													32	1.0	32	31.0
32.0	NO SAMPLE:													32	1.0	32	32.0
32.0	SAND: LIGHT GRAY TO VERY SLIGHT ORANGE GRAY, COARSE TO VERY FINE GRAINED, 12% BASALT, 2% FELD, VERY LITTLE FeOx, POSSIBLE REDUCTION, WET													32	1.0	32	33.0
32.0	SAND: AS ABOVE, MEDIUM TO FINE GRAINED, POSSIBLE SLIGHTLY MORE FeOx													32	1.0	32	34.0
35.0	TOTAL DEPTH: 32.0 FEET													32	1.0	32	35.0

WESTOVER AFB BURN PIT

SITE _____

BORING NUMBER **RU-13**

DATE DRILLED 8/9/99

DRILLED BY ROWAN UNIVERSITY

CHECKED BY L. KENNEDY

1 1

BORING RECORD

DEPTH (FEET)	LITHOLOGIC DESCRIPTION	GRAPHIC SYMBOL	PID ORGANIC VAPOR PPM X 1.0										SAMPLE		
			2	4	6	8	10	12	14	16	18	PID READING	DEPTH		
0	TOPSOIL: BROWN SANDY LOAM WITH ROOTS, DRY														
0.8	SAND: ORANGE TAN, FINE-VERY FINE GRAINED, PARTIALLY GRADED, 10% CLAY, MODERATE-HIGH FeOx, DRY												1.3	1.0	
2.3	SILT: OLIVE TAN, 20% CLAY, HIGH MCA, HIGH FeOx, MOIST												2.2	2.0	
2.3	SAND: ORANGE TAN, FINE TO VERY FINE GRAINED, SUBANGULAR, PARTIALLY GRADED, 8% BASALT, MEDIUM TO HIGH FeOx, SLIGHTLY MOIST												1.4	3.0	
5	SAND: RUSTY TAN, VERY COARSE TO VER FINE GRAINED, WELL GRADED, SUBANGULAR, 6% BASALT, HIGH FeOx, SLIGHTLY MOIST												2.0	4.0	
6.0	SAND: MEDIUM ORANGE TAN, FINE TO VERY FINE GRAINED TO COARSE TO FINE GRAINED, PARTIAL-WELL GRADED, SUBANGULAR, 6% BASALT, HIGH TO MODERATE FeOx, SLIGHTLY MOIST TO MOIST AT BASE												1.3	5.0	
6.5	SAND: LIGHT ORANGE TAN, FINE GRAINED GRADING TO COARSE GRAINE, PARTIAL-WELL GRADED, SUBANGULAR, 8% BASALT, MODERATE-HIGH FeOx, WET												2.3	6.0	
8.0	SAND: SEQUEUNCE AS ABOVE												2.7	7.0	
8.8	SAND: LIGHT ORANGE TAN, VERY COARSE TO VERY FINE GRAINED, WELL GRADED, 8% BASALT, 2% FELD, HIGH FeOx, WET												2.4	8.0	
9.5	SAND: MEDIUM ORANGE TAN, FINE GRAINED GRADING TO VERY COARSE GRAINED, SUBANGULAR, PARTIALLY GRADED, 5% BASALT, 5% FELD, HIGH FeOx, WET, 0.1' LAYER OF GRAVEL IN BASE												2.1	9.0	
10.8	SAND: LIGHT ORANGE GRAY, FINE TO VERY FINE GRAINED, PARTIALLY GRADED, SUBANGULAR, 12% BASALT, 1% ZEOHITE, 1% BIOTITE, POOR FeOx, POSSIBLE Fe REDUCTION, WET												2.7	10.0	
13.5	SAND: ORANGE GRAY TO ORANGE TAN, COARSE TO FINE GRAINED, WELL GRADED, SUBANGULAR, 6% BASALT, 1% FELD, MODERATE FeOx, WET												5.3	11.0	
15	SAND: LIGHT ORANGE GRAY, FINE-VERY FINE GRAINED, PARTIALLY GRADED, SUBANGULAR, 12% BASALT, 5% BIOTITE, VERY POOR FeOx, WET												7.0	12.0	
16.0	SAND: ORANGE GRAY TO GRAYISH TAN, COARSE TO FINE GRAINED, WELL GRADED, PARTIALLY SUBANGULAR, 6% BASALT, SLIGHT-MODERATE FeOx, WET												3.6	14.0	
17.5	SAND: GRAY, FINE TO VERY FINE GRAINED, 16% BASALT, 4% BIOTITE, VERY SLIGHT FeOx, WET												3.2	15.0	
19.3	TOTAL DEPTH: 20.0 FEET												3.4	17.0	
19.8													3.1	18.0	
20													2.2	19.0	
25													2.0	20.0	
30															
35															

WESTOVER AFB BURN PIT

SITE _____

BORING NUMBER **RU-14**

DATE DRILLED 8/9/99

DRILLED BY ROWAN UNIVERSITY

CHECKED BY L. KENNEDY

BORING RECORD

DEPTH (FEET)	LITHOLOGIC DESCRIPTION	GRAPHIC SYMBOL	PID ORGANIC VAPOR PPM X 1.0										SAMPLE			
			2	4	6	8	10	12	14	16	18	PID READING	DEPTH			
0.3	SLAG: BLACK															
1.0	SOIL FILL: BROWN SANDY LOAM MIXED WITH CHARRED SAND													2.1	1.0	0
1.5	SAND: DARK BROWN AND TAN, FINE TO VERY FINE GRAINED, 10% CLAY, SLIGHT-MODERATE FeOx, DRY													1.9	2.0	
2.5	SAND: OLIVE TAN, COARSE TO VERY FINE GRAINED, WELL GRADED, SUBANGULAR, 2% BASALT, MODERATE TO HIGH FeOx, SLIGHTLY MOIST TO DRY													1.1	3.0	
4.3	SAND: OLIVE TAN, FINE TO VERY FINE GRAINED, SUBANGULAR, PARTIALLY GRADED, 4% BASALT, 1% ZEOLITE, SLIGHTLY MOIST													1.8	4.0	
5.3														1.8	5.0	5
5.5														2.3	6.0	
7.0	SAND: LIGHT ORANGE TAN, COARSE TO FINE GRAINED, PARTIALLY GRADED, SUBANGULAR, 4% BASALT, LIGHT FeOx, SLIGHTLY MOIST													1.4	7.0	
	SILT: OLIVE BROWN, 10% CLAY, 30% FINE SAND, MOIST													1.5	8.0	
	SAND: LIGHT ORANGE TAN, COARSE TO FINE GRAINED WITH 8% PEBBLES, SUBANGULAR, WELL GRADED, 8% BASALT, MODERATE FeOx, SLIGHTLY MOIST													1.7	9.0	
9.3														2.3	10.0	10
11.0	SAND: LIGHT ORANGE TAN TO ORANGE GRAY, FINE GRAINED GRADING TO MEDIUM, 8% BASALT, 1% FELD, LIGHT FeOx, WET													1.4	11.0	
12.3	SAND: ORANGE TAN, VERY COARSE TO FINE GRAINED, 15% GRAVEL AND PEBBLES, SUBANGULAR, WELL GRADED, 8% BASALT, 1% ZEOLITE, MODERATE FeOx, WET													1.6	12.0	
13.0														1.3	13.0	
14.0	SAND: LIGHT ORANGE TAN, ORANGE GRAY, MEDIUM TO FINE GRAINED, PARTIALLY GRADED, SUBANGULAR, 8% BASALT, LIGHT FeOx WITH POSSIBLE Fe REDUCTION, WET SAND													0.9	14.0	
15.0														1.8	15.0	15
	SAND: AS ABOVE BUT COARSE TO FINE GRAINED													1.6	16.0	
	SAND: LIGHT ORANGE TAN, MEDIUM TO FINE GRAINED, SUBANGULAR, PARTIALLY GRADED, 8% BASALT, 1% ZEOLITE, MEDIUM FeOx, WET													2.9	17.0	
18.0	SAND: LIGHT ORANGE TAN AND ORANGE GRAY, COARSE TO VERY FINE GRAINED, SUBANGULAR, PARTIALLY GRADED, 8% BASALT, 2% FELD, MODERATE FeOx, WET													2.3	18.0	
20.0	SAND: ORANGE GRAY, VERY FINE GRAINED GRADING TO COARSE-FINE GRAINED WITH DEPTH, ANGULAR-SUBANGULAR, PARTIALLY GRADED, 10% BASALT, SLIGHT FeOx, WET, BASE 0.25' ZONE WITH 10% GRAVEL AND PEBBLES													2.1	20.0	20
	TOTAL DEPTH: 20.0 FEET															
25																25
30																30
35																35

WESTOVER AFB BURN PIT

SITE _____

BORING NUMBER **RU-15**

DATE DRILLED 8/9/99

DRILLED BY ROWAN UNIVERSITY

CHECKED BY L. KENNEDY

BORING RECORD

DEPTH (FEET)	LITHOLOGIC DESCRIPTION	GRAPHIC SYMBOL	PID ORGANIC VAPOR PPM X 20										SAMPLE			
			2	4	6	8	10	12	14	16	18	PID READING	DEPTH			
0	SOIL: BROWN SANDY LOAM, WITH ROOTS, DRY													1.0	1.0	0
0.5	SOIL FILL: LIGHT BROWN SANDY LOAM, LESS ROOTS, DRY															
1.3	CHARRED: BLACK BURNED SANDY LOAM, DRY													25.7	2.0	
2.5	SAND: OLIVE, VERY FINE GRAINED, 25% CLAY, MODERATE TO LIGHT FeOx WITH PROBABLE Fe REDUCTION, MOIST													40.0	3.0	
3.5	SAND: LIGHT OLIVE GRAY, COARSE TO FINE GRAINED, 10% GRAVEL, WELL GRADED, SUBANGULAR, 6% BASALT, 1% BIOTITE, SLIGHT FeOx WITH MOSTLY Fe REDUCTION, SLIGHTLY MOIST TO WET AT - 7													14.4	4.0	
5														5.7	5.0	5
														5.0	6.0	
														2.7	7.0	
8.3	SAND: GRAYISH RUST, COARSE TO FINE GRAINED, SUBANGULAR, WELL GRADED, 4% BASALT, 2% FELD, HIGH FeOx WITH SOME Fe REDUCTION, WET													3.2	8.0	
9.5	SAND: MEDIUM OLIVE GRAY, COARSE TO FINE GRAINED, SUBANGULAR, WELL GRADED, 4% BASALT, 2% FELD, SLIGHT FeOx WITH MUCH Fe REDUCTION, WET													4.5	9.0	
10														2.4	10.0	10
10.5	SAND: AS ABOVE WITH 20% PEBBLES													2.4	11.0	
11.8	SAND: LIGHT ORANGE GRAY-ORANGE TAN, MEDIUM TO FINE GRAINED, PARTIALLY GRADED, SUBANGULAR, 8% BASALT, 5% ZEOLITE, SLIGHT TO MODERATE FeOx, WET													1.8	12.0	
12.0														1.7	13.0	
14.8	SAND: LIGHT ORANGE GRAY, VERY COARSE TO FINE GRAINED, 15% PEBBLES AND GRAVEL, SUBANGULAR, WELL GRADED, 8% BASALT, 1% ZEOLITE, SLIGHT FeOx, SOME Fe REDUCTION, WET													1.3	14.0	
15														0.9	15.0	15
15.3														1.1	16.0	
16.0	SAND: LIGHT ORANGE GRAY, COARSE TO VERY FINE 5% GRAVEL GRAINED, SUBANGULAR, PARTIALLY GRADED, 10% BASALT, 3% ZEOLITE, 5% FELD, SLIGHT FeOx, POSSIBLE Fe REDUCTION, WET													1.2	17.0	
17.5														1.2	18.0	
18.0	SAND: LIGHT ORANGE GRAY, MEDIUM TO FINE GRAINED, PARTIALLY GRADED, SUBANGULAR, 8% BASALT, 5% ZEOLITE, 1% FELD, LIGHT FeOx, POSSIBLE Fe REDUCTION, WET													1.3	19.0	
20														1.4	20.0	20
	SAND: AS ABOVE BUT COARSE TO VERY FINE GRAINED															
	SAND: MEDIUM ORANGE GRAY, FINE TO VERY FINE GRADING TO MEDIUM TO FINE GRAINED, 8% BASALT, 1% FELD, SLIGHT FeOx WITH POSSIBLE REDUCTION, WET															
25	SAND: RUSTY GRAY TAN, VERY COARSE TO FINE GRAINED, SUBANGULAR, WELL GRADED, 8% BASALT, 2% FELD, 3% ZEOLITE, MODERATE TO HIGH FeOx WITH POSSIBLE Fe REDUCTION, WET															25
	SAND: OLIVE GRAY, MEDIUM TO FINE GRADING TO COARSE TO FINE GRAINED WITH 10% PEBBLES, PARTIAL-WELL GRADED, SUBANGULAR, 16% BASALT, 3% ZEOLITE, SLIGHT FeOx WITH PROBABLE Fe REDUCTION, WET															
30	TOTAL DEPTH: 20.0 FEET															30

WESTOVER AFB BURN PIT

SITE _____

BORING NUMBER **RU-16**

DATE DRILLED 8/10/99

DRILLED BY ROWAN UNIVERSITY

CHECKED BY L. KENNEDY

BORING RECORD

DEPTH (FEET)	LITHOLOGIC DESCRIPTION	GRAPHIC SYMBOL	PID ORGANIC VAPOR PPM X 1.0							SAMPLE				
			2	4	6	8	10	12	14	16	18	PID READING	DEPTH	
0	SOIL: BROWN SANDY LOADM, ABUNDANT ROOTS, DRY													0
0.5	SILT: TAN, HIGH FeOx, DRY, SLIGHT ROOTS											0.7	1.0	
1.0	SAND: ORANGE TAN, VERY FINE GRAINED, MEDIUM-HIGH FeOx, DRY											1.4	2.0	
2.0												1.2	3.0	
2.5	SILT: ORANGE GRAY, 35% CLAY, HIGH FeOx, MOIST											1.0	4.0	
	SAND: RUSTY ORANGE, COARSE TO FINE GRAINED, PARTIALLY GRADED, SUBANGULAR, 4% BASALT, 2% FELD, VERY HIGH FeOx, SLIGHTLY MOIST											1.4	5.0	
5	SAND: ORANGE TAN, COARSE-FINE GRAINED, WELL GRADED, SUBANGULAR, 8% BASALT, 3% ZEOLITE, MODERATE TO HIGH FeOx, SLIGHTLY MOIST											1.6	6.0	5
5.3												2.1	7.0	
6.3	SAND: ORANGE, COARSE TO FINE GRAINED, WELL GRADED, SUBANGULAR, 4% BASALT, 2% FELD, HIGH FeOx, VERY MOIST											2.1	8.0	
6.8												2.2	9.0	
8.3	SAND: LIGHT ORANGE GRAY, VERY FINE GRAINED, PARTIALLY GRADED, 6% BASALT, 5% BIOTITE, MODERATE FeOx, WET											2.4	10.0	
9.3	SAND: ORANGE TAN, COARSE TO FINE GRAINED, SUBANGULAR, WELL GRADED, 4% BASALT, 1% ZEOLITE, VERY HIGH FeOx, NO REDUCTION, WET											1.7	11.0	10
10												1.9	12.0	
10.8	SAND: ORANGE TAN, AS ABOVE BUT MEDIUM TO FINE GRAINED											1.9	13.0	
10.9												2.1	14.0	
11.0												1.8	15.0	15
12.3	SAND: RUSTY ORANGE, COARSE-MEDIUM GRAINED, SUBANGULAR, PARTIALLY GRADED, 4% BASALT, 2% FELD, HIGH FeOx, WET											1.5	16.0	
13.3												1.0	18.0	
14.8	SAND: LIGH ORANGE TAN, FINE-VERY FINE GRAINED, SUBANGULAR, PARTIALLY GRADED, 12% BASALT, 2% BIOTITE, MODERATE FeOx, WET											0.9	20.0	20
15.8	SAND: AS ABOVE BUT RUSTY ORANGE, MARKER ZONE!													
16.0	SAND: ORANGE GRAY, FINE TO VERY FINE GRAINED, SUBANGULAR, PARTIALLY GRADED, 12% BASALT, 3% BIOTITE, 1% ZEOLITE, MODERATE TO LIGHT FeOx, WET													
18.0	SAND: ORANGE GRAY, MEDIUM TO FINE GRADING TO COARSE TO FINE GRAINED WITH 15% PEBBLES IN LAST 1', SUBANGULAR, PARTIAL-WELL GRADED, 8% BASALT, 5% FELD, 1% ZEOLITE, MODERATE FeOx, WET													
20	SAND: ORANGE GRAY, MEDIUM-FINE GRAINED GRADING TO COARSE-FINE GRAINED WITH 10% PEBBLES, PARTIAL-WELL GRADED, 8% BASALT, 4% FELD, MODERATE FeOx, WET													
	SAND: LIGHT ORANGE GRAY, MEDIUM TO FINE GRAINED GRADING TO COARSE-FINE GRAINED WITH 15% PEBBLES IN BASE 0.2', PARTIAL-WELL GRADED, SUBANGULAR, 8% BASALT, 5% FELD, MODERATE FeOx, WET													
25	SAND: AS ABOVE BUT MEDIUM GRAINED TO COARSE													
	SAND: AS ABOVE BUT MEDIUM GRAINED TO COARSE													
	TOTAL DEPTH: 20.0 FEET													

WESTOVER AFB BURN PIT

SITE _____

BORING NUMBER **RU-17**

DATE DRILLED 8/10/99

DRILLED BY ROWAN UNIVERSITY

CHECKED BY L. KENNEDY

BORING RECORD

DEPTH (FEET)	LITHOLOGIC DESCRIPTION	GRAPHIC SYMBOL	PID ORGANIC VAPOR PPM X 1.0										SAMPLE				
			2	4	6	8	10	12	14	16	18	PID READING	DEPTH				
0	SOIL: BROWN SANDY LOAM, ABUNDANT ROOTS, DRY																0
0.5	SAND FILL: OLIVE TAN, FINE GRAINED SAND WITH PEA GRAVEL AND SLIGHTLY CHARRED, SLIGHTLY MOIST	•••••													2.4	1.0	
1.75	SILT: BLACK, CHARCOAL WITH 15% CLAY	□□□□													2.3	2.0	
2.5	SILT: OLIVE TAN, 20% CLAY, MOIST	□□□□													1.8	3.0	
2.75	SAND: OLIVE TAN, FINE GRAINED, PARTIALLY GRADED, 20% CLAY, MODERATE FeOx, SLIGHTLY REDUCED, SLIGHTLY MOIST	□□□□													2.1	4.0	
3.0	SILT: OLIVE TAN, 25% CLAY, MODERATE FeOx	□□□□													2.1	5.0	
3.75	SAND: OLIVE TAN, FINE GRAINED, PARTIALLY GRADED, 20% CLAY, MODERATE FeOx, SLIGHTLY REDUCED, SLIGHTLY MOIST	□□□□													2.1	6.0	5
5	SAND: ORANGE TAN, VERY FINE GRADING TO COARSE-VERY FINE GRAINED, 10% PEBBLES IN BASE, PARTIALLY-WELL GRADED, 4% BASALT, 1% ZEOLITE, MODERATE FeOx, SLIGHTLY MOIST	•••••													1.8	7.0	
6.5	SAND: LIGHT ORANGE GRAY, FINE-VERY FINE GRADING TO MEDIUM-FINE GRAINED, SUBANGULAR, PARTIALLY GRADED, 12% BASALT, SLIGHT FeOx, POSSIBLE SLIGHT Fe REDUCTION, WET	•••••													2.0	8.0	
7.25	SAND: LIGHT ORANGE GRAY, FINE-VERY FINE GRADING TO MEDIUM-FINE GRAINED, SUBANGULAR, PARTIALLY GRADED, 12% BASALT, SLIGHT FeOx, POSSIBLE SLIGHT Fe REDUCTION, WET	•••••													2.4	9.0	
8.0	SAND: LIGHT ORANGE GRAY, COARSE-FINE GRAINED, SUBANGULAR, WELL GRADED, 12% BASALT, MODERATE FeOx, POSSIBLE Fe REDUCTION, WET	•••••													2.1	10.0	10
10.25	SAND: ORANGE GRAY, FINE GRAINED GRADING TO COARSE-FINE GRAINED WITH 5% PEBBLES, PARTIAL-WELL GRADED, SUBANGULAR, 6% BASALT, POOR FeOx, POSSIBLE Fe REDUCTION	•••••													1.5	11.0	
12.0	SAND: ORANGE GRAY, FINE GRAINED GRADING TO COARSE-FINE GRAINED WITH 5% PEBBLES, PARTIAL-WELL GRADED, SUBANGULAR, 6% BASALT, POOR FeOx, POSSIBLE Fe REDUCTION	•••••													1.7	12.0	
15	SAND: ORANGE GRAY, VERY COARSE-FINE GRAINED WITH 10% TO 20% GRAVEL AND PEBBLES, WELL GRADED, SUBANGULAR, 4% BASALT, 6% FELD, 3% ZEOLITE, MODERATE FeOx, WET	•••••													1.5	13.0	
16.75	SAND: ORANGE GRAY, COARSE-FINE GRAINED, WELL GRADED, SUBANGULAR, 8% BASALT, 3% FELD, MODERATE FeOx, WET	•••••													1.7	14.0	
18.0	SAND: ORANGE GRAY, COARSE-FINE GRAINED, WELL GRADED, SUBANGULAR, 8% BASALT, 3% FELD, MODERATE FeOx, WET	•••••													1.9	15.0	15
18.0	SAND: GRAY, MEDIUM TO FINE GRAINED, PARTIALLY GRADED, SUBANGULAR, 10% BASALT, 1% ZEOLITE, VERY POOR FeOx, POSSIBLE REDUCTION, WET	•••••													1.8	16.0	
18.0	SAND: GRAY, MEDIUM TO FINE GRAINED, PARTIALLY GRADED, SUBANGULAR, 10% BASALT, 1% ZEOLITE, VERY POOR FeOx, POSSIBLE REDUCTION, WET	•••••													1.4	17.0	
18.0	SAND: GRAY, MEDIUM TO FINE GRAINED, PARTIALLY GRADED, SUBANGULAR, 10% BASALT, 1% ZEOLITE, VERY POOR FeOx, POSSIBLE REDUCTION, WET	•••••													1.0	18.0	
20	TOTAL DEPTH: 18.0 FEET																20
25																	25
30																	30
35																	35

WESTOVER AFB BURN PIT

SITE _____

BORING NUMBER **RU-18**

DATE DRILLED 8/10/99

DRILLED BY ROWAN UNIVERSITY

CHECKED BY L. KENNEDY

Appendix 2. Field Measurements

**Groundwater Measurement
Westover AFRB
Purge, DO, Conductivity, RO, and Depth to Water Measurements**

Well ID	DO mg/L	Purge Vol L	Cond ms	RO mV	Depth to Water Table ft
CF-1A	9.7	50	29.6	635	10.22
CF-7	8.93	120	27.2	518	9.82
CF-4	6.29	75	27.7	436	7.46
CF-8	0.21	60	41.8	204	9.42
CF-6S	0.14	60	174.3	-13.7	7.68
CF-5	0.42	45	102.2	327.1	9.73
CF-3	0.14	45	114.2	-194	8.59
CF-2	0.28	60	338	189	9.15
MP-15S	4.75	1	44.1	326	No Data
MP-10S	9.87	1	29.9	370	No Data
MP-5S	No Data	1	No Data	No Data	No Data

MP wells are very shallow, penetrated only into very top of aquifer at time of sample collection.

**Groundwater Measurement
Westover AFRB
Ground Water Iron, Sulfide, and Sulfate Data**

Well ID	Fe total (mg/L)	S- (mg/L)	Sulfate (mg/L)	Sulfate dup (mg/L)
CF-1A	0.068	0.012	6.9	6.93
CF-7	0.101	0.004	5.87	5.83
CF-4	0.225	0.012	6.2	6.27
CF-8	0.767	0.006	4.23	4.25
CF-6S	31.925	0.081	5.15	5.12
CF-5	12.625	0.021	16.53	16.64
CF-3	17.675	0.41	0.74	0.72
CF-2	1.975	0.105	3.84	3.88
MP-15S	0.5875	0.001	2.51	2.43
MP-10S	0.007	0.003	6.36	6.42
MP-5S	4.5125	0.001	1.52	1.58

**Groundwater Measurement
Westover AFRB
Groundwater Chloride, Nitrite, and Nitrate Data**

Well ID	Cl (mg/L)	Cl dup (mg/L)	NO2 (mg/L)	NO2 dup (mg/L)	NO3 (mg/L)	NO3 dup (mg/L)
CF-1A	1.17	1.07	BDL	BDL	BDL	BDL
CF-7	1.38	1.28	BDL	BDL	1.19	1.17
CF-4	1.67	1.38	BDL	BDL	0.41	0.41
CF-8	1.34	1.39	BDL	0.43	3.6	3.51
CF-6S	13.55	13.68	BDL	BDL	BDL	0.45
CF-5	2.04	1.97	BDL	BDL	BDL	BDL
CF-3	3.53	3.66	BDL	0.47	BDL	BDL
CF-2	1.71	1.67	0.65	0.69	4.11	3.84
MP-15S	2.48	2.36	BDL	BDL	0.77	0.76
MP-10S	1.47	1.37	BDL	BDL	5.11	5.16
MP-5S	4.97	4.99	BDL	BDL	0.86	0.86

Appendix 3. Laboratory Measurements

Table 1
Soils Data Summary
Current Fire Training Area (FT-08)
Westover ARB, Chicopee, MA
0.5N HCl Iron (II)

Sample ID	Result	No. of Data Points	Qualifiers					MDL	PQL
			U	F	B	J	M		
(1)	mg/kg	(3)	(4)	(5)	(6)	(7)	(8)	(9)	(10)
RU1-2	540.8	2				J		8.9	28.3
RU1-4	1033.1	2						8.3	26.5
RU1-6	1268.5	3						120.4	383.4
RU1-8	1211.8	2						8.9	28.3
RU1-10	1439.2	2						141.1	449.5
RU1-12	1558.6	2						140.3	446.7
RU1-14	1797.3	2						137.0	436.5
RU1-16	1512.8	3				J		99.8	317.7
RU1-18	2138.5	2						145.9	464.5
RU1-20	456.6	2						7.8	24.8
RU1-22	686.6	2				J		7.6	24.2
RU1-24	877.8	2			B			8.2	26.2
RU1-26	794.4	4			B	J		10.0	32.0
RU1-28	779.5	2			B	J		8.4	26.9
RU1-30	478.9	2			B			8.8	28.1
RU2-2	427.8	2			B	J		8.0	25.4
RU2-4	1077.8	2			B			9.8	31.3
RU2-6	638.7	3			B			8.5	27.1
RU2-8	839.5	2			B			7.6	24.3
RU2-10	827.0	4			B			8.5	27.2
RU2-12	770.2	2			B			8.9	28.4
RU2-14	603.7	3			B			8.8	27.9
RU2-16	548.6	2			B	J		10.1	32.2
RU2-18	1635.9	2			B	J		96.7	308.0
RU2-20	886.3	2			B			8.7	27.7
RU2-22	890.3	2			B			9.2	29.2
RU2-24	1533.3	3			B	J		100.6	320.5
RU2-26	1598.8	2			B	J		75.1	239.2
RU2-28	3203.2	2			B			170.1	541.8
RU2-30	2172.1	2			B			152.7	486.4
RU3-2	560.0	2			B			7.7	24.4
RU3-4	392.7	3			B			8.5	26.9
RU3-6	584.8	2						7.9	25.2
RU3-8	1402.0	2						68.1	216.9
RU3-10	986.8	2						8.4	26.7
RU3-12	1168.0	2				J		78.2	249.1
RU3-14	909.9	3						7.9	25.1

RU4-2	818.8	2						6.9	22.0
RU4-4	557.5	2				J		9.1	29.1
RU4-6	658.3	2						7.5	23.8
RU4-8	507.8	2				J		8.2	26.0
RU4-10	996.5	3				J		49.3	157.0
RU4-12	1440.0	2				J		67.3	214.5
RU4-13.5	872.5	2				J		7.7	24.5
RU4-14	2745.3	2						162.6	517.9
RU4-18	1188.2	2				J		92.6	295.0
RU4-20	311.6	3				J		8.4	26.7
RU4-24	524.5	2						8.5	27.1
RU5-2	476.9	2						7.6	24.3
RU5-4	512.9	2				J		6.6	21.1
RU5-6	888.2	2				J		7.6	24.3
RU5-8	970.7	3						8.7	27.8
RU5-10	770.5	2				J		8.6	27.2
RU5-12	906.4	2						8.2	26.2
RU5-14	864.8	2						8.1	25.9
RU5-16	665.5	2				J		8.5	26.9
RU5-20	829.0	3						9.0	28.8
RU5-24	2175.4	2						150.6	479.7
RU5-26	2366.1	2						143.9	458.2
RU5-28	1778.2	2				J		74.6	237.4
RU5-32	1682.1	2						143.5	457.1
RU6-2	597.5	2						6.7	21.4
RU6-4	824.3	2						7.7	24.5
RU6-6	1523.9	2						114.2	363.8
RU6-8	596.5	2				J		8.0	25.5
RU6-10	1002.6	3				J		50.3	160.0
RU6-12	932.9	2						8.6	27.5
RU6-14	593.0	2				J		8.5	27.1
RU6-16	401.7	2				J		6.8	21.8
RU6-18	784.4	2				J		8.8	27.9
RU6-20	6734.8	3						133.3	424.5
RU6-36	Missing	0						0.0	0.0
RU7-4	720.3	2				J		7.4	23.6
RU7-7	958.7	2						8.1	25.7
RU7-8	893.2	2						12.8	40.7
RU7-10	1061.7	2				J		12.8	40.9
RU7-12	1175.4	3						13.6	43.2
RU7-14	1082.6	2				J		11.1	35.3
RU7-16	1082.9	2						11.8	37.6
RU7-18	2010.9	2						74.9	238.7
RU7-20	1872.2	2						72.9	232.2
RU8-2	517.9	3						12.2	38.8
RU8-4	859.9	2						11.1	35.2
RU8-6	973.4	2						10.5	33.6

RU8-18	1054.9	2						12.0	38.1
RU8-8	1020.3	2						12.5	39.9
RU8-10	1187.7	2						11.9	37.8
RU8-12	1025.6	3						13.4	42.6
RU8-14	953.7	2						12.7	40.6
RU8-16	1187.3	2						12.9	41.1
RU8-20	1137.1	2						14.5	46.1
RU9-2	993.6	3						11.2	35.5
RU9-4	976.6	2						11.7	37.3
RU9-6	1234.6	2				J		13.0	41.4
RU9-8	930.5	2						11.9	37.8
RU9-10	1316.1	2						11.4	36.3
RU9-12	752.1	3						12.6	40.1
RU9-14	849.3	2						13.0	41.4
RU9-16	632.3	2						11.6	37.0
RU9-18	801.9	2						13.5	43.0
RU9-20	696.4	2						10.3	32.9
RU10-2	1951.5	3						137.0	436.3
RU10-4	1762.2	2						114.5	364.8
RU10-6	1068.6	2						11.2	35.6
RU10-8	1170.4	2						12.0	38.3
RU10-10	1617.3	2						66.8	212.8
RU10-12	1126.8	3				J		13.5	43.0
RU10-13.5	1058.0	3						11.2	35.7
RU10-14	1995.5	2						77.2	246.0
RU10-16	1750.9	2						68.7	218.7
RU10-20	1401.8	2						11.8	37.7
RU10-24	1215.7	2						12.8	40.8
RU10-28	Missing	0						0.0	0.0
RU10-30	1409.7	3						11.9	37.8
RU10-32	1532.5	2						12.0	38.3
RU11-2	630.8	2						11.0	35.1
RU11-4	1418.5	2						12.3	39.1
RU11-6	1134.6	2						12.0	38.3
RU11-8	1207.4	3						12.4	39.3
RU11-10	804.0	2				J		11.8	37.7
RU11-11	1285.3	2				J		12.8	40.7
RU11-12	1500.1	2				J		64.5	205.3
RU11-14	1254.2	2						52.8	168.0
RU11-16	1860.6	3						87.5	278.7
RU11-18	1046.1	2						12.1	38.6
RU11-20	1141.2	2						12.5	39.9
RU11-22	1115.3	2						12.0	38.2
RU11-24	872.9	2						12.2	38.9
RU11-26	753.7	3						13.3	42.5
RU11-28	686.9	2						16.8	53.5
RU12-4	1282.8	2						13.4	42.6

RU12-6	991.9	2						11.2	35.6
RU12-8	1364.8	2						13.7	43.7
RU12-10	1186.3	3						12.0	38.2
RU12-12	870.5	2						11.9	38.0
RU12-14	1455.5	2						16.6	52.9
RU12-16	1187.8	3						12.6	40.2
RU12-20	1635.1	2						15.1	48.1
RU13-4	Missing	0						0.0	0.0
RU13-6	Missing	0						0.0	0.0
RU13-8	1108.3	3						11.9	37.9
RU13-10	1454.4	1						14.5	46.3
RU13-12	1260.0	2						13.2	42.0
RU13-14	1142.2	2						11.6	36.8
RU13-16	1294.0	2						15.3	48.7
RU13-18	1306.1	3						12.7	40.5
RU13-20	1995.2	2						129.1	411.3
RU13-24	1430.0	2						13.3	42.4
RU13-30	1672.9	2						66.1	210.5
RU13-32	1754.8	2						72.2	229.9
RU14-4	721.6	3						9.7	30.9
RU14-6	942.3	2				J		9.4	30.0
RU14-8	975.2	2						13.1	41.8
RU14-10	1277.4	2						16.0	51.0
RU14-12	765.2	2						9.9	31.7
RU14-14	1150.8	4						12.8	40.7
RU14-16	2038.9	2						22.6	71.9
RU14-18	1482.1	2						13.8	44.0
RU14-20	1269.2	2						11.2	35.6
RU15-4	658.9	3						11.6	36.8
RU15-6	787.7	2						10.6	33.8
RU15-10	1196.2	2						11.2	35.7
RU15-12	1122.8	2						36.8	117.3
RU15-14	1125.6	2						13.2	42.0
RU15-16	846.9	2						12.6	40.0
RU15-18	885.0	3						13.0	41.5
RU15-20	Missing	0						0.0	0.0
RU16-4	4348.2	3				J		137.1	436.8
RU16-6	1146.2	2				J		9.6	30.5
RU16-8	1765.2	2						154.0	490.5
RU16-10	1206.3	3						51.1	162.6
RU16-12	1042.4	2				J		72.0	229.2
RU16-14	1953.6	2				J		71.7	228.3
RU16-16	1184.4	3				J		54.5	173.7
RU16-18	1090.2	2				J		77.0	245.2
RU16-20	1672.1	2						147.9	470.9
RU17-4	669.2	3						7.2	23.0
RU17-6	830.8	2						7.9	25.2

RU17-8	724.0	2				J		8.4	26.9
RU17-10	779.5	2						8.2	26.2
RU17-12	917.5	3						8.0	25.6
RU17-14	536.0	2						9.7	30.8
RU17-16	497.9	3				J		9.0	28.6
RU17-18	506.3	2				J		9.1	28.9
RU17-20	381.4	2				J		7.1	22.6
RU18-4	801.3	2						8.4	26.7
RU18-6	683.1	2						7.8	24.9
RU18-8	985.7	3						7.9	25.0
RU18-10	864.9	2						7.6	24.1
RU18-12	576.3	2						7.7	24.6
RU18-14	740.0	3						8.8	28.0
RU18-16	990.1	2						8.0	25.5
RU18-18	907.3	2						8.0	25.6

Results based on one measurement or average of multiple measurements

U = Measured Concentration < MDL (Method Detection Limit).

F = Measured Concentration between MDL and PQL (Practical Quantification Limit).

B = Method or Instrument Blank associated with sample > PQL.

J = Duplicate RPD (Relative Percent Difference) or Triplicate RSD (Relative Standard Deviation) outside of acceptable limit. Only applied to duplicate or triplicate samples, indicated by "No. of Data Points".

M = R (Percent Recovery) outside of acceptable limit for a spike. See QA/QC discussion.

Table 2
Soils Data Summary
Current Fire Training Area (FT-08)
Westover ARB, Chicopee, MA
0.5N HCl Total Iron

Sample ID	Result	No. of Data Points	Qualifiers					MDL	PQL
			U	F	B	J	M		
(1)	(2)	(3)	(4)	(5)	(6)	(7)	(8)	(9)	(10)
RU1-2	1276.2	2						33.4	106.5
RU1-4	1773.1	2						31.3	99.7
RU1-6	1665.0	3						27.2	86.6
RU1-8	1980.4	2						33.4	106.4
RU1-10	1924.8	2						31.9	101.5
RU1-12	2149.6	2						31.7	100.9
RU1-14	3354.5	2				J		30.9	98.5
RU1-16	2788.6	3				J		32.4	103.3
RU1-18	2899.3	2						32.9	104.9
RU1-20	1265.9	2						29.3	93.2
RU1-22	1844.7	2						28.6	91.2
RU1-24	1733.3	2						31.0	98.7
RU1-26	1533.4	4						32.9	104.7
RU1-28	2096.6	2						31.7	101.1
RU1-30	2098.0	2						33.2	105.6
RU2-2	1517.4	2						30.0	95.6
RU2-4	3091.1	2						37.0	117.9
RU2-6	2711.8	3						32.0	102.0
RU2-8	3296.7	2						28.7	91.4
RU2-10	2069.5	4						32.2	102.4
RU2-12	2547.0	2						33.6	107.0
RU2-14	1806.6	3						33.3	106.2
RU2-16	2301.6	2						38.0	121.0
RU2-18	3100.4	2						36.9	117.6
RU2-20	2972.4	2						32.7	104.2
RU2-22	3112.5	2						34.5	109.9
RU2-24	6514.2	3						34.4	109.5
RU2-26	4433.9	2						34.0	108.1
RU2-28	6080.1	2						38.4	122.3
RU2-30	3566.8	2						34.5	109.8
RU3-2	1930.4	2						28.9	92.0
RU3-4	1587.4	3						31.8	101.4
RU3-6	2717.4	2						29.8	95.0
RU3-8	2876.0	2				J		31.8	101.3
RU3-10	1849.5	2						31.5	100.3
RU3-12	2130.5	2						30.9	98.3
RU3-14	2031.5	3						29.6	94.4
RU4-2	4416.9	2				J		25.9	82.6

RU4-4	2373.9	2						34.3	109.4
RU4-6	2086.9	2						28.1	89.6
RU4-8	1900.2	2						30.7	97.7
RU4-10	2534.2	3						31.6	100.7
RU4-12	2234.5	2						30.3	96.5
RU4-13.5	2054.3	2						29.0	92.3
RU4-14	4041.8	2						36.7	116.9
RU4-18	2630.3	2				J		36.5	116.3
RU4-20	1227.4	3						31.6	100.6
RU4-24	1451.7	2						32.1	102.1
RU5-2	1440.8	2						28.7	91.5
RU5-4	1205.4	2						25.0	79.5
RU5-6	1443.7	2						28.7	91.3
RU5-8	1702.2	3						29.6	94.3
RU5-10	2385.9	2						32.2	102.5
RU5-12	1584.5	2						30.9	98.6
RU5-14	1494.4	2						30.6	97.5
RU5-16	1628.1	2						31.8	101.3
RU5-20	1703.9	3						34.0	108.4
RU5-24	2841.5	2						34.0	108.3
RU5-26	3109.3	2						32.5	103.5
RU5-28	3147.2	2						33.5	106.7
RU5-32	2543.0	2						32.4	103.2
RU6-2	4058.4	2						25.3	80.6
RU6-4	3374.4	2						28.9	92.0
RU6-6	2398.1	2						25.8	82.1
RU6-8	1770.1	2						30.2	96.1
RU6-10	1799.8	3						30.0	95.6
RU6-12	1404.6	2						32.5	103.6
RU6-14	2553.2	2						32.0	102.1
RU6-16	1285.0	2						25.7	81.9
RU6-18	1723.3	2						33.0	105.0
RU6-20	1754.1	3						30.1	95.8
RU6-36	Missing	0						0.0	0.0
RU7-4	1877.8	2						27.9	89.0
RU7-7	1599.9	2						30.3	96.5
RU7-8	1702.7	2						48.0	153.0
RU7-10	1575.6	2						48.3	153.9
RU7-12	1278.2	3						51.0	162.5
RU7-14	1851.3	2						25.1	79.8
RU7-16	1378.9	2						26.6	84.9
RU7-18	2723.3	2						30.7	97.8
RU7-20	2607.1	2						31.1	98.9
RU8-2	1531.8	3						27.5	87.6
RU8-4	1628.5	2						25.0	79.6
RU8-6	1524.9	2						23.8	75.8
RU8-18	1333.8	2						27.0	86.0

RU8-8	1466.3	2						28.3	90.2
RU8-10	1581.4	2						26.8	85.3
RU8-12	1377.8	3				J		30.2	96.2
RU8-14	1244.3	2						28.8	91.6
RU8-16	1325.8	2						29.2	92.8
RU8-20	1522.4	2						32.7	104.1
RU9-2	1821.9	3						25.2	80.2
RU9-4	1920.8	2						26.5	84.3
RU9-6	2058.7	2				J		29.4	93.5
RU9-8	1649.4	2						26.8	85.3
RU9-10	2121.7	2						25.7	81.9
RU9-12	1461.1	3						28.4	90.5
RU9-14	1656.4	2						29.4	93.5
RU9-16	1153.3	2						26.2	83.5
RU9-18	1386.9	2						30.5	97.1
RU9-20	1218.1	2						23.3	74.2
RU10-2	2024.4	3						30.9	98.5
RU10-4	2570.9	2						25.9	82.4
RU10-6	1604.0	2						25.3	80.4
RU10-8	1606.7	2						27.2	86.6
RU10-10	1969.0	2						26.4	84.1
RU10-12	1565.8	3						30.5	97.2
RU10-13.5	1439.4	3						25.3	80.5
RU10-14	2460.1	2						31.2	99.3
RU10-16	2156.7	2						29.6	94.2
RU10-20	1752.4	2						26.7	85.1
RU10-24	1554.4	2						28.9	92.1
RU10-28	Missing	0						0.0	0.0
RU10-30	2135.6	3						26.8	85.4
RU10-32	2317.0	2						27.2	86.6
RU11-2	2439.2	2						24.9	79.3
RU11-4	2491.6	2						27.7	88.2
RU11-6	1592.9	2						27.1	86.4
RU11-8	1877.6	3						27.9	88.8
RU11-10	2056.5	2						26.7	85.0
RU11-11	2015.8	2				J		28.9	91.9
RU11-12	2088.9	2				J		27.7	88.1
RU11-14	1647.9	2						23.7	75.3
RU11-16	2388.3	3						29.5	94.0
RU11-18	1475.1	2						27.4	87.2
RU11-20	1553.0	2						28.3	90.0
RU11-22	1647.4	2						27.1	86.1
RU11-24	1379.7	2						27.5	87.7
RU11-26	1312.6	3						30.1	95.9
RU11-28	1249.3	2						37.9	120.9
RU12-4	2364.8	2						30.2	96.2
RU12-6	1553.9	2						25.2	80.3

RU12-8	2066.7	2						30.9	98.6
RU12-10	2212.5	3				J		27.1	86.3
RU12-12	1394.9	2						26.9	85.7
RU12-14	2092.4	2						37.5	119.4
RU12-16	1618.8	3						28.5	90.7
RU12-20	2195.6	2						34.1	108.6
RU13-4	Missing	0						0.0	0.0
RU13-6	Missing	0						0.0	0.0
RU13-8	1615.8	3						26.9	85.5
RU13-10	2029.7	1						32.8	104.6
RU13-12	1789.0	2						29.8	94.8
RU13-14	1625.1	2						26.1	83.1
RU13-16	2031.6	2						34.5	109.9
RU13-18	1736.9	3						28.7	91.4
RU13-20	2491.1	2						29.2	92.9
RU13-24	1853.4	2						30.0	95.7
RU13-30	2136.0	2						26.9	85.7
RU13-32	2234.8	2						30.3	96.6
RU14-4	1878.8	3						21.9	69.8
RU14-6	1547.6	2						21.2	67.6
RU14-8	1592.1	2						29.6	94.3
RU14-10	2259.4	2						36.1	115.1
RU14-12	1485.9	2						22.4	71.5
RU14-14	1521.6	4						28.9	91.9
RU14-16	1219.1	2	U					51.0	162.3
RU14-18	2089.1	2						31.2	99.3
RU14-20	1729.4	2						25.2	80.4
RU15-4	1716.2	3						26.1	83.0
RU15-6	1490.8	2						24.0	76.4
RU15-10	1866.8	2						25.3	80.7
RU15-12	1665.9	2						21.1	67.1
RU15-14	1773.4	2						29.8	94.8
RU15-16	1412.7	2						28.4	90.4
RU15-18	1712.1	3						29.4	93.7
RU15-20	Missing	0						0.0	0.0
RU16-4	3061.4	3						31.0	98.6
RU16-6	2058.7	2						36.0	114.8
RU16-8	2761.2	2						34.8	110.7
RU16-10	2052.6	3						30.6	97.5
RU16-12	1665.3	2				J		28.3	90.2
RU16-14	3005.2	2				J		30.1	95.7
RU16-16	1935.2	3						31.7	100.8
RU16-18	1932.9	2						30.5	97.1
RU16-20	2373.9	2						33.4	106.3
RU17-4	1175.6	3						27.2	86.5
RU17-6	1610.2	2						29.8	94.8
RU17-8	1991.5	2						31.8	101.2

RU17-10	1891.7	2						30.9	98.5
RU17-12	2001.6	3						30.3	96.3
RU17-14	1340.9	2						36.4	116.0
RU17-16	1273.9	3						33.8	107.7
RU17-18	1408.7	2						34.1	108.7
RU17-20	1018.2	2						26.7	85.1
RU18-4	2235.3	2						31.5	100.5
RU18-6	1298.0	2						29.5	93.8
RU18-8	1591.6	3						29.5	94.1
RU18-10	1602.1	2						28.5	90.8
RU18-12	1058.4	2						29.1	92.6
RU18-14	1392.7	3						33.1	105.4
RU18-16	1348.8	2						30.1	95.8
RU18-18	1183.1	2						30.3	96.4

Results based on one measurement or average of multiple measurements

U = Measured Concentration > MDL (Method Detection Limit).

F = Measured Concentration between MDL and PQL (Practical Quantification Limit).

B = Method or Instrument Blank associated with sample > PQL.

J = Duplicate RPD (Relative Percent Difference) or Triplicate RSD (Relative Standard Deviation) outside of acceptable limit. Only applied to duplicate or triplicate samples, indicated by "No. of Data Points".

M = R (Percent Recovery) outside of acceptable limit for a spike. See QA/QC discussion.

Table 3
Soils Data Summary
Current Fire Training Area (FT-08)
Westover ARB, Chicopee, MA
Acid Extractable Sulfide

Sample ID	Result	No. of Data Points	Qualifiers					MDL	PQL
			U	F	B	J	M		
(1)	mg/kg	(3)	(4)	(5)	(6)	(7)	(8)	(9)	(10)
RU1-2	0.1	1	U					0.2	0.7
RU1-4	0.3	1		F				0.2	0.7
RU1-6	0.9	1		F				0.3	0.8
RU1-8	0.1	1	U					0.2	0.8
RU1-10	1.9	3		F		J		0.2	0.7
RU1-12	0.2	1		F				0.2	0.7
RU1-14	0.3	1		F				0.2	0.7
RU1-16	6.1	1		F				0.2	0.6
RU1-18	1.0	1		F				0.2	0.7
RU1-20	0.1	2	U			J		0.2	0.7
RU1-22	0.1	1	U					0.3	0.8
RU1-24	0.1	1	U					0.2	0.7
RU1-26	0.4	1		F				0.2	0.7
RU1-28	0.3	1		F				0.2	0.7
RU1-30	0.2	3	U	F				0.3	0.8
RU2-2	0.1	1	U					0.2	0.8
RU2-4	0.2	1	U					0.3	0.9
RU2-6	0.5	1		F				0.3	0.9
RU2-8	0.6	1		F				0.2	0.6
RU2-10	0.3	3	U	F		J		0.3	0.8
RU2-12	0.4	1		F				0.2	0.8
RU2-14	0.2	1	U					0.2	0.7
RU2-16	0.3	1		F				0.2	0.8
RU2-18	0.4	2		F				0.3	0.8
RU2-20	0.6	1		F				0.2	0.8
RU2-22	0.4	1		F				0.3	0.9
RU2-24	0.2	1	U					0.3	0.9
RU2-26	1.0	1		F				0.3	0.9
RU2-28	0.4	2		F				0.3	0.9
RU2-30	0.6	1		F				0.2	0.7
RU3-2	0.2	1	U					0.2	0.7
RU3-4	0.3	1		F				0.2	0.8
RU3-6	0.4	1		F				0.2	0.7
RU3-8	0.1	3	U			J		0.3	0.8
RU3-10	0.4	1		F				0.3	0.8
RU3-12	0.3	1		F				0.3	0.9
RU3-14	0.1	1	U					0.2	0.7
RU4-2	0.1	1	U					0.2	0.7

RU4-4	0.2	3	U	F		J		0.3	0.9
RU4-6	0.7	1		F				0.2	0.7
RU4-8	0.2	1	U					0.3	0.8
RU4-10	0.3	1		F				0.3	0.8
RU4-12	0.4	1		F				0.2	0.8
RU4-13.5	0.2	3	U	F		J		0.2	0.7
RU4-14	0.4	1		F				0.3	0.8
RU4-18	0.5	1		F				0.3	0.9
RU4-20	0.5	1		F				0.3	0.8
RU4-24	0.3	1		F				0.2	0.7
RU5-2	2.3	3		F				0.2	0.7
RU5-4	0.1	1	U					0.2	0.8
RU5-6	0.2	1		F				0.2	0.5
RU5-8	3.6	1		F				0.3	1.0
RU5-10	0.6	1		F				0.3	0.8
RU5-12	1.0	3		F		J		0.3	1.0
RU5-14	3.9	1		F				0.3	0.8
RU5-16	0.2	1	U					0.3	0.9
RU5-20	1.1	1		F				0.2	0.7
RU5-24	0.6	1		F				0.3	0.9
RU5-26	2.0	3		F				0.3	0.9
RU5-28	1.2	1		F				0.3	0.8
RU5-32	0.7	1		F				0.3	0.8
RU6-2	1.7	1		F				0.2	0.8
RU6-4	1.1	1		F				0.2	0.8
RU6-6	0.9	3		F		J		0.2	0.7
RU6-8	0.7	1		F				0.2	0.7
RU6-10	0.9	1		F				0.2	0.7
RU6-12	1.6	1		F				0.3	0.9
RU6-14	0.6	1		F				0.2	0.8
RU6-16	0.5	3	U	F		J		0.3	0.8
RU6-18	0.3	1		F				0.3	0.9
RU6-20	0.4	1		F				0.2	0.6
RU6-36	0.7	1		F				0.2	0.6
RU7-4	0.5	1		F				0.3	1.0
RU7-7	0.4	3	U	F		J		0.2	0.7
RU7-8	0.2	1	U					0.2	0.8
RU7-10	0.1	1	U					0.2	0.7
RU7-12	0.7	1		F				0.3	0.9
RU7-14	1.0	1		F				0.3	0.9
RU7-16	0.7	3		F				0.3	0.8
RU7-18	0.2	1	U					0.3	0.9
RU7-20	0.1	1	U					0.2	0.6
RU8-2	0.2	1	U					0.2	0.6
RU8-4	0.0	1	U					0.2	0.7
RU8-6	0.4	3	U	F		J		0.2	0.8
RU8-18	0.4	1		F	B			0.3	0.9

RU8-8	0.2	1		F	B			0.2	0.6
RU8-10	0.1	1	U		B			0.3	0.9
RU8-12	0.4	1		F	B			0.2	0.7
RU8-14	0.9	1		F	B			0.2	0.8
RU8-16	1.5	3		F	B	J		0.3	0.8
RU8-20	0.5	1		F	B			0.3	0.8
RU9-2	0.1	1	U		B			0.2	0.7
RU9-4	0.4	1		F	B			0.3	0.8
RU9-6	0.3	1		F				0.2	0.6
RU9-8	0.1	3	U			J		0.3	0.8
RU9-10	0.3	1		F				0.2	0.8
RU9-12	0.1	1	U					0.3	0.8
RU9-14	0.0	1	U					0.2	0.8
RU9-16	0.2	1	U					0.2	0.8
RU9-18	0.1	3	U	F				0.3	0.8
RU9-20	0.1	1	U					0.2	0.7
RU10-2	0.2	1	U					0.3	0.9
RU10-4	0.2	1	U					0.2	0.8
RU10-6	0.2	1		F				0.2	0.7
RU10-8	0.1	3	U			J		0.3	0.8
RU10-10	0.2	1	U					0.3	0.9
RU10-12	0.3	1	U					0.3	1.0
RU10-13.5	0.1	1	U					0.2	0.7
RU10-14	0.7	1		F				0.3	0.9
RU10-16	0.2	3	U			J		0.3	0.9
RU10-20	0.3	1		F				0.3	0.9
RU10-24	0.2	1	U					0.2	0.8
RU10-28	0.1	1	U					0.3	1.0
RU10-30	0.1	1	U					0.3	0.9
RU10-32	0.1	3	U			J		0.3	0.9
RU11-2	0.3	1		F				0.2	0.7
RU11-4	0.1	1	U					0.2	0.8
RU11-6	0.0	1	U					0.2	0.7
RU11-8	0.1	1	U					0.3	0.8
RU11-10	0.3	3	U	F		J		0.3	0.8
RU11-11	0.5	1		F				0.3	0.8
RU11-12	0.7	1		F				0.2	0.8
RU11-14	6.1	1		F				0.2	0.7
RU11-16	3.6	1		F				0.2	0.7
RU11-18	0.4	3	U	F		J		0.3	0.9
RU11-20	Missing	0						0.0	0.0
RU11-22	0.3	1		F				0.3	1.0
RU11-24	0.0	1	U					0.2	0.8
RU11-26	1.7	1		F				0.2	0.8
RU11-28	0.8	3		F				0.2	0.7
RU12-4	0.1	1	U					0.3	0.8
RU12-6	1.7	1		F				0.2	0.7

RU12-8	0.8	1		F				0.3	0.8
RU12-10	0.1	1	U					0.2	0.7
RU12-12	0.6	3	U	F		J		0.2	0.7
RU12-14	0.7	1		F				0.4	1.4
RU12-16	0.4	1		F				0.3	0.9
RU12-20	1.4	1		F				0.2	0.8
RU13-4	0.3	1		F				0.2	0.7
RU13-6	0.3	3	U	F		J		0.2	0.7
RU13-8	0.1	1	U					0.3	0.8
RU13-10	0.0	1	U					0.2	0.8
RU13-12	-0.2	1	U					0.2	0.7
RU13-14	0.3	1		F				0.2	0.8
RU13-16	0.1	3	U	F		J		0.4	1.1
RU13-18	0.1	1	U					0.2	0.8
RU13-20	1.2	1		F				0.3	1.0
RU13-24	0.7	1		F				0.3	0.8
RU13-30	1.8	1		F				0.3	0.9
RU13-32	1.2	2		F				0.2	0.7
RU14-4	0.2	1	U					0.2	0.7
RU14-6	0.1	1	U					0.2	0.6
RU14-8	0.1	1	U					0.3	0.8
RU14-10	0.3	1		F				0.2	0.7
RU14-12	0.3	3	U	F		J		0.2	0.6
RU14-14	0.3	1		F				0.3	0.8
RU14-16	0.8	1		F				0.3	1.0
RU14-18	0.9	1		F				0.3	0.8
RU14-20	0.5	1		F				0.2	0.7
RU15-4	0.9	3		F		J		0.2	0.7
RU15-6	0.4	1		F				0.3	0.8
RU15-10	1.6	1		F				0.2	0.7
RU15-12	0.7	1		F				0.2	0.6
RU15-14	0.7	3		F		J		0.3	0.8
RU15-16	0.3	1		F				0.3	0.8
RU15-18	0.5	1		F				0.3	0.9
RU15-20	0.3	1		F				0.2	0.7
RU16-4	0.7	1		F				0.3	0.8
RU16-6	1.3	1		F				0.2	0.8
RU16-8	2.7	3		F		J		0.2	0.7
RU16-10	0.9	1		F				0.2	0.7
RU16-12	0.8	1		F				0.2	0.7
RU16-14	2.2	1		F				0.3	0.9
RU16-16	1.3	1		F				0.2	0.7
RU16-18	1.5	3		F		J		0.2	0.8
RU16-20	0.6	1		F				0.2	0.7
RU17-4	0.4	1		F				0.2	0.7
RU17-6	0.2	3	U	F		J		0.2	0.7
RU17-8	0.1	1	U					0.2	0.6

RU17-10	0.5	1		F				0.3	0.9
RU17-12	0.8	1		F				0.3	0.9
RU17-14	0.1	1	U					0.2	0.6
RU17-16	1.4	3	U	F		J		0.2	0.7
RU17-18	1.1	1		F				0.2	0.7
RU17-20	3.7	1		F				0.2	0.6
RU18-4	0.7	1		F				0.3	0.8
RU18-6	2.9	1		F				0.2	0.8
RU18-8	0.6	1		F				0.2	0.8
RU18-10	0.4	1		F				0.2	0.7
RU18-12	1.2	3	U	F		J		0.2	0.8
RU18-14	1.1	1		F				0.3	1.0
RU18-16	0.0	1	U					0.3	0.9
RU18-18	0.2	1		F				0.2	0.6

Results based on one measurement or average of multiple measurements

U = Measured Concentration > MDL (Method Detection Limit).

F = Measured Concentration between MDL and PQL (Practical Quantification Limit).

B = Method or Instrument Blank associated with sample > PQL.

J = Duplicate RPD (Relative Percent Difference) or Triplicate RSD (Relative Standard Deviation) outside of acceptable limit. Only applied to duplicate or triplicate samples, indicated by "No. of Data Points".

M = R (Percent Recovery) outside of acceptable limit for a spike. Only applied to laboratory samples. See QA/QC discussion.

Table 4
Soils Data Summary
Current Fire Training Area (FT-08)
Westover ARB, Chicopee, MA
Chromium Extractable Sulfide

Sample ID	Result	No. of Data Points	Qualifiers					MDL	PQL
			U	F	B	J	M		
(1)	(2)	(3)	(4)	(5)	(6)	(7)	(8)	(9)	(10)
RU1-2	64.7	1			B			1.1	3.6
RU1-4	6.5	1			B			0.2	0.7
RU1-6	2.0	1			B			0.3	0.8
RU1-8	0.6	1		F	B			0.2	0.8
RU1-10	29.3	3			B			0.2	0.7
RU1-12	7.4	1			B			0.2	0.7
RU1-14	0.6	1		F	B			0.2	0.7
RU1-16	38.2	1			B			1.0	3.0
RU1-18	21.7	1			B			0.2	0.7
RU1-20	0.8	3		F	B	J		0.2	0.7
RU1-22	2.0	1			B			0.3	0.8
RU1-24	3.4	1			B			0.2	0.7
RU1-26	2.0	1			B			0.2	0.7
RU1-28	0.7	1			B			0.2	0.7
RU1-30	2.6	3			B	J		0.3	0.8
RU2-2	10.7	1						0.2	0.8
RU2-4	1.4	1						0.3	0.9
RU2-6	1.4	1						0.3	0.9
RU2-8	1.0	1						0.2	0.6
RU2-10	1.1	4						0.3	0.8
RU2-12	1.9	1						0.2	0.8
RU2-14	1.0	1						0.2	0.7
RU2-16	1.2	1						0.2	0.8
RU2-18	0.5	2	U			J		0.3	0.8
RU2-20	0.5	1		F				0.2	0.8
RU2-22	0.3	1		F				0.3	0.9
RU2-24	2.4	1						0.3	0.9
RU2-26	NA	0						0.0	0.0
RU2-28	1.9	2		F		J		0.3	0.9
RU2-30	0.7	1		F				0.2	0.7
RU3-2	1.8	1						0.2	0.7
RU3-4	7.8	1						0.2	0.8
RU3-6	3.8	1						0.2	0.7
RU3-8	1.0	3				J		0.3	0.8
RU3-10	1.9	1						0.3	0.8
RU3-12	1.8	1						0.3	0.9
RU3-14	1.3	1						0.2	0.7
RU4-2	19.8	1						0.2	0.7

RU4-4	46.8	3				J		0.3	0.9
RU4-6	14.3	1						0.2	0.7
RU4-8	1.8	1						0.3	0.8
RU4-10	32.8	1						0.3	0.8
RU4-12	1.3	1						0.2	0.8
RU4-13.5	0.9	3		F		J		0.2	0.7
RU4-14	0.2	1	U					0.3	0.8
RU4-18	1.0	1						0.3	0.9
RU4-20	0.8	1		F				0.3	0.8
RU4-24	0.5	1		F				0.2	0.7
RU5-2	35.0	3						0.2	0.7
RU5-4	10.7	1						0.2	0.8
RU5-6	2.4	1						0.2	0.5
RU5-8	4.7	1						0.3	1.0
RU5-10	9.9	1						0.3	0.8
RU5-12	10.3	3				J		0.3	1.0
RU5-14	10.6	1						0.3	0.8
RU5-16	1.2	1						0.3	0.9
RU5-20	17.3	1						0.2	0.7
RU5-24	4.6	1						0.3	0.9
RU5-26	6.6	3						0.3	0.9
RU5-28	1.6	1						0.3	0.8
RU5-32	2.5	1						0.3	0.8
RU6-2	2.9	1						0.2	0.8
RU6-4	1.2	1						0.2	0.8
RU6-6	13.9	3				J		0.2	0.7
RU6-8	1.4	1						0.2	0.7
RU6-10	0.9	1						0.2	0.7
RU6-12	3.5	1						0.3	0.9
RU6-14	0.5	1		F				0.2	0.8
RU6-16	5.6	3				J		0.3	0.8
RU6-18	1.9	1						0.3	0.9
RU6-20	2.2	1						0.2	0.6
RU6-36	0.7	1						0.2	0.6
RU7-4	2.9	1						0.3	1.0
RU7-7	0.6	3		F		J		0.2	0.7
RU7-8	0.6	1		F				0.2	0.8
RU7-10	1.0	1						0.2	0.7
RU7-12	0.3	1		F				0.3	0.9
RU7-14	0.5	1		F				0.3	0.9
RU7-16	3.0	3				J		0.3	0.8
RU7-18	0.7	1		F				0.3	0.9
RU7-20	0.2	1		F				0.2	0.6
RU8-2	2.9	1						0.2	0.6
RU8-4	0.6	1		F				0.2	0.7
RU8-6	1.4	3		F		J		0.2	0.8
RU8-18	0.3	1		F				0.3	0.9

RU8-8	0.5	1		F				0.2	0.6
RU8-10	1.9	1						0.3	0.9
RU8-12	1.6	1						0.2	0.7
RU8-14	0.5	1		F				0.2	0.8
RU8-16	0.5	3		F		J		0.3	0.8
RU8-20	0.6	1		F				0.3	0.8
RU9-2	0.5	1		F				0.2	0.7
RU9-4	0.4	1		F				0.3	0.8
RU9-6	0.8	1			B			0.2	0.6
RU9-8	1.6	3			B	J		0.3	0.8
RU9-10	0.9	1			B			0.2	0.8
RU9-12	0.7	1		F	B			0.3	0.8
RU9-14	0.5	1		F	B			0.2	0.8
RU9-16	0.3	1		F	B			0.2	0.8
RU9-18	0.2	3	U	F	B	J		0.3	0.8
RU9-20	0.5	1		F	B			0.2	0.7
RU10-2	261.6	1			B			1.4	4.6
RU10-4	19.5	1			B			0.2	0.8
RU10-6	1.8	1			B			0.2	0.7
RU10-8	7.4	3			B			0.3	0.8
RU10-10	0.6	1		F	B			0.3	0.9
RU10-12	0.6	1		F	B			0.3	1.0
RU10-13.5	0.7	1		F				0.2	0.7
RU10-14	1.7	1						0.3	0.9
RU10-16	2.1	3						0.3	0.9
RU10-20	1.7	1						0.3	0.9
RU10-24	9.2	1						0.2	0.8
RU10-28	1.3	1						0.3	1.0
RU10-30	0.9	1		F				0.3	0.9
RU10-32	0.6	3		F				0.3	0.9
RU11-2	2.6	1						0.2	0.7
RU11-4	10.4	1						0.2	0.8
RU11-6	2.7	1						0.2	0.7
RU11-8	3.1	1						0.3	0.8
RU11-10	20.0	3						0.3	0.8
RU11-11	23.7	1						0.3	0.8
RU11-12	1.1	1			B			0.2	0.8
RU11-14	68.0	1			B			1.0	3.3
RU11-16	45.3	1			B			0.2	0.7
RU11-18	27.9	3			B			0.3	0.9
RU11-20	38.2	1			B			0.2	0.8
RU11-22	5.6	1			B			0.3	1.0
RU11-24	15.2	1			B			0.2	0.8
RU11-26	4.3	1			B			0.2	0.8
RU11-28	3.8	3			B	J		0.2	0.7
RU12-4	24.6	1			B			0.3	0.8
RU12-6	28.4	1			B			0.2	0.7

RU12-8	13.5	1			B			0.3	0.8
RU12-10	10.7	1			B			0.2	0.7
RU12-12	0.7	3		F	B	J		0.2	0.7
RU12-14	1.6	1						0.4	1.4
RU12-16	0.6	1		F				0.3	0.9
RU12-20	0.8	1						0.2	0.8
RU13-4	0.4	1		F				0.2	0.7
RU13-6	0.4	3		F				0.2	0.7
RU13-8	0.9	1						0.3	0.8
RU13-10	0.0	1	U					0.2	0.8
RU13-12	0.5	1		F				0.2	0.7
RU13-14	2.5	1						0.2	0.8
RU13-16	1.8	3		F		J		0.4	1.1
RU13-18	9.0	1						0.2	0.8
RU13-20	2.2	1						0.3	1.0
RU13-24	6.2	1						0.3	0.8
RU13-30	4.4	1						0.3	0.9
RU13-32	3.7	2						0.2	0.7
RU14-4	0.1	1	U					0.2	0.7
RU14-6	0.3	1		F				0.2	0.6
RU14-8	0.9	1						0.3	0.8
RU14-10	0.3	1		F				0.2	0.7
RU14-12	0.3	3	U	F		J		0.2	0.6
RU14-14	5.3	1						0.3	0.8
RU14-16	1.3	1						0.3	1.0
RU14-18	1.1	1						0.3	0.8
RU14-20	0.8	1						0.2	0.7
RU15-4	0.3	3	U	F		J		0.2	0.7
RU15-6	1.0	1						0.3	0.8
RU15-10	1.4	1						0.2	0.7
RU15-12	0.2	1		F				0.2	0.6
RU15-14	0.4	3	U	F		J		0.3	0.8
RU15-16	0.1	1	U					0.3	0.8
RU15-18	NA	0						0.0	0.0
RU15-20	0.1	1	U					0.2	0.7
RU16-4	6.9	1						0.3	0.8
RU16-6	3.2	1						0.2	0.8
RU16-8	3.9	3				J		0.2	0.7
RU16-10	0.5	1		F				0.2	0.7
RU16-12	0.2	1		F				0.2	0.7
RU16-14	0.2	1	U					0.3	0.9
RU16-16	0.3	1		F				0.2	0.7
RU16-18	0.3	3	U	F		J		0.2	0.8
RU16-20	0.3	1		F				0.2	0.7
RU17-4	0.1	1	U					0.2	0.7
RU17-6	0.1	3	U			J		0.2	0.7
RU17-8	1.3	1						0.2	0.6

RU17-10	0.1	1	U					0.3	0.9
RU17-12	0.4	1		F				0.3	0.9
RU17-14	0.1	1	U					0.2	0.6
RU17-16	0.3	3	U	F		J		0.2	0.7
RU17-18	0.9	1						0.2	0.7
RU17-20	0.4	1		F				0.2	0.6
RU18-4	0.1	1	U					0.3	0.8
RU18-6	0.1	1	U					0.2	0.8
RU18-8	0.0	1	U					0.2	0.8
RU18-10	0.0	1	U					0.2	0.7
RU18-12	0.3	3	U	F		J		0.2	0.8
RU18-14	0.5	1		F				0.3	1.0
RU18-16	0.2	1	U					0.3	0.9
RU18-18	2.5	1						0.2	0.6

Results based on one measurement or average of multiple measurements

U = Measured Concentration > MDL (Method Detection Limit).

F = Measured Concentration between MDL and PQL (Practical Quantification Limit).

B = Method or Instrument Blank associated with sample > PQL.

J = Duplicate RPD (Relative Percent Difference) or Triplicate RSD (Relative Standard Deviation) outside of acceptable limit. Only applied to duplicate or triplicate samples, indicated by "No. of Data Points".

M = R (Percent Recovery) outside of acceptable limit for a spike. Only applied to laboratory samples. See QA/QC discussion.

Table 5
Soils Data Summary
Current Fire Training Area (FT-08)
Westover ARB, Chicopee, MA
Sulfate Pore Water Concentrations

Sample ID	No. of Data Points	Result mg/L	Qualifiers				MDL	PQL
			U	F	B	J	mg/L	mg/L
RU1-2	1	24.9					7.7	24.4
RU1-4	1	8.7					6.2	19.6
RU1-6	1	28.0					6.8	21.6
RU1-8	1	0.0	U				4.8	15.2
RU1-10	1	7.0					5.1	16.2
RU1-12	1	13.4					6.6	21.1
RU1-14	1	4.5	U				5.2	16.6
RU1-16	1	6.7					5.6	17.9
RU1-18	1	21.6					4.8	15.2
RU1-20	1	34.2					5.6	17.8
RU1-22	1	21.4					4.6	14.7
RU1-24	1	18.2					5.1	16.3
RU1-26	1	5.0					3.3	10.6
RU1-28	1	8.5					5.5	17.4
RU1-30	1	7.4					4.4	14.0
RU2-2	1	50.3					10.5	33.4
RU2-4	1	49.8					6.7	21.4
RU2-6	1	28.9					4.2	13.3
RU2-8	1	33.4					5.0	16.0
RU2-10	1	27.1					4.3	13.8
RU2-12	2	22.6					4.0	12.8
RU2-14	1	25.6				J	3.7	11.6
RU2-16	1	34.0				J	4.7	15.1
RU2-18	1	16.3				J	2.8	9.0
RU2-20	1	16.7				J	3.0	9.5
RU2-22	1	3.5	U			J	3.6	11.5
RU2-24	1	17.4				J	4.4	14.0
RU2-26	1	15.1				J	3.0	9.7
RU2-28	1	23.9				J	4.4	14.0
RU2-30	1	21.4				J	4.4	13.9
RU3-2	1	38.5					15.3	48.8
RU3-4	1	23.2					6.4	20.5
RU3-6	1	62.2					5.7	18.1
RU3-8	1	62.7					4.8	15.4
RU3-10	1	65.5					4.8	15.3
RU3-12	1	0.0	U				4.2	13.3
RU3-14	1	63.1					3.8	12.1

RU4-2	missing							
RU4-4	1	5.5				3.5	11.2	
RU4-6	1	7.2	U			8.7	27.7	
RU4-8	1	3.2	U		J	3.7	11.8	
RU4-10	1	2.8	U		J	5.2	16.6	
RU4-12	1	3.1	U		J	4.9	15.5	
RU4-13.5	missing							
RU4-14	1	9.0				4.1	13.0	
RU4-18	1	37.6				3.0	9.5	
RU4-20	1	25.5			J	3.5	11.2	
RU4-24	1	2.4	U		J	3.3	10.6	
RU5-2	missing							
RU5-6	1	12.9	U			14.2	45.1	
RU5-8	1	0.0	U			3.8	12.3	
RU5-10	1	1.5	U			2.9	9.1	
RU5-12	1	1.7	U			2.9	9.3	
RU5-14	1	6.6				3.4	10.9	
RU5-16	1	6.4				3.8	12.2	
RU5-20	1	6.8				4.0	12.8	
RU5-24	1	7.2				3.5	11.2	
RU5-26	1	1.4	U			2.8	8.8	
RU5-28	1	9.8				3.2	10.2	
RU5-32	1	16.2				3.5	11.1	
RU6-2	1	109.3				13.1	41.7	
RU6-4	1	32.7				4.0	12.7	
RU6-6	1	34.9				9.4	29.9	
RU6-8	1	54.0				4.8	15.2	
RU6-10	1	49.8				3.7	11.8	
RU6-12	1	8.1				3.2	10.1	
RU6-14	1	2.9				2.8	8.8	
RU6-16	1	3.1	U			3.7	11.9	
RU6-18	1	1.7	U			3.1	9.9	
RU6-20	1	1.8	U			3.3	10.5	
RU7-4	1	15.1			J	8.4	26.9	
RU7-8	1	23.0			J	3.4	10.8	
RU7-10	1	3.0	U		J	4.4	14.0	
RU7-12	1	1.9	U		J	2.7	8.5	
RU7-14	1	2.1	U		J	3.1	10.0	
RU7-16	1	3.7			J	3.1	10.0	
RU7-18	1	1.5	U		J	2.9	9.1	
RU7-20	1	1.4	U		J	2.6	8.2	
RU8-6	1	22.5			J	3.8	12.2	
RU8-18	1	6.9			J	3.4	10.8	
RU8-8	1	20.0			J	3.3	10.4	
RU8-10	1	11.2			J	3.3	10.5	

RU8-12	1	6.2				J	3.4	10.7
RU8-14	1	11.3				J	2.9	9.4
RU8-16	1	5.6				J	3.4	11.0
RU8-20	1	7.2				J	3.4	11.0
RU9-2	1	40.1			B	J	12.5	39.8
RU9-4	1	51.0			B	J	14.6	46.6
RU9-6	1	24.3			B	J	5.7	18.2
RU9-8	1	17.1			B	J	4.3	13.7
RU9-10	1	15.0			B	J	4.2	13.3
RU9-12	1	15.3				J	3.1	9.9
RU9-14	1	20.5				J	4.0	12.6
RU9-16	1	15.9				J	3.2	10.2
RU9-18	1	18.3				J	4.0	12.7
RU10-2	1	8.3					5.8	18.6
RU10-4	1	12.4					10.7	33.9
RU10-6	1	10.3	U				14.6	46.4
RU10-8	1	2.9	U				5.0	16.0
RU10-10	1	2.1	U				3.4	10.8
RU10-12	1	2.7	U				4.0	12.7
RU10-14	1	2.3	U				3.7	11.9
RU10-16	1	2.2	U				3.1	10.0
RU10-20	1	3.3	U				3.4	10.9
RU10-24	1	2.1	U				3.2	10.1
RU10-30	1	2.6	U				3.2	10.3
RU10-32	1	1.9	U				2.6	8.3
RU11-6	1	52.2					8.5	27.2
RU11-8	1	15.5					3.1	9.8
RU11-10	1	12.8					4.1	13.2
RU11-12	1	10.5					3.7	11.8
RU11-14	missing							
RU11-16	1	3.5	U				3.6	11.6
RU11-18	1	9.3					3.3	10.6
RU11-20	1	2.3	U				3.2	10.2
RU11-22	1	56.6					3.4	10.7
RU11-24	1	46.6					3.2	10.1
RU11-26	1	43.6					3.2	10.0
RU11-28	1	34.8					3.4	11.0
RU12-4	1	21.3					5.5	17.5
RU12-6	1	30.2					9.3	29.7
RU12-8	1	32.0					3.4	10.7
RU12-10	1	46.8					5.8	18.4
RU12-12	1	30.2					3.3	10.4
RU12-14	2	18.1					2.7	8.7
RU12-16	1	25.7					4.7	14.9
RU12-20	1	23.8					3.1	10.0

RU13-6	1	96.6				J	11.4	36.3
RU13-8	1	26.8				J	4.0	12.8
RU13-10	2	37.2				J	3.9	12.3
RU13-12	1	17.9					4.3	13.7
RU13-14	1	3.2	U				4.9	15.6
RU13-16	1	1.6	U				3.6	11.3
RU13-18	1	23.8					4.8	15.2
RU13-20	1	44.0					4.3	13.6
RU13-24	1	28.4					3.7	11.8
RU13-30	1	18.3					3.6	11.5
RU13-32	1	19.5					3.4	10.7
RU14-8	1	20.9					4.1	13.0
RU14-10	1	32.5					4.9	15.5
RU14-12	missing							
RU14-14	1	18.5					4.2	13.4
RU14-16	1	12.6					2.0	6.4
RU14-18	1	21.1					3.1	9.7
RU14-20	missing							
RU15-6	1	88.2					17.1	54.6
RU15-10	1	44.5					7.3	23.2
RU15-12	1	5.8					3.2	10.3
RU15-14	1	2.6	U				3.3	10.4
RU15-16	1	2.4	U				3.7	11.9
RU15-18	1	3.5					3.2	10.1
RU15-20	1	8.1					5.8	18.5
RU16-6	1	144.0					6.5	20.7
RU16-8	1	165.1					5.0	15.8
RU16-10	2	202.4					5.5	17.5
RU16-12	1	159.9					4.1	13.1
RU16-14	1	26.3					3.7	11.8
RU16-16	1	30.5					4.4	14.1
RU16-18	missing							
RU16-20	1	25.6					4.1	13.1
RU17-6	1	20.5					4.2	13.5
RU17-8	1	17.6					3.8	12.3
RU17-10	1	21.9					3.5	11.2
RU17-12	1	19.8					4.0	12.6
RU17-14	1	22.7					3.9	12.5
RU17-18	1	19.1					3.7	11.9
RU18-6	1	36.9				J	6.4	20.4
RU18-8	1	19.2				J	4.0	12.6
RU18-10	2	27.4				J	5.5	17.6
RU18-12	1	19.9					3.6	11.5
RU18-14	1	17.2					3.0	9.6
RU18-16	1	22.5					4.7	14.9

RU18-18	1	16.5					3.6	11.6
---------	---	------	--	--	--	--	-----	------

Results based on one measurement or average of multiple measurements

U = Measured Concentration > MDL (Method Detection Limit).

F = Measured Concentration between MDL and PQL (Practical Quantification Limit).

B = Method or Instrument Blank associated with sample > PQL.

J = Duplicate RPD (Relative Percent Difference) or Triplicate RSD (Relative Standard Deviation) outside of acceptable limit. Only applied to duplicate or triplicate samples, indicated by "No. of Data Points".

M = R (Percent Recovery) outside of acceptable limit for a spike. Only applied to laboratory samples. See QA/QC discussion.

Table 6
Soils Data Summary
Current Fire Training Area (FT-08)
Westover ARB, Chicopee, MA
Iron(II) Pore Water Concentrations

Sample ID	No. of Data Points	Results	Qualifiers			MDL	PQL
		mg/L	U	F	B	mg/L	mg/L
RU1-2	1	2.8				0.9	2.7
RU1-4	1	7.5				0.7	2.2
RU1-6	1	5.3				0.8	2.4
RU1-8	1	2.3				0.5	1.7
RU1-10	1	2.8				0.6	1.8
RU1-12	1	4.3				0.7	2.4
RU1-14	1	8.3				0.6	1.9
RU1-16	1	7.3				0.6	2.0
RU1-18	1	4.1				0.5	1.7
RU1-20	1	2.3				0.6	2.0
RU1-22	1	4.4				0.5	1.7
RU1-24	1	15.8				0.6	1.8
RU1-26	1	1.2		F		0.4	1.2
RU1-28	1	1.6		F		0.6	2.0
RU1-30	1	0.9		F		0.5	1.6
RU2-2	1	0.7	U			1.2	3.7
RU2-4	1	0.4	U			0.8	2.4
RU2-6	1	0.3	U			0.5	1.5
RU2-8	1	0.1	U			0.6	1.8
RU2-10	1	0.2	U			0.5	1.6
RU2-12	1	0.3	U			0.4	1.3
RU2-14	1	0.2	U			0.4	1.3
RU2-16	1	1.3		F		0.5	1.7
RU2-18	1	0.1	U			0.3	1.0
RU2-20	1	0.1	U			0.3	1.1
RU2-22	1	0.0	U			0.4	1.3
RU2-24	1	0.0	U			0.5	1.6
RU2-26	1	0.0	U			0.3	1.1
RU2-28	1	0.2	U			0.5	1.6
RU2-30	1	1.4		F		0.5	1.6
RU3-4	1	1.1		F		0.7	2.3
RU3-6	1	0.0	U			0.6	2.0
RU3-8	1	0.0	U			0.5	1.7
RU3-10	1	0.1	U			0.5	1.7
RU3-14	1	0.1	U			0.4	1.4
RU4-2	1	missing				0.0	0.0
RU4-4	1	5.5				0.4	1.3
RU4-6	1	6.2				1.0	3.1

RU4-8	1	4.1				0.4	1.3
RU4-10	1	3.1				0.6	1.9
RU4-12	1	4.2				0.5	1.7
RU4-14	1	2.0				0.5	1.5
RU4-18	1	1.7				0.3	1.1
RU4-20	1	0.3	U			0.4	1.3
RU4-24	1	1.1		F		0.4	1.2
RU5-6	1	3.8		F		1.6	5.1
RU5-8	1	3.0				0.4	1.4
RU5-10	1	4.4				0.3	1.0
RU5-12	1	2.8				0.3	1.0
RU5-14	1	4.8				0.4	1.2
RU5-16	1	2.6				0.4	1.4
RU5-20	1	2.6				0.5	1.4
RU5-24	1	4.5				0.4	1.3
RU5-26	1	7.0				0.3	1.0
RU5-28	1	2.4				0.4	1.1
RU5-32	1	1.9				0.4	1.2
RU5-36	1	6.0				0.4	1.3
RU6-2	1	0.6	U			1.5	4.7
RU6-4	1	0.1	U			0.4	1.4
RU6-6	1	0.4	U			1.1	3.4
RU6-8	1	0.1	U			0.5	1.7
RU6-10	1	0.2	U			0.4	1.3
RU6-12	1	missing				1.8	5.7
RU6-14	1	missing				1.6	5.0
RU6-16	1	missing				2.1	6.7
RU6-18	1	missing				1.8	5.6
RU6-20	1	missing				1.9	5.9
RU7-4	1	1.3		F		0.9	3.0
RU7-8	1	1.5				0.4	1.2
RU7-10	1	2.6				0.5	1.6
RU7-12	1	3.6				0.3	1.0
RU7-14	1	4.6				0.4	1.1
RU7-16	1	3.6				0.4	1.1
RU7-18	1	4.2				0.3	1.0
RU7-20	1	7.0				0.3	0.9
RU8-6	1	0.3	U			0.4	1.4
RU8-8	1	0.7		F		0.4	1.2
RU8-10	1	3.8				0.4	1.2
RU8-12	1	4.7				0.4	1.2
RU8-14	1	3.9				0.3	1.1
RU8-16	1	9.2				0.4	1.2
RU8-18	1	6.8				0.4	1.2
RU8-20	1	6.3				0.4	1.2

RU9-2	1	0.1	U			1.4	4.5
RU9-4	1	1.3	U			1.6	5.2
RU9-6	1	0.0	U			0.6	2.0
RU9-8	1	0.1	U			0.5	1.5
RU9-10	1	0.2	U			0.5	1.5
RU9-12	1	0.1	U			0.3	1.1
RU9-14	1	1.1		F		0.4	1.4
RU9-16	1	0.7		F		0.4	1.1
RU9-18	1	0.5		F		0.4	1.4
RU9-20	1	missing				0.0	0.0
RU10-2	1	5.0				0.7	2.1
RU10-4	1	7.7				1.2	3.8
RU10-6	1	6.5				1.6	5.2
RU10-8	1	0.9		F		0.6	1.8
RU10-10	1	1.5				0.4	1.2
RU10-12	1	1.8				0.4	1.4
RU10-14	1	2.4				0.4	1.3
RU10-16	1	4.0				0.4	1.1
RU10-20	1	5.1				0.4	1.2
RU10-24	1	7.2				0.4	1.1
RU10-30	1	13.5				0.4	1.2
RU10-32	1	6.2				0.3	0.9
RU11-6	1	6.7				1.0	3.1
RU11-8	1	1.1		F		0.3	1.1
RU11-10	1	3.9				0.5	1.5
RU11-12	1	8.5				0.4	1.3
RU11-14	1	missing				0.0	0.0
RU11-16	1	9.8				0.4	1.3
RU11-18	1	9.1				0.4	1.2
RU11-20	1	6.0				0.4	1.1
RU11-22	1	12.5				0.4	1.2
RU11-24	1	13.9				0.4	1.1
RU11-26	1	8.7				0.4	1.1
RU11-28	1	6.0				0.4	1.2
RU12-4	1	0.7		F		0.6	2.0
RU12-6	1	2.2		F		1.0	3.3
RU12-8	1	0.2	U			0.4	1.2
RU12-10	1	2.4				0.7	2.1
RU12-12	1	2.1				0.4	1.2
RU12-14	1	3.2				0.3	1.0
RU12-16	1	2.5				0.5	1.7
RU12-20	1	7.8				0.4	1.1
RU13-6	1	4.5				1.3	4.1
RU13-8	1	0.5		F		0.5	1.4
RU13-10	1	7.2				0.4	1.4

RU13-12	1	6.5				0.5	1.5
RU13-14	1	20.1				0.6	1.8
RU13-16	1	9.3				0.4	1.3
RU13-18	1	7.5				0.5	1.7
RU13-20	1	12.4				0.5	1.5
RU13-24	1	8.5				0.4	1.3
RU13-30	1	3.5				0.4	1.3
RU13-32	1	2.6				0.4	1.2
RU14-8	1	0.3	U			0.5	1.5
RU14-10	1	3.1				0.5	1.7
RU14-12	1	missing				0.0	0.0
RU14-14	1	6.6				0.5	1.5
RU14-16	1	10.8				0.2	0.7
RU14-18	1	7.4				0.3	1.1
RU14-20	1	missing				0.0	0.0
RU15-6	1	0.7	U			1.9	6.1
RU15-8	1	0.3	U			0.6	1.8
RU15-10	1	1.4		F		0.8	2.6
RU15-12	1	3.1				0.4	1.2
RU15-14	1	3.7				0.4	1.2
RU15-16	1	4.3				0.4	1.3
RU15-18	1	6.5				0.4	1.1
RU15-20	1	12.3				0.7	2.1
RU16-6	1	3.1				0.7	2.3
RU16-8	1	5.7				0.6	1.8
RU16-10	1	9.2				0.6	2.0
RU16-12	1	18.8				0.5	1.5
RU16-14	1	16.2				0.4	1.3
RU16-16	1	21.2				0.5	1.6
RU16-18	1	missing				0.0	0.0
RU16-20	1	12.9				0.5	1.5
RU17-6	1	0.3	U			0.5	1.5
RU17-8	1	0.2	U			0.4	1.4
RU17-10	1	0.8		F		0.4	1.3
RU17-12	1	0.2	U			0.4	1.4
RU17-14	1	2.0				0.4	1.4
RU17-18	1	1.2		F		0.4	1.3
RU18-6	1	1.4		F		0.7	2.3
RU18-8	1	0.8		F		0.4	1.4
RU18-10	1	1.0		F		0.5	1.5
RU18-12	1	0.5		F		0.4	1.3
RU18-14	1	0.8		F		0.3	1.1
RU18-16	1	1.5		F		0.5	1.7
RU18-18	1	5.8				0.4	1.3

Results based on one measurement or average of multiple measurements

- U = Measured Concentration > MDL (Method Detection Limit).
- F = Measured Concentration between MDL and PQL (Practical Quantification Limit).
- B = Method or Instrument Blank associated with sample > PQL.
- J = Duplicate RPD (Relative Percent Difference) or Triplicate RSD (Relative Standard Deviation) outside of acceptable limit. See QA/QC discussion.
- M = R (Percent Recovery) outside of acceptable limit for a spike. See QA/QC discussion.

Table 7
 Aqueous Inorganic Data Summary
 Current Fire Training Area (FT-08)
 Westover ARB, Chicopee, MA

Well ID	Conductivity	Dissolved Oxygen	Oxidation Reduction Potential	Iron(II)	Sulfate
	mS	mg/L	mV	mg/L	mg/L
CF-1A	29.6	9.7	635	0.04	6.9
CF-7	27.2	8.93	518	0.01	5.9
CF-4	27.7	6.29	436	0.09	6.2
CF-8	41.8	0.21	204	0.79	4.2
CF-6S	174.3	0.14	-13.7	22	5.2
CF-5	102.2	0.42	327.1	11.75	16.5
CF-3	114.2	0.14	-194	8.75	0.7
CF-2	338	0.28	189	2.02	3.8
MP-15S	44.1	4.75	326	0.56	2.5
MP-10S	29.9	9.87	370	0.01	6.4
MP-5S	missing	missing	missing	3.12	1.5

Table 1: Compounds Measured by Method 8260

Acetone	Dibromomethane	p-Isopropyltoluene
Acrolein	1,2-Dichlorobenzene	MTBE
Acrylonitrile	1,3-Dichlorobenzene	Methylene Chloride
Benzene	1,4-Dichlorobenzene	MIBK
Bromobenzene	cis-1,4-Dichloro-2-Butene	Naphthalene
Bromochloromethane	trans-1,4-Dichloro-2-Butene	n-Propylbenzene
Bromodichloromethane	Dichlorodifluoromethane	Styrene
Bromomethane	1,1-Dichloroethane	1,1,1,2-Tetrachloroethane
Bromoform	1,2-Dichloroethane	1,1,2,2-Tetrachloroethane
2-Butanone (MEK)	1,1-Dichloroethylene	Tetrachloroethylene
n-Butylbenzene	cis-1,2-Dichloroethylene	Toluene
sec-Butylbenzene	trans-1,2-Dichloroethylene	1,2,3-Trichlorobenzene
tert-Butylbenzene	1,2-Dichloropropane	1,2,4-Trichlorobenzene
Carbon Disulfide	1,3-Dichloropropane	1,1,1-Trichloroethane
Carbon Tetrachloride	2,2-Dichloropropane	1,1,2-Trichloroethane
Chlorobenzene	1,1-Dichloropropene	Trichloroethylene
Chlorodibromomethane	cis-1,3-Dichloropropene	Trichlorofluoromethane
Chloroethane	trans-1,3-Dichloropropene	1,2,3-Trichloropropane
2-Chloroethylvinylether	Ethyl Benzene	1,2,4-Trimethylbenzene
Chloroform	Ethyl Methacrylate	1,3,5-Trimethylbenzene
Chloromethane	Hexachlorobutadiene	Vinyl Acetate
2-Chlorotoluene	2-Hexanone	Vinyl Chloride
4-Chlorotoluene	Iodomethane	m-Xylene
1,2-Dibromo-3-Chloropropane	Isopropylbenzene	o + p Xylene
1,2-Dibromoethane		

Table 2: Aqueous Volatile Organic Compounds

Sample	Analyte	Result	MDL
		mg/kg	mg/kg
RU1-1	All Samples	ND	NA
RU1-3	Ethyl Benzene	0.014	0.002
RU1-3	Isopropylbenzene	0.003	0.002
RU1-3	n-Propylbenzene	0.004	0.002
RU1-3	Toluene	0.031	0.002
RU1-3	1,2,4-Trimethylbenzene	0.023	0.002
RU1-3	1,3,5-Trimethylbenzene	0.01	0.003
RU1-3	m-Xylene	0.059	0.003
RU1-3	o + p Xylene	0.022	0.001
RU1-5	n-Butylbenzene	7.65	0.038
RU1-5	sec-Butylbenzene	5.47	0.033
RU1-5	Ethyl Benzene	27.3	0.033
RU1-5	Isopropylbenzene	6.78	0.033
RU1-5	p-Isopropyltoluene	4.88	0.038
RU1-5	Naphthalene	8.75	0.055
RU1-5	n-Propylbenzene	12	0.044
RU1-5	Toluene	35	0.038
RU1-5	1,2,4-Trimethylbenzene	61.2	0.038
RU1-5	1,3,5-Trimethylbenzene	26.2	0.055
RU1-5	m-Xylene	91.8	0.071
RU1-5	o + p Xylene	29.5	0.027
RU1-7	n-Butylbenzene	8.16	0.041
RU1-7	sec-Butylbenzene	5.83	0.035
RU1-7	Ethyl Benzene	31.5	0.035
RU1-7	Isopropylbenzene	8.16	0.035
RU1-7	p-Isopropyltoluene	5.83	0.041
RU1-7	Naphthalene	8.16	0.058
RU1-7	n-Propylbenzene	12.8	0.047
RU1-7	Toluene	44.3	0.041
RU1-7	1,2,4-Trimethylbenzene	65.3	0.041
RU1-7	1,3,5-Trimethylbenzene	28	0.058
RU1-7	m-Xylene	102	0.076
RU1-7	o + p Xylene	32.6	0.029
RU1-9	n-Butylbenzene	0.132	0.036
RU1-9	sec-Butylbenzene	0.092	0.031
RU1-9	Ethyl Benzene	0.371	0.031
RU1-9	Isopropylbenzene	0.107	0.031
RU1-9	n-Propylbenzene	0.178	0.041
RU1-9	Toluene	0.668	0.036
RU1-9	1,2,4-Trimethylbenzene	0.954	0.036
RU1-9	1,3,5-Trimethylbenzene	0.404	0.051
RU1-9	m-Xylene	1.35	0.066

RU1-9	o + p Xylene	0.412	0.025
RU1-13	Benzene	0.004	0.001
RU1-13	n-Butylbenzene	0.007	0.001
RU1-13	sec-Butylbenzene	0.005	0.001
RU1-13	Ethyl Benzene	0.114	0.001
RU1-13	Isopropylbenzene	0.017	0.001
RU1-13	Naphthalene	0.036	0.001
RU1-13	n-Propylbenzene	0.023	0.001
RU1-13	Toluene	0.2	0.001
RU1-13	1,2,4-Trimethylbenzene	0.234	0.001
RU1-13	1,3,5-Trimethylbenzene	0.059	0.001
RU1-13	m-Xylene	0.367	0.002
RU1-13	o + p Xylene	0.134	0.001
RU1-15	Benzene	0.003	0.001
RU1-15	n-Butylbenzene	0.042	0.001
RU1-15	sec-Butylbenzene	0.029	0.001
RU1-15	Ethyl Benzene	0.123	0.001
RU1-15	Isopropylbenzene	0.034	0.001
RU1-15	p-Isopropyltoluene	0.028	0.001
RU1-15	Naphthalene	0.062	0.002
RU1-15	n-Propylbenzene	0.059	0.001
RU1-15	Toluene	0.328	0.001
RU1-15	1,2,4-Trimethylbenzene	0.78	0.001
RU1-15	1,3,5-Trimethylbenzene	0.148	0.002
RU1-15	m-Xylene	0.832	0.002
RU1-15	o + p Xylene	0.15	0.001
RU1-19	Ethyl Benzene	0.009	0.001
RU1-19	n-Propylbenzene	0.004	0.001
RU1-19	Toluene	0.017	0.001
RU1-19	1,2,4-Trimethylbenzene	0.034	0.001
RU1-19	1,3,5-Trimethylbenzene	0.013	0.002
RU1-19	m-Xylene	0.037	0.002
RU1-19	o + p Xylene	0.014	0.001
RU1-21	Benzene	0.002	0.001
RU1-21	n-Butylbenzene	0.005	0.001
RU1-21	sec-Butylbenzene	0.004	0.001
RU1-21	Ethyl Benzene	0.011	0.001
RU1-21	Isopropylbenzene	0.004	0.001
RU1-21	Naphthalene	0.01	0.002
RU1-21	n-Propylbenzene	0.006	0.001
RU1-21	Toluene	0.019	0.001
RU1-21	1,2,4-Trimethylbenzene	0.04	0.001
RU1-21	1,3,5-Trimethylbenzene	0.015	0.002
RU1-21	m-Xylene	0.044	0.002
RU1-21	o + p Xylene	0.016	0.001

RU1-23	Benzene	0.018	0.006
RU1-23	n-Butylbenzene	0.077	0.007
RU1-23	sec-Butylbenzene	0.051	0.006
RU1-23	Ethyl Benzene	0.162	0.006
RU1-23	Isopropylbenzene	0.052	0.006
RU1-23	p-Isopropyltoluene	0.045	0.007
RU1-23	Naphthalene	0.133	0.01
RU1-23	n-Propylbenzene	0.08	0.008
RU1-23	Toluene	0.275	0.007
RU1-23	1,2,4-Trimethylbenzene	0.576	0.007
RU1-23	1,3,5-Trimethylbenzene	0.22	0.01
RU1-23	m-Xylene	0.612	0.013
RU1-23	o + p Xylene	0.238	0.005
RU1-25	Benzene	0.002	0.001
RU1-25	1,2,4-Trimethylbenzene	0.004	0.001
RU1-25	1,3,5-Trimethylbenzene	0.003	0.002
RU1-25	m-Xylene	0.004	0.003
RU1-25	o + p Xylene	0.002	0.001
RU1-27	All Samples	ND	NA
RU2-1	All Samples	ND	NA
RU2-3	All Samples	ND	NA
RU2-7	All Samples	ND	NA
RU2-11	All Samples	ND	NA
RU2-15	All Samples	ND	NA
RU2-17	All Samples	ND	NA
RU2-21	All Samples	ND	NA
RU2-25	All Samples	ND	NA
RU2-29	All Samples	ND	NA
RU3-3	All Samples	ND	NA
RU3-9	All Samples	ND	NA
RU4-03	Ethyl Benzene	0.009	0.003
RU4-03	Isopropylbenzene	0.005	0.003
RU4-03	n-Propylbenzene	0.006	0.004
RU4-03	1,2,4-Trimethylbenzene	0.034	0.004
RU4-03	1,3,5-Trimethylbenzene	0.016	0.005
RU4-03	m-Xylene	0.027	0.007
RU4-05	n-Butylbenzene	5.25	0.051
RU4-05	sec-Butylbenzene	3.72	0.043
RU4-05	Ethyl Benzene	12.3	0.043
RU4-05	Isopropylbenzene	2.74	0.043
RU4-05	p-Isopropyltoluene	2.96	0.051
RU4-05	Naphthalene	2.7	0.072
RU4-05	n-Propylbenzene	5.76	0.058
RU4-05	Toluene	9.4	0.051
RU4-05	1,2,4-Trimethylbenzene	31.1	0.051

RU4-05	1,3,5-Trimethylbenzene	11.7	0.072
RU4-05	m-Xylene	36.1	0.094
RU4-05	o + p Xylene	12.3	0.036
RU4-05 DUP	n-Butylbenzene	4.21	0.165
RU4-05 DUP	sec-Butylbenzene	2.77	0.141
RU4-05 DUP	Ethyl Benzene	8.11	0.141
RU4-05 DUP	Isopropylbenzene	2.21	0.141
RU4-05 DUP	p-Isopropyltoluene	2.21	0.165
RU4-05 DUP	Naphthalene	2.66	0.235
RU4-05 DUP	n-Propylbenzene	4.65	0.188
RU4-05 DUP	Toluene	6.23	0.165
RU4-05 DUP	1,2,4-Trimethylbenzene	25.3	0.165
RU4-05 DUP	1,3,5-Trimethylbenzene	9	0.235
RU4-05 DUP	m-Xylene	24.2	0.306
RU4-05 DUP	o + p Xylene	8.27	0.118
RU4-09	Benzene	0.11	0.002
RU4-09	n-Butylbenzene	0.009	0.003
RU4-09	sec-Butylbenzene	0.007	0.002
RU4-09	Ethyl Benzene	0.261	0.002
RU4-09	Isopropylbenzene	0.021	0.002
RU4-09	p-Isopropyltoluene	0.006	0.003
RU4-09	Naphthalene	0.035	0.004
RU4-09	n-Propylbenzene	0.029	0.003
RU4-09	Toluene	2.27	0.003
RU4-09	1,2,4-Trimethylbenzene	0.183	0.003
RU4-09	1,3,5-Trimethylbenzene	0.058	0.004
RU4-09	m-Xylene	1.04	0.005
RU4-09	o + p Xylene	0.428	0.002
RU4-11	Benzene	0.016	0.001
RU4-11	Chloroform	0.004	0.002
RU4-11	Ethyl Benzene	0.027	0.001
RU4-11	Isopropylbenzene	0.002	0.001
RU4-11	n-Propylbenzene	0.003	0.002
RU4-11	Toluene	0.174	0.001
RU4-11	1,2,4-Trimethylbenzene	0.02	0.001
RU4-11	1,3,5-Trimethylbenzene	0.006	0.002
RU4-11	m-Xylene	0.075	0.003
RU4-11	o + p Xylene	0.032	0.001
RU4-13	Benzene	0.048	0.037
RU4-13	Ethyl Benzene	0.142	0.037
RU4-13	Toluene	0.142	0.043
RU4-13	1,2,4-Trimethylbenzene	0.186	0.043
RU4-13	1,3,5-Trimethylbenzene	0.136	0.062
RU4-13	m-Xylene	0.223	0.081
RU4-17	n-Butylbenzene	0.002	0.002

RU4-17	Ethyl Benzene	0.015	0.001
RU4-17	Isopropylbenzene	0.003	0.001
RU4-17	n-Propylbenzene	0.004	0.002
RU4-17	Toluene	0.032	0.002
RU4-17	1,2,4-Trimethylbenzene	0.027	0.002
RU4-17	1,3,5-Trimethylbenzene	0.009	0.002
RU4-17	m-Xylene	0.044	0.003
RU4-17	o + p Xylene	0.019	0.001
RU5-02	n-Butylbenzene	0.878	0.062
RU5-02	sec-Butylbenzene	0.488	0.053
RU5-02	Ethyl Benzene	2.58	0.053
RU5-02	Isopropylbenzene	0.612	0.053
RU5-02	p-Isopropyltoluene	0.435	0.062
RU5-02	Naphthalene	1.06	0.089
RU5-02	n-Propylbenzene	1.1	0.071
RU5-02	Toluene	6.27	0.062
RU5-02	1,2,4-Trimethylbenzene	5.93	0.062
RU5-02	1,3,5-Trimethylbenzene	2.88	0.089
RU5-02	m-Xylene	9.76	0.115
RU5-02	o + p Xylene	3.75	0.044
RU5-04	Benzene	1.82	0.11
RU5-04	n-Butylbenzene	20.4	0.128
RU5-04	sec-Butylbenzene	12.1	0.11
RU5-04	Ethyl Benzene	50.2	0.11
RU5-04	Isopropylbenzene	11.6	0.11
RU5-04	p-Isopropyltoluene	11.1	0.128
RU5-04	Naphthalene	15.6	0.183
RU5-04	n-Propylbenzene	22.9	0.147
RU5-04	Toluene	100	0.128
RU5-04	1,2,4-Trimethylbenzene	125	0.128
RU5-04	1,3,5-Trimethylbenzene	62.3	0.183
RU5-04	m-Xylene	180	0.238
RU5-04	o + p Xylene	62.9	0.092
RU5-06	Benzene	2.14	0.141
RU5-06	n-Butylbenzene	21.1	0.165
RU5-06	sec-Butylbenzene	13.9	0.141
RU5-06	Ethyl Benzene	62.7	0.141
RU5-06	Isopropylbenzene	12.7	0.141
RU5-06	p-Isopropyltoluene	11.9	0.165
RU5-06	Naphthalene	18.2	0.236
RU5-06	n-Propylbenzene	22.1	0.189
RU5-06	Toluene	124	0.165
RU5-06	1,2,4-Trimethylbenzene	131	0.165
RU5-06	1,3,5-Trimethylbenzene	63.6	0.236
RU5-06	m-Xylene	220	0.306

RU5-06	o + p Xylene	77.1	0.118
RU5-06 DUP	Benzene	0.783	0.102
RU5-06 DUP	n-Butylbenzene	10.3	0.119
RU5-06 DUP	sec-Butylbenzene	6.5	0.102
RU5-06 DUP	Ethyl Benzene	30.5	0.102
RU5-06 DUP	Isopropylbenzene	6.64	0.102
RU5-06 DUP	p-Isopropyltoluene	5.97	0.119
RU5-06 DUP	Naphthalene	8.93	0.17
RU5-06 DUP	n-Propylbenzene	11.7	0.136
RU5-06 DUP	Toluene	53.9	0.119
RU5-06 DUP	1,2,4-Trimethylbenzene	72	0.119
RU5-06 DUP	1,3,5-Trimethylbenzene	35.7	0.17
RU5-06 DUP	m-Xylene	108	0.221
RU5-06 DUP	o + p Xylene	38.5	0.085
RU5-08	Benzene	2.14	0.158
RU5-08	n-Butylbenzene	19.6	0.185
RU5-08	sec-Butylbenzene	18	0.158
RU5-08	Ethyl Benzene	93.9	0.158
RU5-08	Isopropylbenzene	15.8	0.158
RU5-08	p-Isopropyltoluene	16.6	0.185
RU5-08	Naphthalene	23.5	0.264
RU5-08	n-Propylbenzene	40.6	0.211
RU5-08	Toluene	188	0.185
RU5-08	1,2,4-Trimethylbenzene	193	0.185
RU5-08	1,3,5-Trimethylbenzene	92	0.264
RU5-08	m-Xylene	323	0.343
RU5-08	o + p Xylene	113	0.132
RU5-10	Benzene	0.121	0.002
RU5-10	n-Butylbenzene	0.234	0.002
RU5-10	sec-Butylbenzene	0.012	0.002
RU5-10	Ethyl Benzene	0.719	0.002
RU5-10	Isopropylbenzene	0.058	0.002
RU5-10	p-Isopropyltoluene	0.011	0.002
RU5-10	n-Propylbenzene	0.06	0.002
RU5-10	Toluene	3.24	0.002
RU5-10	1,2,4-Trimethylbenzene	0.595	0.002
RU5-10	1,3,5-Trimethylbenzene	0.133	0.003
RU5-10	m-Xylene	2.44	0.004
RU5-10	o + p Xylene	0.924	0.001
RU5-12	Benzene	0.087	0.002
RU5-12	n-Butylbenzene	0.006	0.002
RU5-12	sec-Butylbenzene	0.005	0.002
RU5-12	Ethyl Benzene	0.317	0.002
RU5-12	Isopropylbenzene	0.029	0.002
RU5-12	p-Isopropyltoluene	0.005	0.002

RU5-12	Naphthalene	0.062	0.003
RU5-12	n-Propylbenzene	0.031	0.003
RU5-12	Toluene	0.994	0.002
RU5-12	1,2,4-Trimethylbenzene	0.195	0.002
RU5-12	1,3,5-Trimethylbenzene	0.066	0.003
RU5-12	m-Xylene	1.06	0.004
RU5-12	o + p Xylene	0.406	0.002
RU5-16	Benzene	0.02	0.001
RU5-16	n-Butylbenzene	0.004	0.001
RU5-16	sec-Butylbenzene	0.004	0.001
RU5-16	Ethyl Benzene	0.207	0.001
RU5-16	Isopropylbenzene	0.021	0.001
RU5-16	p-Isopropyltoluene	0.004	0.001
RU5-16	Naphthalene	0.031	0.002
RU5-16	n-Propylbenzene	0.025	0.002
RU5-16	Toluene	0.559	0.001
RU5-16	1,2,4-Trimethylbenzene	0.139	0.001
RU5-16	1,3,5-Trimethylbenzene	0.05	0.002
RU5-16	m-Xylene	0.771	0.003
RU5-16	o + p Xylene	0.259	0.001
RU5-20	Benzene	0.018	0.002
RU5-20	n-Butylbenzene	0.081	0.003
RU5-20	sec-Butylbenzene	0.051	0.002
RU5-20	Ethyl Benzene	0.208	0.002
RU5-20	Isopropylbenzene	0.056	0.002
RU5-20	p-Isopropyltoluene	0.047	0.003
RU5-20	Naphthalene	0.102	0.004
RU5-20	n-Propylbenzene	0.094	0.003
RU5-20	Toluene	0.223	0.003
RU5-20	1,2,4-Trimethylbenzene	0.334	0.003
RU5-20	1,3,5-Trimethylbenzene	0.248	0.004
RU5-20	m-Xylene	0.39	0.005
RU5-20	o + p Xylene	0.3	0.002
RU5-24	Benzene	0.045	0.035
RU5-24	n-Butylbenzene	0.539	0.041
RU5-24	sec-Butylbenzene	0.313	0.035
RU5-24	Ethyl Benzene	0.678	0.035
RU5-24	Isopropylbenzene	0.244	0.035
RU5-24	p-Isopropyltoluene	0.284	0.041
RU5-24	Naphthalene	0.609	0.058
RU5-24	n-Propylbenzene	0.452	0.046
RU5-24	Toluene	1.5	0.041
RU5-24	1,2,4-Trimethylbenzene	2.6	0.041
RU5-24	1,3,5-Trimethylbenzene	1.21	0.058
RU5-24	m-Xylene	2.55	0.075

RU5-24	o + p Xylene	0.997	0.029
RU5-32	All Samples	ND	NA
RU5-36	Ethyl Benzene	0.002	0.002
RU5-36	Toluene	0.004	0.002
RU5-36	1,2,4-Trimethylbenzene	0.007	0.002
RU5-36	1,3,5-Trimethylbenzene	<1.00	1
RU5-36	m-Xylene	0.007	0.004
RU5-36	o + p Xylene	0.003	0.001
RU6-2	All Samples	ND	NA
RU6-4	All Samples	ND	NA
RU6-8	All Samples	ND	NA
RU6-10	All Samples	ND	NA
RU6-10 DUP	All Samples	ND	NA
RU6-12	Benzene	0.06	0.007
RU6-12	cis-1,2-Dichloroethylene	0.103	0.006
RU6-12	Ethyl Benzene	0.027	0.007
RU6-12	1,2,4-Trimethylbenzene	0.022	0.008
RU6-12	m-Xylene	0.038	0.014
RU6-14	Benzene	0.062	0.002
RU6-14	cis-1,2-Dichloroethylene	0.072	0.002
RU6-14	Toluene	0.08	0.002
RU6-14	Trichloroethylene	0.054	0.003
RU6-14	1,2,4-Trimethylbenzene	0.021	0.002
RU6-14	1,3,5-Trimethylbenzene	0.01	0.003
RU6-14	m-Xylene	0.084	0.004
RU6-14	o + p Xylene	0.021	0.002
RU6-16	Benzene	0.081	0.005
RU6-16	Carbon Disulfide	0.041	0.027
RU6-16	cis-1,2-Dichloroethylene	0.075	0.005
RU6-16	Ethyl Benzene	0.031	0.005
RU6-16	MIBK	BDL	0.08
RU6-16	Toluene	0.022	0.006
RU6-16	1,2,4-Trimethylbenzene	0.018	0.006
RU6-16	1,3,5-Trimethylbenzene	0.01	0.009
RU6-16	m-Xylene	0.058	0.012
RU6-20	Benzene	0.108	0.003
RU6-20	cis-1,2-Dichloroethylene	0.091	0.003
RU6-20	Ethyl Benzene	0.057	0.003
RU6-20	Trichloroethylene	0.23	0.006
RU6-20	1,2,4-Trimethylbenzene	0.04	0.004
RU6-20	1,3,5-Trimethylbenzene	0.018	0.006
RU6-20	m-Xylene	0.14	0.007
RU6-20	o + p Xylene	0.023	0.003
RU7-4	All Samples	ND	NA
RU7-8	Naphthalene	0.013	0.005

RU7-8	1,2,4-Trimethylbenzene	0.006	0.004
RU7-8	1,3,5-Trimethylbenzene	0.006	0.005
RU7-8	m-Xylene	BDL	0.007
RU7-10	All Samples	ND	NA
RU7-12	All Samples	ND	NA
RU7-16	All Samples	ND	NA
RU7-16 DUP	All Samples	ND	NA
RU7-20	m-Xylene	0.024	0.01
RU7-20	o + p Xylene	0.011	0.004
RU8-4	All Samples	ND	NA
RU8-10	All Samples	ND	NA
RU8-14	Benzene	BDL	0.004
RU8-20	Benzene	0.009	0.003
RU8-20	Trichloroethylene	0.024	0.005
RU9-4	All Samples	ND	NA
RU9-6	All Samples	ND	NA
RU9-8	All Samples	ND	NA
RU9-8 DUP	All Samples	ND	NA
RU9-10	Carbon Disulfide	0.064	0.031
RU9-20	Carbon Disulfide	0.033	0.03
RU10-2	sec-Butylbenzene	7.14	0.251
RU10-2	Ethyl Benzene	27.9	0.251
RU10-2	Isopropylbenzene	7.19	0.251
RU10-2	p-Isopropyltoluene	9.56	0.293
RU10-2	Naphthalene	32.3	0.419
RU10-2	n-Propylbenzene	13.3	0.335
RU10-2	Toluene	91.4	0.293
RU10-2	1,2,4-Trimethylbenzene	104	0.293
RU10-2	1,3,5-Trimethylbenzene	49	0.419
RU10-2	m-Xylene	124	0.545
RU10-2	o + p Xylene	41.9	0.21
RU10-4	Benzene	1.94	0.153
RU10-4	n-Butylbenzene	12.3	0.179
RU10-4	sec-Butylbenzene	17.3	0.153
RU10-4	Ethyl Benzene	30.2	0.153
RU10-4	Isopropylbenzene	14.8	0.153
RU10-4	p-Isopropyltoluene	17.3	0.179
RU10-4	Naphthalene	41.9	0.255
RU10-4	n-Propylbenzene	15.5	0.204
RU10-4	Toluene	122	0.179
RU10-4	1,2,4-Trimethylbenzene	101	0.179
RU10-4	1,3,5-Trimethylbenzene	41.9	0.255
RU10-4	m-Xylene	139	0.332
RU10-4	o + p Xylene	51.4	0.128
RU10-6	Benzene	0.025	0.004

RU10-6	n-Butylbenzene	0.59	0.005
RU10-6	sec-Butylbenzene	0.356	0.004
RU10-6	Ethyl Benzene	6.57	0.004
RU10-6	Isopropylbenzene	0.332	0.004
RU10-6	p-Isopropyltoluene	0.359	0.005
RU10-6	Naphthalene	0.58	0.006
RU10-6	n-Propylbenzene	0.606	0.005
RU10-6	Toluene	7.7	0.005
RU10-6	1,2,4-Trimethylbenzene	15.8	0.005
RU10-6	1,3,5-Trimethylbenzene	9.74	0.006
RU10-6	m-Xylene	28.7	0.008
RU10-6	o + p Xylene	10.9	0.003
RU10-8	Benzene	0.146	0.008
RU10-8	n-Butylbenzene	0.047	0.01
RU10-8	sec-Butylbenzene	0.029	0.008
RU10-8	Ethyl Benzene	0.516	0.008
RU10-8	Isopropylbenzene	0.055	0.008
RU10-8	Naphthalene	0.257	0.014
RU10-8	n-Propylbenzene	0.083	0.011
RU10-8	Toluene	0.098	0.01
RU10-8	1,2,4-Trimethylbenzene	0.652	0.01
RU10-8	1,3,5-Trimethylbenzene	0.246	0.014
RU10-8	m-Xylene	1.9	0.018
RU10-8	o + p Xylene	0.885	0.007
RU10-10	Benzene	0.189	0.006
RU10-10	n-Butylbenzene	0.013	0.007
RU10-10	sec-Butylbenzene	0.012	0.006
RU10-10	Ethyl Benzene	0.534	0.006
RU10-10	Isopropylbenzene	0.045	0.006
RU10-10	Naphthalene	0.15	0.01
RU10-10	n-Propylbenzene	0.059	0.008
RU10-10	Toluene	0.203	0.007
RU10-10	1,2,4-Trimethylbenzene	0.474	0.007
RU10-10	1,3,5-Trimethylbenzene	0.17	0.01
RU10-10	m-Xylene	0.808	0.013
RU10-10	o + p Xylene	0.92	0.005
RU10-12	Benzene	0.063	0.002
RU10-12	n-Butylbenzene	0.004	0.002
RU10-12	sec-Butylbenzene	0.004	0.002
RU10-12	Carbon Disulfide	0.018	0.008
RU10-12	Ethyl Benzene	0.181	0.002
RU10-12	Isopropylbenzene	0.015	0.002
RU10-12	Naphthalene	0.044	0.003
RU10-12	n-Propylbenzene	0.019	0.002
RU10-12	Toluene	0.094	0.002

RU10-12	1,2,4-Trimethylbenzene	0.156	0.002
RU10-12	1,3,5-Trimethylbenzene	0.061	0.003
RU10-12	m-Xylene	1.08	0.004
RU10-12	o + p Xylene	0.456	0.001
RU10-16	Benzene	0.027	0.003
RU10-16	n-Butylbenzene	0.011	0.003
RU10-16	sec-Butylbenzene	0.011	0.003
RU10-16	cis-1,2-Dichloroethylene	0.198	0.002
RU10-16	Ethyl Benzene	0.424	0.003
RU10-16	Isopropylbenzene	0.048	0.003
RU10-16	Naphthalene	0.062	0.004
RU10-16	n-Propylbenzene	0.055	0.003
RU10-16	Toluene	0.351	0.003
RU10-16	1,2,4-Trimethylbenzene	0.278	0.003
RU10-16	1,3,5-Trimethylbenzene	0.144	0.004
RU10-16	m-Xylene	0.647	0.006
RU10-16	o + p Xylene	0.445	0.002
RU10-20	Benzene	0.01	0.002
RU10-20	n-Butylbenzene	0.006	0.002
RU10-20	sec-Butylbenzene	0.005	0.002
RU10-20	Carbon Disulfide	0.018	0.01
RU10-20	cis-1,2-Dichloroethylene	0.113	0.002
RU10-20	Ethyl Benzene	0.085	0.002
RU10-20	Isopropylbenzene	0.013	0.002
RU10-20	Naphthalene	0.028	0.003
RU10-20	n-Propylbenzene	0.015	0.003
RU10-20	Toluene	0.078	0.002
RU10-20	1,2,4-Trimethylbenzene	0.077	0.002
RU10-20	1,3,5-Trimethylbenzene	0.047	0.003
RU10-20	m-Xylene	0.197	0.004
RU10-20	o + p Xylene	0.062	0.002
RU10-24	Benzene	0.042	0.003
RU10-24	n-Butylbenzene	BDL	0.7
RU10-24	Carbon Disulfide	0.021	0.013
RU10-24	cis-1,2-Dichloroethylene	0.135	0.002
RU10-24	Ethyl Benzene	0.041	0.003
RU10-24	Isopropylbenzene	0.005	0.003
RU10-24	p-Isopropyltoluene	0.004	0.003
RU10-24	Naphthalene	0.015	0.004
RU10-24	n-Propylbenzene	0.007	0.004
RU10-24	Toluene	0.208	0.003
RU10-24	Trichloroethylene	0.022	0.004
RU10-24	1,2,4-Trimethylbenzene	0.043	0.003
RU10-24	1,3,5-Trimethylbenzene	0.02	0.004
RU10-24	m-Xylene	0.135	0.006

RU10-24	o + p Xylene	0.053	0.002
RU10-28	Toluene	0.004	0.001
RU10-28	m-Xylene	0.003	0.003
RU10-32	Ethyl Benzene	0.002	0.002
RU10-32	Naphthalene	0.018	0.003
RU10-32	Toluene	0.006	0.002
RU10-32	1,2,4-Trimethylbenzene	0.006	0.002
RU10-32	1,3,5-Trimethylbenzene	BDL	0.003
RU10-32	m-Xylene	0.01	0.004
RU10-32	o + p Xylene	0.004	0.001
RU11-4	1,2,4-Trimethylbenzene	0.005	0.001
RU11-4	1,3,5-Trimethylbenzene	0.004	0.002
RU11-4	m-Xylene	0.007	0.003
RU11-6	n-Butylbenzene	4.67	0.076
RU11-6	sec-Butylbenzene	3.8	0.065
RU11-6	Ethyl Benzene	11.2	0.065
RU11-6	Isopropylbenzene	4.01	0.065
RU11-6	p-Isopropyltoluene	3.82	0.076
RU11-6	Naphthalene	8.29	0.109
RU11-6	n-Propylbenzene	6.75	0.087
RU11-6	Toluene	3.95	0.076
RU11-6	1,2,4-Trimethylbenzene	33.6	0.076
RU11-6	1,3,5-Trimethylbenzene	14.7	0.109
RU11-6	m-Xylene	48.5	0.142
RU11-6	o + p Xylene	14.8	0.054
RU11-8	n-Butylbenzene	0.004	0.003
RU11-8	sec-Butylbenzene	0.003	0.003
RU11-8	Ethyl Benzene	0.241	0.003
RU11-8	Isopropylbenzene	0.02	0.003
RU11-8	Naphthalene	0.069	0.004
RU11-8	n-Propylbenzene	0.02	0.003
RU11-8	Toluene	0.972	0.003
RU11-8	1,2,4-Trimethylbenzene	0.124	0.003
RU11-8	1,3,5-Trimethylbenzene	0.041	0.004
RU11-8	m-Xylene	0.684	0.006
RU11-8	o + p Xylene	0.335	0.002
RU11-10	n-Butylbenzene	0.003	0.002
RU11-10	sec-Butylbenzene	0.003	0.001
RU11-10	Carbon Disulfide	0.012	0.007
RU11-10	Ethyl Benzene	0.358	0.001
RU11-10	Isopropylbenzene	0.024	0.001
RU11-10	Naphthalene	0.05	0.002
RU11-10	n-Propylbenzene	0.023	0.002
RU11-10	Toluene	0.212	0.002
RU11-10	1,2,4-Trimethylbenzene	0.138	0.002

RU11-10	1,3,5-Trimethylbenzene	0.047	0.002
RU11-10	m-Xylene	1.38	0.003
RU11-10	o + p Xylene	0.477	0.001
RU11-12	Benzene	0.003	0.002
RU11-12	Carbon Disulfide	0.014	0.009
RU11-12	cis-1,2-Dichloroethylene	0.041	0.002
RU11-12	Ethyl Benzene	0.017	0.002
RU11-12	Isopropylbenzene	0.003	0.002
RU11-12	p-Isopropyltoluene	BDL	0.002
RU11-12	Naphthalene	0.029	0.003
RU11-12	n-Propylbenzene	0.004	0.003
RU11-12	Trichloroethylene	0.348	0.003
RU11-12	1,2,4-Trimethylbenzene	0.022	0.002
RU11-12	1,3,5-Trimethylbenzene	0.008	0.003
RU11-12	m-Xylene	0.022	0.004
RU11-12	o + p Xylene	0.003	0.002
RU11-14	Benzene	0.003	0.001
RU11-14	n-Butylbenzene	BDL	0.002
RU11-14	sec-Butylbenzene	0.002	0.001
RU11-14	Carbon Disulfide	0.058	0.007
RU11-14	cis-1,2-Dichloroethylene	0.053	0.001
RU11-14	Ethyl Benzene	0.025	0.001
RU11-14	Isopropylbenzene	0.006	0.001
RU11-14	Naphthalene	0.015	0.002
RU11-14	n-Propylbenzene	0.008	0.002
RU11-14	Toluene	0.036	0.002
RU11-14	Trichloroethylene	0.434	0.002
RU11-14	1,2,4-Trimethylbenzene	0.041	0.002
RU11-14	1,3,5-Trimethylbenzene	0.015	0.002
RU11-14	m-Xylene	0.066	0.003
RU11-14	o + p Xylene	0.017	0.001
RU11-20	Benzene	0.002	0.002
RU11-20	n-Butylbenzene	BDL	0.002
RU11-20	sec-Butylbenzene	BDL	0.002
RU11-20	Carbon Disulfide	0.029	0.008
RU11-20	cis-1,2-Dichloroethylene	0.144	0.001
RU11-20	Ethyl Benzene	0.044	0.002
RU11-20	Isopropylbenzene	0.005	0.002
RU11-20	n-Propylbenzene	0.006	0.002
RU11-20	Toluene	0.066	0.002
RU11-20	Trichloroethylene	0.059	0.003
RU11-20	1,2,4-Trimethylbenzene	0.033	0.002
RU11-20	1,3,5-Trimethylbenzene	0.012	0.003
RU11-20	m-Xylene	0.101	0.003
RU11-20	o + p Xylene	0.033	0.001

RU11-26	1,2,4-Trimethylbenzene	BDL	0.006
RU11-26	m-Xylene	BDL	0.011
RU11-28	n-Butylbenzene	0.007	0.006
RU11-28	sec-Butylbenzene	0.006	0.005
RU11-28	Carbon Disulfide	BDL	0.025
RU11-28	cis-1,2-Dichloroethylene	0.024	0.004
RU11-28	Ethyl Benzene	0.043	0.005
RU11-28	Isopropylbenzene	0.011	0.005
RU11-28	n-Propylbenzene	0.016	0.007
RU11-28	Toluene	0.043	0.006
RU11-28	Trichloroethylene	0.052	0.008
RU11-28	1,2,4-Trimethylbenzene	0.086	0.006
RU11-28	1,3,5-Trimethylbenzene	0.033	0.008
RU11-28	m-Xylene	0.173	0.011
RU11-28	o + p Xylene	0.054	0.004
RU12-6	All Samples	ND	NA
RU12-8	m-Xylene	BDL	0.016
RU12-8 DUP	Carbon Disulfide	0.032	0.021
RU12-8 DUP	m-Xylene	BDL	0.009
RU12-12	All Samples	ND	NA
RU12-20	Carbon Disulfide	0.01	0.009
RU13-6	All Samples	ND	NA
RU13-8	All Samples	ND	NA
RU13-10	All Samples	ND	NA
RU13-12	Carbon Disulfide	0.01	0.008
RU13-12 DUP	m-Xylene	BDL	0.004
RU13-16	Benzene	0.006	0.002
RU13-16	cis-1,2-Dichloroethylene	0.725	0.001
RU13-16	Ethyl Benzene	0.059	0.002
RU13-16	Isopropylbenzene	0.007	0.002
RU13-16	n-Propylbenzene	0.008	0.002
RU13-16	Toluene	0.067	0.002
RU13-16	1,2,4-Trimethylbenzene	0.056	0.002
RU13-16	1,3,5-Trimethylbenzene	0.019	0.003
RU13-16	m-Xylene	0.13	0.004
RU13-16	o + p Xylene	0.033	0.001
RU13-32	All Samples	ND	NA
RU14-6	All Samples	ND	NA
RU14-8	All Samples	ND	NA
RU14-10	cis-1,2-Dichloroethylene	0.015	0.001
RU14-16	1,2,4-Trimethylbenzene	0.005	0.002
RU14-16	m-Xylene	0.004	0.004
RU15-6	All Samples	ND	NA
RU15-8	All Samples	ND	NA
RU15-10	All Samples	ND	NA

RU15-10DUP	All Samples	ND	NA
RU15-18	All Samples	ND	NA
RU16-6	Ethyl Benzene	0.011	0.002
RU16-6	1,3,5-Trimethylbenzene	0.006	0.003
RU16-6	m-Xylene	0.005	0.003
RU16-8	Carbon Disulfide	0.021	0.008
RU16-8	Ethyl Benzene	0.01	0.002
RU16-8	1,3,5-Trimethylbenzene	0.005	0.003
RU16-8	m-Xylene	0.008	0.003
RU16-8DUP	Ethyl Benzene	0.026	0.002
RU16-8DUP	1,3,5-Trimethylbenzene	0.015	0.003
RU16-8DUP	m-Xylene	0.019	0.004
RU16-10	Ethyl Benzene	0.026	0.002
RU16-10	1,3,5-Trimethylbenzene	0.011	0.003
RU16-10	m-Xylene	0.013	0.004
RU16-14	All Samples	ND	NA
RU16-20	Naphthalene	0.017	0.003
RU16-20	m-Xylene	BDL	0.004
RU17-6	All Samples	ND	NA
RU17-8	All Samples	ND	NA
RU17-10	All Samples	ND	NA
RU17-14	All Samples	ND	NA
RU18-6	All Samples	ND	NA
RU18-8	All Samples	ND	NA
RU18-10	All Samples	ND	NA
RU18-14	All Samples	ND	NA

Table 3: Aqueous Volatile Organic Compounds

Sample	Analyte	Result	MDL
		ug/l	ug/l
CF-01A	All Samples	ND	50
CF-02	Benzene	7.5	0.6
CF-02	cis-1,2-Dichloroethylene	2.2	0.5
CF-02	Ethyl Benzene	31.6	0.6
CF-02	Isopropylbenzene	6.4	0.6
CF-02	Naphthalene	51.6	1
CF-02	n-Propylbenzene	6.7	0.8
CF-02	Toluene	9.4	0.7
CF-02	Trichloroethylene	17.9	1
CF-02	1,2,4-Trimethylbenzene	62.2	0.7
CF-02	1,3,5-Trimethylbenzene	22.8	1
CF-02	m-Xylene	65.2	1.3
CF-02	o + p Xylene	65.2	0.5
CF-03	Benzene	99	60
CF-03	2-Butanone (MEK)	3000	1200
CF-03	cis-1,2-Dichloroethylene	2200	50
CF-03	Ethyl Benzene	578	60
CF-03	Isopropylbenzene	88	60
CF-03	Toluene	2430	70
CF-03	Trichloroethylene	6260	100
CF-03	1,2,4-Trimethylbenzene	743	70
CF-03	1,3,5-Trimethylbenzene	345	100
CF-03	m-Xylene	2320	130
CF-03	o + p Xylene	786	50
CF-03DUP	Benzene	90	60
CF-03DUP	cis-1,2-Dichloroethylene	2380	50
CF-03DUP	Ethyl Benzene	660	60
CF-03DUP	Isopropylbenzene	104	60
CF-03DUP	Toluene	2610	70
CF-03DUP	Trichloroethylene	7020	100
CF-03DUP	1,2,4-Trimethylbenzene	1070	70
CF-03DUP	1,3,5-Trimethylbenzene	129	100
CF-03DUP	m-Xylene	2540	130
CF-03DUP	o + p Xylene	876	50
CF-04	All Samples	ND	50
CF-05	Benzene	6.2	0.6
CF-05	cis-1,2-Dichloroethylene	96.7	0.5
CF-05	trans-1,2-Dichloroethylene	<0.8	0.8
CF-05	Ethyl Benzene	1.3	0.6
CF-05	Isopropylbenzene	1	0.6
CF-05	Trichloroethylene	17.3	1
CF-05	1,2,4-Trimethylbenzene	6	0.7

CF-05	1,3,5-Trimethylbenzene	BDL	1
CF-05	m-Xylene	6	1.3
CF-06	Benzene	1.2	0.6
CF-06	cis-1,2-Dichloroethylene	1.8	0.5
CF-06	Trichloroethylene	24.9	1
CF-07	Carbon Disulfide	6.1	3
CF-08	Benzene	1.4	0.6
CF-08	cis-1,2-Dichloroethylene	2.1	0.5
CF-08	Trichloroethylene	26.9	1
MP-057	Benzene	3.3	0.6
MP-057	Toluene	1.1	0.7
MP-057	Trichloroethylene	3.5	1
MP-057	1,2,4-Trimethylbenzene	1.1	0.7
MP-057	m-Xylene	2.7	1.3
MP-10S	Benzene	1.9	0.6
MP-10S	Ethyl Benzene	0.7	0.6
MP-10S	Toluene	8	0.7
MP-10S	1,2,4-Trimethylbenzene	1.7	0.7
MP-10S	1,3,5-Trimethylbenzene	1.3	1
MP-10S	m-Xylene	4.1	1.3
MP-10S	o + p Xylene	2.1	0.5
MP-15S	Benzene	4.2	0.6
MP-15S	Carbon Disulfide	7.3	3
MP-15S	Ethyl Benzene	1	0.6
MP-15S	Naphthalene	4.4	1
MP-15S	Toluene	11.7	0.7
MP-15S	1,2,4-Trimethylbenzene	2.4	0.7
MP-15S	1,3,5-Trimethylbenzene	1.7	1
MP-15S	m-Xylene	5.2	1.3
MP-15S	o + p Xylene	3.3	0.5

QA/QC SUMMARY

In this section, summary Quality Control / Quality Assurance information is given. Specific information is given in the data tables.

Sediment samples – Inorganic Analyses

Table 1 is used to provide a summary for inorganic parameters associated with sediment sampling. Sixteen hundred and eighty-two inorganic analyses were conducted. Overall, data completeness is 97%. Only 3% of data are associated with failed Blanks and 10% are associated with failed duplicates or replicates. Considering the heterogeneity of sediment samples, the 10 % failure rate for duplicates and replicates is reasonable.

Table 1: Sampling locations, samples, completeness, blanks, and duplicates/replicates – Inorganic Data

Parameter	Sampling Locations	No. of Samples Analyzed at Sampling Locations			Missing Data	Completeness	Sampling Locations Associated With Failed...	
		1	2	3			(%)	Blank
(1)	(2)	(3)	(4)	(5)	(6)	(7)	(8)	(9)
Fe(II)	190	1	144	40	5	97	21	47
Fe Total	190	1	144	40	5	97	0	12
AVS	193	155	3	35	0	100	5	6
CrES	193	155	3	35	0	100	0	4
PW SO ₄	173	161	5	0	7	96	5	45
PW FE(II)	172	161	0	0	11	94	NA	NA
Total	1111	634	299	150	28	NA	31	114
Percent	100	57	27	13	3	97	3	10

NA = Not Applicable. Fe(II) and Fe Total are 0.5 HCl extracted.

Spikes were conducted for 0.5 N HCl Fe(II), Pore water sulfate, and Sulfide. All of the 0.5 N HCl Fe(II) spike recoveries were within 30 % of the target. All of the pore water sulfate spikes had recoveries within 30 % of the target. For sulfide, ground glass spiked with a sulfide mineral was used for spikes. For each individual test, a portion of the ground glass / spike material was sampled and subjected to the full analysis method. The average error for the spikes was 10.8 %. An average error is reported due to heterogeneity of the ground glass / spike material used.

Sediment samples – Organic Analyses

One hundred and fifteen sediment samples were analyzed for volatile organic compounds (VOC) using EPA method 8260. Nine field blanks, 8 equipment blanks, and 10 duplicate samples were collected in the field. All of the field blanks had all parameters below detection limits. Of the equipment blanks, seven contained measurable levels of Carbon Disulfide. The average Carbon Disulfide reading for sixth of the equipment blanks was 13.4 ug/L. The seventh had a reading of 205 ug/L. One equipment blank had a measurable concentration of chloroform (1.3 ug/L). Carbon disulfide data for the site should be treated with caution. Two of the trip blanks had low levels of Methyl Chloride (8/5/99 - 4.5 ug/L and 8/10/99 - 3.9 ug/L). However, Methyl Chloride levels in all other samples taken on these days had levels below the detection limit.

For four duplicates (RU 2-9, 6-10, 7-16, and 9-8), all of the parameters were non-detect. RU 4-5 had 12 non-detect parameters, with 8 passing the precision test. Two duplicates had one non-detect parameter each (RU 12-8 and 13-2), with passing precision. RU 16-8 had four non-detects, with each failing a precision test. RU 5-6 had 13 non-detect parameters, with each failing a precision test. The duplicate results indicate that the distribution of VOCs in the sediment is very heterogeneous.

Surrogate recovery, matrix spike recovery, and method blanks were also analyzed. All surrogate recovery and method blank results were within acceptable ranges. Two matrix spike recoveries were outside of acceptable ranges. For RU 10-2, the recovery of a Toluene spike was 245.6%; however, the ratio of sample to spike was greater than 4 to 1, which is expected to lead to greater than usual variation in spike recovery. Also, for RU 10-2, the recovery of a TCE spike was 148%, greater than acceptable.

Aqueous samples – Inorganic Analyses

Conductivity, Dissolved Oxygen, and Oxidation Reduction Potential were measured in the field using meters calibrated in the field. Iron(II) was measured in the field using Hach Method 8146. The calibration of the spectrophotometer used to measure Iron(II) was checked before and after fieldwork. Sulfate was measured using an Ion Chromatograph at Rowan University following EPA Method SW9056. Duplicate analyses of each sulfate sample were completed. All duplicates were acceptable.

Aqueous samples – Organic Analyses

Ten aqueous samples were analyzed for volatile organic compounds using EPA method 8260. **The duplicate analyses provided results in acceptable ranges.** Surrogate recovery, matrix spike recovery, and method blanks were also analyzed and all were within acceptable ranges.